

1-1-2011

# A multi-species analysis of biomechanical responses of the head to a shock wave

Richard Bolander  
*Wayne State University,*

Follow this and additional works at: [http://digitalcommons.wayne.edu/oa\\_dissertations](http://digitalcommons.wayne.edu/oa_dissertations)

 Part of the [Biomechanics Commons](#), and the [Biomedical Engineering and Bioengineering Commons](#)

---

## Recommended Citation

Bolander, Richard, "A multi-species analysis of biomechanical responses of the head to a shock wave" (2011). *Wayne State University Dissertations*. Paper 406.

This Open Access Dissertation is brought to you for free and open access by DigitalCommons@WayneState. It has been accepted for inclusion in Wayne State University Dissertations by an authorized administrator of DigitalCommons@WayneState.

**A MULTI-SPECIES ANALYSIS OF BIOMECHANICAL RESPONSES OF THE HEAD  
TO A SHOCK WAVE**

by

**RICHARD BOLANDER**

**DISSERTATION**

Submitted to the Graduate School

of Wayne State University,

Detroit, Michigan

in partial fulfillment of the requirements

for the degree of

**DOCTOR OF PHILOSOPHY**

2012

MAJOR: BIOMEDICAL ENGINEERING

Approved by:

---

Advisor

Date

---

Co-advisor

Date

---

Date

---

Date

---

Date

© COPYRIGHT BY  
RICHARD BOLANDER  
2012  
All Rights Reserved

## DEDICATION

This work is dedicated to my wife Sarah Elyse Bolander.

## ACKNOWLEDGEMENTS

I would like to thank many people for the completion of this dissertation. This includes my wife Sarah for her love and support. My friends and family have also had a significant effect on the completion of this project.

I would like to also thank my committee for their guidance in developing this dissertation and their willingness to challenge me along the way. I would also like to acknowledge the BME center staff and students for helping me to complete this project, and having the patience to help me learn about impact biomechanics theory and testing.

## TABLE OF CONTENTS

Dedication.....	ii
Acknowledgements.....	iii
List of Tables.....	viii
List of Figures.....	x
Chapter 1 Introduction.....	1
1.1 Statement of the Problem .....	1
1.2 Background and Significance.....	2
1.3 Hypotheses of PBI Mechanism .....	4
1.4 Investigating biomechanical responses of different biological models in blast injury research.....	10
1.5 Specific Aims and Hypotheses.....	11
Chapter 2 Shock Waves and Simplified Physical Models.....	15
2.1 Blast waves in air .....	15
2.2 Shock tubes .....	18
2.3 Wayne State University shock tube.....	22
2.4 Modal response of a system .....	24
2.5 Shock wave loading on an object.....	25
2.6 Experimental modes of response for a cylinder exposed to a shock wave .....	26
2.7 Theoretical modes of response of a sphere .....	28
2.8 Experimental modes observed in simplified physical models.....	29
2.9 Relationship between strain and ISP in simplified spherical models .....	32
2.10 Modes observed in simplified physical models .....	35
Chapter 3 Rat Model of Blast Biomechanics.....	37
3.1 The rat in blast research .....	37

3.2	Methods for investigating skull strain and ICP in the rat.....	38
3.3	Results of SG Measurements .....	42
3.4	Results of ICP measurements.....	44
3.5	MicroCT results .....	47
3.6	Observed modes of the rat skull when subjected to a shock wave .....	48
3.7	Limitations of study .....	49
3.8	Assessing frequency response changes of the DOA mode in the rat .....	50
3.9	Methods for assessing frequency response changes of the DOA mode in the rat.....	51
3.10	Results for top mounted versus back mounted sensors .....	53
3.11	Discussion of the effect of the IC vs OIC mount on the DOA flexural mode .....	57
3.12	FEM model of the rat head when exposed to a shock wave .....	59
3.13	Conclusion of rat model analysis .....	61
Chapter 4 Pig Model of Blast Biomechanics .....		63
4.1	The pig in blast research .....	63
4.2	Expected contribution of flexural modes of the pig skull when subjected to a shock wave .....	64
4.3	Methods for investigating biomechanical responses of the pig head when exposed to shock wave.....	65
4.4	ICP response for Pig 1 .....	70
4.5	Skull strain response of the pig head to shock wave exposure .....	71
4.6	ICP responses of the WSU pigs.....	72
4.7	Relationship between skull strain and ICP for WSU pigs .....	73
4.8	Relationship between principal strain and ICP .....	76
4.9	ICP response of pig compared to simplified physical models .....	76
4.10	Conclusion of WSU pig head testing.....	82

4.11	Methods from PREVENT series of tests .....	82
4.12	ICP response results from PREVENT biomechanics data set.....	86
4.13	ICP responses from PREVENT pigs.....	88
4.14	Pressure in the major vessels during blast wave exposure .....	89
4.15	Comparison between PREVENT and WSU pig results.....	92
4.16	Conclusion of pig testing.....	95
Chapter 5 Cadaver Model of Blast Biomechanics .....		97
5.1	Measurement of skull flexure and ICP in the cadaver when exposed to a shock wave .....	97
5.2	Methods for assessing biomechanical responses of the cadaver head during shock wave exposure .....	101
5.3	Observed flexural modes of the cadaver skull.....	107
5.4	Frequency content of ICP oscillations .....	115
5.5	Comparison of principal strain to ICP.....	119
5.6	Investigation of shock wave loading compared to blunt impact.....	122
5.7	Formation of internal pressure gradients.....	128
5.8	Frequency response of the cadaver head to impact .....	133
5.9	Hypothesis of response.....	134
5.10	Conclusion of Cadaver Testing.....	135
Chapter 6 Identification of Relevant Biomechanical Responses Across Species.....		138
6.1	Introduction .....	138
6.2	Relationships between the rat, pig, and cadaver.....	138
6.3	Biomechanical responses occurring across species during a front facing exposure .....	140
6.4	ICP comparison between the pig and cadaver by orientation .....	145
6.5	Discussion of results .....	147

6.6	CNS susceptibility to imparted pressure gradients.....	150
6.7	Discussion of hypotheses .....	151
6.8	Conclusion .....	152
	Appendix A Rat Data.....	154
	Appendix B Pig Data .....	172
	Appendix C Cadaver Data.....	201
	References.....	238
	Abstract.....	247
	Autobiographical Statement.....	249

## LIST OF TABLES

Table 3.1 Sample of research where rats are exposed to shock waves .....	38
Table 3.2 Peak skull flexure increases with shock wave intensity for the superior rat skull .....	44
Table 3.3 ICP increase with shock wave intensity ( $p < .0001$ ). .....	44
Table 3.4 A description of the weight and mount type for each rat used in the study.....	52
Table 4.1 A sample of blast research involving the pig model. The method of creating the shock wave, area of body exposed, number of specimens tested, measurement techniques applied, and rationale are all provided. S/W = shock wave, A/R = assault rifle, U/W = under water, Phys = physiological measurements, Hist = histology of brain tissue, Acc = Acceleration.....	63
Table 4.2 Protocol for a pig specimen exposed to multiple shock waves.....	69
Table 4.3 Distribution summary of strain results by sensor and orientation. ....	72
Table 4.4 Summary statistics of ICP response between specimens at each orientation for the low pressure intensity. ....	73
Table 4.5 A summary of the data collected from the PREVENT Phase 1 biomechanical studies. ICP= all fiber optic sensors in the brain, c = carotid, IVC= inferior vena cava, Cis= cisterna, TA= Thoracic Aorta, J= jugular, V= ventricle. ....	86
Table 4.6 Channel assessment of the ICP data from the PREVENT Phase 1 biomechanics study. ....	87
Table 5.1 A summary of characteristics of the cadavers used in this series of tests. CHF stands for chronic heart failure. ....	101
Table 5.2 Number of exposures to which each head was subjected at each orientation and pressure magnitude. ....	101
Table 5.3 Location of ICP sensors on the cadaver head (Leonardi 2011) .....	104
Table 5.4 The calculated ICP oscillation frequencies associated with the DOA mode of skull flexure for the front facing and rear facing orientations.....	119

Table 5.5 The pressure responses for this study were compared to the un-helmeted blunt impacts results reported by Hardy et al. (2007). * Indicate probable erroneous data. ....	126
Table 6.1 Bone thickness measurements for the three species tested in this project. Human (frontal bone), Pig (frontal bone), and rat (parietal bone). .....	139
Table 6.2 Shock front interaction times between different species. The skull lengths and braincases were measured from the specimens tested in this study.....	140
Table 6.3 The frequency of the DOA waveform was significantly different (* p < 0.05) between species.....	145

## LIST OF FIGURES

Figure 1.1 Intracranial pressure response of a monkey head exposed to a shock wave. This event took place despite thorax protection (Romba and Martin 1961). .....	8
Figure 1.2 FEM output of shock wave causing deformation to the skull, causing pressure gradients in the brain (Moss et al. 2008).....	9
Figure 1.3 The biomechanical responses observed in this study can be used to mitigate the effects of PBI in the warfighter. ....	11
Figure 1.4 The multi-modal skull flexure response was assessed by measuring shell deformation (strain) and stress on brain tissue (pressure). ....	12
Figure 1.5 The hypothesis of the project was that the skull is deformed by the shock wave, the resulting response will cause the formation of pressure gradients in the brain that may be damaging to the cells composing the central nervous system.....	14
Figure 2.1 : During detonation of an explosive charge (a) and (b) the rapid expansion of detonation products will create a contact surface, labeled as C, that will transfer its momentum to the ambient air as a blast wave (c). The blast wave will then propagate (d) (e) and (f). Figure taken from Ritzel et al. (2011). ....	16
Figure 2.2 Diagram of a Friedlander waveform (Kinney, 1962).....	17
Figure 2.3 Properties associated with air will change when a blast wave propagates through and are dependent on the distance of the blast wave relative to the fireball. The responses associated with pressure, density, flow velocity, and temperature are more variable in the near-field regime (a) than in the far-field regime (b). Figure taken from Ritzel et al. (2011). ....	17
Figure 2.4 Shock tube diagram prior to diaphragm rupture (McMilian 2004).....	18
Figure 2.5 Definition of regions within the shock tube following rupture of the membrane (McMilian 2004).....	19
Figure 2.6 Shock tube diagram and corresponding pressure and temperature profiles for each distinct region following membrane rupture (Ritzel et al. (2011))......	20
Figure 2.7 An X-t diagram of a close ended shock tube (Lamanna 1996).....	21
Figure 2.8 Multiple wave interactions occur within the shock tube in order to create a representative free-field blast wave profile (Ritzel et al. (2011)). ....	21

Figure 2.9 Graphic indicating dimensions of the WSU shock tube and placement of sensors .....	24
Figure 2.10 The axial strain response of a cylinder exposed to an underwater shock wave.....	28
Figure 2.11 The breathing mode response of a cylinder exposed to an underwater shock wave. The compression of the ends of the cylinder cause the center to go into tension, oscillate, and return to baseline (Kwon and Fox 1993). .....	28
Figure 2.12 Pressure sensor and strain gage locations on the glycerin filled sphere used by Leonardi (2011).....	30
Figure 2.13 The strain response of the aqueous filled sphere to shock wave exposure. The DOA, HFLA, and QSC modes have been highlighted (figure adapted from Leonardi (2011)).....	31
Figure 2.14 The ISP response for the occipital pressure sensor. Responses associated with the three identified modes on the shell surface are highlighted in this series. The HFLA oscillations are superposed on the DOA oscillations (adapted fromLeonardi (2011)).....	32
Figure 2.15 As the FEM shell was stiffened, the calculated pressure profile better approximated the experimentally measured pressures within the sphere. Figure is taken from Mediavilla Varas et al. 2011. Physics of IED blast shock tube simulations for mTBI research. Frontiers in Neurology 2, 1-14. ....	33
Figure 2.16 The experimental strain response of the 7mm sphere when compared to the FEM calculations. Figure is taken from Mediavilla Varas et al. 2011. Physics of IED blast shock tube simulations for mTBI research. Frontiers in Neurology 2, 1-14. ....	34
Figure 2.17 The waveforms to which the simulant is subjected are dependent on shell stiffness. Figure is taken from Mediavilla Varas et al. 2011. Physics of IED blast shock tube simulations for mTBI research. Frontiers in Neurology 2, 1-14.....	35
Figure 2.18 Modes of response observed for the sphere when exposed to a shock wave.....	36
Figure 3.1 Placement of strain gage on surface of the rat skull (A) and fiber optic pressure sensor installation on a rat skull (B).....	40
Figure 3.2 The rat was placed 114 cm within the shock tube and was placed on a trolley system to reduce the level of dynamic pressure shifts that are not representative of a free-field shock wave. ....	41

Figure 3.3 Principal strain response profiles of the superior brain case for both a 262 and 247 gram rat when exposed to shock waves of increasing intensity. For the presented data, tension is positive and compression is negative. (1) (red) A compression with an associated damped oscillation. (2) (green) A quasi-steady compression closely following the decay of the external static overpressure. (3) (blue) A response beginning in tension that followed the incident shock.....	43
Figure 3.4 The intracranial pressure response of a rat is dependent on shock wave intensity. The ICP responses for a 249 gram rat show distinct pressure oscillations (1) (red) that are present in each of the profiles. The waveforms also undergo a quasi-steady compression response that approximates the external loading response invoked by the shock wave (2) (green).....	46
Figure 3.5 The rise time of the external pressure wave is shorter (solid) than the rise time of the recorded intracranial pressure for a 249 gram rat. The actual rise time of the shock wave is shorter than what is measured by the penci gage (~ 1 microsecond) (dotted).....	46
Figure 3.6 (A) Measurements were taken of the MicroCT images of the rat skull to determine key structural elements. (B) A 3-dimensional reconstruction of the images depict that there are considerable gaps between the bone plates with significant reinforcement on the lateral bone folds, suggesting that the midline suture would be a probable place for skull flexure to take place.....	47
Figure 3.7 A diagram of the mounting procedures for the IC (A) and OIC (B) mounting positions of the rat skull. Drawings are not to scale. ....	51
Figure 3.8 . Intracranial pressure measurements with the fiber optic pressure sensor mounted on the top of the skull (IC). For the 437 gram rat (A) the pressure response associated with the DOA mode was the most harmonic at the 172 kPa incident intensity. For the 256 gram rat (B) the response was most harmonic when the 117 kPa incident shock wave was introduced.....	55
Figure 3.9 The OIC instrumented rats report higher frequencies but show similar results to the IC rats. The ICP response for both a 232 gram rat (A) amd 317 gram rat (B) demonstrate a high frequency content associated with the DOA mode of skull flixture and a ressonance associated with the QSC mode. ....	56
Figure 3.10 A contour chart describing the role of incident peak pressure intensity and rat weight for determining the frequency response associated with the DOA flexural mode for the IC group. It is generally shown that as	

the rats get heavier; greater incident shock wave intensity is required to invoke the DOA mode to oscillate the most harmonically.....	57
Figure 3.11 ICP response of the FEM rat head. The data suggest that the pressures within the brain are variable with some regions greater than the incident pressure. Additionally, the contrecoup pressure measured a tensile pressure before undergoing compression. Figure taken from Zhu et al. 2010. Development of an FE model of the rat head subjected to air shock loading. Stapp car crash journal. 54: 211-225.....	60
Figure 3.12 Flexural modes of the rat skull affecting ICP response. ....	62
Figure 4.1 Three dimensional microCT sections of the pig skull. The brain consists of a smaller portion of the total head volume than the human. ....	65
Figure 4.2 Strain gage locations on the pig head. ....	66
Figure 4.3 The pressure sensor fiber was secured to the pig skull at the foramen magnum. ....	67
Figure 4.4 The fiber optic sensor was mounted into the skull using a threaded insert. A rubber stopper compressed the fiber and a threaded cap was used to prevent the sensor from pulling out.....	67
Figure 4.5 A fastening system was used to hold the insert in place. The cable ties also prevented the strain wires from whipping, causing loss of contact of the strain gages to the skull bones. ....	69
Figure 4.6 The pig was positioned in three orientations. (A) Front (B) Side (C) Back. ....	70
Figure 4.7 The ICP response was dependent on skull flexure as measured by strain gages (Second Frontal). When the max and min principal strain responses oscillated in unison the greatest ICPs were measured (when in tension). Especially within the first millisecond. (Pig subject 5, 69 kPa incident pressure, front facing). ....	75
Figure 4.8 The large oscillations associated with the DOA flexural mode were observed in the brain when the max and min principal strains oscillated in unison. Oscillation peaks in the pressure response were observed when max and min principal strain were both in peak tension. ....	75
Figure 4.9 The ICP response was similar to the transient min principal strain response. The pressurization associated with the QSC mode was related to the max principal strain response. (Pig subject 5, 69 kPa Incident).....	76

Figure 4.10 An increase in ICP may result from axial compression of the long axis of the bone. The compression will cause the surface of the bone to symmetrically bow out, raising ICP .....	78
Figure 4.11 It is hypothesized that reflecting phenomena on the surface of the occipital bone can cause changes to the ICP response within the brain. ....	79
Figure 4.12 ICP comparison of two front facing pigs. The responses are similar to the open and closed sphere results described by Mediavilla Varas et al. (2011). ....	81
Figure 4.13 A comparison of ICP between a 7mm sphere with a closed or open hole. Figure is taken from Mediavilla Varas et al. 2011. Physics of IED blast shock tube simulations for mTBI research. Frontiers in Neurology 2, 1-14. ....	81
Figure 4.14 The blast tube used for the PREVENT studies (Bauman et al. 2009). ....	83
Figure 4.15 A graphic of the acrylic block that was mounted to the skull surface of the specimen. The sensors were placed one centimeter below the dura. ....	84
Figure 4.16 A graphic of the aluminum box where each fiber optic sensor connected and then was fed out of the protected compartment to the data acquisition system. ....	86
Figure 4.17 The pig was supported in a canvas sling within the test section. The graphic is facing the explosive end of the tube and the pencil probe can be observed above the support shaft. ....	86
Figure 4.18 The ICP and pressure response in the thoracic aorta for pig 032608. Multiple shock reflections were observed in the pencil response. ....	90
Figure 4.19 The ICP response for pig 030308. ....	90
Figure 4.20 The pressure response for pig 031708. The inferior vena cava was pressurized at a later time, and the rise time of the pressurization was longer than for the ICP responses. ....	91
Figure 4.21 The ICP response for pig 040308. The rise time of the jugular was similar to the ICP responses. The thoracic aorta was pressurized at a later point with an associated longer rise time. ....	91
Figure 4.22 The ICP response for pig 040108. These pressure traces showed a rise in pressure, a decline, and a secondary rise that then decayed. ....	92
Figure 4.23 ICP responses for PREVENT pig 0404108 (3 month old, 175 kPa incident shock wave) and WSU pigs 4 and 5 (> 7 months, 69 kPa incident shock wave). The responses were separated to observe that multiple	

modes of skull flexure may cause the formation of the ICP response in the pig.....	94
Figure 4.24 The filtered ICP signal for the PREVENT pig subject shows an initial oscillation of approximately 1000 Hz. Similar responses to the WSU pigs were observed. This frequency band appears to be dominated by skull flexure as was shown for the WSU pigs prior. ....	95
Figure 5.1 The human is a species that has evolved such that the brain mass per body mass is considerably greater than any other recent ancestor, average mammal, or primate (Schoenemann 2006). ....	99
Figure 5.2 A three dimensional CT reconstruction of the human skull. ....	100
Figure 5.3 Summary of the variance in thickness of bone composing the human skull (Moreira-Gonzalez 1963). Units are in mm.....	100
Figure 5.4 A graphic of the quick disconnect valves attached to the major vasculature centers of the brain.....	103
Figure 5.5 Mounting for the fiber optic pressure sensor. The fiber was adhered to a threaded insert that was then threaded into the skull. ....	103
Figure 5.6 The fiber optic pressure sensor was mounted to the skull, surgical screws were threaded into the bone and bone cement was applied to the surface to prevent sensor pull out.....	104
Figure 5.7 A graphic demonstrating the placement of strain gages on the cadaver skull. Tissue was removed so that the sensor could be bonded to the bone surface. To prevent sensor whip, an incision was made in the tissue to run the wires away from the head without creating additional strain on the sensor / wire interface. ....	105
Figure 5.8 A graphic of the cadaver head hanging inverted in the expansion region of the shock tube. ....	107
Figure 5.9 The strain results for each location during a single front facing exposure. The frequency of oscillation was dependent on the bone being measured.....	108
Figure 5.10 The strain response of the temporal bone for cadaver 5 (fresh cadaver 4) was dependent on the orientation of the head relative to the incident shock wave. With the head facing forward the bone went into tension prior to compression. When the bone was directly exposed to the reflected pressure it directly went into compression. ....	109
Figure 5.11 When filtered at a 360 Hz – 8 kHz band pass filter, the temporal bone will have a more defined series of oscillations when exposed to a left side	

exposure. The negative time is relative to the point in which the trigger was activated for these strain channels.....	111
Figure 5.12 The strain response of the parietal bone for cadaver 4 (fresh cadaver 3) approximated the loading conditions of the external static pressure response. When the side of the head was exposed to the incident shock wave, a tension would develop prior to compression. ....	112
Figure 5.13 The strain response of the occipital bone for cadaver 2 (fresh cadaver 1). When the sensor was facing the incident shock it would directly measure compression. ....	112
Figure 5.14 The max principal strain response for the frontal bone of cadaver 5 (fresh cadaver 4) was one of the few cases where the strain channels were considered appropriate for calculations of principal strain. ....	113
Figure 5.15 When measuring the ICP response of the cadaver head, the ventricle sensor had a similar response to the frontal sensor whereas the parietal sensor had a similar response to the occipital sensor for a front facing shock wave exposure. ....	115
Figure 5.16 The initial pressure responses measured by the frontal ICP sensor increase with increasing incident shock wave intensity in the face forward orientation. As the magnitude of the incident shock wave increased, the shock wave would interact with the head at an earlier time due to its higher Mach number. These ICPs were greater than the incident pressure. ....	116
Figure 5.17 The ICP profiles in the cadaver head are dependent on the orientation in which the head was subjected to the incoming incident shock wave. The sensor nearest to the reflected pressure (either occipital or frontal) initially measures a compressive pressure whereas the sensor furthest from the reflected pressure measures a tensile pressure. ....	117
Figure 5.18 The pressure response of the frontal bone was separated into three different phases. (1) A positive or negative pressurization dependent on orientation. (2) A high frequency component and (3) a low frequency component.....	118
Figure 5.19 The principal strain responses for the frontal bone is similar to the ICP response measured by the frontal pressure sensor.....	122
Figure 5.20 Comparison of ICP near the frontal bone. Cadavers were exposed to either a face forward shock wave or blunt impact to the forehead. The blunt impact pressures are reported from Nahum et al. (1977) (Experiments 48 and 49). Each blunt impact trace consists of 8 pts. ....	128

Figure 5.21 The coup pressure response of a cadaver where the occipital bone was impacted or the back of the head was exposed to the incident shock wave. The blunt impact responses were reported from Hardy et al. (2007). Eight points were used to plot the blunt impact ICP responses.....	128
Figure 5.22 A tensile pressure field develops in front of an advancing compression wave in a thin walled fluid filled cylinder. This negative pressure region will focus on the opposite side of the incident load. Which results from and outbending of the shell. (Figure is reproduced with permission from Iakovlev (2006). External shock loading on a submerged fluid-filled cylindrical shell: Fluid-Structure interaction effects, J. Fluids and Structures 22, 997-1028).....	130
Figure 5.23 The formation of the tensile pressure is greater against the interior skull surface and is greatest at the point opposite of impact. ICPs were measured using a fluid filled cadaver skull with either a rigid or elastic cap covering the foramen magnum. (Photo reproduced from Thomas et al. 1966. Experimental intracranial pressure gradients in the human skull. J. Neurol. Neurosurg. Psychiat. 29. 404.....	132
Figure 5.24 The frequency response of the cadaver head during a frontal impact is dependent on the rise time of the initial event. As the rise time of the impact decreases, higher frequency content will be present. (Graphic taken from Gurjidan et al. 1970. Studies on mechanical impedance of the human skull: Preliminary report. J Biomech. 3; 239-247 .....	134
Figure 6.1 A side by side comparison of the different species that were tested in this project. ....	139
Figure 6.2 The strain response for each of the species tested at the low pressure intensity. ....	142
Figure 6.3 The ICP response for each species when exposed to a low intensity shock wave.....	143
Figure 6.4 Isolated ICP pressure profiles for each species during a front facing exposure so that frequency content was observable.....	144
Figure 6.5 Band pass filtering was applied to allow better observe the DOA waveform. When this filtering is applied, the DOA response in the rat became much more evident. ....	144
Figure 6.6 The ICP responses for the pig and cadaver when subjected to a shock wave during a face forward exposure.....	146
Figure 6.7 The ICP responses of the cadaver and pig when subjected to a side facing exposure. ....	146

Figure 6.8 The ICP responses of the cadaver and pig when subjected to a back facing exposure.....147

## CHAPTER 1 INTRODUCTION

### 1.1 Statement of the Problem

In 1585, Antwerp, Belgium, 7 tons of gunpowder was detonated to destroy a bridge on the River Schelt, reportedly killing 1,000 soldiers, among whom “. . . some dropped dead without any wounds, sheerly from concussion”, this was probably the first known description of primary blast injury (Frykberg 2002). Since the discovery of black powder over 2000 years ago, explosives have been used as weapons. Evidence for this statement includes; the terrorist actions in Ireland in the 70's and 80's (Mellor and Cooper 1989), the constant conflicts in the Middle East (Katz et al. 1989), the train bombings in Madrid (Turegano-Fuentes et al. 2008), and the current conflicts in Iraq and Afghanistan (Bird and Fairweather 2007). The victims of these bombings include both military and civilian populations. It has been shown that, in the current conflicts, 78% of injuries among the US military have been explosive related. This includes a significantly greater occurrence of head injuries when compared to previous conflicts (Owens et al. 2008).

As protective equipment and more efficient medical evacuation and higher-tech medical care become more technologically advanced, a greater number of soldiers exposed to explosions survive. These increasing survival rates further the need to investigate the complicated nature of blast related brain injury. The rationale for this statement includes reports of increased occurrences of mild traumatic brain injury (mTBI) among soldiers that are strongly associated with Post Traumatic Stress Disorder (PTSD) and physical health problems 3 to 4 months post deployment (Hoge et al.

2008). It was also reported that veterans with impairments from blast exposure were more likely to have severe headaches, severe pain, and impaired sleep with nightmares (Ruff et al. 2008). Unfortunately, the best methods for treating blast related mTBI are not known, and further complications arise because the exact biomechanical mechanisms of cellular neuropathology in the brain are unknown.

## **1.2 Background and Significance**

Multiple models are used in the study of traumatic brain injury (TBI). Physical models are used to understand mechanical responses of simplified systems that can be extrapolated to understand the biomechanical responses of more complex biological systems. Theoretical models involve the use of mathematics to predict biomechanical responses under given input conditions; such as force, acceleration, or pressure. Multiple biological models are used in TBI research. Cadavers are used to measure biomechanical responses and determine material thresholds. The purpose for the use of animals in TBI research is to replicate certain pathological components or phases of clinical trauma, aiming to address pathology and/or treatment (Lighthall and Anderson 1994). Additionally, the use of biological models can also include the measurement of in vitro cellular biochemical changes to a given stimulus. Mild traumatic brain injuries (mTBI) are even more difficult to diagnose as the resulting pathology is much harder to detect (Van Boven et al. 2009). This is especially true for blast related neurotrauma as the mechanisms of primary blast injury are still under debate (Courtney and Courtney 2009).

Injuries from an explosion can result in considerable polytrauma to the person that is exposed to the event (Sayer et al. 2008). A primary blast injury (PBI) involves

injuries incurred from immediate effects of shock wave interaction. Secondary blast injury is defined as the trauma caused by projectiles, shrapnel, and ejecta. Tertiary blast injury is defined as acceleration based damages that result from impacting a surface. Quadrinary blast injury is defined as the result of chemical exposure and other trauma incurred at the event (Sayer et al. 2008). Finally, quinary blast injury is defined as post-exposure effects that do not have a defined time in which the delayed effects occur; this injury type can include hyper-inflammatory behavior (Kluger et al. 2007).

The mechanics of blast wave interaction (primary blast injury) with different biological tissues are of interest given the levels of strain and shear that are produced (Cooper and Taylor 1989). When a pressure wave propagates through a given medium, the greatest pressures result at the interface. This effect is maximized if there is a large impedance differential between the two media (Alley et al. 2010). When a pressure wave is propagating in a tissue and arrives at a cellular lining, the lining may experience extreme tensile stress that can lead to trauma. This phenomenon is called “spalling” and is of concern for air-backed tissues such as the aveoli in the lungs and the inner layers of the intestines (Ho 2002). These types of injuries, historically in the air-backed organs, have led to the largest number of casualties associated with PBI (Phillips 1986).

When a shock wave in air interacts with the head, the impedance mismatch between the two materials is great. The shock wave in the less dense medium (air) will partially reflect against the denser medium (skull) but can also deform the structure (Ho 2002). Magnified pressures can develop on surfaces directly facing the incident blast wave (Chafi et al. 2010). It has been hypothesized, aided by computer models, that these magnified pressures can cause deformations of the skull and as a result pressure

gradients will form within the brain (Moss et al. 2008; Chafi et al. 2010), although these models have not been validated with experimental results.

### **1.3 Hypotheses of PBI Mechanism**

There are multiple hypotheses regarding the manner in which blast wave interaction with the body results in neurotrauma. Currently, there are four hypotheses regarding how this phenomenon occurs (Courtney and Courtney 2010): thoracic mediated, acceleration based, and direct interaction of the shock wave with the head, by either direct wave transmission or skull flexure.

Multiple researchers have proposed that brain injuries from PBI are the result of a thoracic mechanism (Cernak et al. 1996; Cernak et al. 2001; Courtney and Courtney 2009; Courtney and Courtney 2010), although, this hypothesis has been suggested as early as 1916 (Mott 1916). These groups have suggested that shock wave interaction with the thorax will cause a pressure surge that will propagate through the vasculature and damage the more sensitive vessels in the brain. Researchers investigated whether isolation of the blast to the chest only, when compared to the entire body, would yield different results. Their conclusions were that whole body and local chest shock wave exposure cause ultrastructural changes of the neurons in the hippocampus and biochemical alterations, along with cognitive deficits in the rat (Cernak et al. 2001).

It was shown that by removing the vagus nerve of rabbits that detrimental physiological effects such as vasoconstriction and bradycardia were lessened during shock wave exposure (Cernak et al. 1996). The pulmonary C fibers imbedded in the lung tissue converge to the vagus cranial nerve. It was hypothesized that deafferentation of these fibers prevent vasoconstriction, bradycardia, and other

autonomic compensatory physiological mechanisms that may lead to pathological responses in the brain due to inability to maintain proper PH balance and cellular metabolism. The possibility of these physiological changes causing pathological responses in the brain are more plausible than a pressure surge that will propagate in the brain, due to time it would take for fluid to be compressed and translated into the intracranial contents. Additionally, it needs to be mentioned that these animals were tested outside of the shock tube and because of which were subject to post shock wave gas dynamic effects not representative of a free field blast wave, which will cause testing artifacts that may cause an exaggerated pathological response.

The second hypothesis of injury caused from PBI is that there is a combination of rotational and translational accelerations of the head that are being invoked by the primary blast wave (Courtney and Courtney 2010). It has been reported that the combination of linear and rotational acceleration of the head invoke high strain rates on the neurons in the brain (Zhang et al. 2006) although this has only been shown for impact and has not been proven for blast wave exposure. It was hypothesized that a rapid acceleration results from the shock wave interacting with the soldier's personal protective gear (Finkel 2006). This has not been shown experimentally under true blast wave exposure conditions.

The response of a head to a blast wave is distinct because the rise time of the pressure wave is much shorter and loading is diffuse when compared to traditional blunt impact conditions. In recent experiments, it was determined that global motion of a crash test surrogate head does not become observable until 2 ms following exposure to a shock wave within a shock tube. Low levels of acceleration were reported for a 120

kPa incident shock wave (Progress report: DOD Award W81XWH-09-1-0498). Another research team also reported that global motion following shock wave exposure did not take place for a sphere supported outside of a blast tube until 3-4 ms following the initial shock wave interaction for a series of exposures ranging 110 – 455 kPa (Alley et al. 2010). Unfortunately, by testing outside of the blast tube, gas dynamic events not associated with a blast wave exposure interact with the test specimen. This includes high flow velocities that can cause external translation of the test specimen. Therefore the sphere may not have even translated to the degree that it had if it were subjected to a free-field shock wave. These results suggest that global acceleration may not be the primary injury mechanism during blast wave exposure. While it is expected that damage will result from global translation and rotation, the injury patterns associated with this mode of damage are better classified under tertiary injury.

A third hypothesis discussed by Courtney and Courtney (2010) is by transmission of the blast energy directly to the cranium. However, the physics of direct pressure wave transmission should be distinguished from pressure gradients formed in the brain caused by skull flexure. Direct wave transmission (trans-osteal wave propagation) concerns the processes by which an air-borne shock wave interacts with the material interface of the skull and transmits a 'through-thickness' stress by direction compression of the skull material. This will result in lower amplitudes and higher frequencies than what would be associated with skull flexure. The development of the reflected pressure on the skull surface can be high enough to cause deformation which will form new pressure gradients within the intracranial contents. Finite element models (FEM) have predicted responses that could be associated with this phenomenon, but

have yet to validate the results against experimental data (Moss et al. 2008; Taylor and Ford 2009; Chafi et al. 2010).

Courtney and Courtney (2011) reference the work of Chavko et al. (2007) which reports that ICP records within the cranium closely follow the external static pressure condition. However, Leonardi et al. (2011) compared records from unsealed and completely sealed intracranial pressure (ICP) sensors from rats exposed to a shock wave which indicated that the conclusions by Chavko et al. (2007) may have been an artifact of an unsealed ICP gage. The study by Leonardi et al (2011) indicated that by creating a fully sealed testing environment, mimicking the actual physiological environment, peak ICP profiles exceeding the external static pressure environment could be developed. The unsealed environment produced similar recordings to those of the external pressure measurements since the enhanced fluid pressurization was able to be relieved through the leaking seal. They also noted distinct oscillations in ICP taking place in the signal following the initial pressure rise, the amplitude and frequency of the imparted ICP was likely linked to skull dynamics.

An oscillatory response has been observed following an initial rise in ICP during shock wave exposure (Clemenson and Criborn 1955; Romba and Martin 1961). In order to determine the source of ICP oscillations, Romba and Martin (1961) investigated the effect of shielding the thorax of a monkey while subjecting the head to blast wave exposure. Their results indicated that oscillations in ICP occurred regardless of the presence of thorax protection. The Romba and Martin (1961) study investigated this phenomenon by placing pressure sensors in a euthanized primate brain and reported the intracranial pressure profiles. They found distinct pressure waveforms in the brain

that did not mirror the ambient pressure profile (Figure 1.1). Additionally, they found that if the thorax was protected and the head was not, these pressure pulses were observed. If the head was protected from the shock wave and the thorax was not, no distinct pressure profiles were observed in the brain.

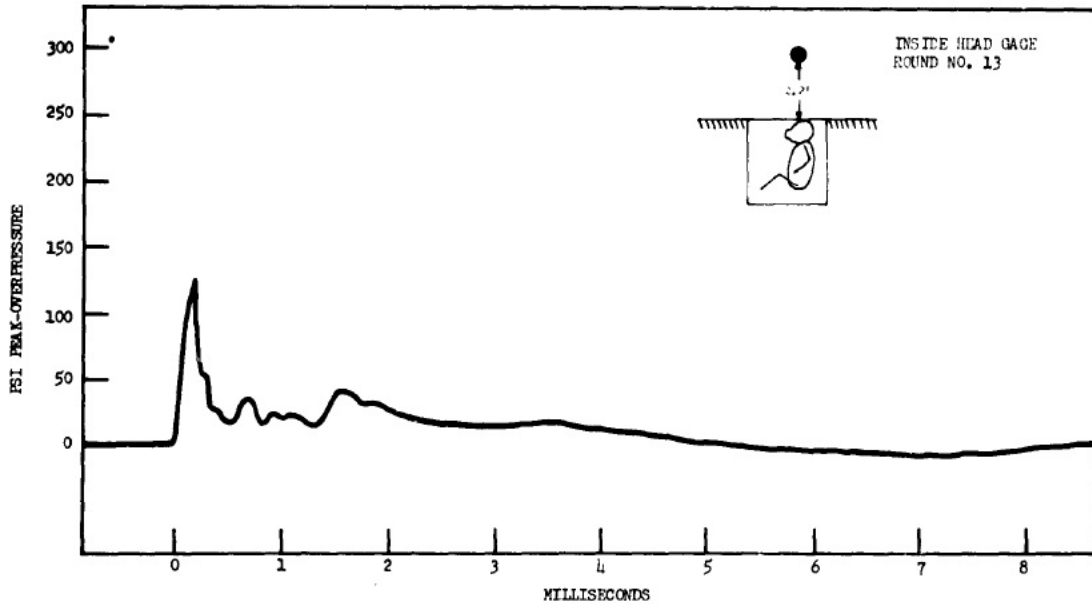


**Figure 1.1 Intracranial pressure response of a monkey head exposed to a shock wave. This event took place despite thorax protection (Romba and Martin 1961).**

Sophisticated FEM models have been developed to investigate the response of the head to blast wave exposure, although current limitations are related to properly defining the material characteristics of biological tissues and how they interact with each other. Moss et al. (2009) created a simulation of the human head interacting with the shock wave from a blast. The main conclusion from this work is that the blast wave will cause the skull to dynamically flex inwards; this will then create a ripple effect on the skull surface that will propagate outwards (Figure 1.2). This rippling will then result in variable pressure regions that produce pressure gradients in the brain (Moss et al.

2008). It was also reported that the deflections caused by the shock front will lead to magnified levels of pressure within the brain, potentially leading to significant neurotrauma. This model has not been experimentally tested and remains hypothetical.

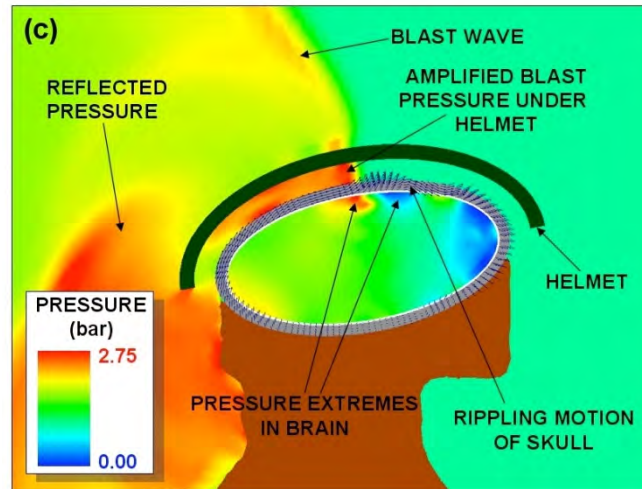


**Figure 1.2 FEM output of shock wave causing deformation to the skull, causing pressure gradients in the brain (Moss et al. 2008).**

Results from other FEM models have suggested that intracranial pressure oscillations exist during shock wave exposure (Moore et al. 2009). The authors have reported that these pressure profiles can be caused by flexural waves of the skull. Additionally they reported that due to the geometry of the brain, the pressure profiles that occur within it will be location specific (Moore et al. 2009).

The mechanical responses of the simplified physical models have also been theoretically calculated. Spherical shells, with and without apertures, and with two different gelatin cores of varying mechanical properties (viscosity, density, modulus, and Poisson's ratio) were used to determine the effects of impedance mismatch on the resulting pressure within the gelatin core (Alley et al. 2010). Their results indicated that there were noticeable pressure oscillations within the gelatin and those regions of

varying compression and tension could possibly lead to neurotrauma in an organism. Based on the presented studies, the loading resulting from shock wave interaction with the head may be able to cause the formation of intracranial pressure gradients within the brain, by means of shell deformation.

#### **1.4 Investigating biomechanical responses of different biological models in blast injury research**

The response of the head to blast wave loading is dependent on the mechanical properties of the the skull and brain. Therefore it is expected that physical differences between animals and humans will yield different responses during shock wave interaction. This is of concern given that different animal models are utilized in blast testing. Previous research has utilized mice, rat, rabbit, and pig models (Clemenson 1957; Clemenson and Nelson 1957; Cernak et al. 1996; Cernak et al. 1996; Bauman et al. 1997; Saljo et al. 2000; Cernak et al. 2001; Cernak et al. 2004; Cernak 2005; Chavko et al. 2007; Saljo et al. 2008; Bauman et al. 2009; Saljo et al. 2009; Bolander et al. 2011; Leonardi et al. 2011; Mao et al. 2011; VandeVord et al. 2011). Without a biomechanical analysis of the physical systems being tested, there cannot be a proper identification of how to mitigate and protect against the mechanisms that may be causing the resulting neuropathology from PBI.

To address the issue of the variability among biological models, it was proposed that three be assessed under similar conditions to quantify the differences among each. A small (rat) and large (pig) animal, and human analog (cadaver), all underwent a similar series of experiments to measure and compare their biomechanical responses. Each of these models has their own distinct advantages and disadvantages. Therefore,

it is important to understand the biomechanical responses of each in order to provide data that can be of use to mitigate the pathological effects associated with PBI in the warfighter (Figure 1.3).

## Models of Primary Blast Injury Research

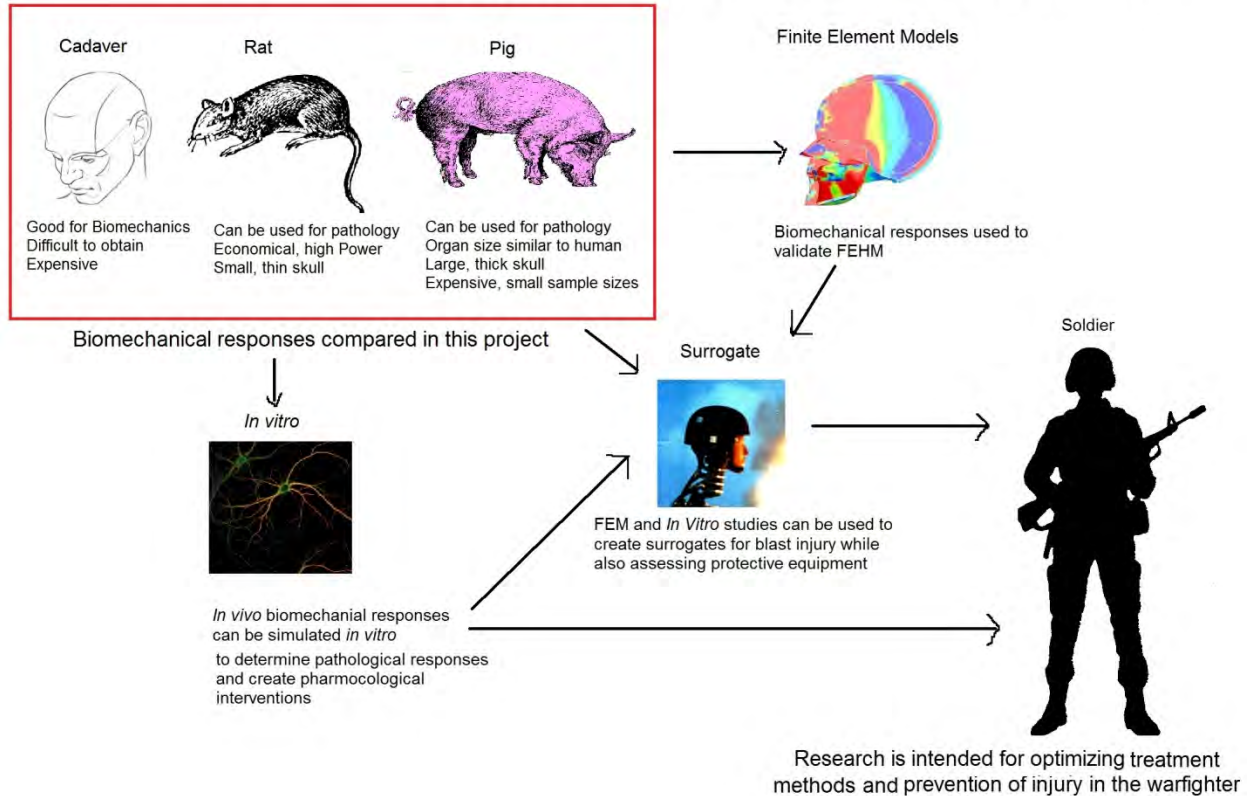


**Figure 1.3** The biomechanical responses observed in this study can ultimately lead to the mitigation of deleterious effects of PBI in the warfighter.

### 1.5 Specific Aims and Hypotheses

The purpose of this research was to evaluate the hypothesis of multi-modal skull flexure. In the previous discussion it was suggested that skull deformation, caused by shock wave interaction, is the most likely candidate for describing the formation of pressure responses in the brain that could be damaging to the cells composing the

central nervous system. The term 'multi-modal' has been included as it was discussed that the resulting pressure responses within the brain or simplified models may consist of a combination of multiple pressure profiles. It is possible that these pressure profiles are being driven by distinct phenomena or modes taking place in the skull. To evaluate the multi-modal skull flexure hypothesis, it was required to measure the response of the skull to shock wave exposure. This was accomplished by measuring the strain on the skull surface. The environment in which the brain was subjected was measured using pressure sensors. Figure 1.4 has been included to provide a framework for assessing the multi-modal skull flexure hypothesis.

## Evaluating Multi-Modal Flexure Hypothesis

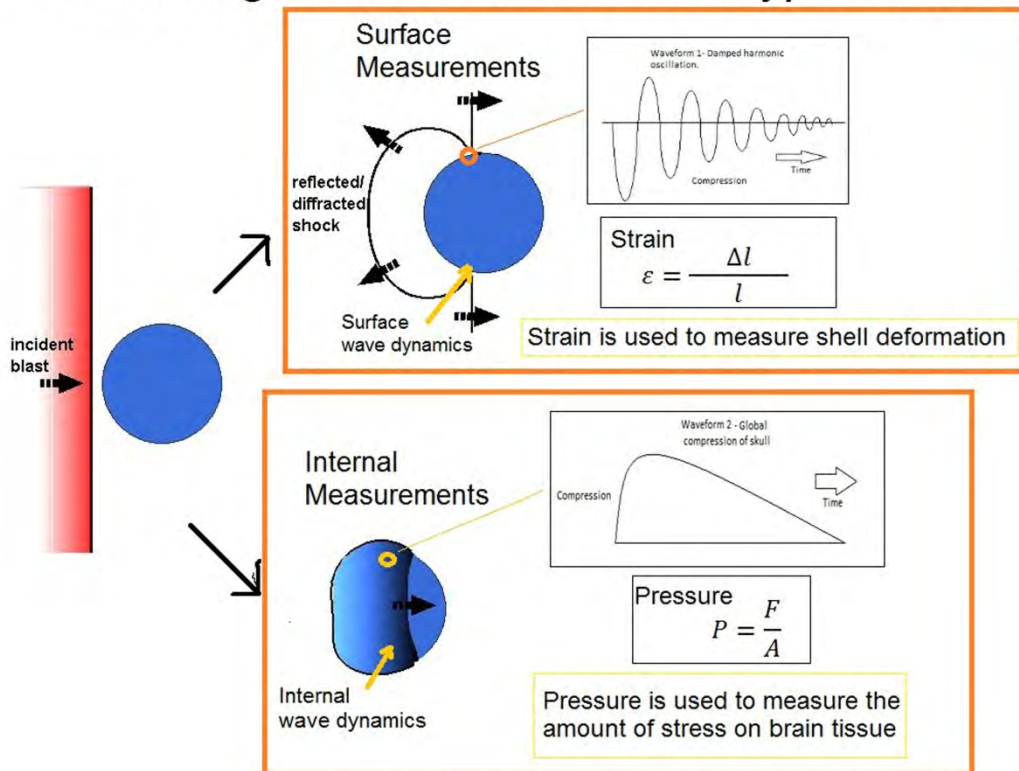


Figure 1.4 The multi-modal skull flexure response was assessed by measuring shell deformation (strain) and stress on brain tissue (pressure).

The specific aims for this research were:

- **Specific Aim 1:** Measure the biomechanical responses of skull strain and intracranial pressure (ICP) in the rat, pig, and cadaver when exposed to a simulated single free field shock wave.
- **Specific Aim 2:** Compare biomechanical responses occurring across species to identify what similarities and differences exist between species.

Based on these specific aims two hypotheses were able to be formed and a diagram of these hypotheses was provided in Figure 1.5:

- **Hypothesis 1:** Shock wave exposure will excite multiple modes of response of the skull and due to the coupling at the skull/brain interface, pressure gradients will be propagated into the intracranial contents.
- **Hypothesis 2:** Physical differences between species (such as thickness of the bones and geometry of the skull) will significantly affect the skull/brain biomechanical responses.

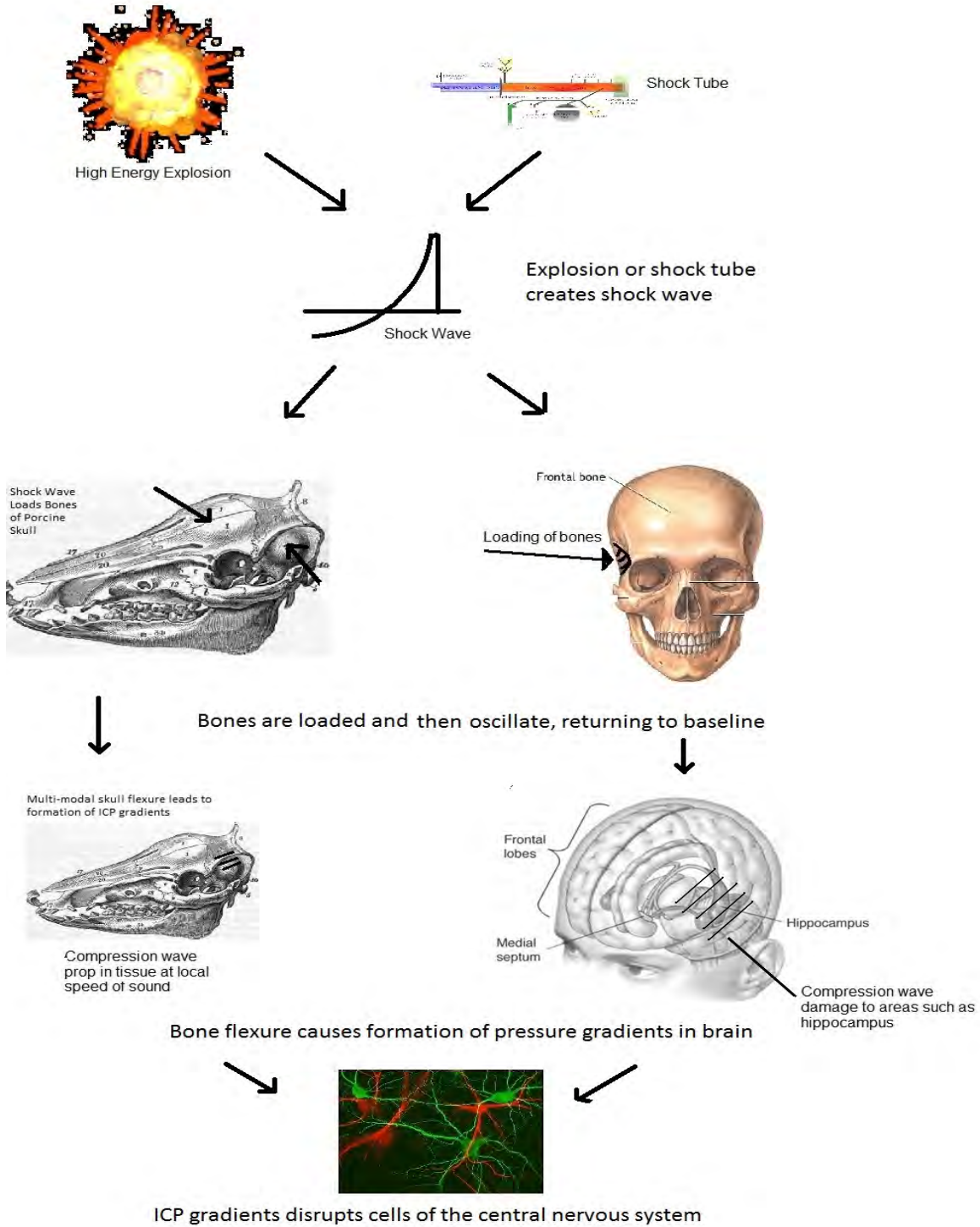


Figure 1.5 The hypothesis of the project was that the skull is deformed by the shock wave, the resulting response will cause the formation of pressure gradients in the brain that may be damaging to the cells composing the central nervous system.

## CHAPTER 2 SHOCK WAVES AND SIMPLIFIED PHYSICAL MODELS

### 2.1 Blast waves in air

When an explosion occurs near a person, they may be subjected to fragmentation, ejecta (accelerated sediment and other materials), and a blast wave, all can be devastating to the body. The injury mechanisms and patterns associated with projectiles and ejecta will not be discussed in this dissertation as the focus is on injuries associated with the blast wave exclusively (primary blast injury). Blast waves can be generated by chemical, physical, thermal, and nuclear sources. Blast waves formed by chemical explosion will be discussed in this section.

Assuming a spherical charge in an open field, when detonation occurs there is a rapid expansion of gas and fireball that result as products of the chemical reaction. The leading edge of the expanding gas/fireball is called a contact surface. A blast wave is driven by the expanding contact surface, which is a result of an exchange in momentum between the contact surface and the ambient air. Following the point of peak expansion of detonation products, the blast wave will then propagate in air Figure 2.1 (Ritzel et al. 2011).

The blast wave will expand with time and distance and decay into a sound wave (Kinney 1962). Outside of the fireball of the explosion, the blast wave consists of a leading edge shock front, a positive pressure pulse, a rarefaction (expansion phase), and a return to baseline pressures. This waveform is called the Friedlander waveform and is representative of what is observed when the blast wave is not reflecting against surfaces and outside of the fireball (Figure 2.2) (Kinney 1962).

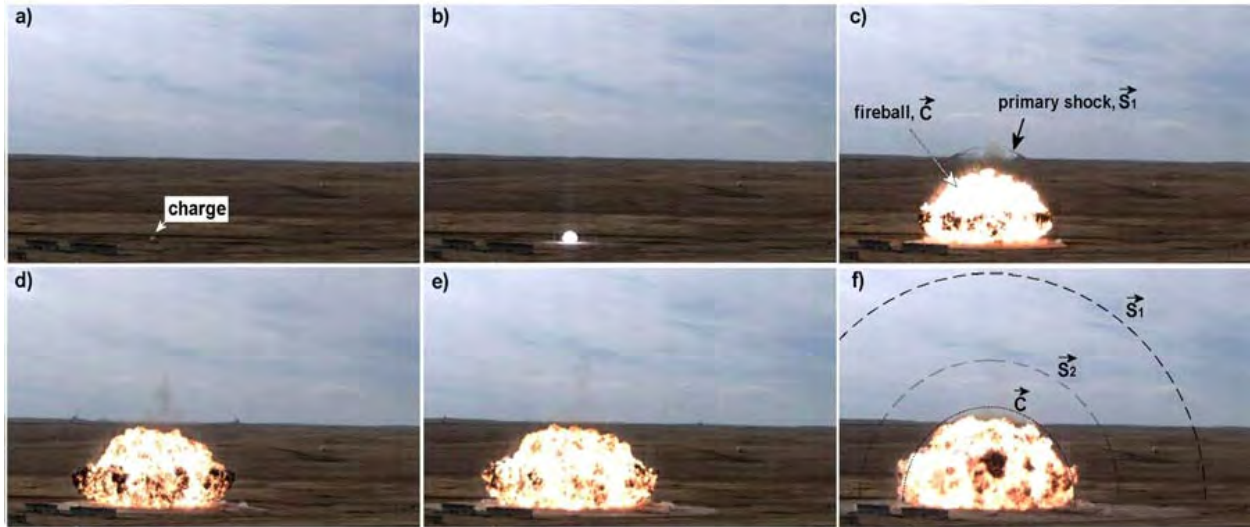


**Figure 2.1 :** During detonation of an explosive charge (a) and (b) the rapid expansion of detonation products will create a contact surface, labeled as C, that will transfer its momentum to the ambient air as a blast wave (c). The blast wave will then propagate (d) (e) and (f). Figure taken from Ritzel et al. (2011).

Blast waves are described by several characteristics, examples include: peak pressure, positive duration, impulse, and rise time. Peak pressure is associated with the amplitude of the wave. The positive duration is the time from the initial pressure spike to the first crossing past zero overpressure. Impulse is measured as the integral of pressure and time. Rise time is the time in which the shock wave will rise from ambient to peak pressure (Command 1986). The rise time of the shock wave is exceedingly short, on the order of one microsecond.

As the blast wave propagates it will change properties associated with the air. These properties include pressure, density, temperature, and flow velocity. General relationships between these properties are classified by distance away from the detonation source. Three regimes have been defined to describe these relationships.

The near-field regime is the region within the maximum extent of the fireball. It is within this regime that the properties are most variable (Figure 2.3 A). The mid-field regime is a region beyond the near-field but still has non-uniform wave dynamics. The far-field regime is where the wave dynamics have equilibrated to a quasi-spherical decay (Figure 2.3 B).

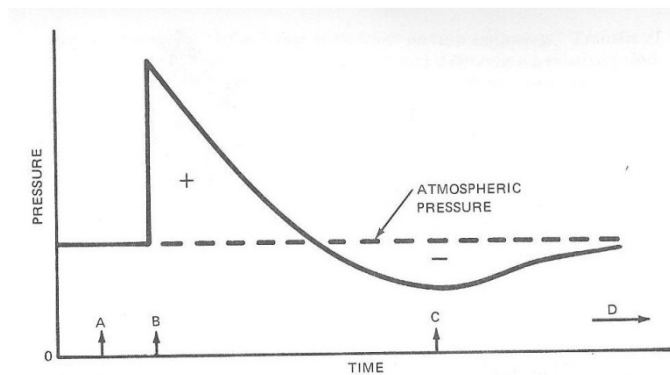


Figure 2.2 Diagram of a Friedlander waveform (Kinney, 1962).

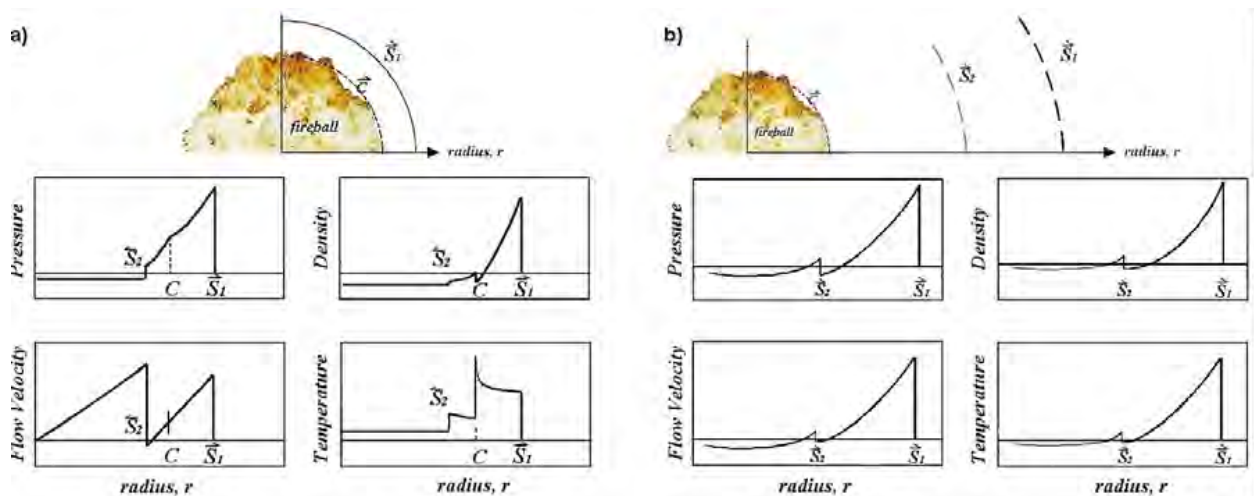
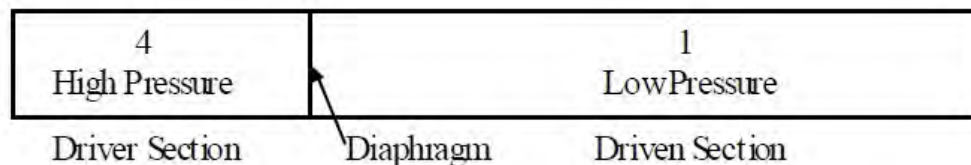


Figure 2.3 Properties associated with air will change when a blast wave propagates through and are dependent on the distance of the blast wave relative to the fireball. The responses associated with pressure, density, flow velocity, and temperature are more variable in the near-field regime (a) than in the far-field regime (b). Figure taken from Ritzel et al. (2011).

## 2.2 Shock tubes

Blast waves are a type of shock wave. One way to simulate blast waves within a laboratory environment is through the use of shock tubes (Bowman 1966). Different methods can be undertaken to create simulated blast waves within a shock tube, for example; detonation of charges, the ignition of fuel/air mixtures, or by rupture of a membrane in a compressed gas driver. The shock tube at Wayne State University (WSU) was designed for the purpose of simulating mid to far-field blast wave conditions using a compressed gas driver. For this reason, this method for creating shock waves within a shock tube will be discussed.

The WSU shock tube was designed to create shock fronts by the rapid expansion of gas from a “high” pressure region to a “low” pressure region. The shock tube consists of two regions separated by a frangible membrane (Figure 2.4). The “high” pressure region is called the driver section. The “low” pressure region is called the driven section. Generally, the driven section is annotated as region 1 and the driver section is notated as region 4 (McMilian 2004).



**Figure 2.4 Shock tube diagram prior to diaphragm rupture (McMilian 2004).**

At initial conditions, the pressure in region 4 is greater than region 1. The driver section is filled with gas until the frangible membrane ruptures. The expansion of the high pressure gas causes a contact surface to form between the driver and driven

gases (regions 2 and 3) (Figure 2.5). It is the expansion of the gas that drives the formation of a shock wave. The shock wave will propagate into the low pressure ambient gas region ahead of the contact surface. A region of “shocked” gas exists between the shock wave and the contact surface (2), which is associated with greater temperatures and pressures than the ambient driven gas as a result of interaction with the shock front (Figure 2.6). When the shock wave reaches the open end of the tube, part of the wave will reflect, creating a rarefaction (expansion) wave that will then propagate upstream. A separate rarefaction wave will propagate into the driver section during membrane rupture, reducing pressure.

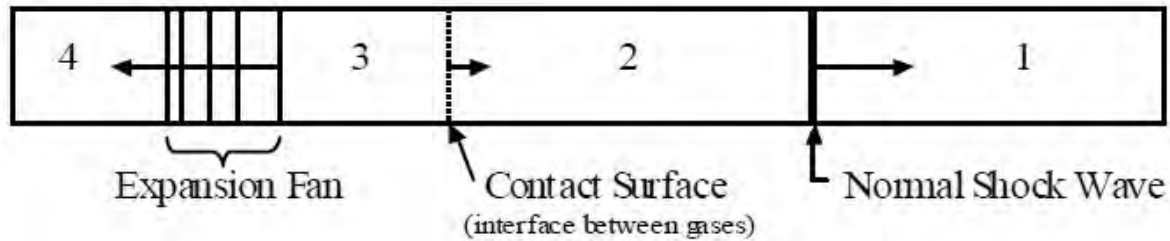


**Figure 2.5 Definition of regions within the shock tube following rupture of the membrane (McMilian 2004)**

The position – time ( $x-t$ ) diagram is used to describe how the interactions associated with each region progress (Figure 2.7). As the shock wave propagates, it will separate from the contact surface. The rarefaction wave in the driver will propagate towards the end of the driver section, reflect and propagate in the driven gas direction (Lamanna 1996).

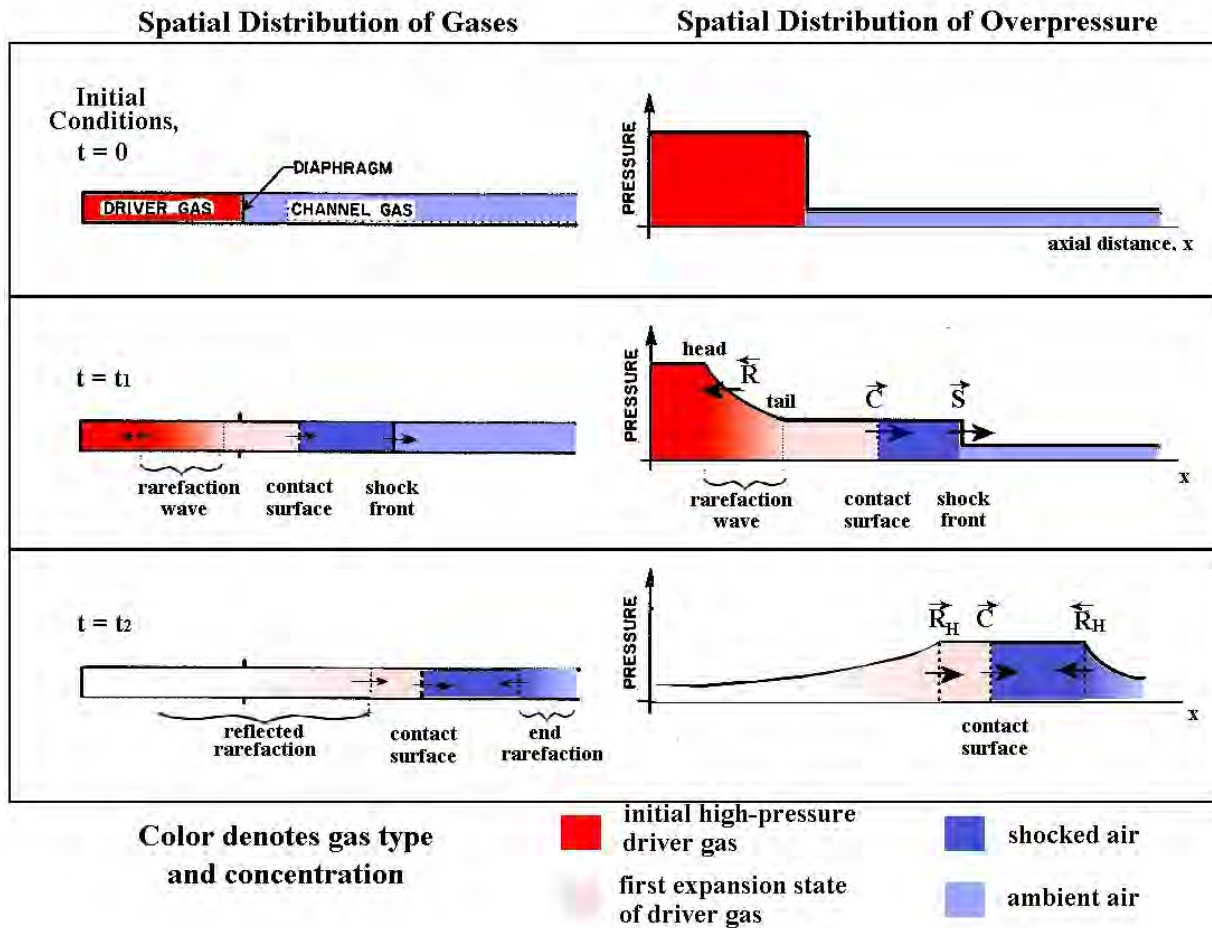


Figure 2.6 Shock tube diagram and corresponding pressure profiles for each distinct region following membrane rupture (Ritzel et al. (2011)).

A shock wave generated within a shock tube is not the same as a blast wave generated in a free-field explosion. The pressure environment within the tube is variable due to the interaction between the various wave phenomena described prior. To approximate loading conditions associated with a free-field blast wave, a test specimen has to be placed at a specific location in the tube where the various waves interact to create a similar profile to a blast wave. The major components associated with the loading profile are the shock wave, contact surface, rarefaction from the driver, rarefaction from the open end of the tube, and the upstream shock wave (Ritzel et al.

2011). A graphic of ideal manner in which these different waves interact is provided in Figure 2.8.

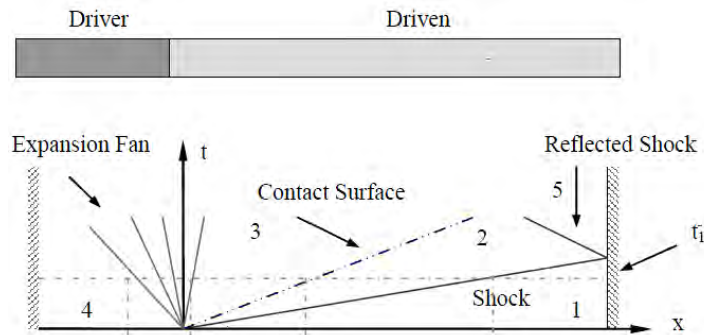


Figure 2.7 An X-t diagram of a close ended shock tube (Lamanna 1996).

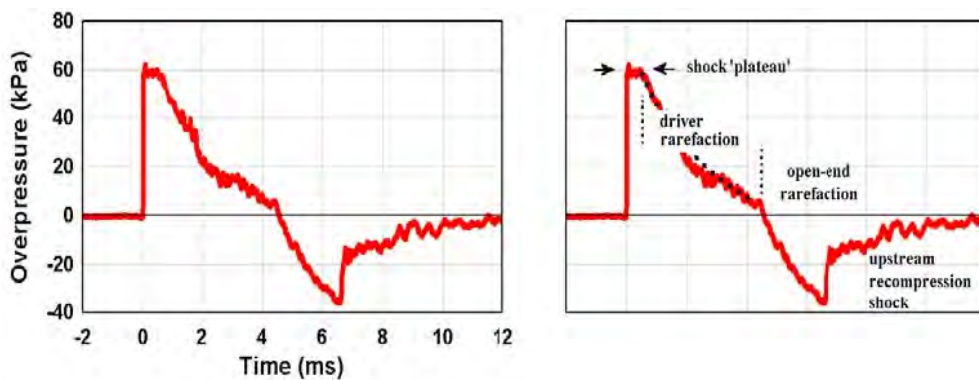


Figure 2.8 Multiple wave interactions occur within the shock tube in order to create a representative free-field blast wave profile (Ritzel et al. (2011)).

Multiple factors need to be taken under consideration when subjecting a specimen to a properly tailored shock wave within a shock tube. During a blast wave exposure, the rarefaction below zero overpressure will result in a suction that will want to pull a specimen towards the detonation center and a may also expose the specimen to a secondary shock of lower magnitude in the same direction as the first. For specimens within the tube both, rarefaction waves will increase the intensity of the flow

velocity. The flow velocity will become further increased at the time the open-end rarefaction arrives at the test section (Ritzel et al. 2011). This will put shear on the specimen in the direction towards the open end of the tube and not the driver. Additionally, the upstream recompression shock wave will first interact with the back side of the specimen. Therefore a specimen will experience shocks to both the front and back sides.

A final note should be made regarding experiments that occur outside of the shock tube. The combination of the emerging shock wave and venting gas cause the formation of a vortex and high flow velocity region called end-jet. Studies that include the testing of specimens outside of the tube subject the specimens to artifacts that are not associated with a blast wave or shock waves created within the shock tube at the test section. These artifacts can create high levels of force on an animal specimen that may create trauma that may not have occurred if tested within the tube. Multiple studies discussed in this dissertation have tested outside of the tube, which requires a higher level skepticism when interpreting the author's conclusions.

### **2.3 Wayne State University shock tube**

The Wayne State University shock tube has a 0.762 m long driver with a 0.304 m diameter. Three sections are bolted together to the driver to create the medium for the shock wave to travel longitudinally. The driven section consists of two 2.440 m metal sections; a clear Lexan tube of 1.2 m length is attached at the end such that high speed video can record an event within the tube. Mylar ® sheets of various thicknesses are secured between the driver and driven tubes. Helium is forced into the driver until the membrane ruptures; the expanding gas drives a shock wave that propagates down the

tube. Helium was selected for the driver gas and air was selected as the driven gas for the WSU shock tube because Helium will cause a shock wave profile that will result in an initial increased amplitude, a steeper decay rate, reduction of the negative pressure phase, and a delay in the upstream shock (Ritzel et al. 2011).

One pressure sensor is placed in the driver; another two pressure sensors are placed 2.4 meters apart in the driven section (Figure 2.9). A fourth pencil pressure sensor is mounted on a platform 1.12 m within the test section. This platform is attached to a long hollow aluminum tube which is attached to an external fixture which can translate to mitigate some of the post-shock wave gas dynamic responses.

To investigate how a small specimen will respond to a shock wave. It is secured to the platform. To test larger specimens, the clear Lexan portion and the second driven section are removed and an expansion section is added. The dimensions of this expansion section are provided in Figure 2.9. Two different test sections are required because the ratio of front facing surface area of the specimen to the cross sectional area of the tube need to be small enough so that the waveform to which the specimen is subjected is approximate of the free-field shock wave.

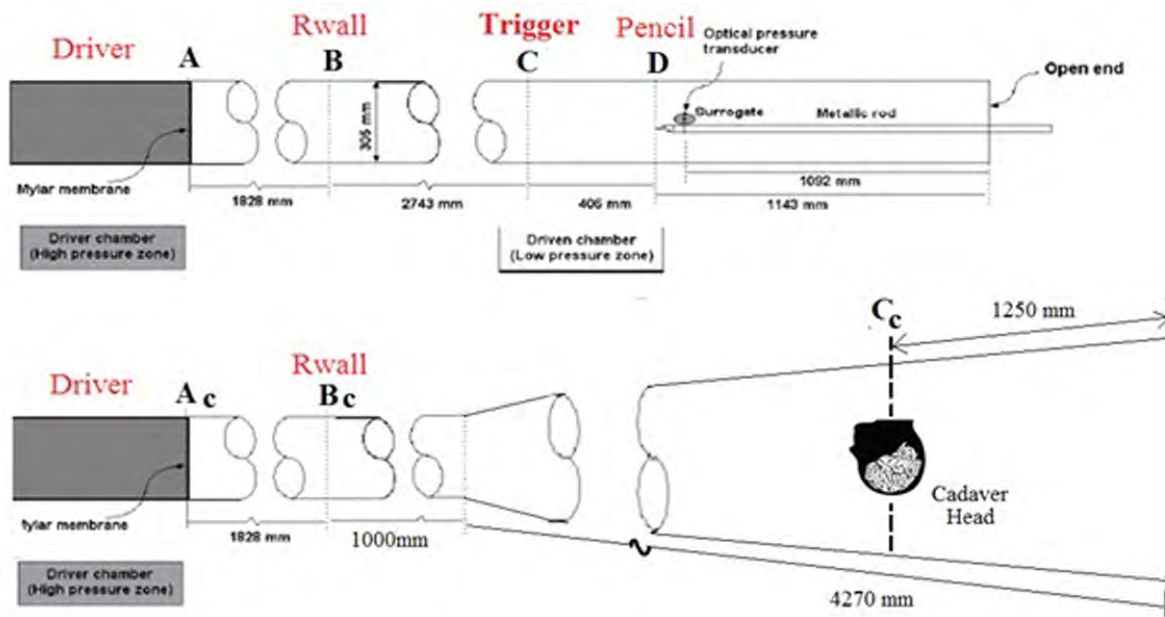


Figure 2.9 Graphic indicating dimensions of the WSU shock tube and placement of sensors (graphic courtesy of Sumit Sharma, Wayne State University).

## 2.4 Modal response of a system

When an object is subjected to a mechanical input, energy from the input can be stored in the object as elastic potential energy. One way in which the object can dissipate this elastic potential energy is through mechanical vibrations. Mechanical vibrations are a series of oscillations about a given point (Halliday et al. 2005). Due to the effects of friction, among other forms of energy loss, a vibrating system will dampen out and return to resting energy state unless the system remains excited through external forcing. In the case of a simplified physical model, such as a sphere, a shock wave will cause an initial deformation (increasing elastic potential energy) which will then oscillate in order to dissipate some of this energy in order to return to its resting state.

The manner in which a system will respond to a given input is dependent on its mechanical properties, primarily mass and stiffness. Stiffness incorporates such factors

as cross sectional area, length, and elastic modulus of the system. These properties will dictate the natural frequency (cycles/second) of the system. The natural frequency of a system is a frequency at which a system will tend to oscillate under excitation (Halliday et al. 2005). Multiple natural frequencies may exist for a given system. The natural frequency will be excited to a greater extent if the period ( $1/\text{frequency}$ ) of the forced excitation and the system are similar.

Modes of response of a system are the patterns of motion in a system where all the parts move sinusoidal and in phase. Modes are classified by the frequency and shape of response. Many modes may exist for a given system and only some may be excited during a given event (Halliday et al. 2005).

## **2.5 Shock wave loading on an object**

Energy from the shock wave is transferred to a given object with which it is interacting at a very fast rate due to its short rise time. The short rise time of the shock front is associated with wide band frequency content ( $\sim 1\text{MHz}$ ). This excitation allows for the possibility of exciting additional modes of responses in an object, when compared to a lower frequency excitation, such as a padded blunt impact.

The shock wave has other properties that will cause a system to respond in a given manner. When a shock wave interacts with an object, the surface normal to the propagating shock wave will experience magnified pressures (reflected pressure). The magnitude of this reflected pressure can exceed over twice the incident pressure (peak pressure of the propagating shock wave). As the shock wave traverses about the object, the wave will diffract across the surface, causing additional loading. The magnitude of this loading on the sides of the object will be similar to the magnitude of

the incident pressure. Although, depending on the angle of interaction, a region of magnified pressure may form, which is called a mach stem (Kinney 1962). Depending on the size of the object, the shock wave may cause large pressure differentials on the object's surfaces.

## **2.6 Experimental modes of response for a cylinder exposed to a shock wave**

The cadaver, pig, and rat vary in geometry, and mechanical properties. To understand of the response of each system to shock wave loading, it is first important to investigate how simplified physical models respond under similar loading conditions. This will allow for insight in identifying the modes of response of the more complex biological models. For this reason, the rat head can be simplified to a cylinder because its skull is long relative to its cross-sectional diameter and the cadaver can be simplified to a sphere due to its rounded curvature.

A relevant study for identifying potential modes of response in the rat involved subjecting a submerged cylinder to a shock wave (Kwon and Fox 1993). In the study, a large aluminum tube was submerged 3.66 meters under water and exposed side-on to a 16.3 MPa shock wave in water. The tube was 1.067 m long, with a 0.305 m diameter, and a 0.006 m wall thickness. The ends of the tube were sealed with 0.025 m plates. Fourteen strain gages were attached to the surface. Following testing the data were filtered at 2kHz. The experiment was also simulated using finite element (FE) methods.

While the test differed considerably from a rat head exposed to a shock wave in air, the modes of response of the tube were of interest. In Figure 2.10 a plot of the strain response of the system was provided. A series of damped oscillations were observed in the strain response. Higher modes may have been observed if the data

were not filtered at 2000 Hz. The FEM results allowed for the visualization of three response modes. Two were directly related to the presented strain response (Kwon and Fox 1993).

The first identified mode was called a whipping mode. This mode was parallel to the direction of shock wave. The center of the cylinder was displaced, oscillated and returned to baseline. The other two modes were called accordion and breathing. These modes resulted from axial compression and release, which caused the system to oscillate and return to baseline. The compression of the ends caused tension on the surface at the mid-shaft of the cylinder. These modes were the same frequency and thus assumed to be closely related (Kwon and Fox 1993). An FEM representation of the breathing mode is provided in Figure 2.11. Due to the similar cylindrical geometry between the rat skull and the thin walled cylinder, it is possible that the rat skull will undergo a similar mode of response as the breathing mode described by Kwon and Fox.

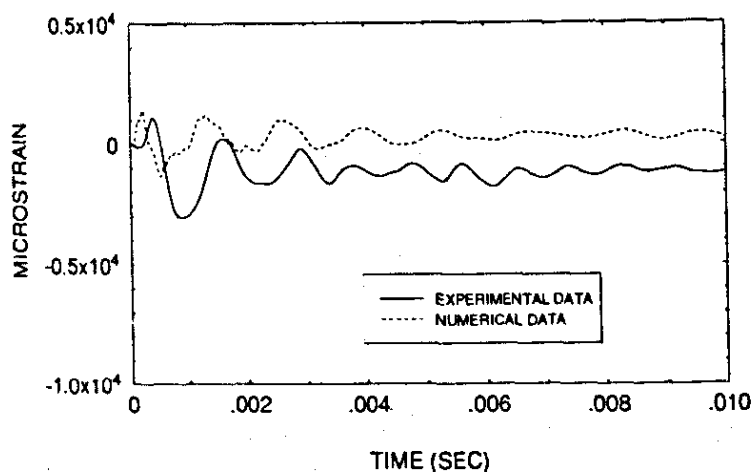
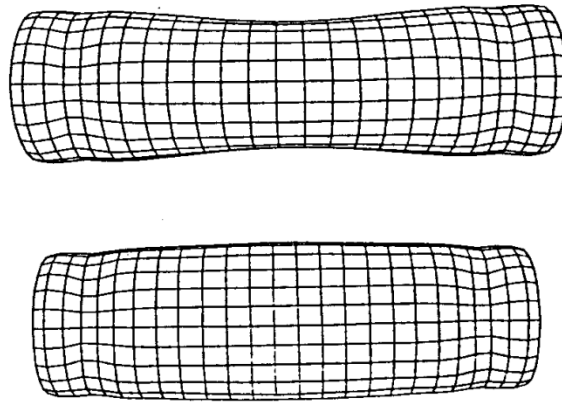


Figure 2.10 The axial strain response of a cylinder exposed to an underwater shock wave (Kwon and Fox 1993).



**Figure 2.11** The breathing mode response of a cylinder exposed to an underwater shock wave. The compression of the ends of the cylinder cause the surface at center to go into tension (bulge), oscillate, and return to baseline (Kwon and Fox 1993).

## 2.7 Theoretical modes of response of a sphere

Shock wave loading of thin walled spheres with a simulated brain core has been an area of research due to its implications for identifying brain injury mechanisms. The sphere has been shown to exhibit two types of modes; membrane and composite (Nayfeh and Arafat 2005). Membrane modes take place on the surface of the sphere and are not sensitive to shell thickness. Whereas composite modes are associated with bending, and as such are sensitive to shell thickness. Most of the dissipation of strain energy from resulting from deformation is associated with these composite modes. Nayfeh and Arafat (2005) also described a breathing mode for a sphere. The mode is associated with radial expansion and is also termed volumetric or pulsating mode.

The theoretical stress (and therefore strain) responses of the surface of the sphere during radial impulsive loading were shown to be axisymmetric about the load point (Engin 1969; Engin and Liu 1970). In this study the tangential stresses on the surface of sphere were shown to experience two major responses. One response

resulted from a compression at the location of impact and an out bending of the sides. The other response consisted of high frequency response across the entire surface of the shell. The high frequencies were of lower magnitude than the first response. While these studies were theoretical, they suggest multiple modes of response for the sphere that can then be verified experimentally.

## **2.8 Experimental modes observed in simplified physical models**

In a recent dissertation, Leonardi (2011) examined the mechanical responses of surface strain and intra-spherical pressure (ISP) of thin shelled spheres filled with aqueous glycerin at 40% weight. The thin walled spheres were made of polyurethane foam, composed of a spongy inner core and a stiffer outer shell simulating cortical bone. The thickness of these spheres were either 5 mm or 7mm (Leonardi 2011).

Leonardi subjected the spheres to shock waves with incident pressures of 69, 88, and 120 kPa at four orientations: front, side (left and right), and back facing relative to the incoming incident shock wave. The protocol included one exposure at four orientations with a repeat of the front orientation for each intensity. Four fiber optic pressure sensors (FOP-MIV, Fiso Inc) and four strain gages (FAER-25B-35SX, Vishay Inc.) were used to measure the ISP and surface strain response (Figure 2.12).

When the shock wave interacted with the sphere, the shell went into compression at the surface nearest the shockwave along with the region opposite of this location. The lateral strain gages would undergo tension during this time. When the sphere was rotated 90 degrees the lateral strain gages would undergo compression, oscillate, and eventually dampen out (Figure 2.13). This mode was similar to the breathing mode described by Nayfeh and Arafat (2005). Although, because when one

axis goes into compression the other two would go into tension, the term Damped Oscillation Axisymmetric (DOA) response mode has been chosen because there was not a uniform radial expansion and reduction across the entire surface, but was symmetric about the principal axis loaded by the reflected pressure. Two other modes were also identified in the strain records. The first was a High Frequency Low Amplitude (HFLA) response mode. It has not been determined if this response was similar to that predicted by Engin (1960). The other response was a compression that mirrored the external pressure environment. This mode has been called the Quasi-Steady Compression (QSC) response mode.

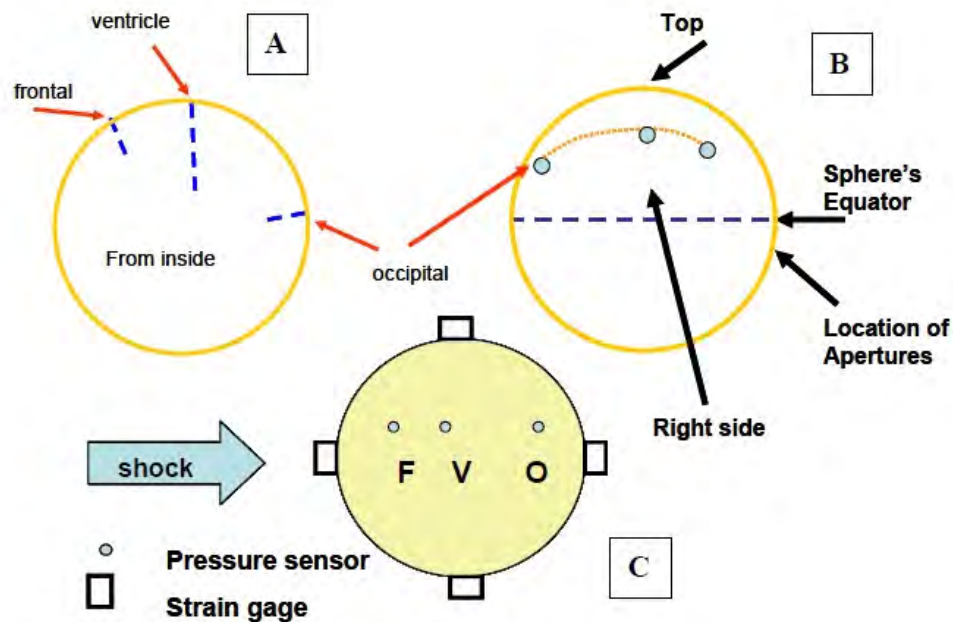
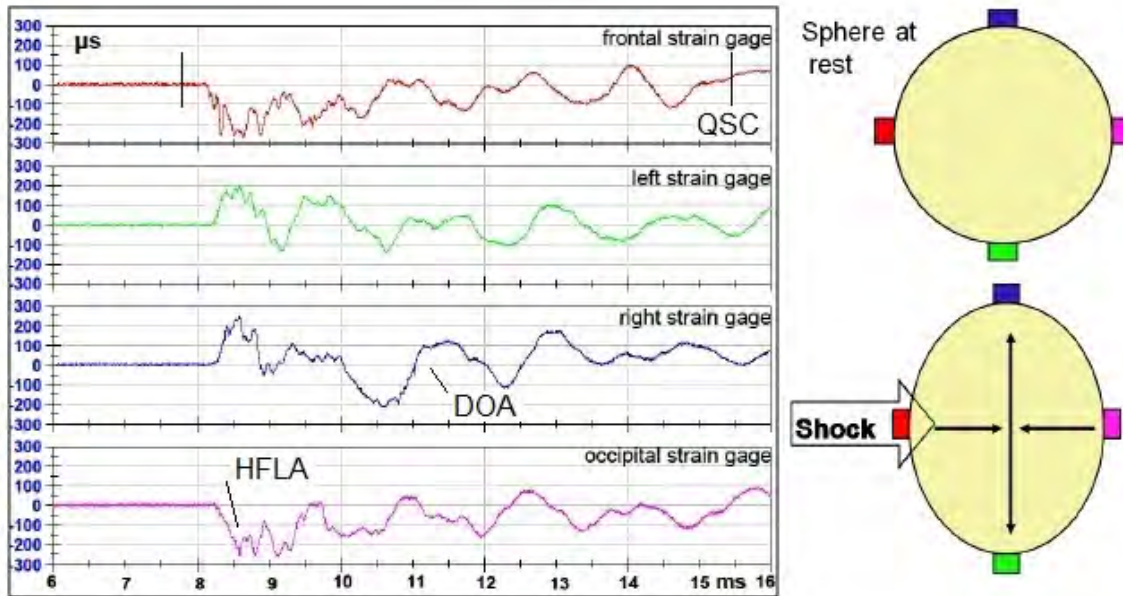


Figure 2.12 Pressure sensor and strain gage locations on the glycerin filled sphere used by Leonardi (2011).



**Figure 2.13** The strain response of the aqueous filled sphere to shock wave exposure. The DOA, HFLA, and QSC modes have been highlighted (figure adapted from Leonardi (2011)).

Pressure responses associated with the three flexural modes observed in the shell strains were observed within the sphere. Examples of these responses are shown in Figure 2.14 for the 7mm sphere. The pressures recorded by this sensor were taken on the side opposite of impact (occipital). Therefore when the sphere was in the front facing position, the sensor would measure a negative pressure prior to positive pressure.

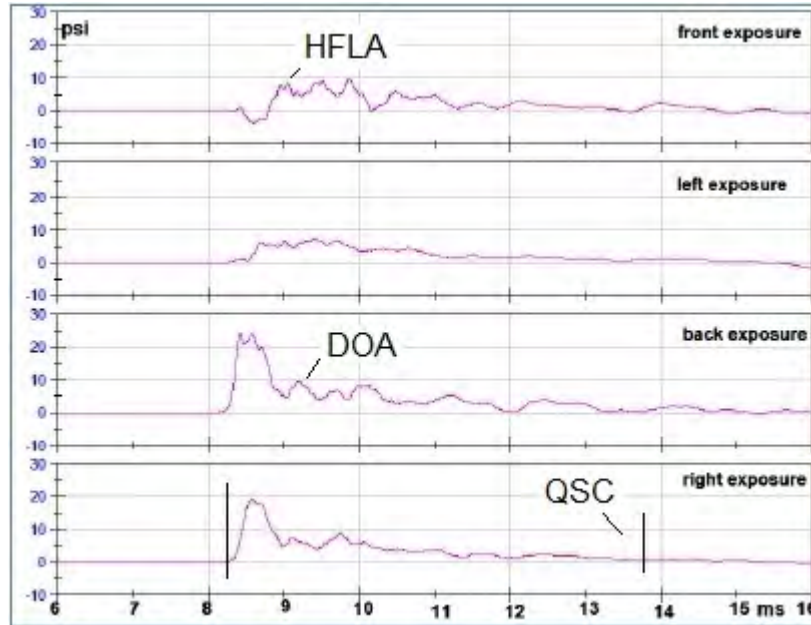
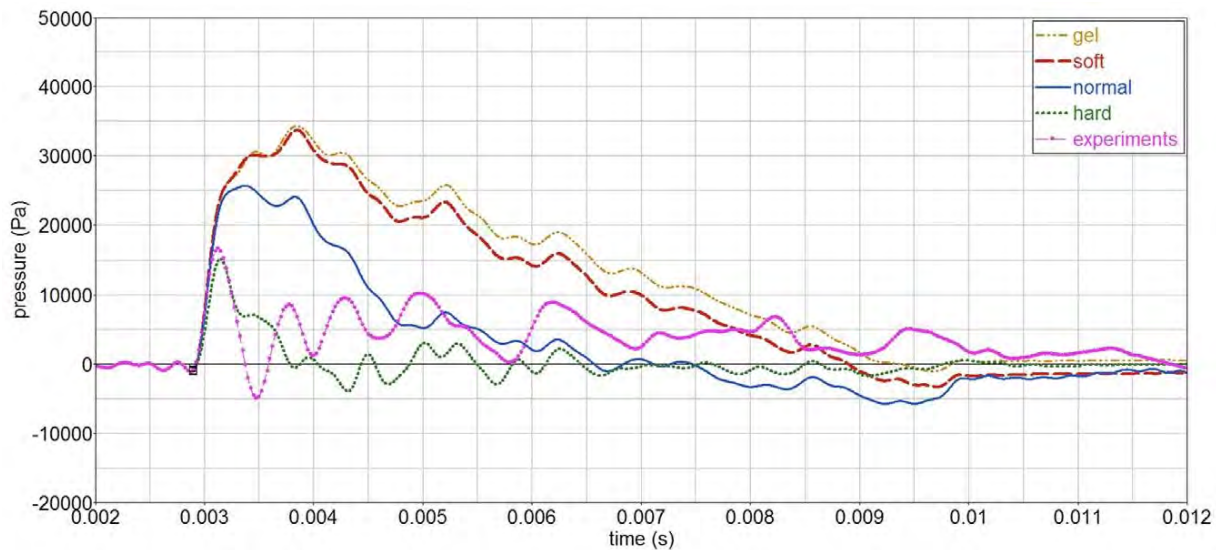


Figure 2.14 The ISP response for the occipital pressure sensor. Responses associated with the three identified modes on the shell surface are highlighted in this series. The HFLA oscillations are superposed on the DOA oscillations (adapted from Leonardi (2011)).

## 2.9 Relationship between strain and ISP in simplified spherical models

The investigation of simplified physical models when subjected to a shock wave has also been undertaken by other researchers (Mediavilla Varas et al. 2011). In this study, the intra-spherical pressure (ISP) and shell strain response of a similar 7mm thick sphere used by Leonardi (2011) was measured. The sphere was filled with 10% mass ballistic 3 gelatin and subjected to a 40 kPa shock wave. Three pressure sensors (8530B-200, Endevco Inc.) were placed .03 m apart in the center of the sphere. Strain gages were mounted to the surface. Aside from the experimental study, the authors also created a finite element model (FEM) of the sphere and a computational fluid dynamic (CFD) model of the shock wave in order to carry out parametric analyses of the sphere/simulant response characteristics.

A parametric analysis of shell stiffness was undertaken to determine how increasing the stiffness of the shell would affect the pressure response within the gelatin. The FE results over predicted the pressure response within the sphere. As the FEM shell was stiffened, the ISP amplitude decreased and the overall waveform better approximated the experimental results (Figure 2.15).



**Figure 2.15** As the FEM shell was stiffened, the calculated pressure profile better approximated the experimentally measured pressures within the sphere. Figure is taken from Mediavilla Varas et al. 2011. Physics of IED blast shock tube simulations for mTBI research. *Frontiers in Neurology* 2, 1-14.

The strain gage results were also useful for describing how shell stiffness will affect the pressure response within the sphere. An example of the strain that was calculated on the surface of the sphere was shown in Figure 2.16. The authors described that the phase delay between the FEM and experimental strain was the result of an overly soft behavior of the FEM simulant.

The effect of shell stiffness was also investigated for the frequency of oscillation within the simulant. In Figure 2.17 it was shown that increased stiffness in the shell will

increase the frequency of the pressure response within the sphere, demonstrating the role of surface strain on the ISP response.

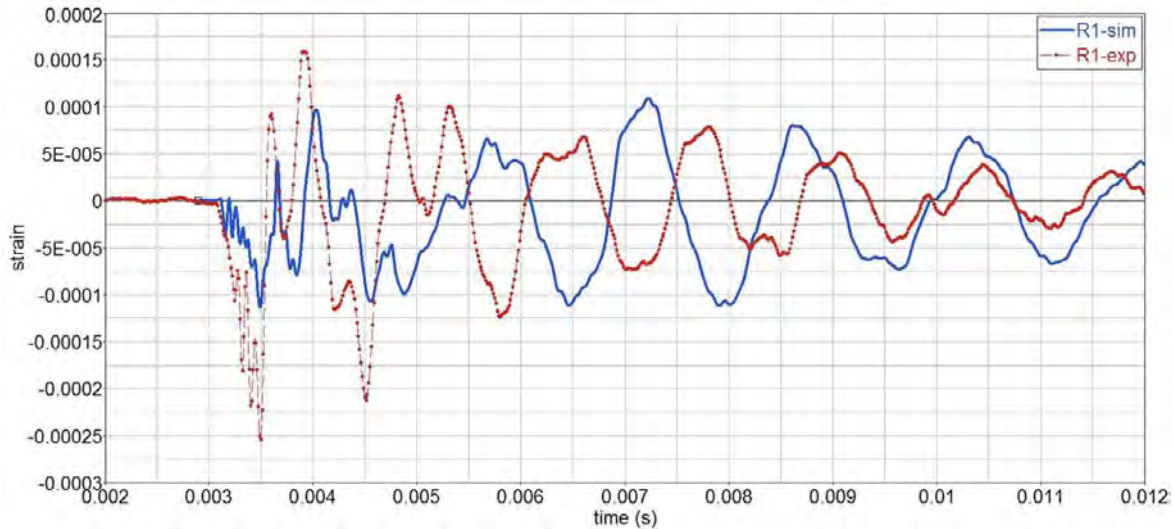


**Figure 2.16** The experimental strain response of the 7mm sphere when compared to the FEM calculations. Figure is taken from Mediavilla Varas et al. 2011. Physics of IED blast shock tube simulations for mTBI research. *Frontiers in Neurology* 2, 1-14.

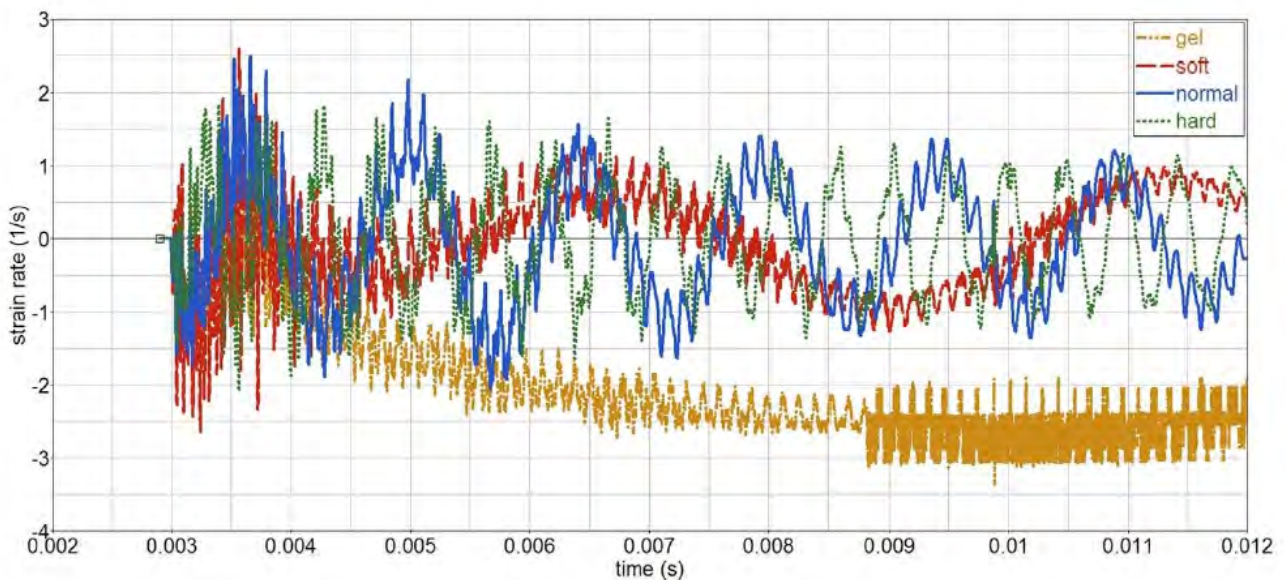
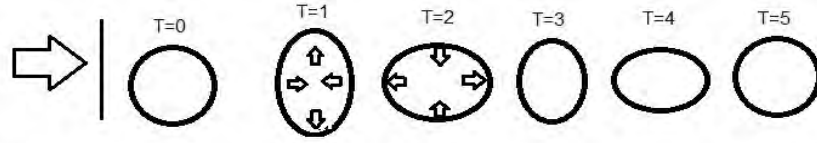


**Figure 2.17** The waveforms to which the simulant is subjected are dependent on shell stiffness. Figure is taken from Mediavilla Varas et al. 2011. Physics of IED blast shock tube simulations for mTBI research. *Frontiers in Neurology* 2, 1-14.

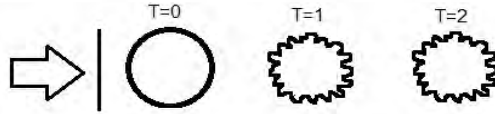
## 2.10 Modes observed in simplified physical models

The modes of response of biological specimens are difficult to identify given the complexity of each structure. Simplified physical models reduce this variability to easier identify these modes and to understand how different mechanical properties (such as shell stiffness) will dictate the overall response of the system. The work of Leonardi (2011) and Mediavilla-Varas et al. (2011) allow for the identification of three modes of response in the sphere. Each of the modes of the shell and their resulting effect on the intra-spherical pressure response are described in Figure 2.18. The description of these modes and their responses provide a framework in which to evaluate the biomechanical responses of each of the three species evaluated.

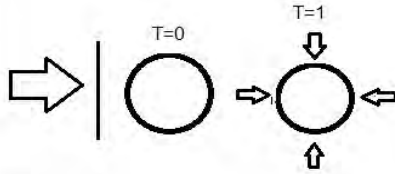
Flexural Modes of Shell



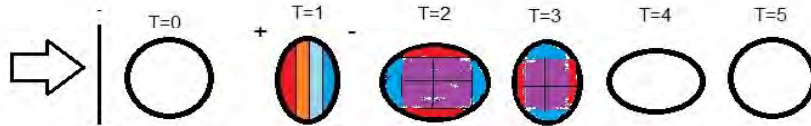
Damped oscillation axisymmetric response mode: Shock wave deforms surface of object. Side exposed to reflected pressure is compressed. Sides go into tension. System oscillates in damped manner back to baseline.



Low amplitude high frequency mode: Shock wave excites high frequency flexural response. Response loses energy, returns to baseline.

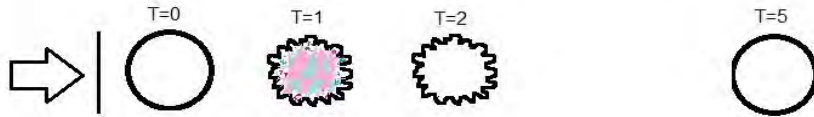


Quasi-steady compression: Shock wave loading compresses object globally, and weakens with time, returning to baseline.

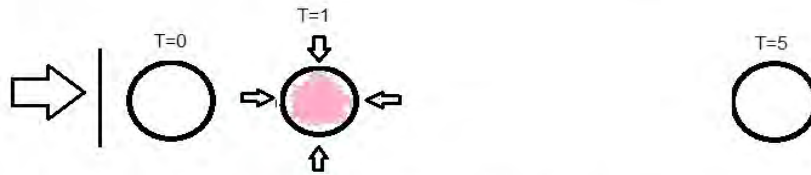


Coup/contrecoup pressure response results from initial deformation during damped oscillation axisymmetric response. Oscillations of shell cause pressure gradients in the object.

Pressure Responses



Low amplitude high frequency mode causes pressure pulses of higher frequency, but has less of an overall effect on pressure response.



Quasi-steady compression causes slight increase in pressure within the object.

Figure 2.18 Modes of response observed for the sphere when exposed to a shock wave.

## CHAPTER 3 RAT MODEL OF BLAST BIOMECHANICS

### 3.1 The rat in blast research

One of the roles of animal models in blast research is to understand the pathological responses that result from shock wave exposure. The rat remains one of the most widely used animal models to understand these responses. Table 3.1 provides a summary of some of this research that has been carried out within the last 15 years. Despite the concern that the rat is grossly undersized when compared to the human, research with rats continues to be undertaken. Of the studies summarized in the table, only one had investigated the intracranial pressure (ICP) biomechanical response within the rat brain during shock wave exposure.

The lack of studies investigating the biomechanical responses of the rat head is important to point out because the environments in which the rat brain is subjected may be significantly different than what the human brain would experience under the same external loading conditions. This is relevant for studies that investigate biochemical, physiological, or cognitive changes in the rat resulting from shock wave exposure. Scaling factors of injury response from animals to humans will be erroneous if the responses are based on conditions which the human brain may never be subjected. For the results of experiments utilizing rats to be useful to the entire blast community, an understanding the biomechanical responses of the rat head during shock wave exposure is required.

To investigate the biomechanical responses of the rat head, multiple specimens were exposed to shock waves of increasing intensity. The first set of tests investigated

the relationship between skull strain and intracranial pressure (ICP). A second set of tests was conducted in order to evaluate the effects of the instrumentation modifying the biomechanical responses of the system. Collectively, these experiments provided an insight to the biomechanical responses of the rat head to shock wave exposure. This insight included identification of multiple modes of response of the rat skull and subsequent intracranial pressure responses.

**Table 3.1 Sample of research where rats are exposed to shock waves**

Researcher	Methods	Pressure Range	Exposure Orientation	Placement	Findings
Kaur <i>et al.</i> 1995	Histology	Severe, exact pressures not known	N/A	Cages in a concrete bunker	Shock wave will induce wide spread microglial activation, leading to increased endocytosis and immunological responses
Bauman <i>et al.</i> 1997	Physiology	83-129 kPa	Side	In net on the open end of the tube	Shock wave exposure decreases exercise and food intake
Irwin <i>et al.</i> 1999	Physiology	91-109 kPa	Xiphoid	Small Diameter tube opening placed over ventral side	Circulatory shock brought on by shock wave is reduced when vagus nerve is deafferented
Saljo <i>et al.</i> 2000	Histology	154-240 kPa	Side	In blast tube	Shock wave exposure may lead to disturbed axonal transport in the brain
Cernak <i>et al.</i> 2001	Cognitive Physiology Histology	440 kPa	Thoracic region, side (50 ms)	Outside of shock tube	Shock wave exposure induces ultrastructural and biochemical impairments in the hippocampus along with cognitive deficits
Moochhala <i>et al.</i> 2004	Cognitive Histology	2.8 - 20 kPa	N/A	Cages in bunker	Shock waves cause neurobehavioral decrements, aminoguanidine may be protective
Chavko <i>et al.</i> 2007	Biomechanics	33-47 kPa	Front	Inside of shock tube	Pressure waves develop in brain during exposure
Long <i>et al.</i> 2009	Physiology, Cognitive	126 , 147 kPa	Side	Outside of shock tube	Protection of thorax reduces mortality, Shock waves can cause TBI
Saljo <i>et al.</i> 2009	Cognitive ICP	10-60 kPa	Front	Inside of shock tube	Low intensity exposure increases ICP and decreases cognitive performance

### 3.2 Methods for investigating skull strain and ICP in the rat

Approval of all experiments was obtained from the Wayne State University Institutional Animal Care and Use Committee (IACUC) prior to testing. A total of ten male Sprague Dawley rats, age 65-70 days old, were procured. All animals were given food and water ad lib. Animals were randomly assigned to one of two groups based on

instrumentation used during the testing: strain gage (SG) or intracranial pressure sensor mounted to the top of the skull (IC).

For the SG group, (5) rats were sacrificed immediately prior to testing. The dermal tissue was removed from the medial dorsal surface of the head exposing a 1.5 cm wide region of the skull extending from 1-cm rostral to the bregma to 1-cm caudal to the lambda. The skull surface was then cleaned using acetone to ensure a solid and durable mechanical bond with the strain gage. A three-axis rectangular Rosette-style strain gage (FAER-25B-35SX, Vishay Inc) was then attached to the skull surface using cyanoacrylate and allowed five minutes to cure. The channels were named rostral, medial, and caudal (Figure 3.1 A). To limit motion of the rat's head during exposure and prevent mechanical stress on the instrumentation fibers, the nose was secured such that the head was pitched down at approximately 45 degrees to the shock front.

For the IC group, five rats were anesthetized using a ketamine/xylazine mixture (80mg/kg/10 mg/kg; I.P) and immobilized in a stereotaxic frame. A longitudinal incision was made along the dorsal medial surface of the head, exposing the skull from the bregma to the lambda. A 1.5mm diameter hole was drilled using a stereotaxic high-speed drill at the following location: +3.0 (A-P (mm) from Bregma), -2.0 (M-L (mm)), and -1.0 (D-V (mm)), exposing the frontal cortex.

A plastic guide cannula (18-gage; 1.2 mm, CMA Microdialysis Inc) with a small pedestal was implanted through the hole and fixed to the skull using two small stainless steel screws inserted at 45 degree angles from the horizontal into the skull adjacent to the cannula. Cranioplastic cement was applied to fix the pedestal to the skull and was anchored by the screws. The surgical wound was closed with sutures, as needed. A

dummy cannula insert with a threaded cap was inserted in the guide cannula until testing; the rats were allowed five days recovery time.

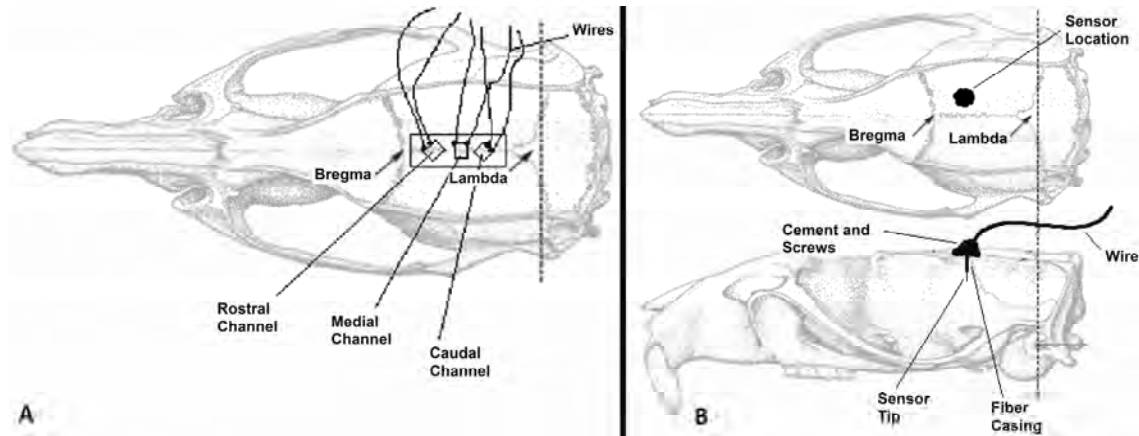


**Figure 3.1 Placement of the strain rosette on the surface of the rat skull (SG) (A) and fiber optic pressure sensor installation on the rat skull (IC) (B).**

Prior to testing, rats were anesthetized using a ketamine/xylazine mixture (80mg/kg/10 mg/kg; I.P). The cannula was then filled with a sterile saline solution. The cannula cap was filled with petroleum jelly and a fiber optic pressure sensor (FOP-MIV, Fiso Inc.) was inserted into the cannula and threaded onto the cannula pedestal (Figure 3.1B).

All animals were affixed to a trolley-mounted stage using a nylon harness, and inserted into the shock tube. The rat's nose was positioned 114 cm inside the end of the Lexan® tube facing the driver (Figure 3.2). The harness maintained the rat's longitudinal axis perpendicular to the shock front and in fixed proximity to a side-on pressure sensor. The trolley system reduced the effects of post-shock dynamic pressure flow on the rat.

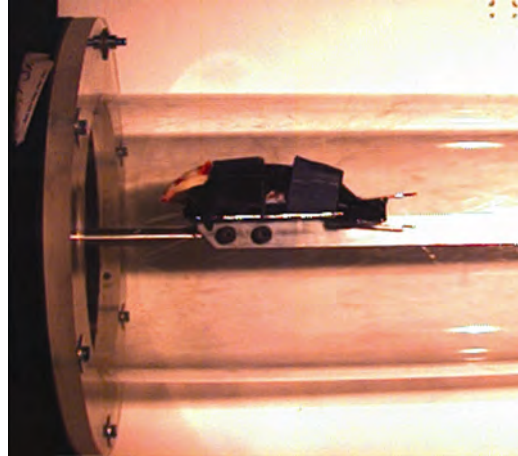


**Figure 3.2** The rat was placed 114 cm within the shock tube and was placed on a trolley system to reduce the effect of dynamic pressures that are not representative of a free-field blast wave.

Once placed in the harness, the SG rats were subjected to three exposures, each at 69, 97, 117, and 172 kPa incident pressures or until sensor failure for a total of 12 exposures maximum per animal. The IC rats were exposed to three repeated exposures at three intensities (69, 97, and 117 kPa). In order to conserve the integrity of the ICP sensors, the highest pressure intensity (172 kPa) was not applied. The intensities used in the protocol were determined from previous tests to maximize the amount of useful data. The time in between exposures was approximately two minutes for both groups of animals.

Both ICP and strain data were collected at 400 kHz using the Dash 8HF data acquisition system (Astro-med Inc). The data were then post-processed using Diadem 11.0 (National Instruments Inc). Calculations of maximum principal strain (Equation 1) were undertaken; the rostral gage measured  $\epsilon_1$ , the medial gage,  $\epsilon_2$ , and the caudal gage,  $\epsilon_3$ .

$$\varepsilon_{P,Q} = \frac{\varepsilon_1 + \varepsilon_3}{2} \pm \sqrt{\left[ (\varepsilon_1 - \varepsilon_2)^2 + (\varepsilon_2 - \varepsilon_3)^2 \right] / 2} \quad (1)$$

The data were reported in microstrain and the magnitude of the first compressive peak was recorded. The peak intracranial pressure was also recorded. Data were grouped by incident shock wave intensity and responses were compared using ANOVA with post hoc Tukey HSD used to determine significant differences (\* p < .05) between groups.

Computer tomography (CT) scans were obtained for the SG rats by means of a microCT device (Scanco VivaCT, Scanco Medical Inc). ICP rats were not scanned as the instrumentation installed into the skull made it difficult to measure bone thickness. Variability of SG rat skull thickness throughout the skull was determined to help identify structural weaknesses that could be considered candidates for flexure. Skulls were scanned using a voltage of 70 kVp and a current of 114 uA at a 30 um resolution with a 320 ms integration time. Thickness measurements were calculated by using MicroCT Analysis software (Scanco Medical Inc.). Measurements were taken at the midpoint between the lambda and bregma sutures. Three-dimensional reconstruction of the skull was undertaken to appreciate the skull geometry.

### 3.3 Results of SG Measurements

The data collected from the strain gages were useful for determining the flexural response of the superior braincase during shock wave loading. There were characteristic superposed response patterns that were observed consistently as follows:

(1) A strong and rapid compression with an associated damped oscillation at relatively

high frequency (less than 3kHz) (red). (2) A quasi-steady compression closely following the decay of the external static overpressure condition that developed as the strain returned to pre-blast levels (green). (3) A waveform of lower frequency with its pulse beginning in tension following the rapid compression (blue). These responses were present for all the rats tested (Figure 3.3).

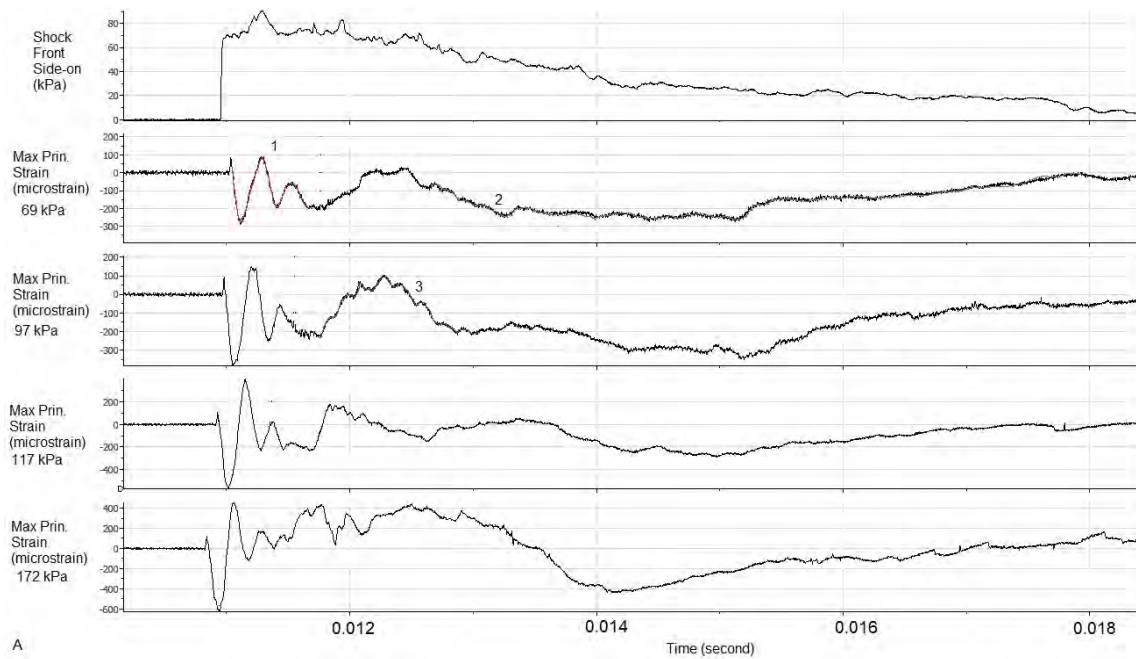


**Figure 3.3 Principal strain response profiles of the superior brain case for both a 262 gram rat when exposed to shock waves of increasing intensity. For the presented data, tension is positive and compression is negative. (1) (red) A compression with an associated damped oscillation. (2) (green) A quasi-steady compression closely following the decay of the external static overpressure. (3) (blue) A response beginning in tension that was dependent on the initial compression.**

The first trace of the series included the side-on (static) pressure sensor exposed to the incident shock wave. Following the incident shock front, reflections from the fixture holding the specimen develop and create pressure artifacts on the sensor's surface that are not representative of the environment to which the specimen is

exposed. This effect is expected from theory; the arrival and amplitude of the perturbation coincides with those expected of that reflection disturbance.

The peak compression was calculated for all exposures. In Table 3.2, it was shown that as the incident shock wave intensity increased, the calculated maximum principal strain also increased for the rats instrumented with strain gages. The means were significantly different between exposure intensities (\* $p < .05$ ,  $p < 0.0001$ ).

**Table 3.2 Peak skull flexure increases with shock wave intensity for the superior rat skull**

Pressure (kPa)	Number	Mean (microstrain)	Standard Dev.
69	15	253	52
97	15	359	66
117	12	533	98
172	12	760	124

### 3.4 Results of ICP measurements

For intracranial pressure, two response patterns were observed consistently between specimens: (1) a rise in pressure followed by dampened oscillations, (2) a rapid increase in pressure that approximated the external loading environment and returned to pre-exposure conditions. In Table 3.3 it was shown that as the incident shock wave intensity increased, the peak pressure increased, all groups were significantly different from each other (\* $p < 0.05$ ,  $p < 0.0001$ ).

**Table 3.3 ICP increased with shock wave intensity (  $p < 0.0001$ ).**

Pressure (kPa)	Number	Mean (kPa)	Standard Dev.
69	15	100	14
97	15	144	8
117	15	178	11

The pressure response profiles for a 249 gram rat were shown in Figure 3.4. The three profiles have been time shifted to begin at the same point. The increase in peak pressure as a function of an increase in incident pressure can be observed for this series of waveforms. The duration of the rise times is also a function of intensity, where the highest intensities resulted in the shortest rise times. To further this point, the 97 kPa ICP pressure response was time shifted so that its pressure profile could be compared to a 97 kPa incident shock wave without the shock reflections that were observed in Figure 3.4 (Figure 3.5). The rise times between the incident wave on the external pressure sensor and the intracranial pressure response was 27 compared to 195 microseconds, respectively. Although, this 27 microsecond response is an artifact of the pressure gage and boundary layer (contact surface). The actual rise time is on the order of one microsecond. Regardless, the external pressure measurement was provided because it allowed for a basis of comparison to the ICP response where there was a significant increase in rise time as a result of deformation of the skull caused by the shock wave.

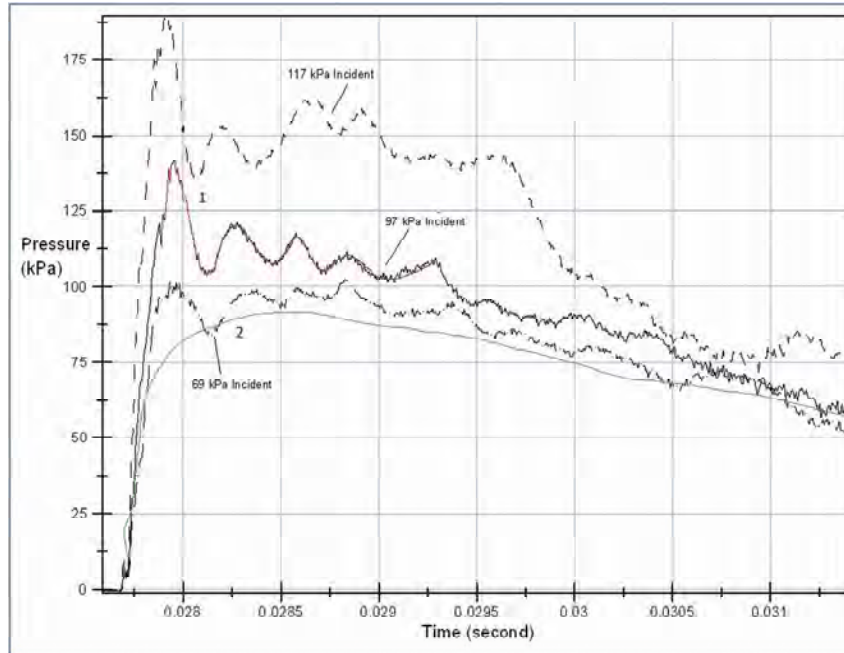


**Figure 3.4** The intracranial pressure response of a rat is dependent on shock wave intensity. The ICP responses for a 249 gram rat show distinct pressure oscillations (1) (red) that are present in each of the profiles. The waveforms also undergo a quasi-steady compression response that approximates the external loading response invoked by the shock wave (2) (green).

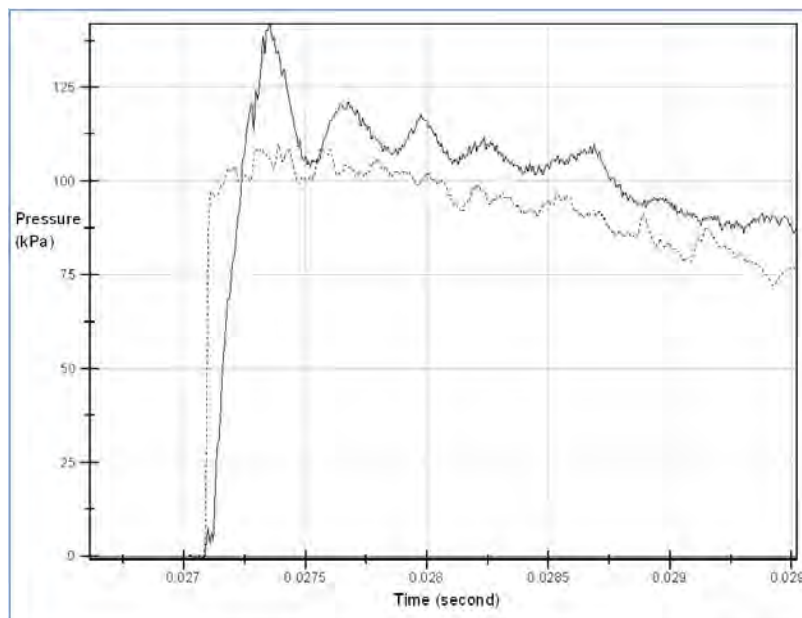


**Figure 3.5** The rise time of the external pressure wave is shorter (solid) than the rise time of the recorded intracranial pressure for a 249 gram rat. The actual rise time of the shock wave is shorter than what is measured by the penci gage (~ 1 microsecond) (dotted).

### 3.5 MicroCT results

The results from the micro CT imaging provided information regarding the geometry and thicknesses of specific bones in the skull (Figure 3.6 A). The mid plate thickness between lamda and bregma sutures was approximately  $0.354 \pm 0.061$  mm thick (1) where the thickness increases near the midline suture to  $0.630 \pm 0.082$  mm thick (3). The gap between the suture itself was approximately  $0.162 \pm 0.016$  mm thick (2). The distance from horn to horn was  $11.72 \pm 0.114$  mm (5). Additionally the distance from horn to suture top was  $5.78 \pm 0.207$  mm (4). The term horn is in reference to the folds of bone on the lateral aspects of the skull, acting as reinforcements. Values were reported as (mean  $\pm$  standard deviation).

In Figure 3.6 B, a three dimensional reconstruction of the rat skull was provided. The rostral end was rotated down to the bottom of the graphic; the caudal region is near the top. The reinforcement of bone on the lateral aspects of the skull and the gaps between of the suture lines allow for inward flexure of the superior bones of the skull case during exposure to the external pressure wave as it diffracts across the head.

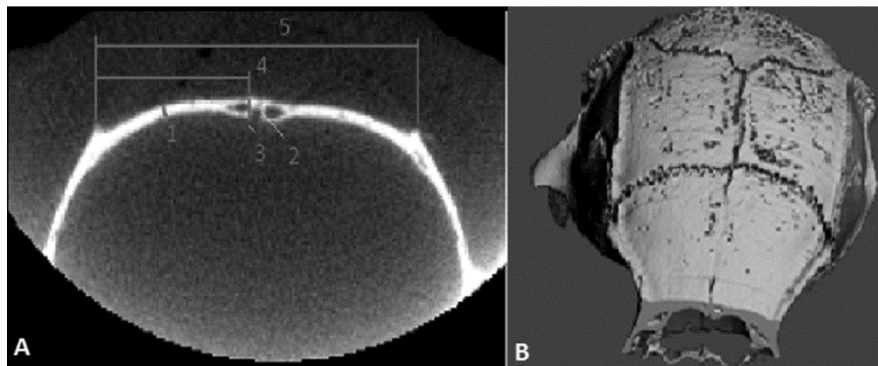


**Figure 3.6 (A) Measurements were taken of the MicroCT images of the rat skull to determine key structural elements. (B) A 3-dimensional reconstruction of the images depict that there are considerable gaps between the bone plates with significant reinforcement on the lateral bone folds, suggesting that the midline suture would be a probable place for skull flexure to take place.**

### 3.6 Observed modes of the rat skull when subjected to a shock wave

The MicroCT imaging of the superior braincase of the rat revealed that the bones are not completely fused and the lateral aspects are reinforced with thicker layers of bone. It is hypothesized that when the incident shock wave diffracts across the surface of the skull, the shock wave loads the surface. This loading will cause the greatest deflections in the regions with the least reinforcement. When examining the specific anatomical features of the rat skull, the region between the lambda and bregma suture appears to offer the greatest amount of deflection as the bone plates may hinge about the major sutures.

Results from the strain gage data further substantiates the hypothesis that the incident shock wave is causing the skull to flex. The rapid compression that increases in magnitude with the intensity of the incident shock is believed to be the direct result of the shock wave compressing the skull surface. The damped oscillation phase that developed as a result of the compression is hypothesized to be due to the return of the deflected surface regions back to equilibrium. This mode of response is believed to be similar to the breathing or accordion mode described in Chapter 2 although the mode is better described as the damped oscillation axisymmetric (DOA) response mode due to the increase in radius in one plane while decreasing in another during the same motion. The quasi-steady compression (QSC) mode that approximates the external pressure environment was best observed as the DOA mode would subside. The third mode described for the rat included a low frequency tension wave that appeared to be related to the DOA mode. It has been observed that this mode is dependent on the intensity of the incident shock wave. The shape of this mode steepens as the intensity increases.

Due to the flexibility of the plates composing the surface of the superior braincase of the rat, it is possible that this mode is the result of additional interactions between these plates.

Because of these observations in both the strain gage and intracranial pressure responses, it is proposed that there are two major responses occurring. The first is the transient phase which consists of a rapid compression and damped oscillations (DOA mode); the other is the quasi-steady compression (QSC mode).

### **3.7 Limitations of study**

Some limitations exist with the current data. The placement of the strain gage on the skull was problematic because mounting on the suture lines will cause an amplification of the signal or measure modes of response that may not have an effect on the ICP. An example of this would be mode (3). Principal strain calculations were not made on a homogenous surface and the sensors were relatively widely distributed. But, given the consistency of the signals between exposures and that similar responses were observed between specimens, the data are useful for describing responses of the rat to shock wave exposure.

The ICP data were of concern because the skull was modified with small screws and bone cement, modifying the native surface. If the superior skull case was acting as a diaphragm, the additional mass of the sensor mounting complex will change the period of each of the oscillations.

To determine if mounting of the ICP sensor on the surface of the skull case modified the frequency of oscillations in the pressure record, a second set of experiments were undertaken. The study was designed to determine what effect

mounting on the superior aspect of the skull when compared to mounting on the occipital bone will have on the imparted ICP response. If it was shown that the frequency of oscillations for the DOA mode was an artifact of the instrumentation, then to associate this frequency of pressure fluctuations with a potential brain injury mechanism would be erroneous.

### 3.8 Assessing frequency response changes of the DOA mode in the rat

It had been previously discussed in this chapter that because the rat skull is so thin, the mounting of the fiber optic pressure sensor on the superior skull case may change the frequency response of the DOA mode of the skull when subjected to the diffracted shock wave. The two factors that will change the frequency response of a system are its mass and stiffness (equation 2):

$$f_n = \frac{1}{2\pi} \sqrt{\frac{k}{m}} \quad (2)$$

Where  $k$  is the system's stiffness and  $m$  is the mass of the system. To assess what effects mass and stiffness would have on the DOA mode, a series of tests were conducted. To determine the effect of changing the mass of the system, the ICP responses were compared between mounting of the fiber optic pressure sensor on the occipital bone to mounting of the sensor to the superior brain case. To address effects associated stiffness, older rats were included in this study to determine if age (as a correlate to increased skull stiffness) (Gefen et al. 2003) will affect the frequency of the ICP response associated with the DOA mode.

### 3.9 Methods for assessing frequency response changes of the DOA mode in the rat

Two different groups were designated for this study. Group 1 consisted of male Sprague-Dawley rats (N=12) that were instrumented with a cannula mounted to the superior aspect of skull (IC). Group 2 consisted of male Sprague Dawley rats (N=6) that were instrumented with a cannula mounted through the occipital bone (OIC).

The superior mounted test set-up (IC) was similar to the methodology described prior and is demonstrated in Figure 3.7 A. The installation procedure for the rats with the occipital mount (OIC) differed from the IC. In brief, rats were euthanized with a mixture of ketamine/xylazine. The scalp of the posterior region was removed. A small hole was then drilled into the bone to allow for the cannula to be placed. Screws were then drilled into the bone at four positions on the occipital bone to be used as anchor points. The cannula with its threaded cap was placed and bone cement was applied to hold the cannula system. Following curing of the cement (~ 10 minutes) the ICP sensor was then sealed within the cannula, with the sensor tip exposed beneath the region between the lambda and bregma (Figure 3.7B).

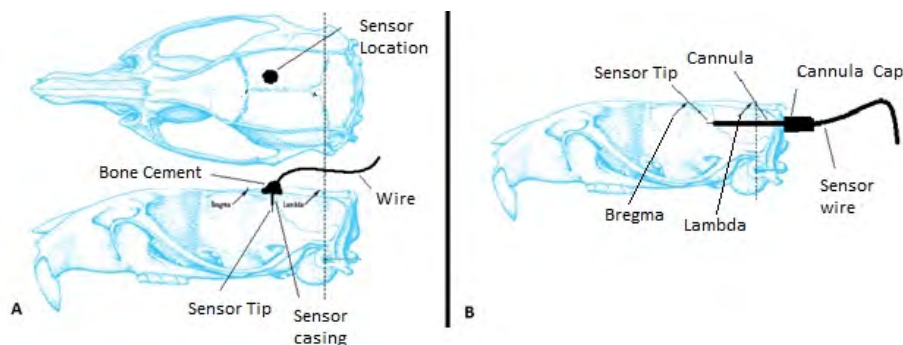


**Figure 3.7 A diagram of the ICP sensor location for the IC (A) and OIC (B) mounting positions of the rat skull. Drawings are not to scale.**

Each rat was subjected to three shock wave exposures at a given intensity. The intensities ranged from 69 to 172 kPa peak incident. The time in between each exposure was approximately two minutes. Following testing, rats from the IC group were euthanized. The purpose for euthanizing the OIC group prior to testing was undertaken due to the severity of the surgical technique. A table describing characteristics of the rats tested in the study was provided in Table 3.4.

**Table 3.4 A description of the weight and mount type for each rat used in the study.**

Mount	Weight	Mount	Weight
Top	239	Occipital	264
Top	240	Occipital	232
Top	244	Occipital	238
Top	249	Occipital	290
Top	256	Occipital	317
Top	259	Occipital	325
Top	273		
Top	301		
Top	368		
Top	369		
Top	437		

Pressure data were collected at 400 kHz by the DASH HF (Astromed Inc). The peak ambient pressure and peak ICP magnitudes were recorded. The peak ICP pressures were grouped by incident intensity and compared with ANOVA and post hoc Tukey HSD test to determine significance amongst groups.

For each rat, a frequency associated with the DOA mode was observed and the first five cycles were counted for the response where the waveform oscillated the most harmonically. Approximate frequencies were then calculated from these cycles using simple waveform analysis (number of cycles divided by time between first and last cycle). For the IC rats the relationship between weight of the rat, shock wave intensity,

and calculated frequency were described graphically using the contour map method, where weight of the specimen and shock wave intensity were graphed on the x and y axes creating a “contour” of the frequency response using DPLOT (Hydesoft Computing LLC). A contour map was not created for the OIC rats due to the smaller sample size.

### **3.10 Results for top mounted versus back mounted sensors**

The peak pressure amplitude measured in the rats was observed to increase with incident shock wave intensity. For both the IC (\*p < 0.05, p < 0.0001) and OIC (\*p < 0.05, p < 0.0001) groups, the data indicated that the maximum ICP response of each population was significantly different to each other when grouped by incident intensity.

For the IC group, the intracranial pressure response for a 256 gram and a 437 gram rat was shown in Figure 3.8. Two major pressure responses associated with the previously described flexural modes of the skull were observed in the overall pressure profile; (1) damped oscillatory pressure oscillations (DOA) and (2) a pressure response that approximated the external shock wave loading (QSC).

For the OIC group, pressure responses for a 232 gram and 317 gram rat were provided in Figure 3.9. Without instrumentation on the external superior aspect of the skull, pressure oscillations associated with the DOA mode were measured within the brain at higher frequencies. The QSC component was also present in the pressure profiles.

At specific incident intensities, seeming to be partially dependent on skull stiffness (associated with rat weight), the pressure response associated with the DOA mode of skull flexure would oscillate the most harmonically. This response was associated with a 256 gram IC rat during a 117 kPa incident shock Figure 3.8.

Unfortunately the mounting fixture broke following this pressure intensity and the higher incident pressure could not be assessed for this rat. The response was associated with a 437 gram IC rat during a 172 kPa incident shock. The relationship was not able to be defined as clearly for the OIC rats Figure 3.9.

The calculated frequencies from the IC group were analyzed. In Figure 3.10, the rat weight (as an analog to skull stiffness), incident shock intensity, and frequency were all compared. The data indicated that as the rat weight and shock wave intensity increased, the calculated frequency decreased for the IC group. The results from the OIC group were not graphed due to the smaller sample size and less clearly defined responses. The calculated frequency for the OIC group was  $7030 \pm 1341$  Hz and frequency results for the IC group were  $4984 \pm 1316$  Hz.

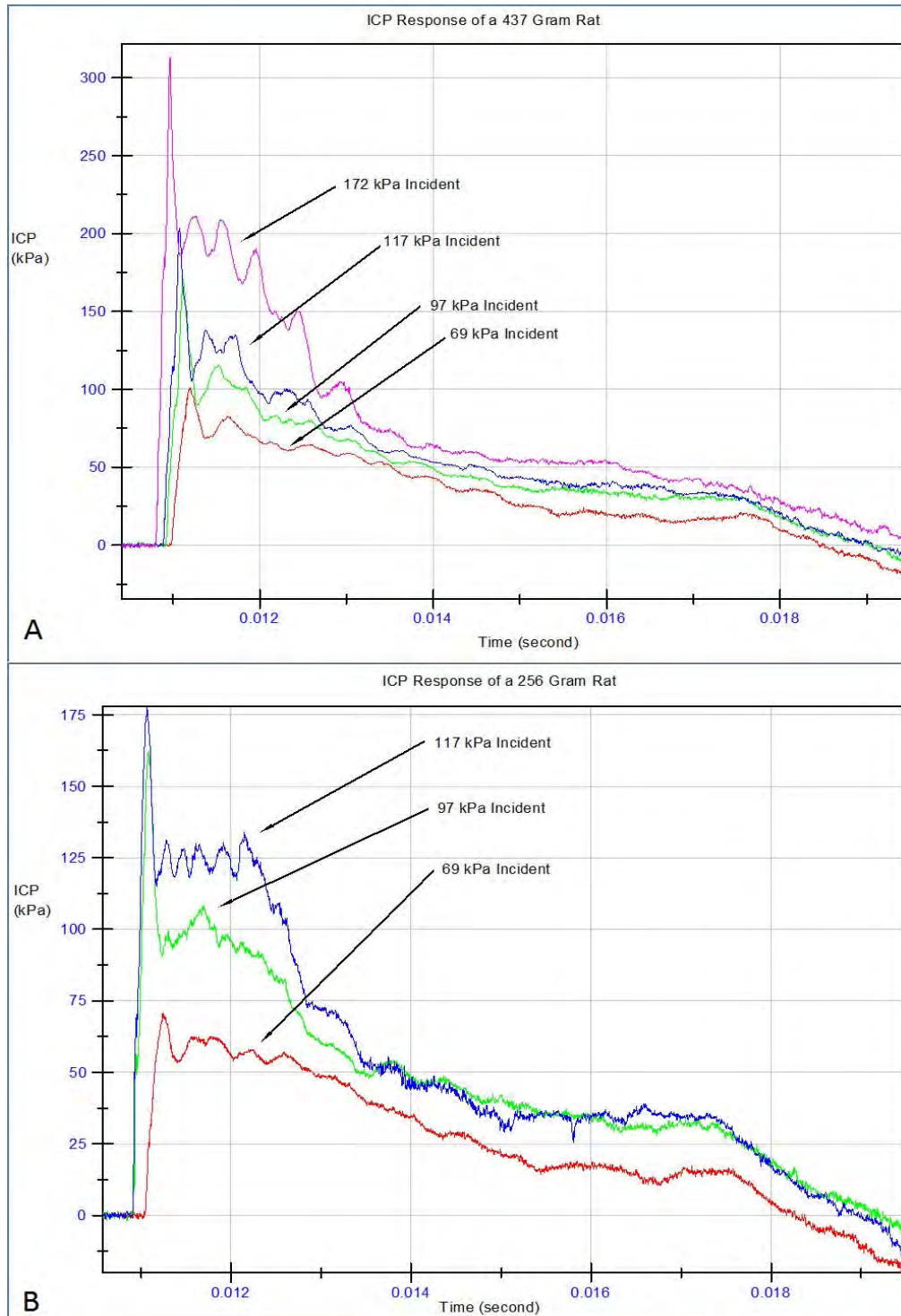


**Figure 3.8 . Intracranial pressure measurements with the fiber optic pressure sensor mounted on the top of the skull (IC). For the 437 gram rat (A) the pressure response associated with the DOA mode was the most harmonic at the 172 kPa incident intensity. For the 256 gram rat (B) the response was most harmonic when the 117 kPa incident shock wave was introduced.**

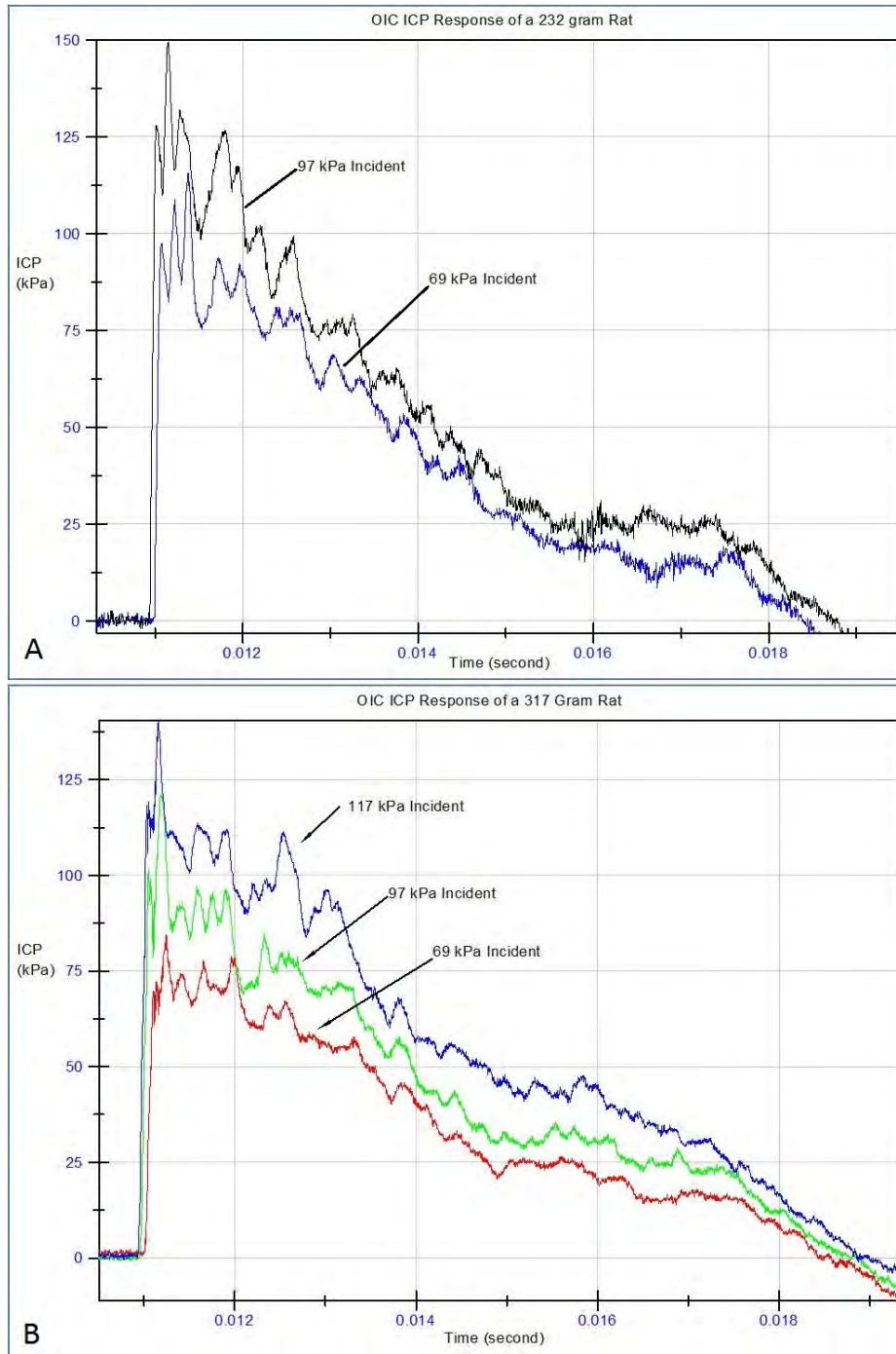


**Figure 3.9 The OIC instrumented rats report higher frequencies but show similar results to the IC rats. The ICP response for both a 232 gram rat (A) and 317 gram rat (B) demonstrate a high frequency content associated with the DOA mode of skull flexure and a response associated with the QSC mode.**

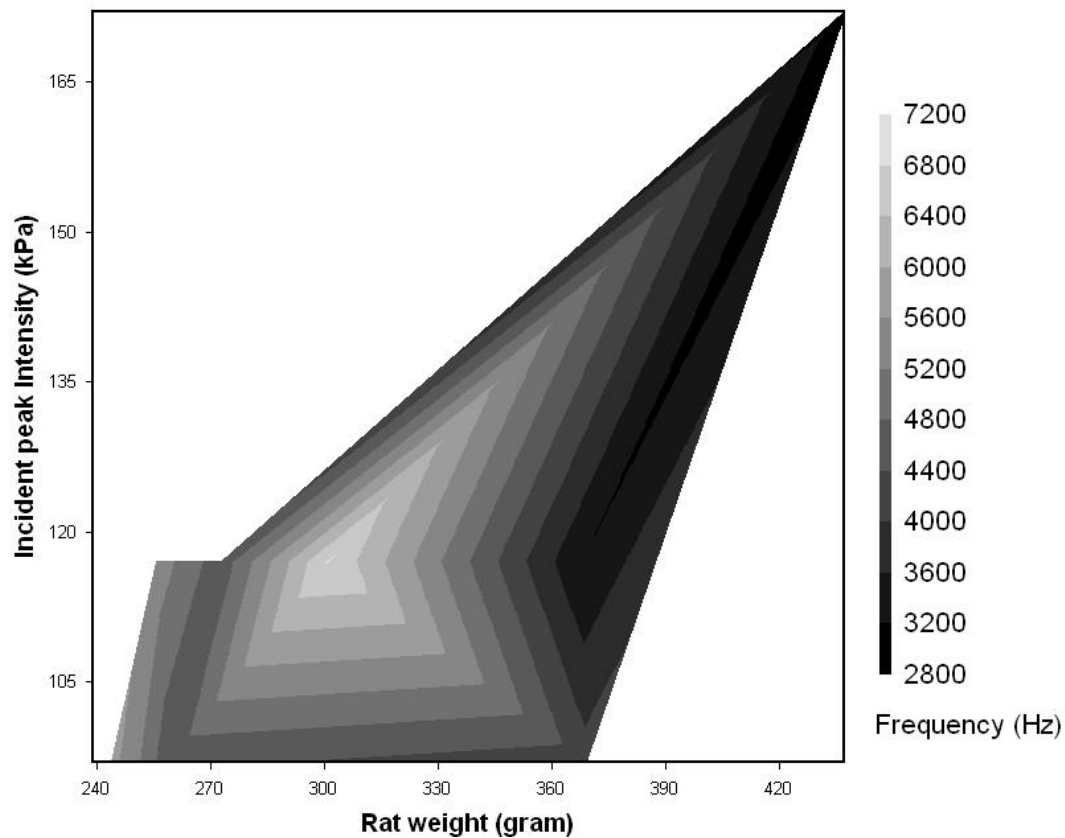


**Figure 3.10** A contour chart describing the role of incident peak pressure intensity and rat weight for determining the frequency response associated with the DOA flexural mode for the IC group. It is generally shown that as the rats get heavier; greater incident shock wave intensity is required to invoke the DOA mode to oscillate the most harmonically.

### 3.11 Discussion of the effect of the IC vs OIC mount on the DOA flexural mode

The results from this series of tests show that the mounting location of the ICP sensor will change the frequency of the pressure response associated with the DOA mode of flexure. It can therefore be assumed that the superior rat brain case is acting as a damped harmonic oscillator. In the introduction for this test series it was shown that the frequency of response will change when either the mass or the stiffness of the system changes. These tests assessed both of these properties.

By mounting the ICP sensor to the occipital bone, the superior brain case was able to oscillate at a higher frequency due to the reduction of mass in the system. To address the property of stiffness, a larger number of IC rats were tested that included a larger range of rat weights. Increasing rat weight was associated to be an analog of skull stiffness (Gefen et al. 2003).

For the IC rats was shown that as a rat became heavier the ICP response associated with the DOA flexural mode would oscillate at lower frequencies, and that greater incident shock wave intensities were required to invoke the response. Because the older rat skull is stiffer, more energy was required to displace the surface in order for it to oscillate and return to baseline levels. The geometry of the rat skull will change with age, it is expected that the lower pressure oscillation frequency that was observed with increasing shock wave intensity was a result of increasing the surface area of the superior brain case or by other mechanisms such as increasing the thickness of the bones, but remaining to be incompletely fused.

If the mechanical properties of the skull are able to dictate the imparted pressure profiles in the brain, then the neuropathological response in the rat as a result of shock wave exposure might be predicted by exposure intensity. The frequency and expression of the pressure oscillations associated with the DOA mode of skull flexure that developed are specific to intensity. Potentially, there could be specific pressure intensities the lead to exaggerated neurotrauma in the rat.

VandeVord et al. (2011) recently demonstrated that rats would exhibit exaggerated cognitive declines and neuropathological increases at a specific band of pressures (VandeVord et al. 2011). The most exaggerated trauma for the rats (average

weight ~ 300 grams) was around 117 kPa. When exposed to greater intensities the rats would experience less of the neuropathological and cognitive declines. It is hypothesized that the rats may be injured to a greater degree when the pressure oscillations associated with the DOA mode of skull flexure are the most harmonic. Studies will need to be undertaken to confirm this association.

### **3.12 FEM model of the rat head when exposed to a shock wave**

In addition to the experimental data collected in these series of experiments, an FEM simulation of the rat head when exposed to a shock wave was undertaken by Zhu et al. (2010). In the study, ICP data for 350 and 355 gram rats with the top mounted ICP sensor were used to validate the model. The experimental tests were undertaken at Wayne State University using the same fiber optic pressure sensors described previously (FOP-MIV, Fiso Inc.). The amplitude of the incident shock wave was approximately 83 kPa and resulted in greater ICP than the external environment. A full description of the methods of the study are available in the reference (Zhu et al. 2010).

The results of the simulations provided theoretical ICP at different locations in the brain, including the anterior and posterior sections. In Figure 3.11, an example of how these theoretical pressures develop was provided. Contrecoup pressurization was observed in the posterior region. The greatest levels of shear stress were observed in the brain region just below to the superior brain case. The authors concluded that the response of the rat head was more sensitive to peak overpressure than impulse.

The authors described the origin of the pressure oscillations in the brain to be the result of “complicated wave interactions taking place at the two boundaries (anterior and posterior)”. This suggests that the pressure oscillations in the brain would be the result

of the reflections of an internal stress wave. One of the major assumptions in the model was that the skull was a solid surface and descriptions of the flexural response of the skull were not included. Additionally it has been shown that measurements taken using the IC mounting technique will give results that are biased due to the modification of the frequency of oscillation of the superior brain case. In this chapter, it was discussed that the midline suture on the superior brain case may act as a hinge in which additional deformations of the skull may occur. Because the pressure oscillations associated with the DOA flexural mode were able to be modified based on the location of the sensor, to make the claim that the pressure oscillations are due to reflections of the internal stress wave may be premature until further experimental and theoretical studies determine the nature of that response.

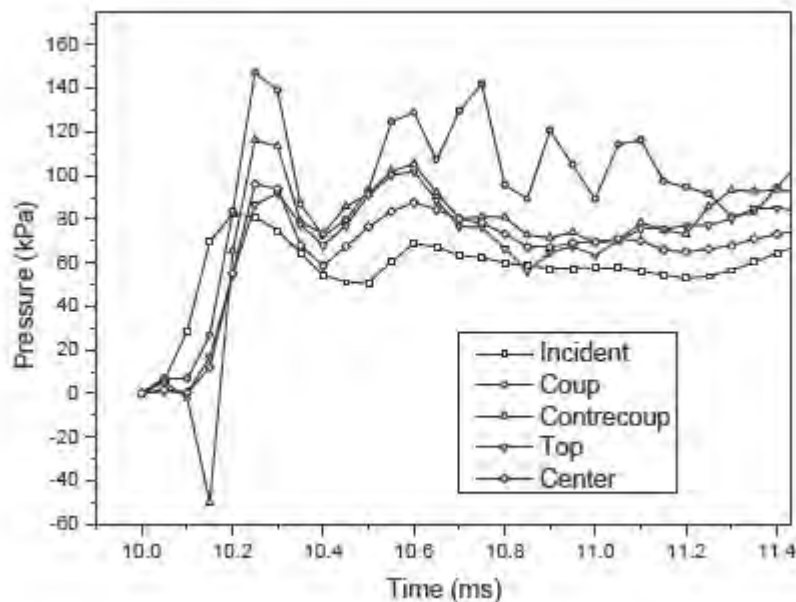


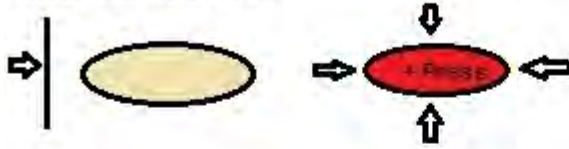
**Figure 3.11 ICP response of the FEM rat head. The data suggest that the pressures within the brain are variable with some regions greater than the incident pressure. Additionally, the contrecoup pressure measured a tensile pressure before undergoing compression. Figure taken from Zhu et al. 2010. Development of an FE model of the rat head subjected to air shock loading. Stapp car crash journal. 54: 211-225.**

### 3.13 Conclusion of rat model analysis

The biomechanical response of the rat to shock wave loading was assessed in this chapter. The data suggests that the skull flexural modes may be the major factor in developing intracranial pressures in this model. The strain and ICP data both support this hypothesis. Analysis of the strain data allowed for the identification of three flexural modes. The first mode was a damped oscillatory axisymmetric (DOA) mode, similar to the breathing or whipping mode described by Kwon and Fox (1993) in chapter 2. This mode responds similarly to a damped harmonic oscillator, where it has been shown that by modifying the superior braincase, the frequency of the DOA mode will change, altering the dynamic response of the system. The second mode was a quasi-steady compression that mirrored the loading from the shock wave. Both of these modes were shown to have an effect on the intracranial pressure response. The third mode identified in the strain records did not appear in the ICP records and is believed to be a result of shifting of the skull plates which the strain gages were mounted. Based on the observed modes in the rat, a diagram of the flexural modes and pressure responses of interest is provided in Figure 3.12. The conclusion from this chapter is that the pressure environment within the rat brain can be explained by the multi-modal skull flexure hypothesis.

## Flexural Modes and Pressure Responses in the Rat

Quasi-Steady Compression(QSC): Skull is globally compressed by external shock wave-raises ICP



Damped Oscillation Axisymmetric (DOA) mode: Skull is loaded by shock wave, regions such as superior brain case deflect to greater degree- system oscillates and returns to resting energy

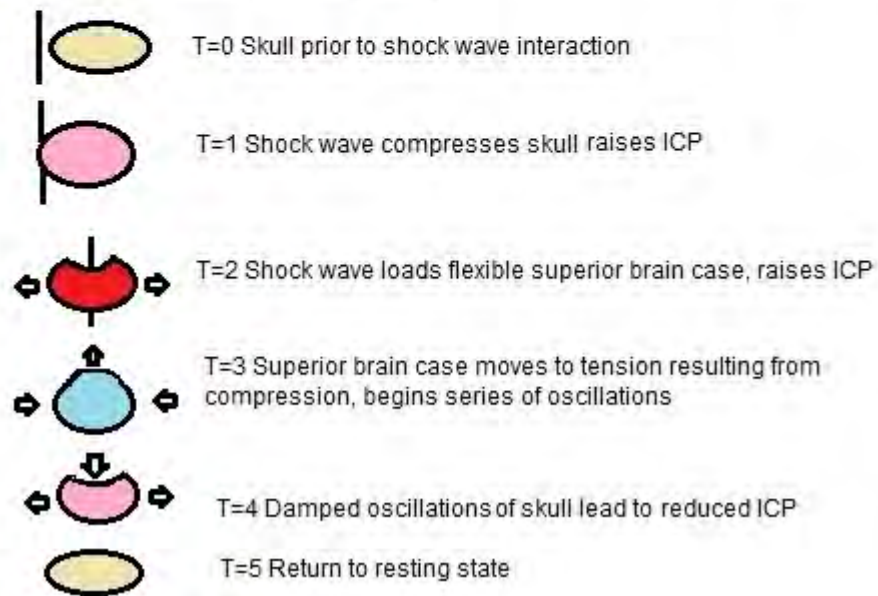


Figure 3.12 Flexural modes of the rat skull affecting ICP response.

## CHAPTER 4 PIG MODEL OF BLAST BIOMECHANICS

### 4.1 The pig in blast research

The pig model has been previously utilized in blast injury related research. This species is not used as extensively as the rat in blast research because it is relatively large, expensive, and larger shock tubes are required to properly conduct experiments. These conditions cause pig sample sizes to decrease for a given study. Despite these issues, the pig model has continued to be tested because its organs are more human like anatomically than other animal models used in blast research. Because the pig is used in blast research, it is important that studies assessing biomechanical responses take place. In one study, fiber optic pressure sensors were placed in the brain to measure ICP changes during the shock wave exposure (Bauman et al. 2009).

**Table 4.1 A sample of blast research involving the pig model. The method of creating the shock wave, area of body exposed, number of specimens tested, measurement techniques applied, and rationale are all provided. S/W = shock wave, A/R = assault rifle, U/W = under water, Phys = physiological measurements, Hist = histology of brain tissue, Acc = Acceleration.**

Researcher	S/W creation	Areas exposed	Number	Measurement	Purpose
Axelsson et al., 2000	Explosion: Free-field	Total Body	10	Phys	Resp., circ., and brain activity changes from blast
Saljo et al., 2008	Shock tube, Howitzer, A/R, U/W	Head / Abdomen/ Total body	115	Acc., ICP, Hist.	Damage caused by different initiators of shock waves
Bauman et al., 2009	Blast tube, Explosion: HUMVEE/ Building	Head / Total Body	175	ICP, Hist., Angio, ECG, EEG	Response changes across environments
Garner et al., 2009	Explosion: Free-field	Total Body	18	Hemorrhage, Phys.	Pathology of Blast + Hemorrhage
Phillips et al., 1989	Explosion: Armored Vehicle	Total Body	~67	Anatomy, Phys.	Complex Wave / Ear Injury

Without biomechanical data for both skull strain and ICP, it is difficult to develop a hypothesis that addresses how a pig brain is injured from a shock wave. The purpose of this chapter was to determine if the pig brain will experience pressure responses in the brain that can be associated with the multi-modal skull flexure hypothesis. Tests measuring skull strain and ICP were undertaken to provide necessary insight into the response of this unique system. Additionally, an analysis of ICP data from real explosions with living pigs was undertaken to determine what differences can be expected between experiments conducted with just a head and a living specimen.

#### **4.2 Expected contribution of flexural modes of the pig skull when subjected to a shock wave**

The pig head differs from the human head with respect to tissue architecture. Anatomically, the pig cranial vault is considerably less than the human cranial vault with respect to total bone volume. The muzzle is considerably elongated and the superior aspect of the skull is reinforced by a thick region of trabecular bone in between the two layers of compact bone (Figure 4.1). Sun et al. (2004) measured the bone thickness of 7 month old pig specimens and found that the mean thickness for the frontal bone was approximately 12 mm (Sun et al. 2004). The approximate thickness for the adult human frontal bone is 6mm (Moreira-Gonzalez 1963). Differences in skull thickness and geometry between the human and pig allow for an analysis in which the biomechanical responses of the human head can be compared to a skull/brain system that is thicker (assumed to be an analog to stiffness) with a smaller brain mass during shock wave exposure.

It was hypothesized that flexural modes observed on the skull would be related to the ICP response. Because the pig skull is relatively thick when compared to the rat, it was expected that the ICP profile would show less dependence on the quasi-steady compression mode (QSC). At the same pressure intensity, the thicker stiffer skull should deform less under loading from the shock wave. Therefore, the largest contribution in the ICP response was hypothesized to result from the DOA mode of the transient phase of response.



**Figure 4.1** Three dimensional microCT sections of the pig skull. The brain consists of a smaller portion of the total head volume than the human.

#### **4.3 Methods for investigating biomechanical responses of the pig head when exposed to shock wave**

The testing undertaken at Wayne State University (WSU) involved five pig heads weighing between three and four kilograms. The heads were acquired from a local meat distributor and were purchased frozen and thawed prior to testing. For specimen

preparation, soft tissue was removed to allow for positioning of the sensors and for reduction of overall weight.

The scalp was removed from the skull to allow for the positioning of four three channel rosette strain gages (FAER-25B-35SX, Vishay Inc). The “frontal” strain gage was mounted 16 cm posterior to the snout and approximately 1cm lateral of the midline suture. The “second frontal” was 4.5 cm posterior to and 1.5 cm lateral to the frontal sensor. The “temporal” sensor was placed in the center of the temporal bone on the left side of the head (Figure 4.2). The “occipital” sensor was placed on the occipital bone in the region with the greatest concave curvature.

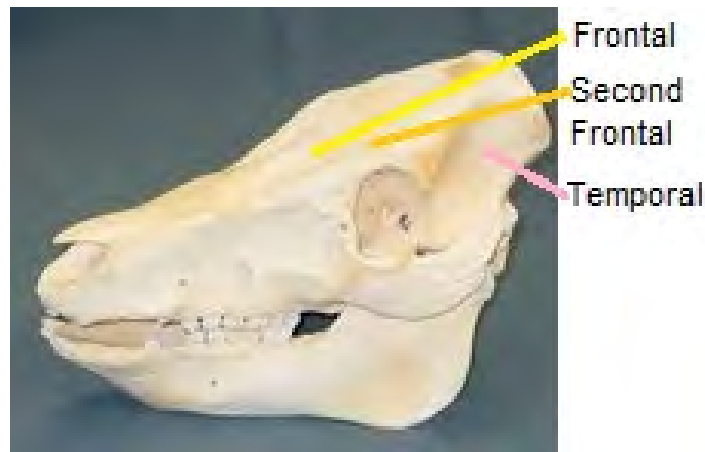


**Figure 4.2 Strain gage locations on the pig head.**

To measure intracranial pressure, a threaded insert was machined to attach the fiber optic pressure sensor (FOP-MIV, Fiso Inc) to the foramen magnum (Figure 4.3). The foramen magnum was first filled with phosphate buffer solution to pressurize the system and the insert was threaded into the base of the occipital bone. The fiber optic sensor was fed into the brain until it touched the interior brain case at the meninges, which was then retracted one centimeter. It was believed that this retraction would have

negligible effects on the overall ICP response. The brain was filled with cerebral spinal fluid and would therefore prevent any sort of cavity from forming and the overall diameter of the sensor was minimal (0.515 mm). A rubber stopper was attached to the fiber and compressed by a threaded cap. The compression fit prevented the fiber from moving (Figure 4.4). The fiber was then fed through a plastic tube to shield the fiber from the dynamic pressure that is generated within the shock tube. The insert was also held in place by cable ties if the threads loosened (Figure 4.5).

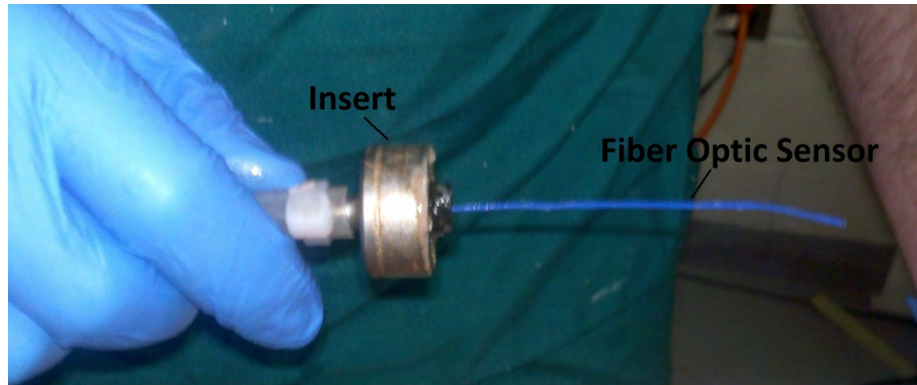


Figure 4.3 The pressure sensor fiber was secured to the pig skull at the foramen magnum.

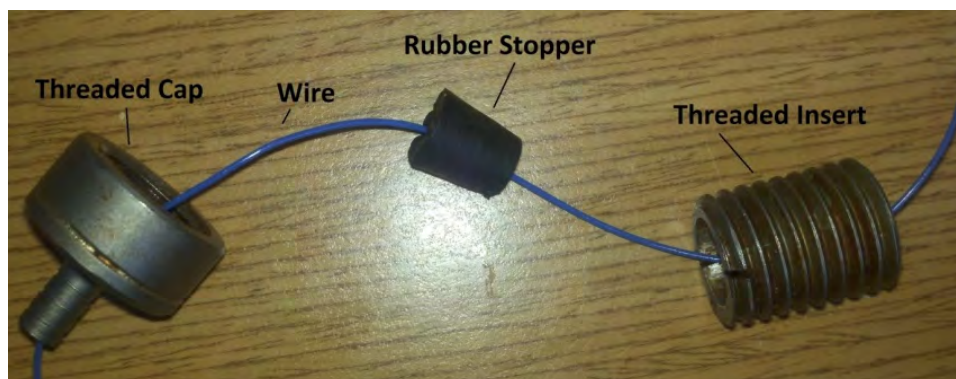
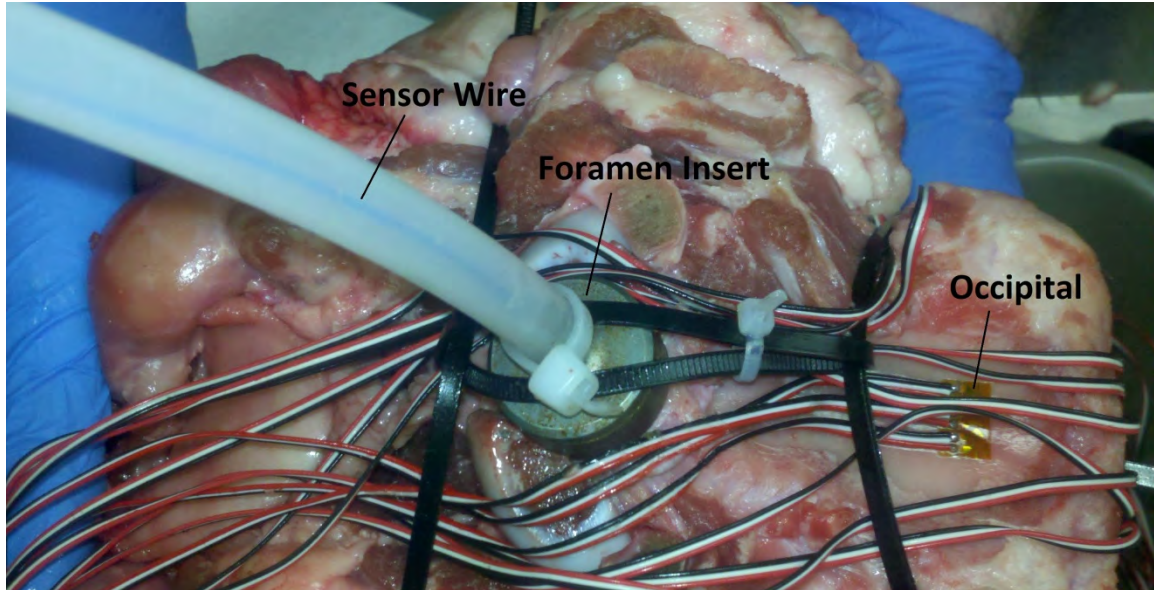


Figure 4.4 The fiber optic sensor was mounted into the skull using a threaded insert. A rubber stopper compressed the fiber and a threaded cap was used to prevent the sensor from pulling out.



**Figure 4.5** A fastening system was used to hold the insert in place. The cable ties also prevented the strain wires from whipping, causing loss of contact of the strain gages to the skull bones.

Following sensor installation, cable ties were attached to a chain that was used to hang the head within the shock tube. When the specimen was positioned, the guide protecting the pressure sensor fiber from the dynamic pressure was fed out of the shock tube through a hole at the base. The strain gage wires were secured and fed out the opening of driven end of the tube. The fiber optic pressure sensor was connected to a Veloce 50 (FISO Inc.) signal conditioning unit where the signal was then sent to the DASH HF DAQ (Astro-med Inc.) data acquisition system. The data were collected at 500 kHz. The strain data were collected at 150.943 kHz using the TDAS (DTS Inc.) data acquisition system. The data were post-processed using Diadem 11 (National Instruments Inc.).

The specimens were subjected to multiple exposures in multiple orientations (Table 4.2). Each head was tested in three orientations. The frontal orientation

subjected the muzzle to the reflected pressure loading. The side orientation exposed the temporal bone to the reflected pressure. And the back orientation exposed the occipital bone to the reflected pressure. A graphic of the three positions of the head is provided in Figure 4.6. During and following testing, the head was examined for sensor failure locations. This inspection was achieved by observing the data output and visually inspecting the gage/bone interface to determine if the sensor surface was peeling.

Individual peak maximum and minimum principal strains and peak ICP magnitudes were measured and reported in Appendix B for all trials. The time series data was included for each sensor at each location at the low pressure intensity to provide an example of how each region of the skull surface and ICP in the frontal lobe responded to shock wave exposure. The lowest intensity provided the most consistent results due to less sensor failure. The peak ICP was compared between specimens and orientation using an ANOVA with a post hoc Tukey HSD test (significance set at \*  $p < 0.05$ ). The frequency of the oscillations associated with the DOA mode of skull flexure were also calculated using simple waveform analysis (number of cycles / change in time) and compared by orientation using the same ANOVA procedures as the pressure analyses.

**Table 4.2 Protocol for a pig specimen exposed to multiple shock waves.**

<b>Incident Pressure</b>	<b>Front Position (exposures)</b>	<b>Side Position (exposures)</b>	<b>Back Position (exposures)</b>
<b>69 (kPa)</b>	3	3	3
<b>120 (kPa)</b>	1	1	1

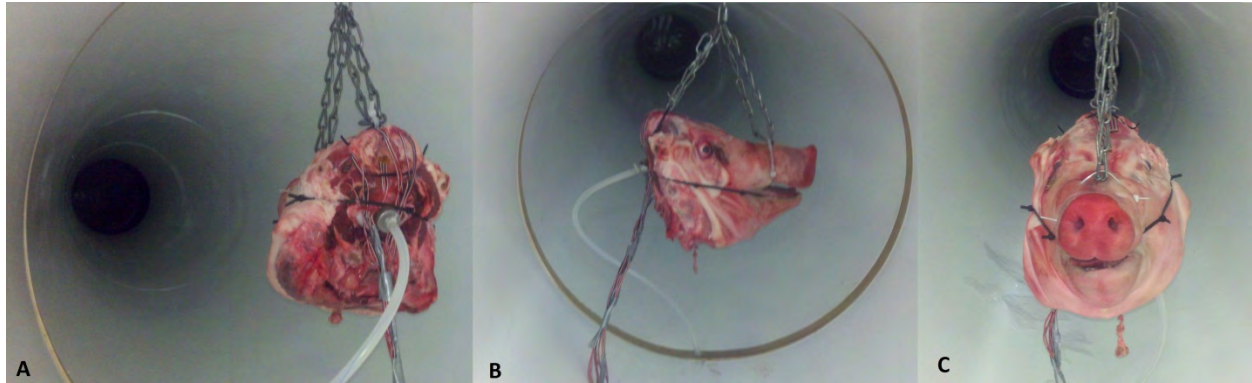


**Figure 4.6** The pig was positioned in three orientations. (A) Front (B) Side (C) Back.

#### **4.4 ICP response for Pig 1**

The degree in which ICP develops is partially the result of coupling of the intracranial contents to the skull. Pig 1 was left out of the cooler overnight prior to testing. During the night the brain collapsed within the brain case. Despite the collapsed brain, the braincase was filled with artificial cerebral spinal fluid and sealed. Initial tests within the shock tube failed to produce significant pressure responses within the brain. The strain data were collected from these tests and the brain was removed. The head was then filled with a two part gelatin and allowed to cure overnight. The following morning, a second series of tests were conducted. The magnitude of the pressure responses within the gelatin filled cavity was higher, but the response still appeared to be minimal. Post examination results found that the mixture had barely cured and as a result the brain simulant was actually a viscous liquid. Subsequent experiments with additional pigs had a greater degree of coupling to the interior skull case due to the intact brain and meninges, which resulted in significantly greater ICP at similar incident shock wave intensities.

This observation can be used to further validate the multi-modal skull flexure hypothesis. The experiment demonstrated that a decoupled system (relative to the skull/brain interface) will transmit less energy from the shell layer. The transmission phenomenon has been addressed prior, but not for the pig skull/brain boundary.

#### **4.5 Skull strain response of the pig head to shock wave exposure**

The calculation of maximum and minimum principal strains was undertaken for each rosette gage set at each location on the head. In these series of tests, the sensors remained intact for the duration of testing for most experiments. For example, the interface between one gage of the occipital rosette and the skull weakened and biased results (Fig 5).

Similar to the rat, the strain responses for the pig subjects were consistent within subjects and relationships could be demonstrated between subjects. The response of the skull was dependent on location and orientation. The individual strain channels, along with the maximum and minimum principal strains, were useful for describing these responses.

One issue that was believed to induce some variability between the strain responses was the amount of adhesive that was used to hold the sensor in place. Too much adhesive may mitigate strain on the sensor or cause it to measure artifacts associated with the mounting. Too little adhesive may cause premature failure of the sensor.

The peak maximum and minimum principal strain magnitudes are summarized in Table 4.3. The quartile distributions for the principal strains were grouped by sensor and location. As discussed prior, the amount of adhesive between the gages and skull

surface will affect the outputted results. This will cause skewness in the data that would bias the mean response. Therefore it was more appropriate to determine where the central tendency in the data occurred by using quartiles to determine if the data was skewed high, low, or was balanced. For example, the 75% quartile for a front facing frontal sensor was 701 microstrain where the median and 25% were within the hundreds. This meant the data was skewed low with some outliers with greater magnitudes. Trends can be observed in the data: The frontal rosette reported greater strains than the second frontal rosette and in some cases the minimum principal strains were greater than the respective maximum principal strains.

**Table 4.3 Distribution summary of max (p) and min (q) principal strain results by sensor and orientation.**

Sensor	Orientation	N	$\epsilon_p$ 25%	$\epsilon_p$ 50%	$\epsilon_p$ 75%	$\epsilon_q$ 25%	$\epsilon_q$ 50%	$\epsilon_q$ 75%
Frontal	Front	10	113	131	701	90	125	352
2 Frontal	Front	10	85	99	141	58	126	205
Occipital	Front	10	164	175	199	81	85	228
Temporal	Front	10	54	62	214	57	90	167
Frontal	Side	10	159	191	574	73	84	240
2 Frontal	Side	10	92	233	385	86	147	417
Occipital	Side	10	115	134	164	34	53	384
Temporal	Side	10	56	100	372	86	193	222
Frontal	Back	10	100	142	440	90	105	235
2 Frontal	Back	10	76	121	158	93	107	142
Occipital	Back	8	154	165	190	98	107	120
Temporal	Back	8	68	81	97	27	59	94

#### 4.6 ICP responses of the WSU pigs

The intracranial pressure response of the pig head was measured in the frontal lobe. In all specimens there was a transient component and a quasi-steady component. All ICP values were less than the magnitude of the incident shock wave. Each head was exposed to shock waves in three orientations; front, side, and back. When the head

was facing front the pressure in the frontal lobe was initially compressive. The side and back facing head would initially undergo a tensile response.

The ICP differences were significantly different between pig 1 and the other specimens for the reason described earlier (collapsed brain/viscous fluid surrogate). ICP was not significantly different between specimens 2-5; it was significantly different between orientations. Each orientation was significantly different from each other (\*  $p < 0.05$ ,  $p < 0.0001$ ) (Table 4.4). The front facing head reported the highest magnitudes and the back facing reported the lowest.

A series of oscillations associated with the transient phase, possibly associated with the DOA flexural mode, was observed. Frequency of oscillation was determined using simple waveform analysis. It was determined that there was no significant difference between these oscillations and orientation. The grand mean was 1055 Hz with a standard deviation of 272 Hz ( $p=0.648$ ).

**Table 4.4 Summary statistics of ICP response between specimens at each orientation for the low pressure intensity.**

Orientation	N	Mean (kPa)	SD (kPa)
Front	10	51	13
Side	11	36	6
Back	11	31	5

#### **4.7 Relationship between skull strain and ICP for WSU pigs**

Skull strain was shown to be similar to the ICP response within the brain. Within each response profile, elements of the flexural modes described in chapter 2 were observed. The three hypothesized modes of response were; a damped oscillation axisymmetric (DOA) response mode, a high frequency low amplitude (HFLA) response

mode, and a quasi-steady compression (QSC). These responses were used to describe the pig results.

For the pig, both maximum and minimum principal strains were important for describing the ICP response. In Figure 4.7, the max and min principal strains and ICP response are provided for a front facing pig. In the following figures, for strain, tension is positive and compression is negative. For this figure, the min principal strain response trace approximated the ICP response to a great degree. The max principal strain response also approximated the ICP response following an initial compression. The greatest peaks in ICP resulted when both the max and min principal strains had the same shape when in tension. Following an initial increase in ICP, there were a series of large oscillations associated with the DOA mode, a series of higher frequency oscillations associated with the HFLA mode, and a mild global compression.

The strain and ICP responses for the same specimen during a side facing exposure are provided in Figure 4.8. For this series, it was shown that the large oscillations associated with the DOA flexural mode occurred when the max and min principal strains oscillated in union. The initial transient ICP response was similar to the min principal strain response.

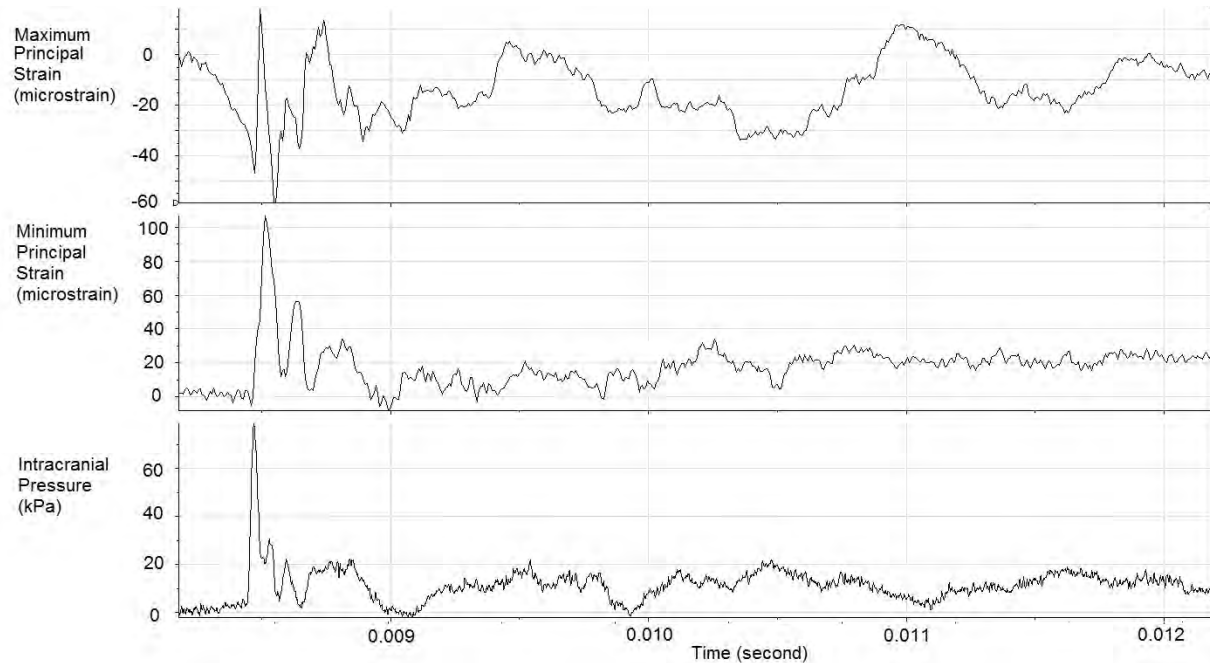


**Figure 4.7** The ICP response was dependent on skull flexure as measured by strain gages (Second Frontal). When the max and min principal strain responses moved in unison the greatest ICPs were measured (when in tension). Especially within the first millisecond. (Pig subject 5, 69 kPa incident pressure, front facing).

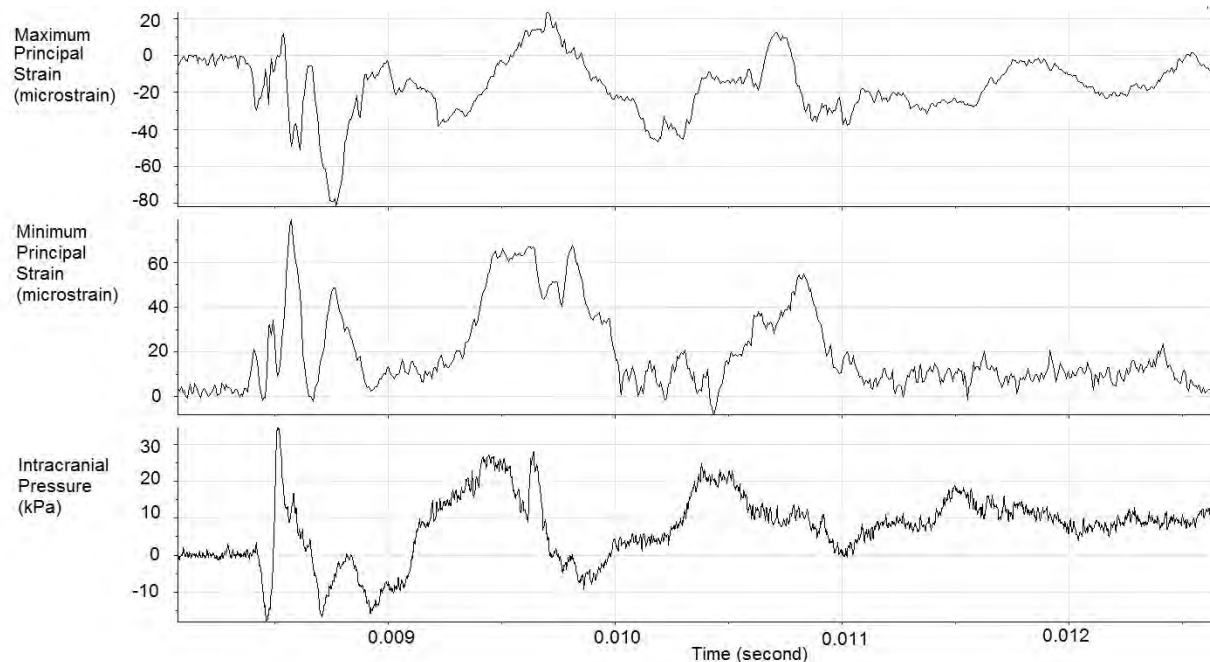


**Figure 4.8** The large oscillations associated with the DOA flexural mode were observed in the brain when the max and min principal strains oscillated in unison. Oscillation peaks in the pressure response were observed when max and min principal strain were both in peak tension. (Pig subject 5, 69 kPa incident pressure, side facing).

For the same pig, when back facing, the ICP response shape was best related to the occipital strain gage Figure 4.9. When the min principal strain response would initially move into tension, the ICP response would become negative. When the max principal strain went into compression the ICP response returned to baseline, then mirrored the minimum principal strain response. An increase in ICP was associated with a global compression in the max principal strain response.

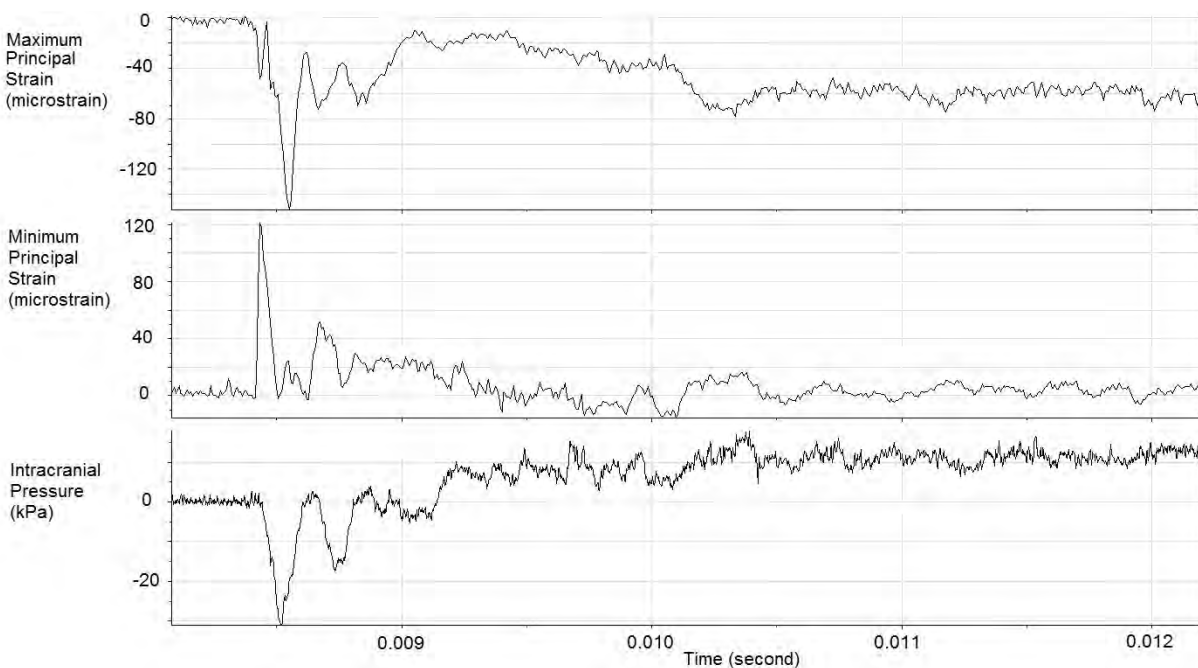


**Figure 4.9 The ICP response was similar to the transient min principal strain response. The pressurization associated with the QSC mode was related to the max principal strain response. (Pig subject 5, 69 kPa Incident).**

#### 4.8 Relationship between principal strain and ICP

In this series of experiments the relationship between skull flexure (as measured by strain) and ICP was investigated. The experiments that were undertaken isolated the mounting of the ICP sensor from any of the bones composing the skull. Because of this

novel mounting technique, the strong relationship between skull flexure and the ICP response does not appear to be an artifact of the mount.

For the pig, the min principal strain response showed the most similarities to the ICP response. On a surface such as a bone, the three strain gages will measure the strain in the direction in which they are adhered to the surface. The strain on a surface can be described by its normal strains and shear strains. Therefore each of the three sensors will measure some combination of shear strains. The principal strain calculations are used separate out the shear strains into their two principal components. The max principal strain is the normal strain in one direction on the surface (usually x) and the min is the normal strain in the other direction of the surface.

It was shown that when the front facing and side facing pig was exposed to the incident shock, the time points in which the ICP had the highest magnitudes were when the max and min principal strains were oscillating in union, and the peaks were in tension. Physically this suggested that pressure was the greatest in the brain when the bone was bowing out. In the rat, it was shown that the ICP was greatest when the bone was in compression. It is hypothesized that the reason for this discrepancy was the result of axially compressing the bones of the skull, which will then cause the bones to bow out. It is expected that there would be a symmetric effect where if the external layer of compact bone was bowing out, the inner layer of compact bone would also bow out, raising ICP (Figure 4.10).

For the back facing pig head, the response appeared to be reversed. The tension reported by the min principal strain best approximated the ICP response, but, ICP began in tension and each peak of the oscillation in tension corresponded to the

tension peaks in the min principal strain response. This ICP response was believed to be caused by a different mechanism.

The occipital bone is a concave surface. It is hypothesized that the shock wave will act as a planar wave and when the wave is focused by the surface, it will reflect as a circular wave. The point at which this wave focuses will result in a tension wave on the surface then a compression and subsequent oscillations. Because the loading taking place in this orientation is not compressive to the long axis of the occipital bone, but to the surface, the tension on the bone could be described as a “pulling” against the brain case, reducing ICP (Figure 4.11).

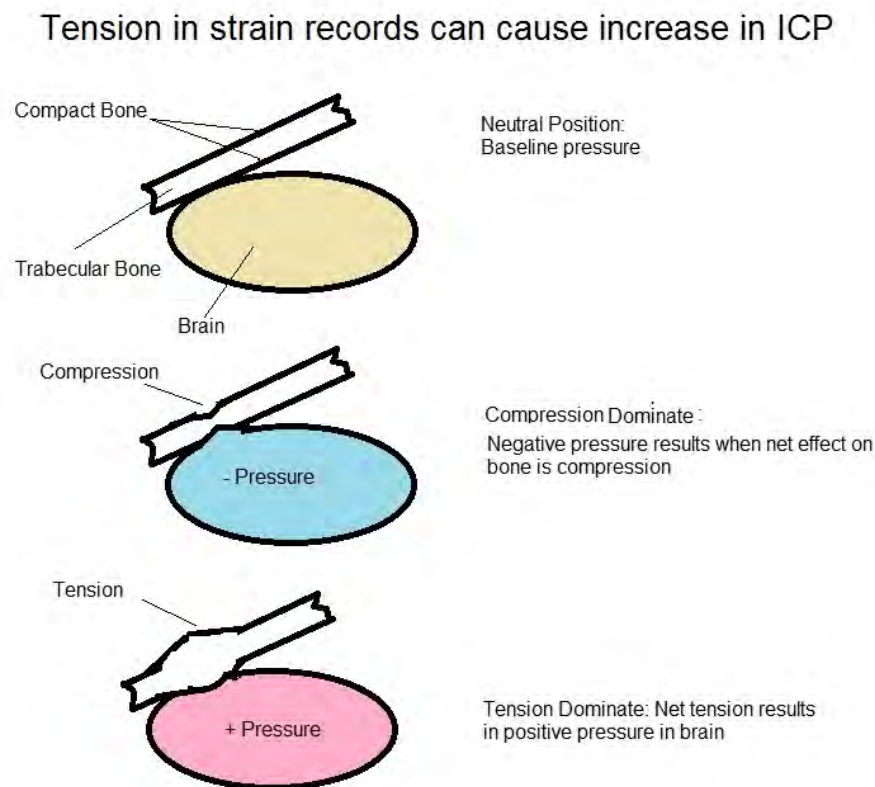


**Figure 4.10** An increase in ICP may result from axial compression of the long axis of the bone. The compression will cause the surface of the bone to symmetrically bow out, raising ICP

### ICP response resulting from shock wave interaction with concave surface

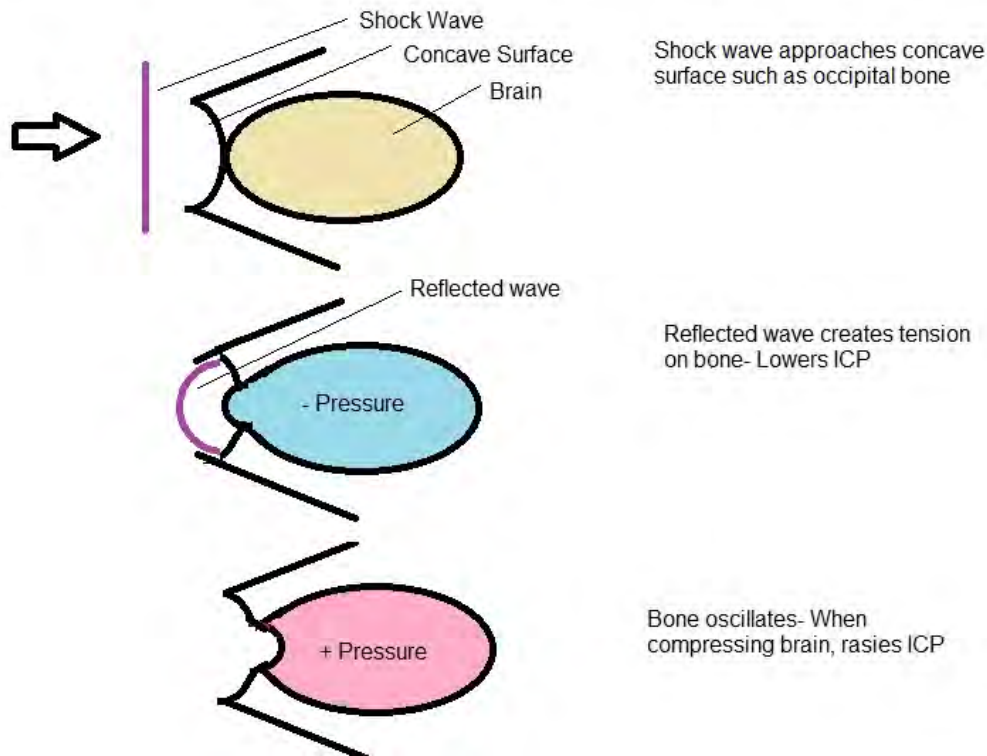


**Figure 4.11** It is hypothesized that reflecting phenomena on the surface of the occipital bone can cause changes to the ICP response within the brain.

#### 4.9 ICP response of pig compared to simplified physical models

Depending on the specimen tested, the ICP response would either present as shown in the previous figures, or with the development of a secondary rise in ICP that would appear to result from the QSC mode. An example of the differences in response is provided in Figure 4.12.

An explanation for the differences in response can be related to a simplified physical model study discussed in chapter 2. In that study a thin (7mm) shelled sphere with a gelatin core was exposed to shock waves within a shock tube. One of the

variables assessed was the effect of having a hole in the shell. An example of this response is provided in Figure 4.13. The completely closed spherical surface would present with a rise in intra-spherical pressure (ISP) and then follow with a series of oscillations. This mode was associated with the DOA flexural mode. For the sphere with an open hole, there would be a secondary large amplitude rise in the pressure response in the brain (blue).

The authors of the study indicate that the reason for this change in response was the result of some of the external pressure of the shock wave entering the inside of the sphere through the hole and pressurizing the environment. At this point it cannot be determined if the authors' assessment was correct. It is unlikely that there was a leak in the ICP sensor mount in the pig that would allow for this pressure to increase within the brain in such a short period of time. When this secondary pulse occurred, it was consistent in all orientations and exposures for a given specimen.

The response associated with the QSC mode could be the result of a "leak" or hole in the system, but an alternative hypothesis could be that the secondary rise in pressure may result in compression of the surface of shell layer. When a hole is introduced in a sphere the overall stiffness of the sphere will decrease. It is possible that the decreased stiffness will cause the shell to deform to a greater degree that will increase ICP. Further experiments will be required in both simplified models and pig specimens to determine the nature of this response.

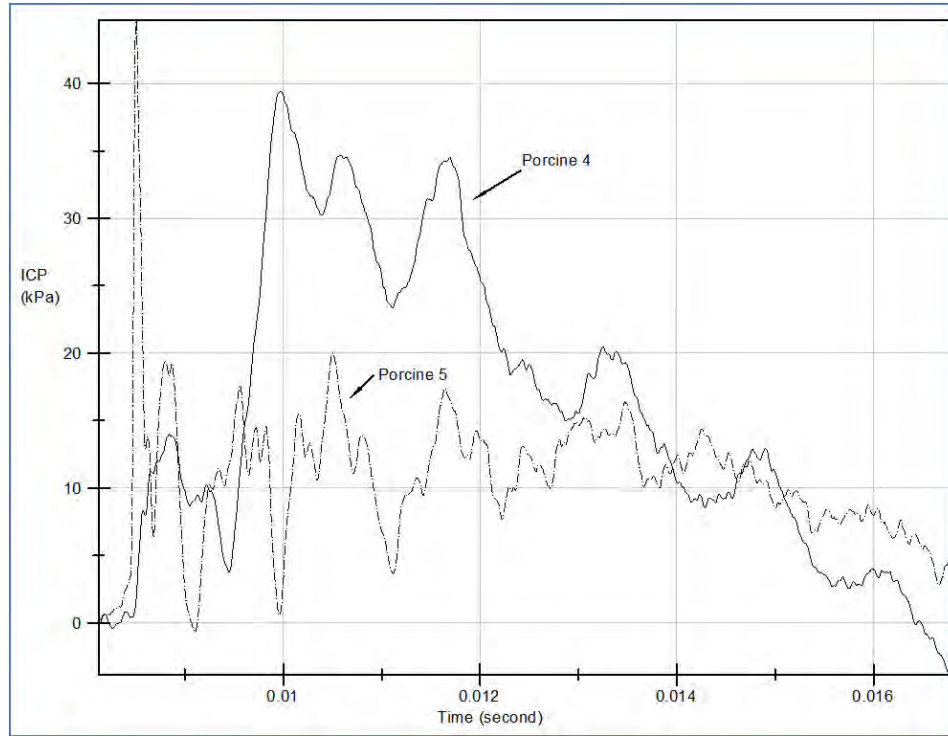


**Figure 4.12 ICP comparison of two front facing pigs. The responses are similar to the open and closed sphere results described by Mediavilla Varas et al. (2011).**

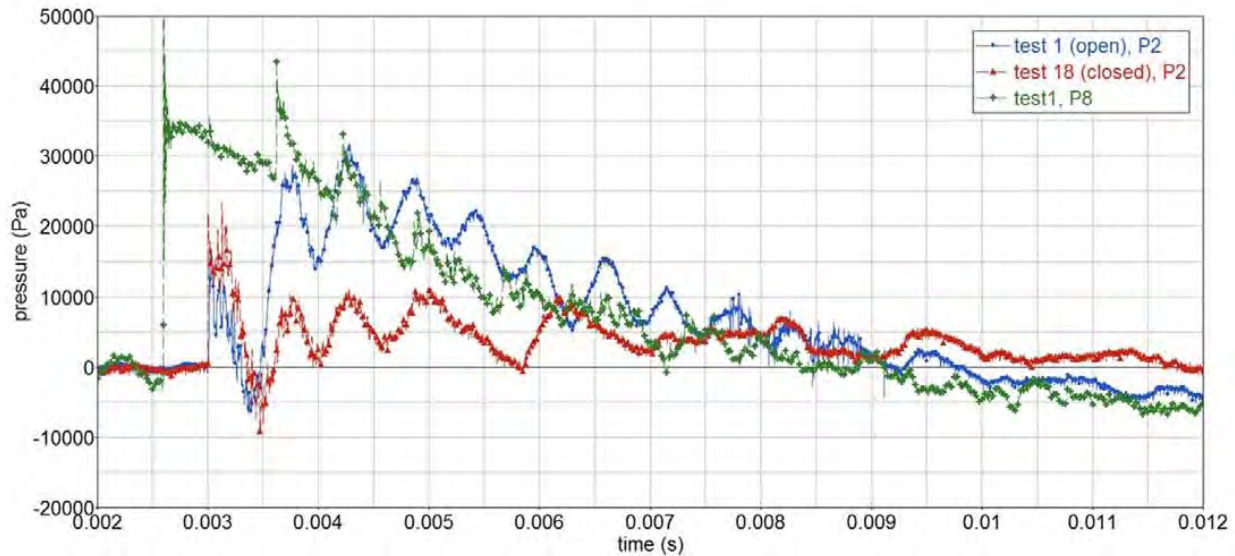


**Figure 4.13 A comparison of ICP between a 7mm sphere with a closed or open hole. Figure is taken from Mediavilla Varas et al. 2011. Physics of IED blast shock tube simulations for mTBI research. Frontiers in Neurology 2, 1-14.**

#### **4.10 Conclusion of WSU pig head testing**

The pig head was tested under multiple conditions to determine the relationship between skull flexure and ICP during shock wave exposure. The results from the testing show that there is a dependence of ICP response on skull flexure. Modes of skull flexure were observed for the strain profiles and ICP responses that would result from these flexural modes were also identified. Additionally, multiple hypotheses, based on the results, were developed to explain the processes in which these events occur.

One of the concerns with this work is that only the pig head was tested. Attempts were made to pressurize the brain, but this method is only an approximation. To further investigate the ICP response of the pig, it was necessary to investigate the ICP response of the living pig. Such experiments were undertaken in the DARPA PREVENT Phase 1 experiments. The ICP response data during blast wave exposure was made available to Wayne State University, an analysis of the data was undertaken.

#### **4.11 Methods from PREVENT series of tests**

As a supplement to the pig biomechanics studies undertaken at WSU, pig experimental data were obtained from ORA Inc. This biomechanics data was a part of the Phase 1 PREVENT study. In this study, 3 month old (n=16) Yorkshire pigs (40-50 kg) were each exposed to a single blast wave resulting from an explosive detonation. The pigs were anesthetized with a mixture of acepromazine (2 mg/kg) and midazolam (1 mg/kg) and maintained on 1-2% isoflourane.

The explosive driven blast tube consisted 0.0762 m thick metal piping with a 2.8343 m by 0.8636 m driver, a 3.048 m expansion section, and a 15.24 m by 1.8034 m test section. An uncased charge was hung in the driver chamber, and as a result of the

explosion, a blast wave propagated to the test section where the pig was supported. The pig itself was held in a sling within the test section between 4.3 m and 7.3 m from the charge (Figure 4.14).

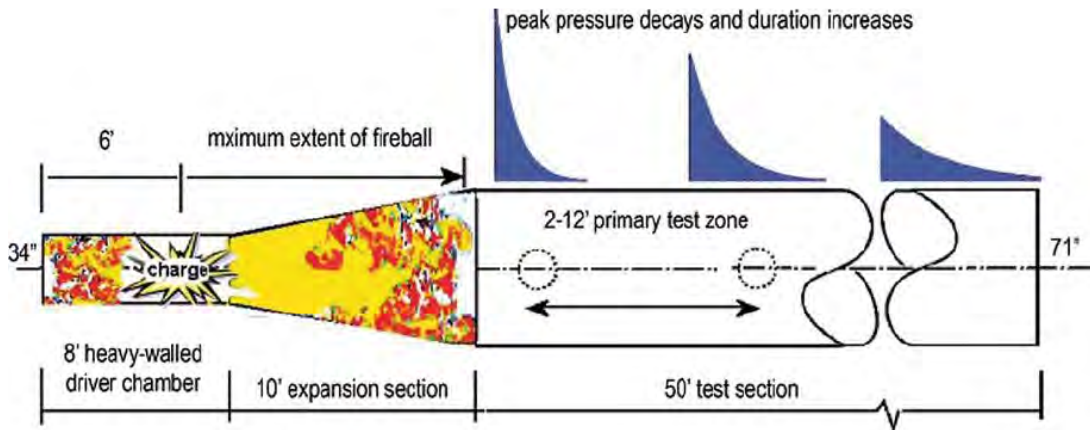


**Figure 4.14** The blast tube used for the PREVENT studies (Bauman et al. 2009).

To measure ICP, four pressure sensors (FOP-MIV, FISO Inc.) were placed in the brain. An acrylic mount was fabricated that attached to the skull at the parietal bones across the midline suture (Figure 4.15). Within this mount there were four flexible tubes that were able to house the sensors. Holes were drilled into the skull so that these housings reached into the brain tissue so that ICP gradients could be measured. The hole pattern was designed so that three pressure sensors would be axially aligned rostral to caudal (names: rostral, medial, and caudal) with a fourth sensor symmetric to the medial sensor about the midline suture (medial 2). The sensors were placed one centimeter below the dura.

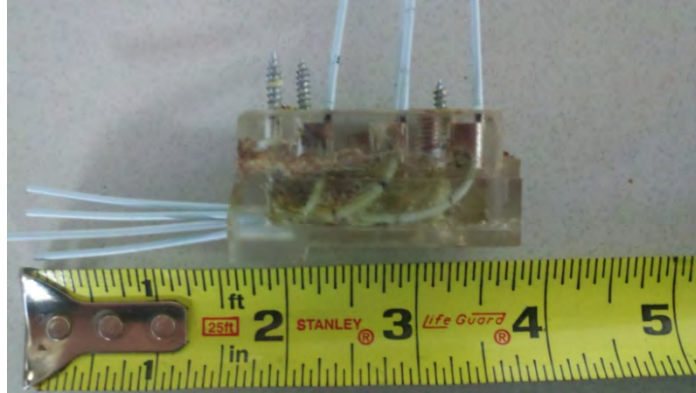


**Figure 4.15** A graphic of the acrylic block that was mounted to the skull surface of the specimen. The sensors were placed one centimeter below the dura.

The mount was attached across the parietal bones. Outside of the acrylic mount the sensor fibers were covered in a leather sheath that was sutured to the midline above the spine. These fibers were then connected to plugs within an aluminum box that was held in a leather pouch that was sutured to the sacral region of the specimen (Figure 4.16). The cables were then sheathed in a metal tube that connected to the data acquisition system. A graphic of the restrained pig in the test section is provided in Figure 4.17. In some instances the pig was protected with a lead vest (Table 4.6).



**Figure 4.16** A graphic of the aluminum box where each fiber optic sensor connected and then was fed out of the protected compartment to the data acquisition system.



**Figure 4.17** The pig was supported in a canvas sling within the test section. The graphic is facing the explosive end of the tube and the pencil probe can be observed above the support shaft.

In addition to the measurement of ICP, fiber optic sensors were placed in other regions of the body to measure pressure gradients in those locations. The locations included the jugular vein, the Inferior vena cava, the left ventricle, the common carotid artery, and the thoracic aorta. Up to three of these locations were hooked up at any given time, and during some events the ICP was measured exclusively. A table describing the series of events is provided (Table 4.5).

Following exposure the animals were euthanized. The pressure data were collected using Labview (National Instruments Inc.) and each channel was collected at 1 mHz for 5 seconds. The data were then post processed using both Matlab (Mathworks Inc.) and Diadem (National Instruments Inc.), where the data were truncated and disjointed signals were corrected. The useable data were then analyzed in terms of peak magnitude and arrival of pressure waves relative to different locations in the body.

**Table 4.5 A summary of the data collected from the PREVENT Phase 1 biomechanical studies. ICP= all fiber optic sensors in the brain, c = carotid, IVC= inferior vena cava, Cis= cisterna, TA= Thoracic Aorta, J= jugular, V= ventricle.**

<b>Pig ID</b>	<b>Weight (kg)</b>	<b>Sensor Locations</b>
30308	53	ICP
30508	56	ICP
30608	48	ICP, C, IVC, Cis
31108	49	ICP, C, IVC
31208	48	ICP, TA, J
31708	49	ICP, V, C, IVC
40308	49	ICP, J, V, TA
31408	50	ICP, V, TA, J
31908	47	ICP, V, C, IVC
32108	52	ICP, V, TA, J
32408	54	V, C
32608	54	ICP, V, J, TA
40108	n/a	ICP, J, V, TA
22808	n/a	ICP, V, J, IVC

#### **4.12 ICP response results from PREVENT biomechanics data set**

Based on the nature of the testing, there were a significant number of sensor failures. Laboratory experience suggests that the erroneous pressure profiles resulted from excessive strain on the fibers. The dynamic pressure associated with the blast wave may have been what had caused the sensors to fail. The pressure trace of each sensor for each experiment was evaluated; those that could be modified to create a useable pressure trace were changed. A summary of an evaluation of the data was provided in Table 4.6.

**Table 4.6 Channel assessment of the ICP data from the PREVENT Phase 1 biomechanics study.  
Pencil pressure in psi.**

PREVENT	Data analysis		Blast tube exposures								
	Pig#	Protected	Pencil	Rostral	Medial	Caudal	Medial2	Jugular/Carotid	Ventricle	Thoraorta/IVC	
22808	n		50	Yellow							
30308	n		31	Green			Blue				
30508	n		42	Yellow			Red	Blue			
30608	n		42	Yellow							
31108	n		38	Yellow							
31208	n		39	Yellow							
31408	p		32	Yellow							
31708	p		40	Yellow		Red		Green	Red	Green	
f31908	p		40	Purple							
f031908	p		40	Yellow			Green	Yellow	Green		
32108	p		35	Yellow							
32408	p		25	Red							
32608	n		25	Purple							
f32608	n		25	Yellow			Green	Yellow	Green		
40108	p		24	Purple							
f040108	p		24	Green						Red	
40308	p		23	Purple							
f040308	p		23	Green			Yellow	Green			
Legend											
			Not included								
			Not useable								
			Cautionary								
			Good for amplitude and rise time								
			Disconnects were corrected for some channels and these events were included to be used as a comparison								

There were five experiments that had associated pressure profiles that were used to interpret the ICP response during blast wave exposure. The rise time to peak pressure is longer for ICP when compared to the incident shock wave as measured by the pencil sensor (which is an artifact of the time in which it takes the shock front to diffract across the sensing surface). The actual rise time of the shock front is approximately one millisecond. Depending on the specimen, the ICP responses were either of higher or lower magnitudes than the external incident shock wave. It has not been determined if this inconsistency was the result of an instrumentation artifact or was

the result of a property inherent in the pig being tested. Despite the concerns associated with the amount of sensor failure, two observations were made. The first observation was that pressure gradients associated with external shock wave loading formed within the brain. The second observation involved the response of the vessels of the neck and thorax during the exposure.

#### **4.13 ICP responses from PREVENT pigs**

Overall, the ICP results were difficult to interpret due to artifacts in the signals. Multiple shock reflections were measured by the pencil sensor (Figure 4.18, Figure 4.19, and Figure 4.20 ). These reflections did not show up in the ICP pressure traces and were not assumed to be interacting with the head.

The ICP response appeared to be dominated by the quasi-steady compression flexural mode. The ICP would increase to a peak and then decay similar to the external shock wave, although the response was of shorter duration. For experiments where the medial 2 pressure sensor reported reliable results, lower amplitude than the three other sensors on the contralateral side of the midline suture would be recorded (Figure 4.1, Figure 4.22).

Beyond these observations, the utility of the data are limited. But the data do show a dominate mode of response that was not as dominate in the WSU pig tests. Unfortunately the nature of the responses occurring in the PREVENT tests will have to be repeated to collect data that is consistent across specimens, assuming that a response is consistent across specimens. The large differences in peak amplitude across species and large number of sensor disconnects are grounds for this observation.

#### **4.14 Pressure in the major vessels during blast wave exposure**

The PREVENT data were most useful for describing the response of the major vessels in the neck and thorax during shock wave exposure. These data show that a pressure pulse does develop in the thorax, but there exists a significant delay in the formation of this pulse in compression to that observed in the brain (ranging from 1-5 ms). The rise time was much longer for the pressure rise in the thorax, and the pulse shape resembled a half sinusoid response. There was no evidence of this pulse pressurizing the brain, which refutes the thoracic compression hypothesis of brain injury during blast wave exposure.

Generally speaking, when the shock wave interacted with the pig subject, the pressure vessels in the neck experienced a rise in pressure at the same time as the brain or earlier. Therefore, it cannot be ruled out that there may be some sort of pressure effect taking place at the boundary between the neck and the head. While it would not be the fluid within the vessels of the neck that are pressurizing the brain, an alternative hypothesis would be that the boundary at the foramen magnum could be pressurized; altering the way the ICP develops. In chapter 5, a discussion of how altering this boundary condition will alter the ICP gradients within the cadaver is included.

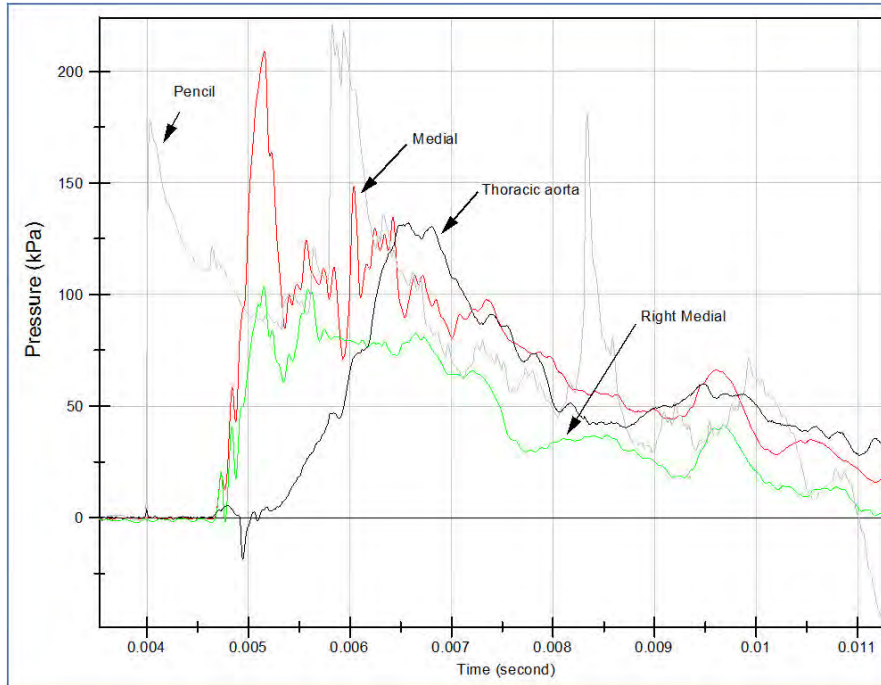


Figure 4.18 The ICP and pressure response in the thoracic aorta for pig 032608. Multiple shock reflections were observed in the pencil response.

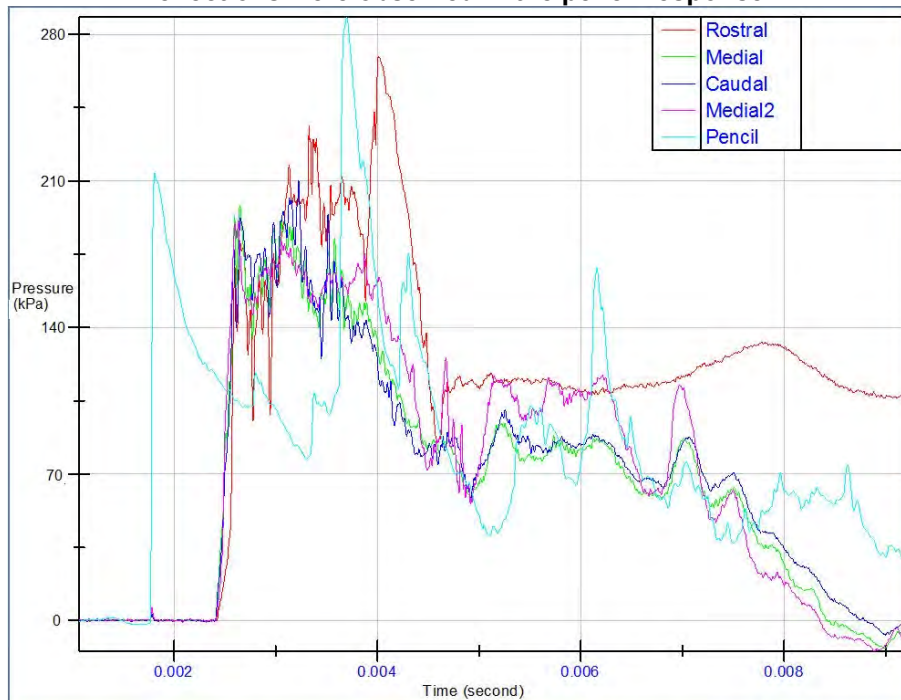
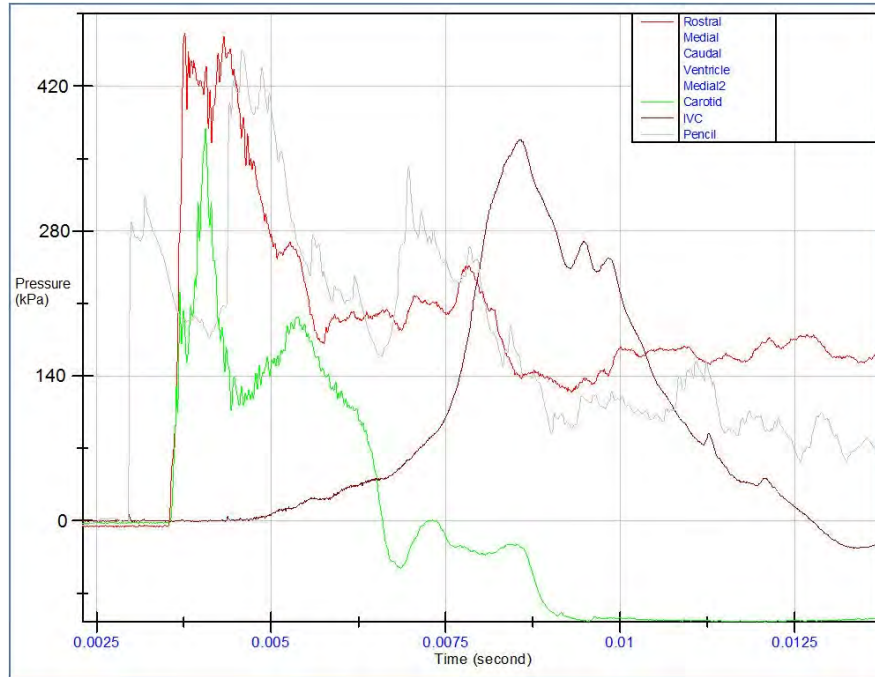
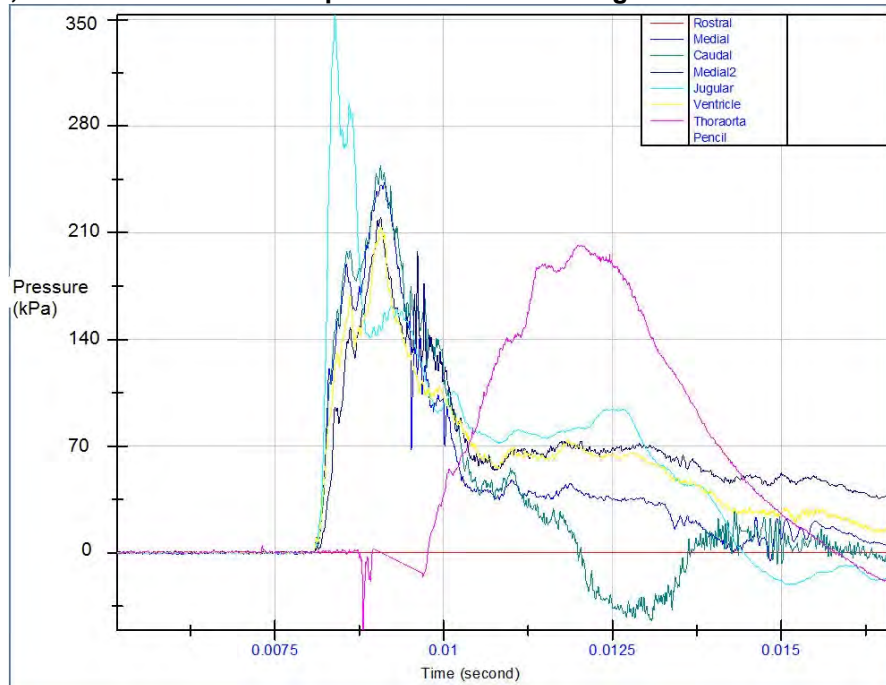


Figure 4.19 The ICP response for pig 030308.



**Figure 4.20** The pressure response for pig 031708. The inferior vena cava was pressurized at a later time, and the rise time of the pressurization was longer than for the ICP responses.



**Figure 4.21** The ICP response for pig 040308. The rise time of the jugular was similar to the ICP responses. The thoracic aorta was pressurized at a later point with an associated longer rise time.

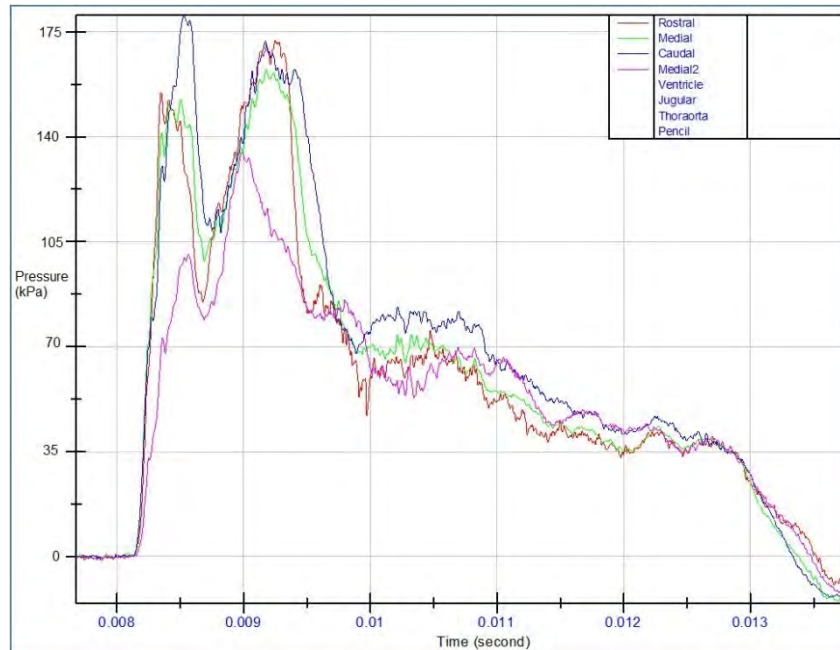


**Figure 4.22** The ICP response for pig 040108. These pressure traces showed a rise in pressure, a decline, and a secondary rise that then decayed.

#### 4.15 Comparison between PREVENT and WSU pig results

Both studies discussed in this chapter were useful for describing the response of the pig head to shock wave exposure. The WSU study investigated the relationship between skull flexure and ICP of pig heads in multiple orientations. The PREVENT study measured ICP in a living pig during shock wave exposure. The magnitudes of the incident shock waves were higher in the PREVENT study and the pigs were younger (3 months). The WSU pigs were at least 7 months old. Sun et al. (2002) measured the differences in skull thickness between pigs of different ages. The three month old Yorkshire pig will have a skull thickness of 4.2 mm where the 7 month old will have a skull thickness of 12 mm. Therefore it is probable that the skull thickness (as an analog for stiffness) would be greater for the pig tested at WSU. Because the magnitudes of the incident shock wave were greater for the PREVENT studies, it is possible that the

thinner, less stiff skull, of the PREVENT pig, exposed to greater magnitude shock waves, would have a greater contribution of the QSC mode than the WSU pigs.

The other possibility is that the greater QSC response is the result of changing of the boundary conditions at important regions such as the foramen magnum. While attempts were made to seal and pressurize the WSU pigs, this technique cannot replicate the sealing, and possible pressurizing, for regions such as the neck achieved by testing a living system. Further testing will be required to determine the biomechanical mechanisms that affect the degree of expression of the QSC response in the pig.

It was observed that the QSC component was the most dominate mode of response on the ICP of the PREVENT pigs. To determine if other modes associated with skull flexure were observed in the pressure traces, two WSU pig ICP profiles were compared to a PREVENT pig ICP profile in . In the non-filtered ICP responses, there were oscillations imbedded that appeared to have a similar response between specimens. When filtered, the QSC component was removed. The PREVENT pig response showed a series of oscillations. The response was considerably more damped than the WSU pigs with a frequency of the first oscillation approximately 1000 Hz. The WSU frequencies were also within this regime. These data suggest that the living pig may also experience ICP gradients associated with multiple modes of skull flexure.. A 500-7000 Hz band pass filter was applied to the pressure profiles to better observe the damped oscillations hypothesized to correspond to the DOA flexural mode of the skull. This band pass was selected as it filtered out the effects of the QSC

component and also filtered out very high frequency content that was not observed to have a pattern of oscillation that could be associated with a specific flexural mode.

In the non-filtered ICP responses, there were oscillations imbedded that appeared to have a similar response between specimens. When filtered, the QSC component was removed. The PREVENT pig response showed a series of oscillations. The response was considerably more damped than the WSU pigs with a frequency of the first oscillation approximately 1000 Hz. The WSU frequencies were also within this regime. These data suggest that the living pig may also experience ICP gradients associated with multiple modes of skull flexure.

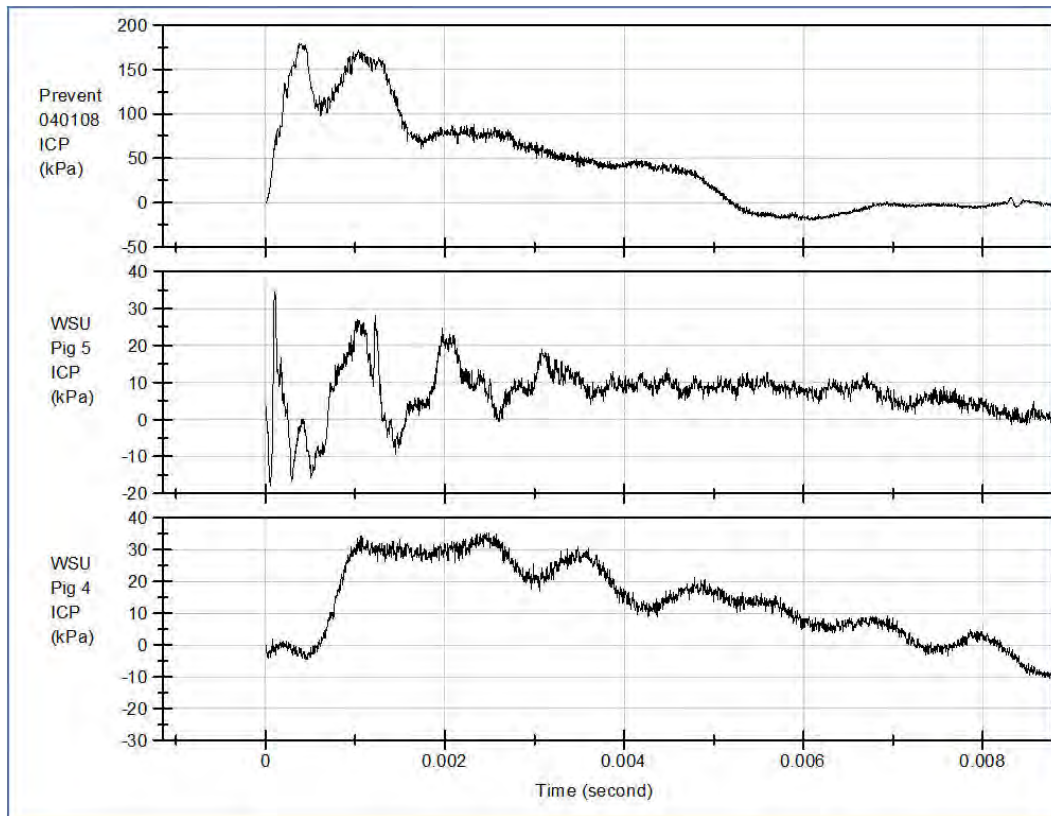


**Figure 4.23 ICP responses for PREVENT pig 0404108 (3 month old, 175 kPa incident shock wave) and WSU pigs 4 and 5 (> 7 months, 69 kPa incident shock wave). The responses were separated to observe that multiple modes of skull flexure may cause the formation of the ICP response in the pig.**

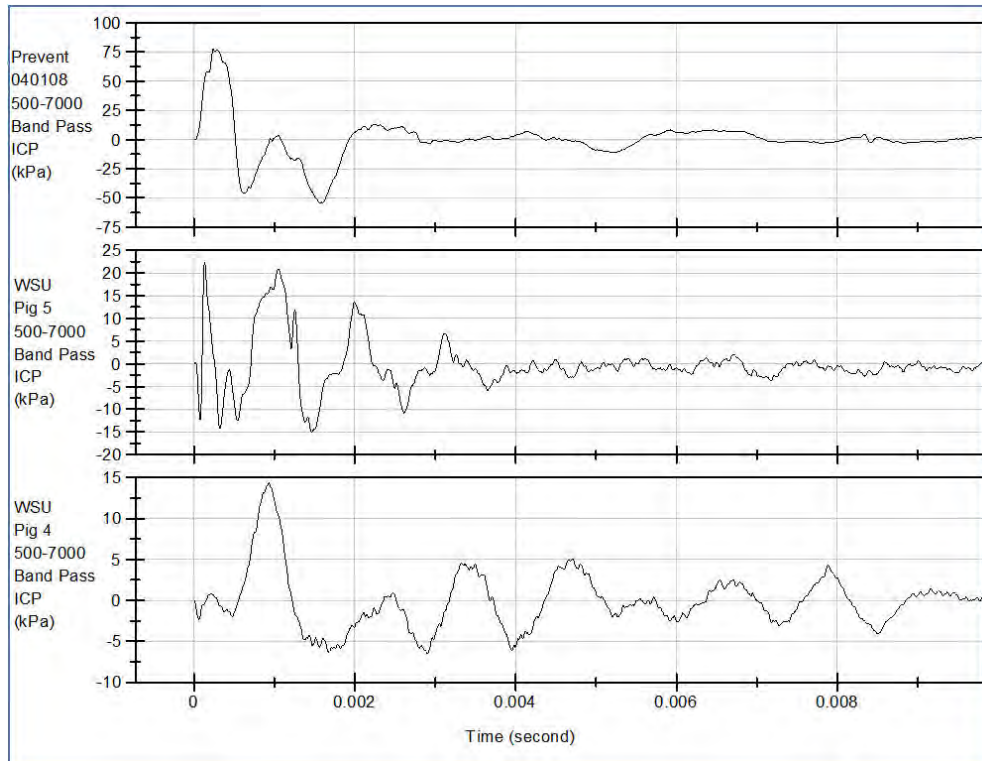


**Figure 4.24** The filtered ICP signal for the PREVENT pig subject shows an initial oscillation of approximately 1000 Hz. Similar responses to the WSU pigs were observed. This frequency band appears to be dominated by skull flexure as was shown for the WSU pigs prior.

#### 4.16 Conclusion of pig testing

In this chapter the biomechanical responses of pig specimens were compared from two different studies. For the WSU pig study, only the heads were tested within a shock tube. Both the biomechanical responses of skull flexure (as revealed by strain) and ICP were measured. The effect of orientation was also assessed. The relationship between the strain and ICP records indicate that for the pig head, skull flexure has a dominate effect on the overall pressure response within the frontal lobe of the brain and that the response is orientation specific. These statements were validated by the relationship between the skull strain and ICP response. For the front facing and side

facing pig, when the bones on the pig head “bowed” the pressure within the brain increased. For the examples provided, the ICP response followed the strain response through the major series of oscillations associated to result from multiple modes of skull flexure. With the back facing pig, the negative phase that developed was hypothesized to result from the “pulling” of the occipital bone away from the brain.

The PREVENT study investigated the ICP responses of side exposed living pigs and also measured pressure within major vessels. The results from the study indicated that the ICP waveforms were dominated by the quasi-steady compression (QSC) phase but there was also frequency content associated with a DOA mode. The results also refute the hypothesis that the thorax is being compressed by the ribcage and is sending a pressure surge up into the brain that may cause significant neurotrauma. However, pressurization at the neck may occur, creating a boundary condition that specific to a living organism.

The PREVENT pigs were younger and exposed to greater incident shock wave intensities than the older WSU pig. One hypothesis is that the increased quasi-steady phase of the PREVENT pig was a result of these characteristics. A thicker (as an analog to stiffness) skull exposed to lower intensity shock waves would be expected to protect against the external pressure compression, but the pressure oscillations in the brain associated with the DOA and HFLA modes of skull flexure would still be able to form. The other possibility is that by testing living organisms, the boundary conditions change so that there is additional pressurization associated with the QSC mode. Further studies will be required to address this question using standardized specimens and shock wave amplitudes.

## CHAPTER 5 CADAVER MODEL OF BLAST BIOMECHANICS

**NOTE:** The data that were collected in this chapter was primarily undertaken by Dr. Alessandra Leonardi. Her dissertation is a complement to the cadaver data presented in this dissertation (Leonardi 2011). All figures taken from her dissertation have been referenced. All data that were analyzed and presented in this chapter was completed by R. Bolander.

### 5.1 Measurement of skull flexure and ICP in the cadaver when exposed to a shock wave

For assessing the biomechanical responses of the human head, fresh cadavers are the most appropriate model to study because the ratios in geometry and bone thickness best approximate those of living humans. Unfortunately, testing with cadavers does not allow for measurement of physiological or living tissue responses resulting from shock wave exposure. Additionally, cadavers are more complicated to procure than other species and it is difficult to simulate homeostatic conditions such as normal ICP levels during an experiment (Hardy 2007).

There is little research that has been completed in the cadaver model with regards to experimental blast injury, particularly in the brain. Rafaels et al. (2010) have recently published a report that compared responses of the cadaver head to a Hybrid III crash test dummy head when exposed to a shock wave outside of a shock tube. In the study, cadavers were instrumented with pressure sensors and accelerometers. During a front facing exposure, the pressure records in the brain were shown to diminish anterior to posterior. Only the peak pressures of the records were reported and a

description of the overall ICP waveform profile within the brain was not provided. It was concluded that helmets reduced the pressure on the surface of the skull, but increased head acceleration values due to coupling of the head to the helmet by means of the loose fitting chin strap. The authors concluded that a primary blast injury criterion should include the effects of overpressure, positive phase duration, and impulse on resulting blast neurotrauma.

An in depth analysis of the potential biomechanical mechanisms causing injury from blast exposure was not conducted, therefore an injury criterion based on the factors stated above is not possible. It is imperative to first present a hypothesis of what is actually causing neurotrauma in live humans and then create tests to address that hypothesis. This reflects the need for further cadaver research to take place which examines biomechanical responses associated with an injury hypothesis. In this study, the testing was designed to assess the multi-modal skull flexure hypothesis.

Experiments with cadavers are needed to test the multi-modal skull flexure hypothesis. As stated previously, an advantage of conducting experiments with cadavers is that these specimens have the same bone geometries to living humans. When compared anatomically, the human skull is different than the other species discussed. The most apparent difference is the reduction of the muzzle (Figure 5.1) and an increase in total brain volume relative to total body mass. Due to the bipedal evolution of the human, the orientation of the brain has shifted to where the brain appears to be folded on itself when compared to mammals that ambulate on four legs (Weidenreich 1947). This evolution has caused the human skull to be more spherical which results from a change in the proportions and curvature of each specific bone

(Figure 5.2). Studies have been undertaken to characterize the thickness of human skull bones (Moreira-Gonzalez 1963; Lynnerup et al. 2005). By measuring 281 human skulls, the mean thickness of the frontal bone was approximately 7mm thick with thinner region of bone near the lambda and sagittal suture intersection (Moreira-Gonzalez 1963) (Figure 5.3).

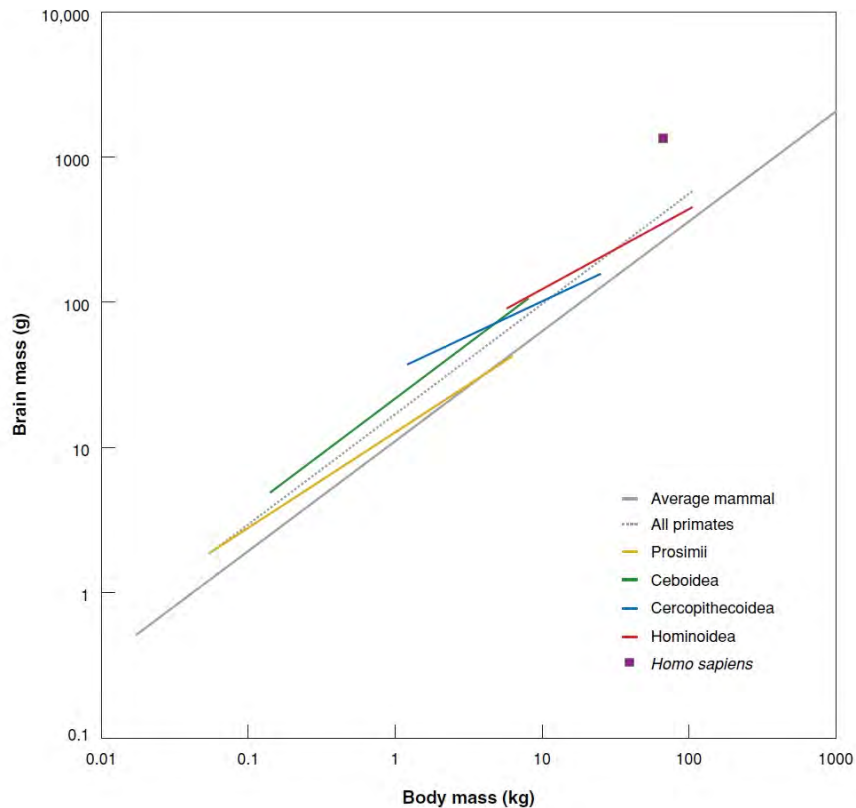


**Figure 5.1 The human is a species that has evolved such that the brain mass per body mass is considerably greater than any other recent ancestor, average mammal, or primate (Schoenemann 2006).**

The purpose of this study was to assess the multi-modal skull flexure hypothesis in the cadaver head when exposed to a shock wave. In the experiments, both strain gages and pressure sensors were used to quantify skull flexure and pressure profiles within the brain during shock wave exposure. If a relationship between skull strain and

ICP was observed and associated with specific flexural modes of the skull, then the hypothesis would have further credibility as a potential injury mechanism associated with primary blast injury.



Figure 5.2 A three dimensional CT reconstruction of the human skull.

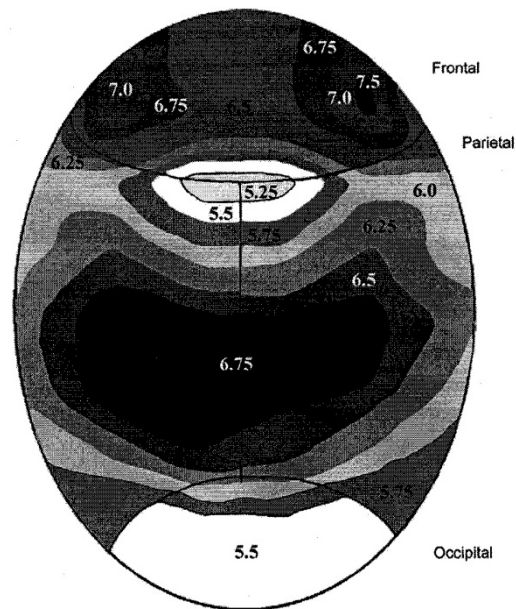


Figure 5.3 Summary of the variance in thickness of bone composing the human skull (Moreira-Gonzalez 1963). Units are in mm.

## 5.2 Methods for assessing biomechanical responses of the cadaver head during shock wave exposure

A total of four cadavers were utilized in these series of tests (Table 5.1). Each specimen was subjected to a total of 15 exposures at four different orientations, except for the third specimen which received 17 exposures (Table 5.2). Two additional experiments were undertaken for cadaver 3 due to issues with the trigger for the strain measurements.

**Table 5.1 A summary of characteristics of the cadavers used in this series of tests. CHF stands for chronic heart failure.**

	Cadaver 1	Cadaver 2	Cadaver 3	Cadaver 4	Avg	Std. Dev.
Age	52	87	73	87	74.75	16.5
Sex	M	F	F	F	-	-
Mass (kg)	63.5	49.9	76.6	63.5	63.375	10.9
Stature (cm)	162.6	160	152.4	165	160	5.46
Head Width (cm)	14.4	14.5	15.2	15	14.8	0.3
Head Length (cm)	16.5	16.8	16.2	16.5	16.5	0.2
Head Circum. (cm)	51.1	51.5	52.4	52	51.8	0.5
C.O.D.	CHF	CHF	CHF	N/A	-	-
# Exposures	15	15	17	15	15.5	1

**Table 5.2 Number of exposures to which each head was subjected at each orientation and pressure magnitude.**

Incident Pressure	Front	Left	Back	Right
69 kPa	2	1	1	1
88 kPa	2	1	1	1
120 kPa	2	1	1	1

FOP-MIV (Fiso Inc.) fiber optic pressure sensors were used to measure intracranial pressure (ICP). The ICP sensors were connected to a Veloce-50 (Fiso Inc.) system which was connected to the Dash 8HF (Astro-Med Inc) data acquisition system. The sampling rate was set to 250 kHz with 90% pre-trigger over a one-second duration.

All specimens were handled and prepared per guidelines outlined by Wayne State University School of Medicine Willed Body Program and the Human Investigation Committee. Each head was disarticulated from the body between the third and fourth cervical vertebrae with the exception of the first specimen. Careful attention was given to preserving the carotid arteries and jugular veins. Upon disarticulating the head, the carotid arteries and jugular veins were fitted with quick disconnect fittings to aid with perfusion of the system as shown in Figure 5.4. The spinal cord was also fitted with a quick disconnect fitting in the initial two specimens. In the last two specimens, the spinal cord was tied off with string to prevent leaking of the pressurized system. A small square portion of skin 2 X 2 cm was removed at the ICP sensor site. A hole was drilled at each site and tapped (6-32). The plastic cannula was threaded into the hole. The assembly of the ICP sensor and cannula was shown in Figure 5.5. Three screws were arranged around each ICP sensor. A mixture of bone cement was poured into the space between the screws as shown in Figure 5.6. This method of ICP sensor placement provided the greatest survivability for the conditions. Four ICP sensors were used per head for this study (Table 5.3).

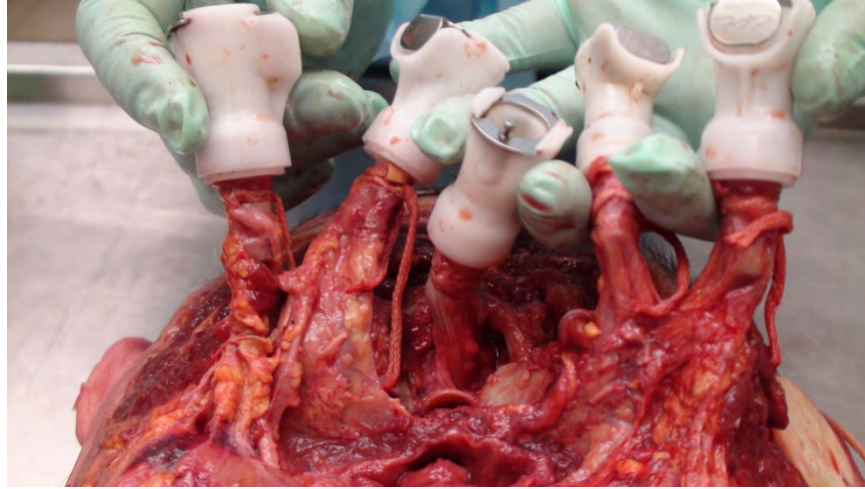


**Figure 5.4** A graphic of the quick disconnect valves attached to the major vasculature centers of the brain.

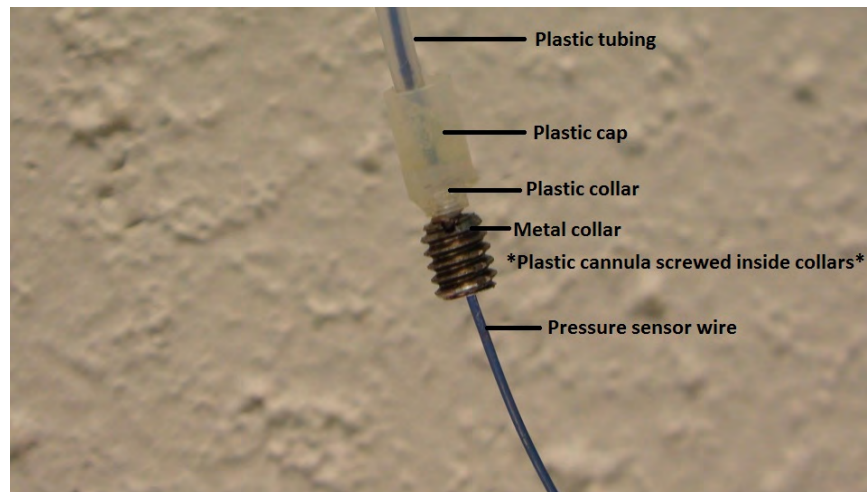


**Figure 5.5** Mounting for the fiber optic pressure sensor. The fiber was adhered to a threaded insert that was then threaded into the skull.



**Figure 5.6** The fiber optic pressure sensor was mounted to the skull, surgical screws were threaded into the bone and bone cement was applied to the surface to prevent sensor pull out.

**Table 5.3** Location of ICP sensors on the cadaver head (Leonardi 2011)

ICP sensor	Measurements for Location
frontal	10 mm away from midline; 70 mm from nasion going towards the back of the skull
ventricle	20 mm away from midline; 50 mm from frontal going towards the back of the skull; usually on coronal suture line
parietal	10 mm away from midline; 70 mm from ventricle going towards the back of the skull
occipital	10mm away from midline; 50 mm from parietal going towards the back of the skull

Rosette strain gage (FAER-25B-35SX, Vishay micro-measurements Inc.) sites were prepared a day prior to testing. A 2 X 2 cm square of skin was removed and underlying tissue was removed with a scalpel. The strain gages were not attached until the day of testing. M-Bond (Vishay Inc.) electronics adhesive was used to attach each sensor to the bone which was then protected with M-coat (Vishay Inc.). The wire was

sutured under the skin as shown in Figure 4 to prevent translation. This configuration provided the greatest survivability of strain gage sensors (Figure 5.7). Five rosette strain gages were applied to the skull surface. Sensors were applied to the frontal bone, the occipital bone, the temporal bone, the parietal bone, and the zygomatic bone. The frontal, parietal, and occipital gages were placed 20 mm left of the sagittal suture. The strain data were collected at 150.943 kHz using the TDAS (DTS Inc.) data acquisition system.

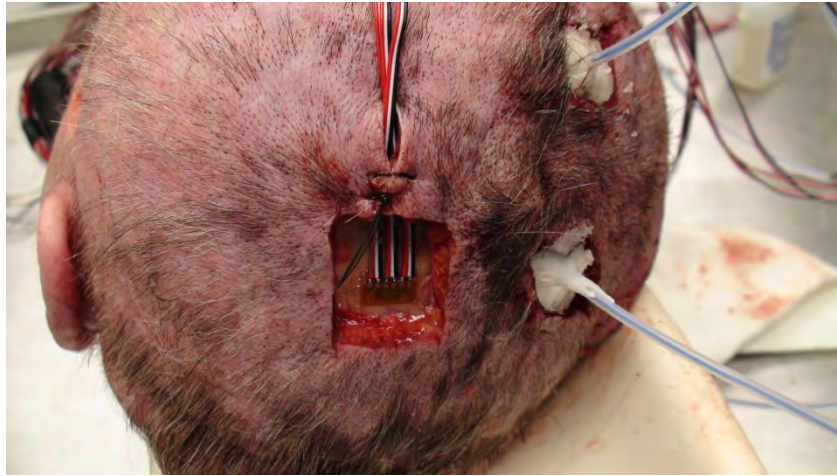


**Figure 5.7** A graphic demonstrating the placement of strain gages on the cadaver skull. Tissue was removed so that the sensor could be bonded to the bone surface. To prevent sensor whip, an incision was made in the tissue to run the wires away from the head without creating additional strain on the sensor / wire interface.

The specimens were placed in an inverted configuration within the Wayne State University Bioengineering center shock tube. All specimen heads were centered 1.25 m from the end of the expansion portion of the shock tube. The head was contained with a net. A metal chain was used to support the net and to hold the head in place during testing (Figure 5.8). The ICP fibers were passed through a hole at the base of the expansion tube. The strain gage wires were run along the base of the tube and out the

driven end. Prior to testing, the specimen head was re-pressurized with an artificial cerebral spinal fluid (aCSF) solution. The aCSF was introduced with a tubing system that was connected to the quick disconnect fittings. The specimens were then subject to the series of exposures described in Table 5.2.

The collected data were then analyzed. The peak strains and pressures were collected for each trial and are available in appendix C. The rate of pressure increase was also calculated and reported. Because of the high number of strain gage losses, calculation of principal strain was only able to be accomplished with select gages. A full description of the analysis of the ICP results was undertaken by Leonardi (2011). The secondary large oscillation frequencies within the ICP waveforms associated with the DOA mode of skull flexure were calculated using simple waveform analysis. The strain and ICP data were considered separately and together to understand the relationships between the two responses. Additionally, the ICP response of the frontal and occipital sensors were compared to blunt impact studies with cadavers that also measured ICP to better appreciate how shock wave exposure is unique.

Following testing, each specimen was thoroughly examined. Strain gage sensors were inspected for any wire damage or peeling from the skull. The skin was removed from the specimen calvaria to inspect sensor placement in relation to bony landmarks and skull sutures. The left portion of the calvaria was removed to inspect brain tissue consistency and/or abnormalities. The left hemisphere was removed to inspect ICP sensor depth. This was accomplished by removing small layers of brain tissue to locate ICP sensor within the right hemisphere.

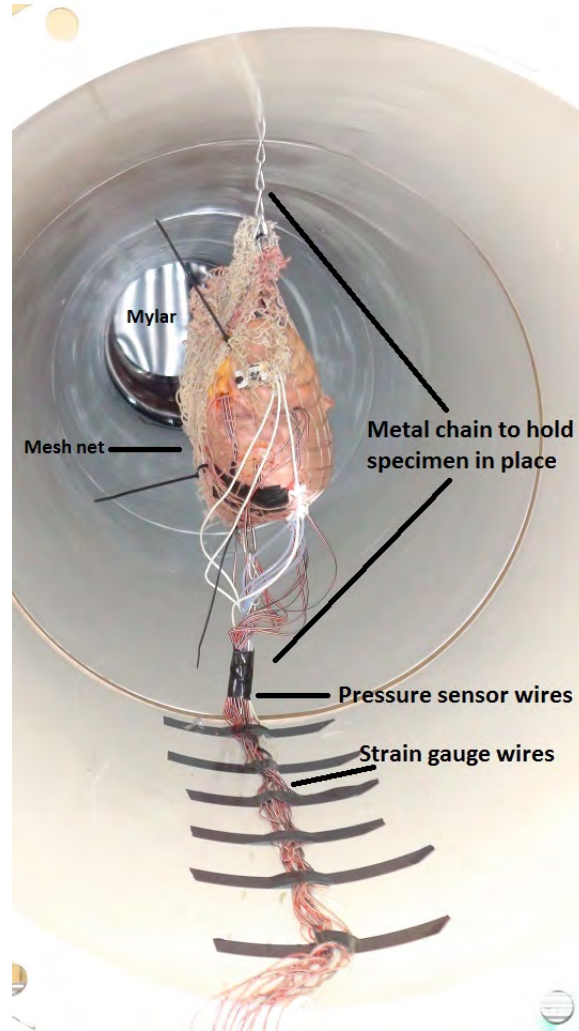


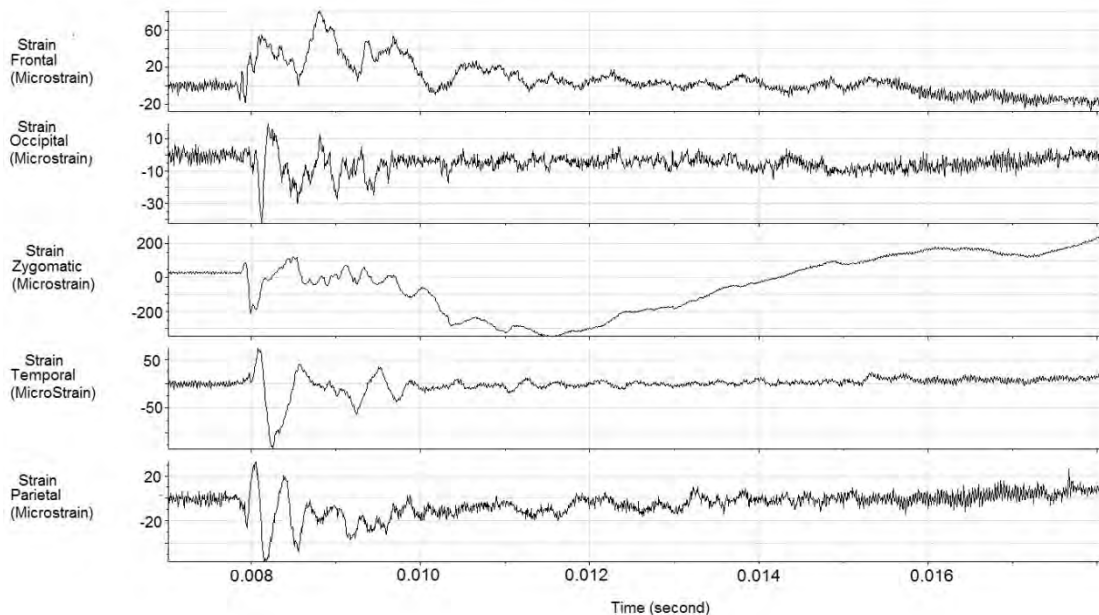
Figure 5.8 A graphic of the cadaver head hanging inverted in the expansion region of the shock tube.

### 5.3 Observed flexural modes of the cadaver skull

Due to the highly dynamic pressure environment in which the cadaver head was exposed, multiple strain gages failed during testing. Some sensors became completely delaminated during these tests. Each sensor was assessed by visual inspection to determine if proper bonding had remained intact following testing as a check to decide if a specific channel had a greater probability of errors. However, enough sensors survived to provide an understanding of how the cadaver skull will flex under shock

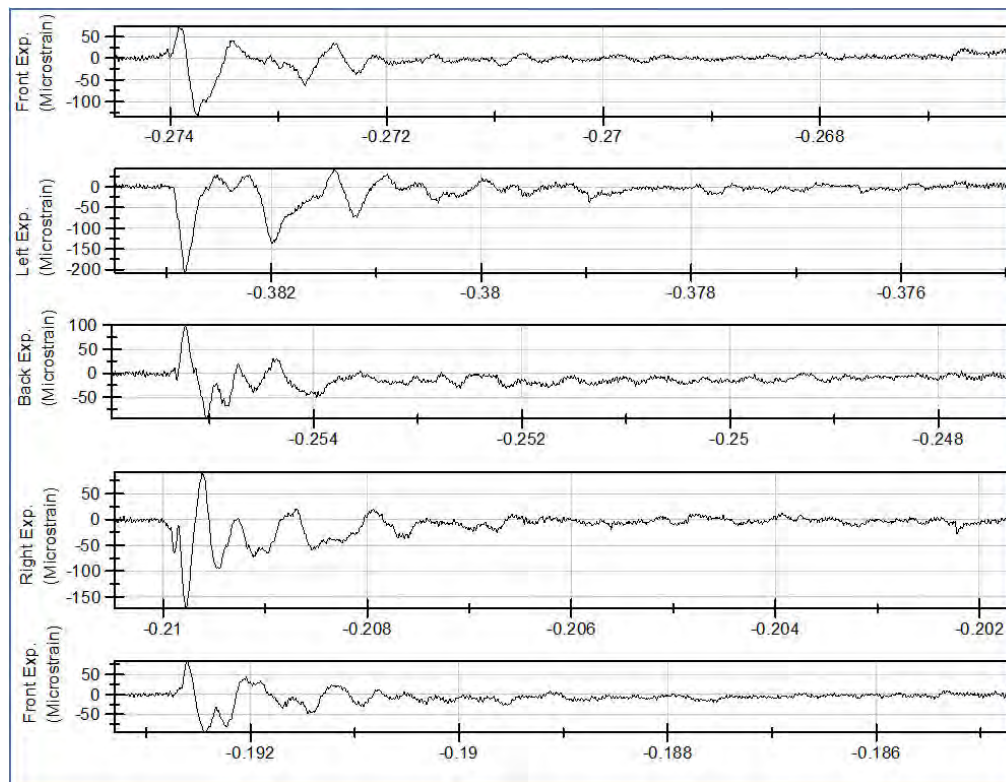
wave loading. The most important aspects of this data are: (1) the biomechanical responses of the skull are dependent on orientation relative to the incident shock and (2) the biomechanical responses of the skull are dependent on the bone being measured and (3) the three flexural modes (DOA, HFLA, and QSC) were observed in the profiles. The strain profiles presented are typical across specimens when the strain gages were properly adhered to the skull surface.

Figure 5.9 demonstrates the variability in strain profiles on the surface of the skull during a single front facing exposure. Some sensors begin in tension while others in compression. The frequency of oscillation is associated with the bone being measured. For example the frequencies of the large oscillations in Figure 5.9 were: Frontal = 1250 Hz, Occipital = 2222 Hz, Zygomatic = 3215 Hz, Temporal = 2083 Hz, and Parietal = 3704 Hz.



**Figure 5.9** The strain results for each location during a single front facing exposure. The frequency of oscillation was dependent on the bone being measured.

The strain response of the temporal bone to shock wave exposure was presented in order to appreciate how the skull will respond in different orientations. With the head facing front to the incident shock wave, the strain profile began in tension then oscillated and returned to baseline strain. When the temporal bone was directly facing the incident shock wave, the bone was compressed, oscillated, and returned to baseline. This initial tension was also measured when the back of the head was exposed to the incident shock (Figure 5.10).



**Figure 5.10** The strain response of the temporal bone for cadaver 5 (fresh cadaver 4) was dependent on the orientation of the head relative to the incident shock wave. With the head facing forward the bone went into tension prior to compression. When the bone was directly exposed to the reflected pressure it directly went into compression.

The frequency response for the temporal bone during a front facing and left side facing exposure was quantified using fast Fourier transform. The signals were then

post-filtered with a 360- 8000 Hz band pass to better observe the frequencies of interest. The frequency versus amplitude graph of the left side exposure resulted in a more defined frequency spectrum than the front facing exposure (Figure 5.11). When the head was facing forward, the frontal bone underwent compression due to reflected pressure loading on the surface. This will cause the temporal bone to undergo tension as a response, which will then oscillate and dampen out. When directly facing the shock front, the temporal bone will directly go into compression during the loading, this will cause the bone to oscillate and then return to baseline.

The strain response of the parietal bone included a larger component of the QSC mode. Because this sensor was near the apex of the head, the peak strains were fairly similar between orientations. For this sensor, when the head was face forward or face backward the sensor recorded compression, when turned to the side, tension developed prior to compression (Figure 5.12).

For the occipital strain gages, when the front of the head was facing to the sides, tension would develop prior to the compression. When facing backward, a compression followed by distinct oscillations, similar to the temporal bone was observed (Figure 5.13).

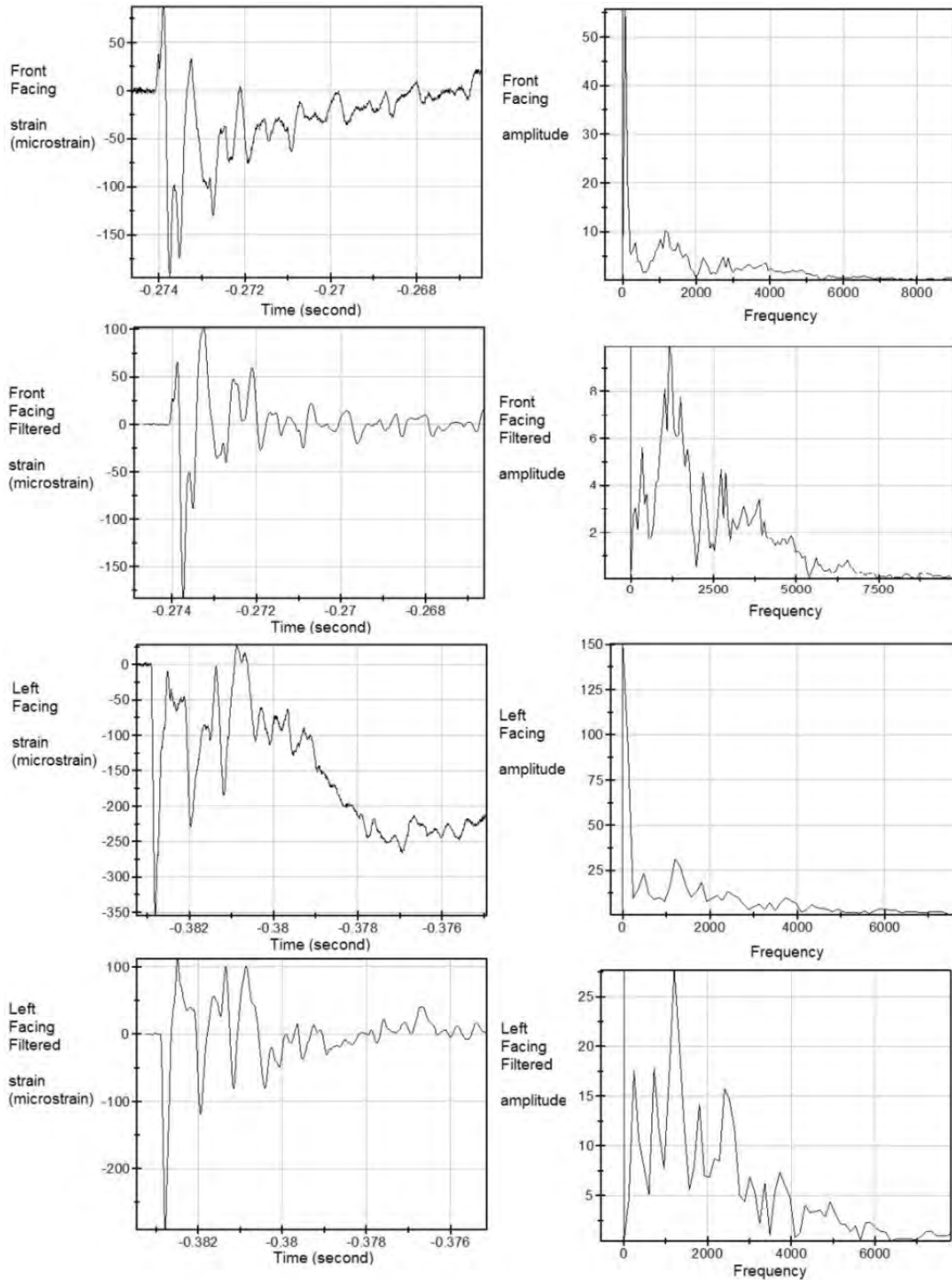


**Figure 5.11** When filtered at a 360 Hz – 8 kHz band pass filter, the temporal bone will have a more defined series of oscillations when exposed to a left side exposure. The negative time is relative to the point in which the trigger was activated for these strain channels.

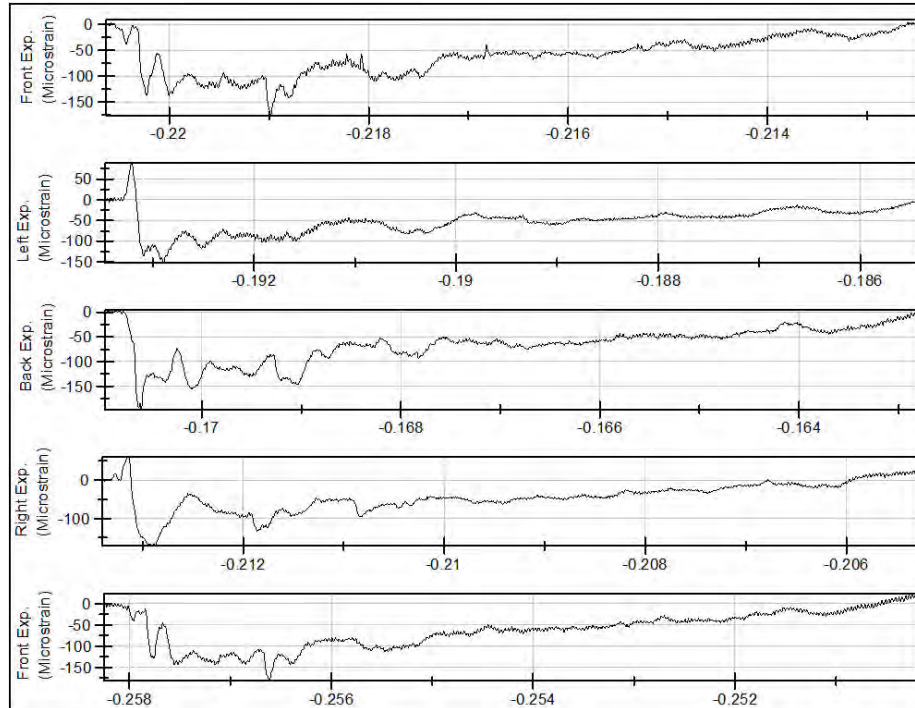


**Figure 5.12** The strain response of the parietal bone for cadaver 4 (fresh cadaver 3) approximated the loading conditions of the external static pressure response. When the side of the head was exposed to the incident shock wave, a tension would develop prior to compression.

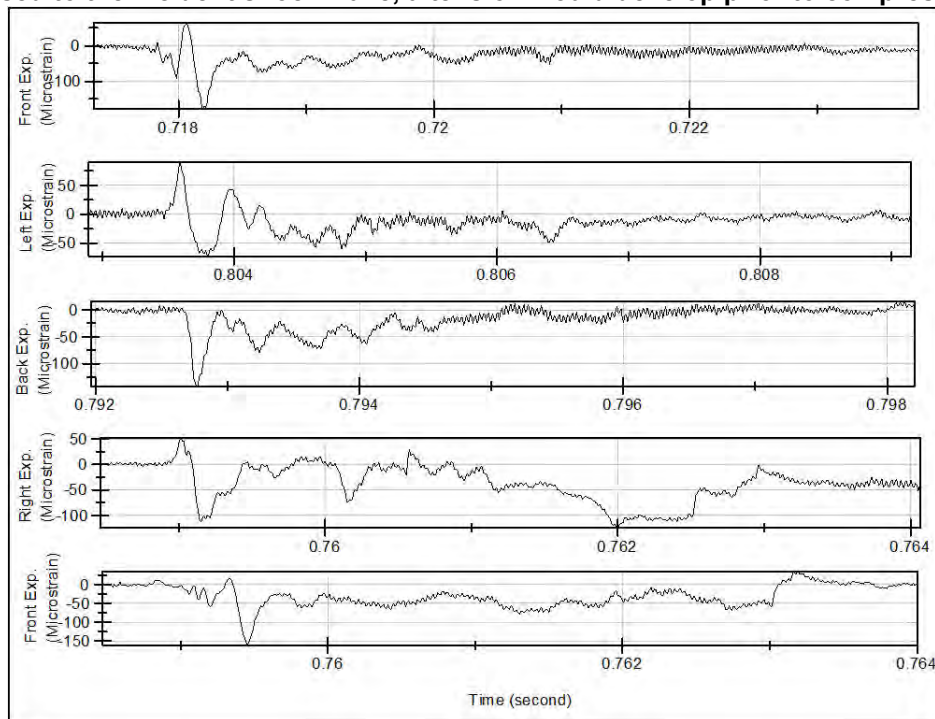


**Figure 5.13** The strain response of the occipital bone for cadaver 2 (fresh cadaver 1). When the sensor was facing the incident shock it would directly measure compression.

The strain series just presented were taken from single strain gages. In most cases, a channel would be lost over the series that would make calculations of principal strain not possible. A frontal sensor series using principal strain was able to be identified (Figure 5.14). The series show frequency content that lasts for a greater duration, with less distinct responses in the first millisecond.

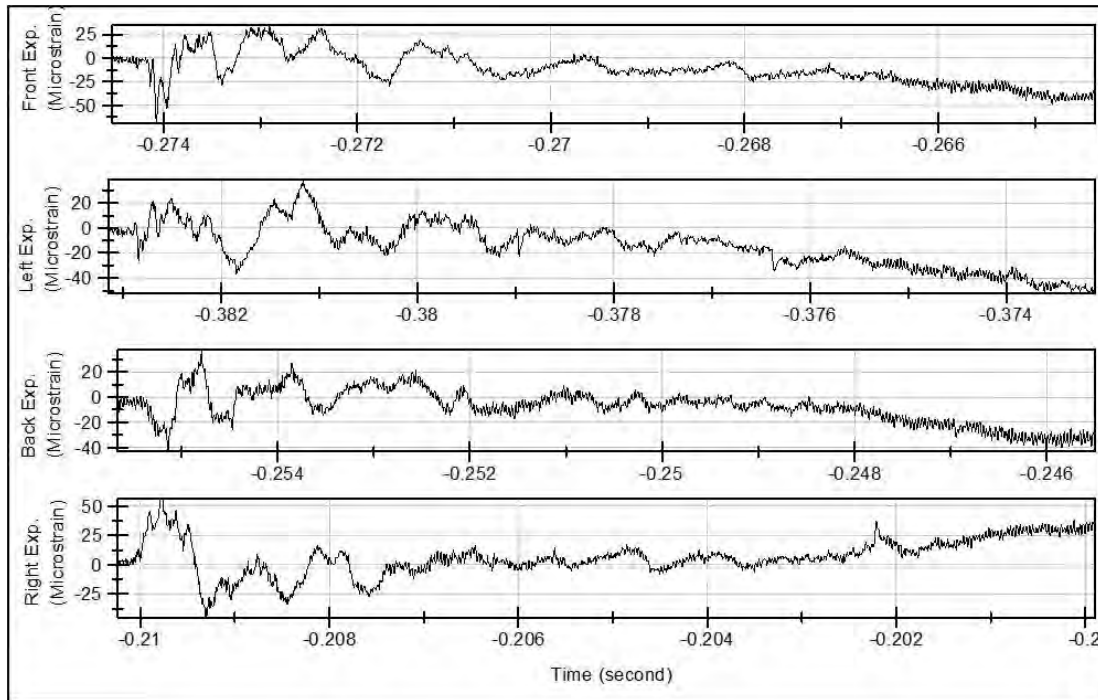


**Figure 5.14** The max principal strain response for the frontal bone of cadaver 5 (fresh cadaver 4) was one of the few cases where the strain channels were considered appropriate for calculations of principal strain.

The zygomatic bone was not included in these results as the magnitudes and wave shapes were not reliable. Following interaction with the shock wave, the measured strains on the zygomatic bone would not return to baseline. It is believed that the unreliable data was partially the result of having to mount the sensor on a very concave surface. Additionally, this region resulted in the greatest number of sensor

failures by delamination. In appendix C the peak strains for all series are provided. Descriptive statistics were not completed for the strain results due to the number of sensors that failed during testing.

Overall, the results from the strain gages indicate that the response of the skull is dependent on the orientation of the head relative to the incident shock wave. The flexural modes discussed for the sphere in chapter 2 are useful for describing the flexural response of the cadaver skull. When a region of the head was exposed to the reflected pressure, that region would directly go into compression, oscillate, and return to baseline. The regions on the side would go into tension initially, oscillate, and return to baseline. The same response would then happen if the head was rotated 90 degrees.

It was shown that the frequency of oscillation of the single strain channels were generally over 1500 Hz and would dissipate within the first millisecond. Whereas the calculated principal strain for the frontal rosette showed oscillations of lower frequency for longer durations. Both of these frequency regimes were observed in the ICP profiles and were associated with the DOA and HFLA modes of skull flexure, which will be discussed later.

#### **5.4 Frequency content of ICP oscillations**

Leonardi (2011) undertook a thorough analysis of the cadaver ICP response using this data set. The analysis that was presented will not be re-discussed. For this dissertation, the frequency content associated with the ICP responses were of interest. Although, some ICP magnitudes were presented in order to compare the ICP responses that develop during a blunt impact, to those that develop during shock wave exposure.

It was observed for all experiments that the ventricle and parietal pressure sensors would generally report lower absolute magnitudes when compared to the frontal and occipital sensors. Secondary oscillations would result following an initial tension or compression. The ventricle would approximate the frontal sensor and the parietal sensor would approximate the occipital sensor (Figure 5.15). Due to the similarities between the two middle sensors to the frontal and occipital sensors, only results from the frontal and occipital sensors were included in further discussion. The second purpose for this was that the frontal and occipital sensors were in similar locations to blunt impact studies with cadavers that measured ICP and served as a comparison.

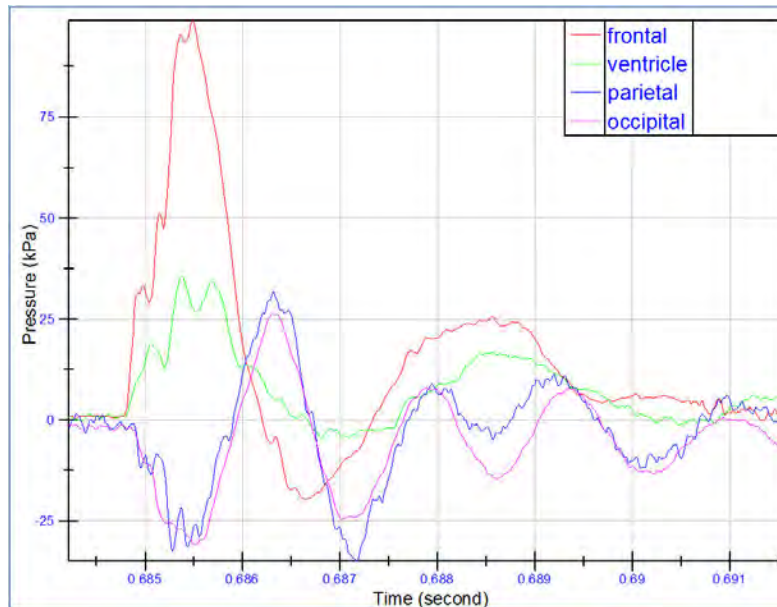


**Figure 5.15** When measuring the ICP response of the cadaver head, the ventricle sensor had a similar response to the frontal sensor whereas the parietal sensor had a similar response to the occipital sensor for a front facing shock wave exposure.

As the intensity of the incident shock wave increased, the magnitude of ICP would increase (Figure 5.16). During the face forward orientation, the frontal ICP

sensor exhibited a compressive pressure pulse followed by damped oscillations. Near the same time, the occipital sensor developed a tensile pressurization followed by damped oscillations. In Figure 5.17, it was demonstrated that when either the frontal or occipital bone is facing the incident shock, their respective pressure sensors record a compressive pressure phase duration prior to the damped oscillations. The sensor mounted on the opposite side of the incident shock wave will measure a tensile pressurization.

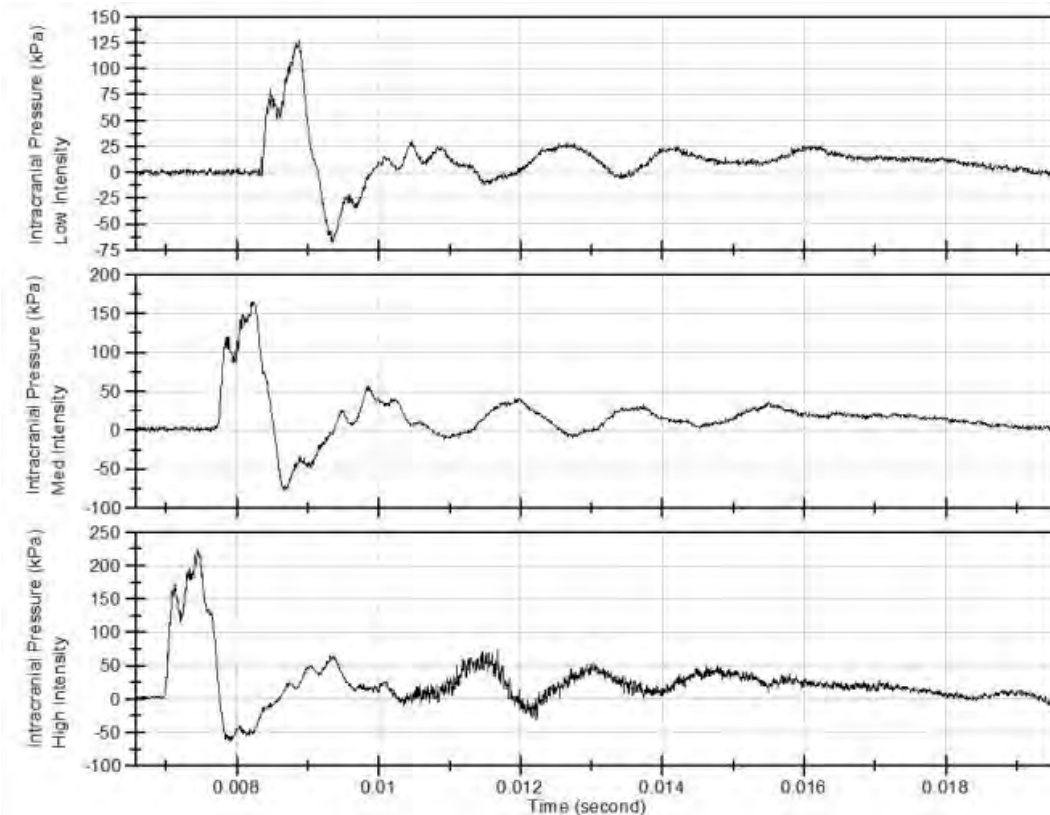


**Figure 5.16** The initial pressure responses measured by the frontal ICP sensor increase with increasing incident shock wave intensity in the face forward orientation. As the magnitude of the incident shock wave increased, the shock wave would interact with the head at an earlier time due to its higher Mach number. These ICPs were greater than the incident pressure.

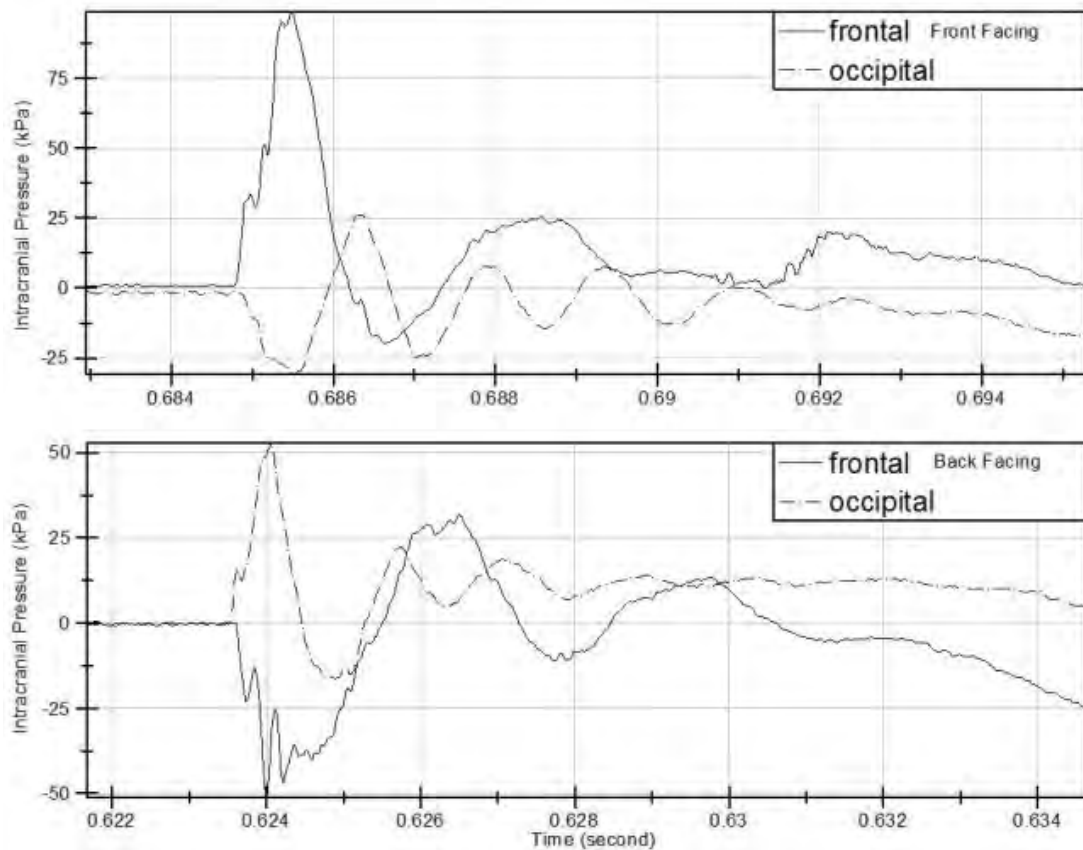


**Figure 5.17** The ICP profiles in the cadaver head are dependent on the orientation in which the head was subjected to the incoming incident shock wave. The sensor nearest to the reflected pressure (either occipital or frontal) initially measures a compressive pressure whereas the sensor furthest from the reflected pressure measures a tensile pressure.

In some instances, perhaps due to either sensor mounting or the properties of the bones being tested, multiple phases could be identified in the ICP waveform (Figure 5.18). The first phase (1) has been identified as either a positive or negative pressurization dependent on orientation. Phases (2) and (3) consist of two major frequencies; a higher frequency (~2500 Hz) and lower frequency (~500 Hz) oscillations, respectively.

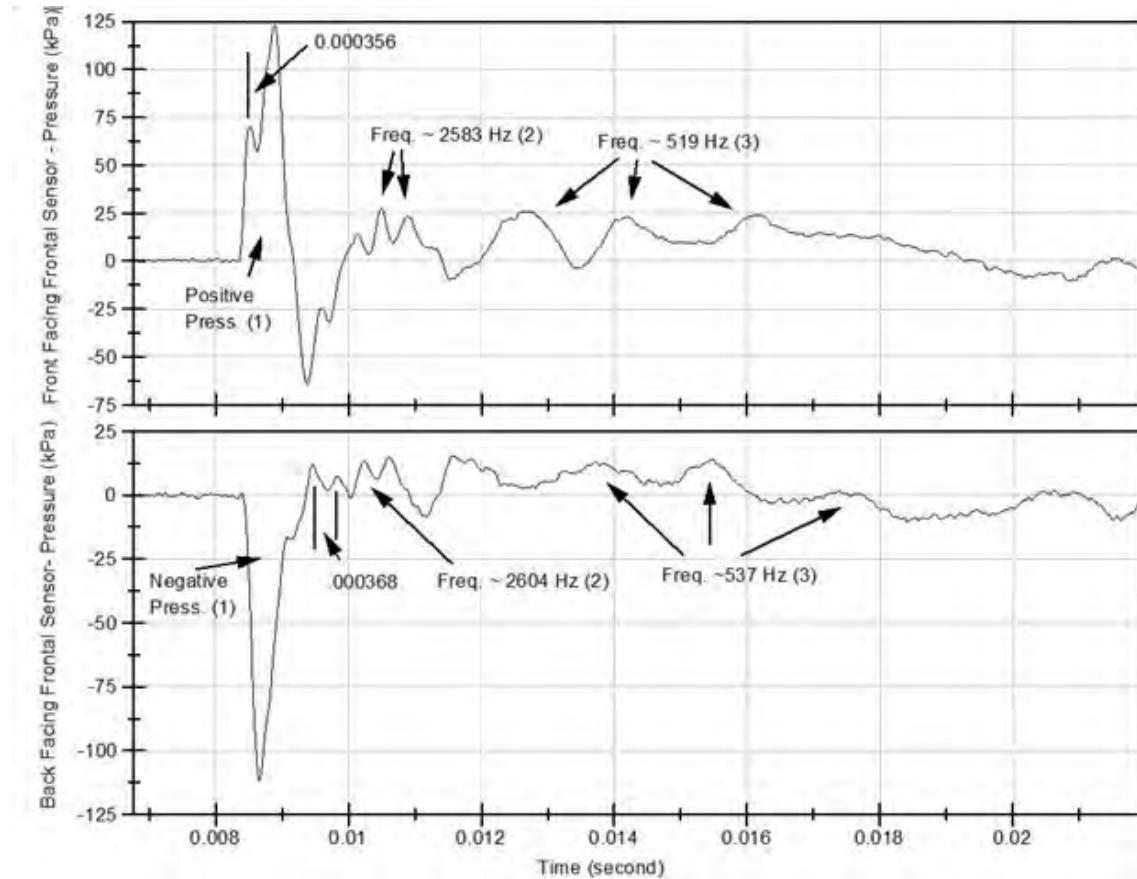


**Figure 5.18** The pressure response of the frontal bone was separated into three different phases. (1) A positive or negative pressurization dependent on orientation. (2) A high frequency component and (3) a low frequency component.

The frequencies were calculated using simple waveform analysis for the large damped oscillations associated with the DOA mode of skull flexure ( $< 1000$  Hz) and analyzed by bone which the sensor was mounted (frontal or occipital) and specimen (Table 5.4). The occipital sensor measured higher frequencies of oscillation than the frontal sensor. It is possible that following the initial compression or tension occurring at each location, the bones will then oscillate at their own characteristic frequencies, based on their own specific mechanical properties. This would then potentially cause localized pressure responses within the brain.

**Table 5.4 The calculated ICP oscillation frequencies associated with the DOA mode of skull flexure for the front facing and rear facing orientations.**

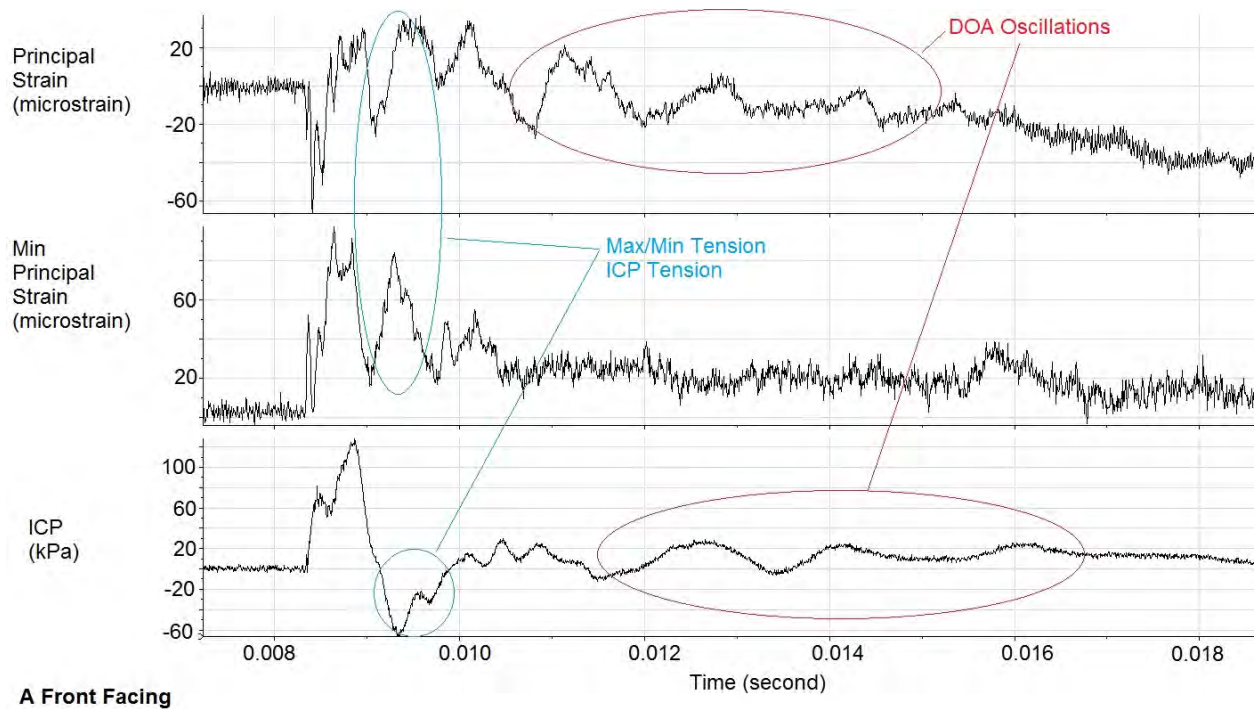
Specimen	Sensor	N	Frequency (Hz)
Cadaver 1	Frontal	1	462
Cadaver 2	Frontal	4	390 ± 201
Cadaver 2	Occipital	4	775 ± 45
Cadaver 3	Frontal	8	320 ± 24
Cadaver 3	Occipital	8	649 ± 66
Cadaver 4	Frontal	8	528 ± 44

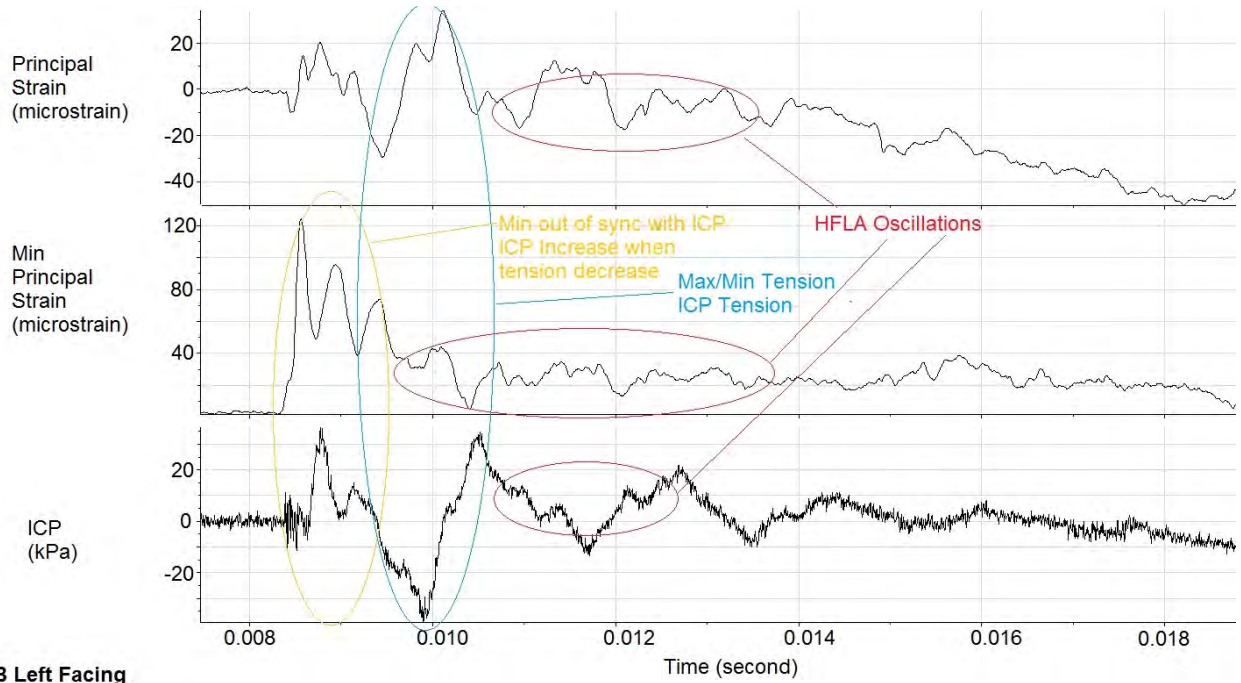
### 5.5 Comparison of principal strain to ICP

As stated before, due to the number of strain gage sensor losses, calculations of principal strain could not be made consistently. A series of the four orientations at the low intensity could be analyzed for the frontal sensors for the fourth fresh cadaver. The principal strain responses for the frontal strain gages were plotted against the frontal pressure sensor at each orientation at the low pressure intensity in Figure 5.19. The purpose for this was to determine which ICP responses could be related to a mode of skull flexure during shock wave exposure.

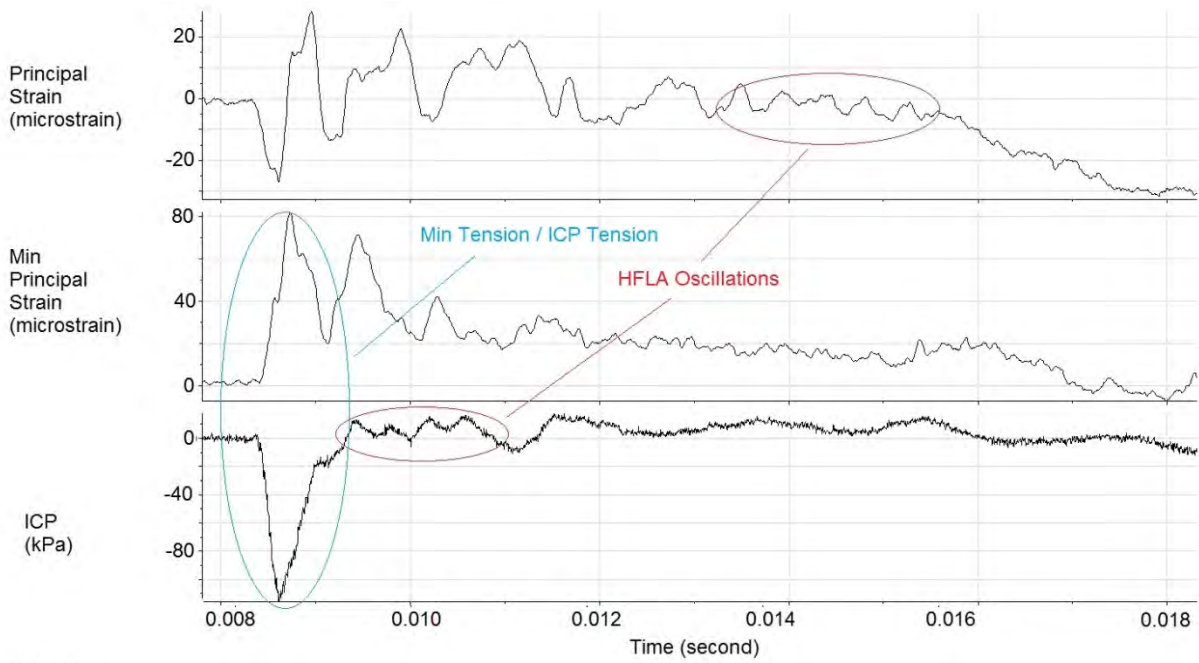
Multiple observations were made comparing the principal strains to the ICP response. Both the max and min principal strains were important for describing the response of the system. Within the first millisecond following shock wave exposure, the ICP response would go into tension when both the max and min principal strains moved in tension. Instances when this phenomenon occurred are highlighted in blue. Oscillations associated with the DOA and HFLA modes were also highlighted. The

DOA oscillations were best associated with the max principal strain response and presented in the ICP response when the min principal strain response was minimized. HFLA oscillations were observed in both the max and min principal strain responses. For the left facing orientation, a phenomenon occurred where the peak compressions taking place in the first 2 milliseconds for the ICP were out of sync with the min principal strain response. This showed that when the bone was moving into compression the ICP would increase.





**B Left Facing**



**C Back Facing**

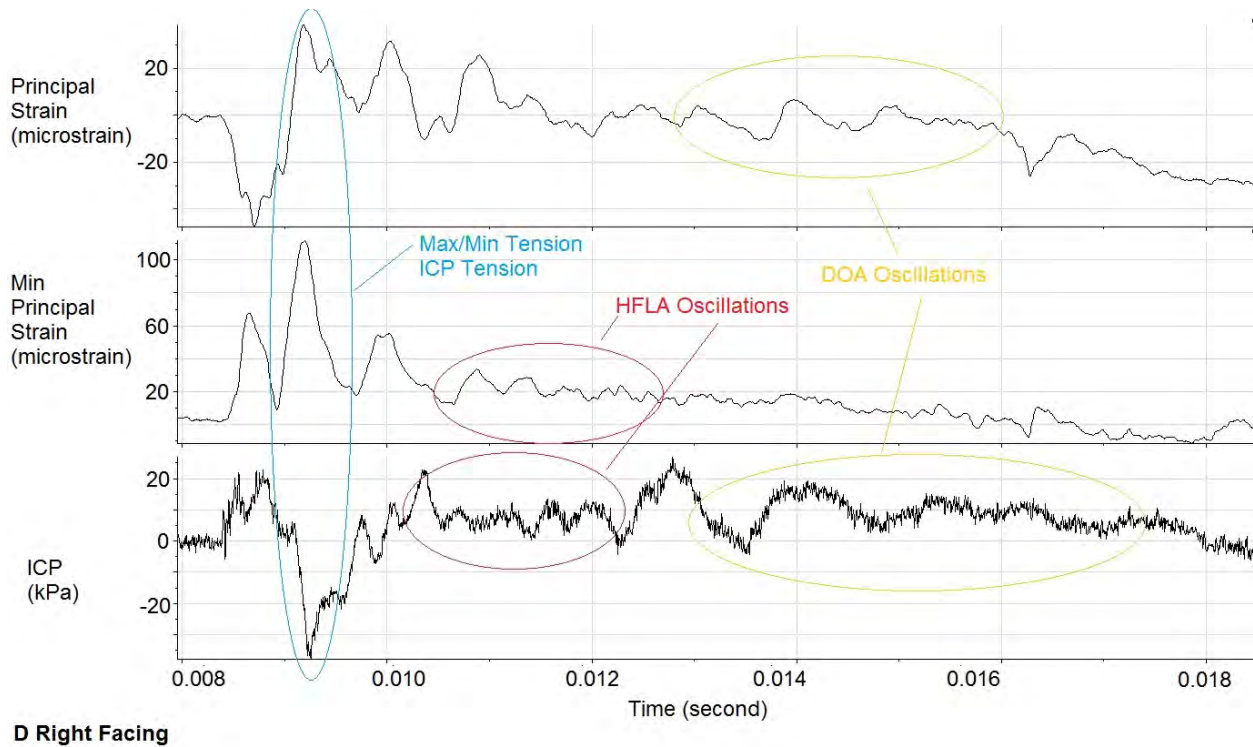


**Figure 5.19** The principal strain responses for the frontal bone are similar to the ICP response measured by the frontal pressure sensor.

The relationship between skull flexure (as measured by strain) and ICP was demonstrated. Oscillations associated different flexural modes were observed in the strain and ICP responses. These results suggest that the localized pressure environments within the brain may be explained by skull flexure. When the max and min principal strain went into tension, the ICP would drop. This suggests a “pulling” of the cranial bone against the brain, will lower the ICP response. Conversely, ICP will increase when the bones “pushes” on the brain.

## 5.6 Investigation of shock wave loading compared to blunt impact.

It had been shown through the data in this chapter that there is a relationship between skull flexure and ICP in the cadaver head when exposed to a shock wave. It is

hypothesized that it is the flexing skull that is creating the pressure gradients in the brain. To further understand the response of the head to shock wave loading, the ICP data from this study were compared to multiple studies investigating blunt impact response of the cadaver head.

In Hardy et al. (2007), multiple perfused cadaver heads were suspended upside down on a trolley system. Each head was pressurized and a piston mechanism accelerated the trolley. While in motion, the head impacted an acrylic block on the occipital region. The velocity of the head ranged between 3 to 4 m/s. Pressure sensors were placed in the frontal and occipital regions of the brain.

The coup/contrecoup response was observed in the specimens tested. The rate of pressure change and amplitude increased with increased head acceleration. This relationship of loading of the head to pressure formation in the brain was observed for cadaver heads that were exposed to shock waves in this study, except that the pressure responses were of shorter duration and had shorter rise times for the shock wave exposed cadavers.

In Table 5.4, ICP data for the front and back facing cadaver head, measured by the frontal and occipital sensors, were separated by sensor and orientation of the head. The peak pressures, rate of pressure increase, and duration of the initial phase were included in the summary. Under similar loading conditions, the peak pressures, and rates of pressure increase for the shockwave exposed cadavers were higher when measured from the frontal sensor when compared to the occipital sensor. The pressure responses reported by Hardy et al. (2007) were included at the bottom of the table to be used as a comparison. The values associated with occipital sensor were similar to the

coup pressurization results for blunt impact in terms of peak pressure and rate of pressure change, but the measurements reported by the frontal bone were higher. The durations of the ICP response for the blunt impact studies were longer than the shock wave exposure studies.

To better appreciate the differences in the ICP response between a blunt impact and a shock wave exposure, the time series ICP responses measured in this study were compared to those of Nahum et al. (1977) and Hardy et al. (2007). Specific points of interest in those pressure profiles were collected to generate representative traces (8 points). In Figure 5.20, the front facing cadaver ICP response was compared to two pressure traces from Nahum et al. (1977), where the frontal bone of cadavers were impacted using a pendulum. The blunt impacts were padded. ICP responses are dependent on the stiffness of the padding during blunt impact as it changes the duration and rise time of the input excitation. Also, the types of sensors used were different and may have had very low frequency response when compared to the fiber optic sensors used to measure the ICP response for the shock wave exposed cadaver heads. In Figure 5.21, the back facing shock wave exposed cadaver head was compared to pressure traces from Hardy et al. (2007) and Nahum et al. (1977).

The shock waves that the cadavers were exposed to in this study had rise times of approximately 1 microsecond with overall positive phase durations of approximately 7.5 milliseconds. Whereas the rise time of the excitation and imparted pressure waves reported by Nahum et al. (1977) was approximately 2.5 milliseconds with a similar duration. The impactor mass was approximately 5 kg with velocities ranging from 4 to 12 m/s. The peak force ranged from 5200 to 1400 N with impulses of 10 to 30 N\*s.

To determine if similar loading conditions were applied to the cadavers exposed to a shock wave in the current experiments, peak horizontal force and impulse were calculated (Glasstone and Dolan 1977). The calculation of peak input force for an arced structure is the product of peak reflected pressure and surface area of the front face. The impulse of the diffracted shock was calculated as:

$$\text{Impulse} = \text{Peak Reflected Pressure} * \text{Surface Area} (2 * \text{radius of arc} / \text{Wave Velocity})$$

A radius of 6.5 cm was assumed, based on measurements of the occipital bone of a human skull surrogate. The surface area ( $0.02653 \text{ m}^2$ ) and the wave velocity (490 m/s) were both calculated. For a 69 and 120 kPa incident shock wave with an assumed double magnification, the input force is approximately 3600 and 6200 N with impulses of 0.97 and 1.64 N\*s respectively. Therefore, the calculated peak load for the shock wave exposed cadavers is within the same regime as the input forces from Nahum et al. (1977), but the impulses are an order of magnitude less.

In both orientations, the blunt impact ICP responses did not show the pressure inversion and series of oscillations that were observed for the shock wave exposed cadaver head. The ICP waveforms associated with the shock wave exposed cadaver heads were shown to be directly related to the flexural modes of the skull resulting from shock wave exposure. It is probable that these flexural modes exist as a result of the specific loading conditions associated with shock wave exposure.

**Table 5.5** The pressure responses for this study were compared to the un-helmeted blunt impact results reported by Hardy et al. (2007). \* Indicate probable erroneous data.

Identification	Cadaver	Sensor	Orientation	Intensity	Pressure (kPa)	Pressure Rate (kPa/ms)	Duration (ms)
I1	1	Frontal	front	69 kPa	135.7	251.4	1.12
I2	2	Frontal	front	69 kPa	77.3	91.1	1.66
I6	2	Frontal	front	69 kPa	74.4	91.7	1.4
I10	3	Frontal	front	69 kPa	71.0	98.2	1.416
I14	3	Frontal	front	69 kPa	67.6	93.1	1.42
I26	4	Frontal	front	69 kPa	119.5	204.6	0.9
I28	4	Frontal	front	69 kPa	126.2	214.7	0.9
					<b>95.9 ± 29.7</b>	<b>149.2 ± 71</b>	<b>1.3 ± 0.3</b>
I8	2	Frontal	front	88 kPa	98.5	128.4	1.4
I16	3	Frontal	front	88 kPa	96.5	125.3	1.4
I20	3	Frontal	front	88 kPa	98.6	119.0	1.6
I29	4	Frontal	front	88 kPa	158.6	262.7	0.9
I31	4	Frontal	front	88 kPa	150.9	271.4	0.8
					<b>120.6 ± 31.2</b>	<b>181.4 ± 78.3</b>	<b>1.22 ± 0.3</b>
I32	4	Frontal	front	120 kPa	207.5	399.2	0.8
I34	4	Frontal	front	120 kPa	184.8	342.4	0.8
					<b>196.2 ± 16.1</b>	<b>370.8 ± 40.2</b>	<b>0.8 ± 0</b>
	Group average				<b>119.1 ± 43.9</b>	<b>192.4 ± 101.4</b>	<b>1.2 ± 0.3</b>
I3	2	Occipital	front	69 kPa	67.4	131.7	1
I7	2	Occipital	front	69 kPa	64.3	114.0	1.03
I11	3	Occipital	front	69 kPa	13.4	18.4	1.14
I15	3	Occipital	front	69 kPa	18.3	31.0	1.2
					<b>40.8 ± 28.9</b>	<b>73.8 ± 57.3</b>	<b>1.09 ± 0.1</b>
I9	2	Occipital	front	88 kPa	73.8	139.0	1.1
I17	3	Occipital	front	88 kPa	28.6	35.6	1.2
I21	3	Occipital	front	88 kPa	28.8	52.1	1.1
					<b>43.7 ± 26</b>	<b>75.6 ± 55.6</b>	<b>1.13 ± 0.06</b>
I23	3	Occipital	front	120 kPa	86.8	152.8	0.9
	Group average				<b>47.7 ± 28.4</b>	<b>84.3 ± 55.3</b>	<b>1.1 ± 0.1</b>
I4	2	Frontal	back	69 kPa	23.2	40.7	1.3
I12	3	Frontal	back	69 kPa	29.3	33.4	1.76
I27	4	Frontal	back	69 kPa	107.8	390.8	1
					<b>53.5 ± 47.2</b>	<b>155 ± 204.3</b>	<b>1.35 ± 0.6</b>
I18	3	Frontal	back	88 kPa	44.0	62.2	1.96
I30	4	Frontal	back	88 kPa	128.2	433.8	1.1
					<b>86.1 ± 59.6</b>	<b>248 ± 262.8</b>	<b>1.5 ± 0.6</b>
I24	3	Frontal	back	120 kPa	142.0	181.4	1.5
I33	4	Frontal	back	120 kPa	152.4	452.7	1.4
					<b>147.2 ± 7.3</b>	<b>317 ± 192.8</b>	<b>1.45 ± 0.07</b>
	Group average				<b>-89.6 ± 55.7</b>	<b>-227.9 ± 192.3</b>	<b>1.4 ± 0.3</b>
I5	2	Occipital	back	69 kPa	120.0	243.9	1
I13	3	Occipital	back	69 kPa	21.3	35.1	1
					<b>70.6 ± 69.8</b>	<b>139.5 ± 147.7</b>	<b>1 ± 0</b>
I19	3	Occipital	back	88 kPa	51.4	86.8	0.99
I25*	3	Occipital	back	120 kPa	39.9	60.9	0.8
	Group average				<b>-58.1 ± 43</b>	<b>-106.6 ± 93.9</b>	<b>1 ± 0.1</b>
	Coup pressure values from Hardy et al. (2007)				<b>68.1 ± 47.6</b>	<b>88.5 ± 64.9</b>	<b>16 ± 18.0</b>

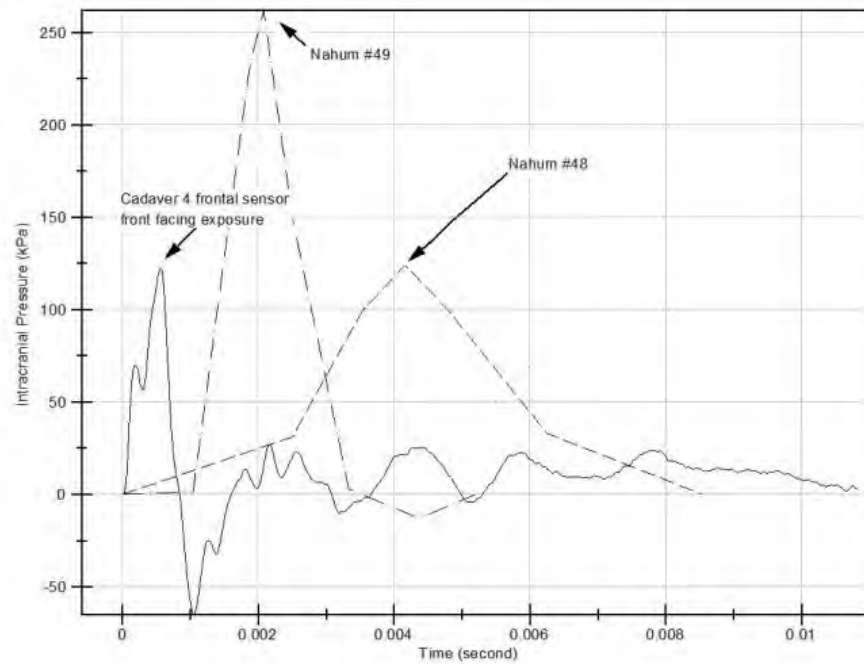


**Figure 5.20 Comparison of ICP near the frontal bone. Cadavers were exposed to either a face forward shock wave or blunt impact to the forehead. The blunt impact pressures are reported from Nahum et al. (1977) (Experiments 48 and 49). Each blunt impact trace consists of 8 points.**

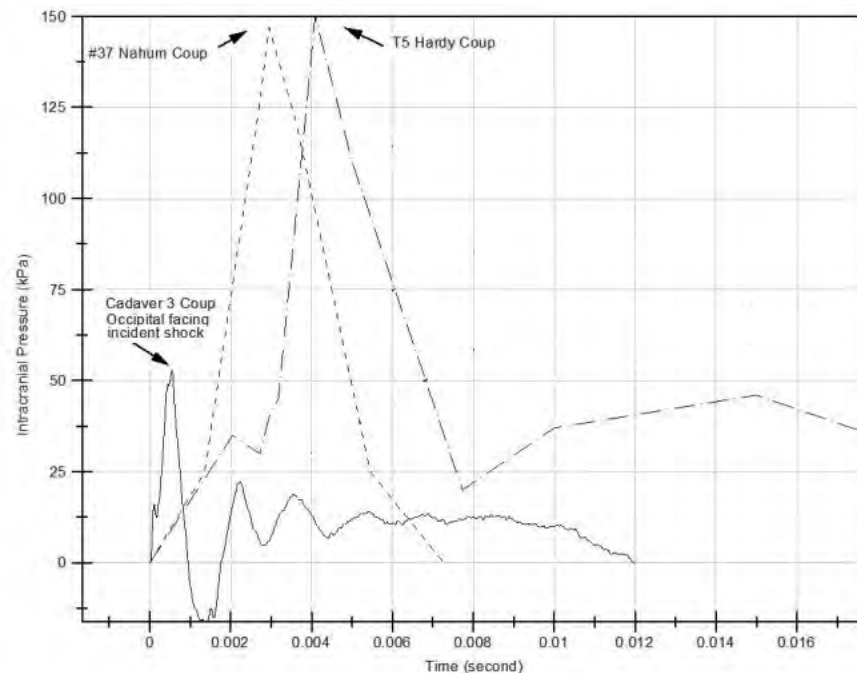


**Figure 5.21 The coup pressure response of a cadaver where the occipital bone was impacted or the back of the head was exposed to the incident shock wave. The blunt impact responses were reported from Hardy et al. (2007). Eight points were used to plot the blunt impact ICP responses.**

## 5.7 Formation of internal pressure gradients

It had been proposed that there are two events that take place during a blunt impact that affect the intracranial pressure gradients within the human brain (Gujidan et al. 1966). The first event results from skull deformation and the second results from head acceleration. It had been reported that the significant pressure gradients will develop and subside prior to significant rotation of the skull (Nahum et al. 1977). As demonstrated from the current shock wave exposed cadaver head ICP data, there was not a secondary pressure pulse during shock wave exposure that would be related to total head acceleration observed during blunt impacts.

The response of simplified physical models exposed to shock waves can provide insights into the response of the human head to shock wave exposure. A series of theoretical studies based on experimental data conducted by Iakovlev (Iakovlev 2006; Iakovlev 2007; McGinn et al. 2009) investigated the response of thin shelled fluid filled cylinders that were submerged in a fluid medium and exposed to external shock waves.

When the thin shelled cylinder was exposed to a shock wave, elastic waves would develop from the site of the incident load and propagate within the shell layer. These elastic waves propagate at the speed of sound in the shell and radiate into both the internal and external environments (Iakovlev 2006; Iakovlev 2007). During this time there will also be an out-bending of the shell.

A pressure wave propagates internally through the contained fluid. It is a compression wave and its amplitude, wave shape, and wave speed are dependent on the properties of the shell and the external and internal mediums. It was shown that in the case of a denser (along with the square root of modulus multiplied by density)

internal fluid compared to an external fluid, the speed of the wave within the internal fluid will increase. Also, as the stiffness or density of the shell increases, the magnitude of the pressure wave will decrease (Iakovlev 2006; Iakovlev 2007).

The combination of the advancing pressure wave and out-bending of the shell will create a tensile pressure region on the internal wall following the passage of the midline. The negative pressure is the result of the out-bending of shell wall which decompresses the fluid. This translation can be very small, and the rate at which the fluid decompresses has a significant role in the response. These regions of reduced pressure will then focus at the contrecoup area of the internal wall. This focusing is the result of constructive superposition that results from the symmetry of the cylindrical edges (personal communication with Dr. Iakovlev). The terms coup and contrecoup are defined as the locations of the formation of the positive and negative pressures during an impact and are not associated with pathology. Figure 5.22 shows the development of this negative region on the inner wall of the 2D cross section of the cylinder. The lightest region indicates compressive pressure, the dark region indicates tensile pressure, and the gray region indicates neutral pressure.

Theoretical work by Engin (1969), and Engin and Liu (1970) investigated the manner in which fluid filled spherical shells would respond to a radial impulsive load (3764 kPa). The purposes of their studies were to determine which regions of the brain would be the best candidates for injury due to interactions between the shell and the brain. They concluded that the skull will have the most significant effects on the pressure in the brain at the point of impact, at regions of out-bending of the bone, and the site opposite of impact where the regions of out-bending will be the highest which

will cause the greatest levels of tensile stress (Engin 1969). It was also shown that a thinner or more compliant shell will emphasize the fluid-structure interaction (Engin and Liu 1970).

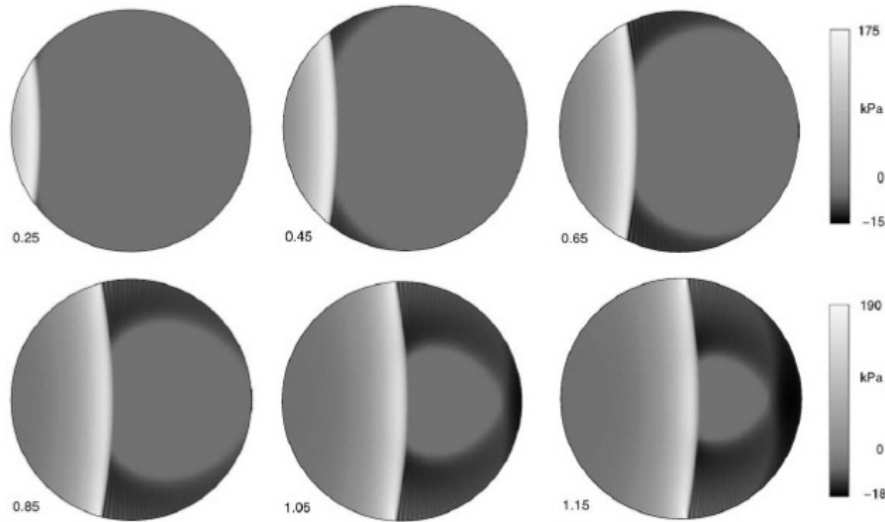


**Figure 5.22** A tensile pressure field develops in front of an advancing compression wave in a thin walled fluid filled cylinder. This negative pressure region will focus on the opposite side of where the incident load occurred. This tensile region results from an outbending of the shell. (Iakovlev (2006). External shock loading on a submerged fluid-filled cylindrical shell: Fluid-Structure interaction effects, *J. Fluids and Structures* 22, 997-1028).

The cadaver head has a more complex geometry and wall thicknesses that are variable and dependent upon location when compared to a sphere (Moreira-Gonzalez 1963). The response of the cadaver head to blunt impact was evaluated using intracranial pressure sensors (Thomas et al. 1966). A five pressure sensor array was placed in each principal axis to determine how pressure gradients develop in the brain during a blunt impact. The head was hung and exposed to pendulum impacts. The acceleration magnitudes ranged from 11 to 80 G. The rise times and durations were not

reported. The results of the study indicated that the pressure gradients developed in the fluid filled skull (Figure 5.23). Additionally, the pressure sensors near the internal skull surface opposite of impact (countercoup zone) developed the greatest tensile pressures. The wave profiles maintained greater tensile pressures when the foramen magnum was replaced with a rigid plug when compared to an elastic plug, suggesting the importance of boundary conditions on ICP response.

The coup/countercoup phenomenon has also been described by numerous computer models undertaking shock wave injury research (Moss et al. 2008; Chafi et al. 2009; Taylor and Ford 2009). Taylor and Ford have extensively investigated this phenomenon using mathematical modeling techniques and predicted the event occurs within the first .1-.2 ms following shock wave interaction.

This synopsis of research investigating the formation of ICP gradients within the brain has direct relevance to data provided in this chapter. The relationship between skull flexure and ICP demonstrated that when the bones of the skull went into tension, out-bending or “pulling” from the brain, a tensile pressure would develop. The literature cited supports these results that it is the flexing skull that is driving the ICP gradient formations. The DOA mode is believed to be the cause of this “out-bending”, forcing the formation of the tensile pressure in the brain.

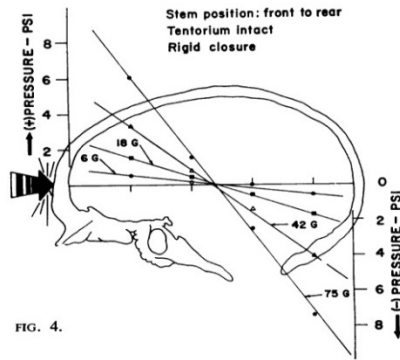


FIG. 4.

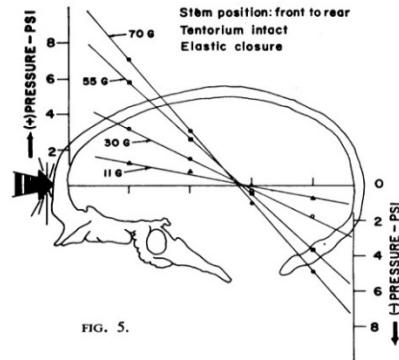


FIG. 5.

FIG. 4. Distribution of pressure (lb./sq. in.) along the antero-posterior axis due to a blow, with increasing magnitudes of acceleration, to the front of the skull with the falx and tentorium intact and a rigid closure over the foramen magnum.

FIG. 5. Pressure distribution along the antero-posterior axis with a frontal blow, with increasing magnitudes of acceleration, to the skull with the falx and tentorium intact and an elastic closure over the foramen magnum.

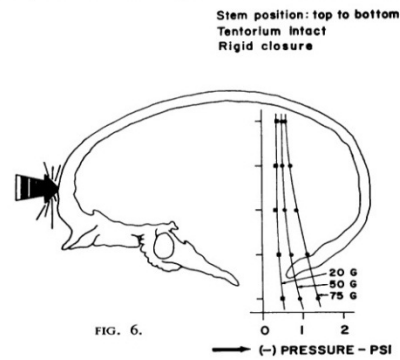


FIG. 6.

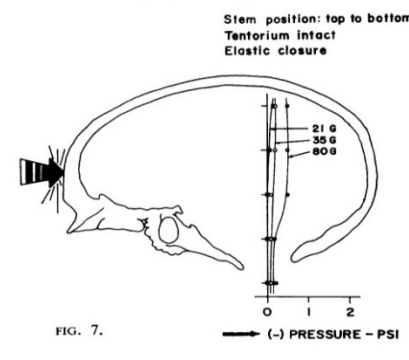


FIG. 7.

FIG. 6. Pressure distribution in the vertical axis with a blow, with increasing magnitudes of acceleration, to the forehead with the falx and tentorium intact and a rigid closure over the foramen magnum.

FIG. 7. Pressure distribution, with increasing magnitudes of acceleration, in the vertical axis with the falx and tentorium intact and an elastic closure over the foramen magnum.

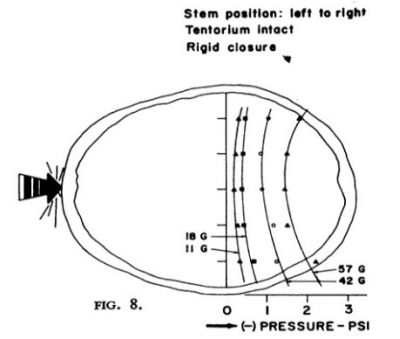


FIG. 8.

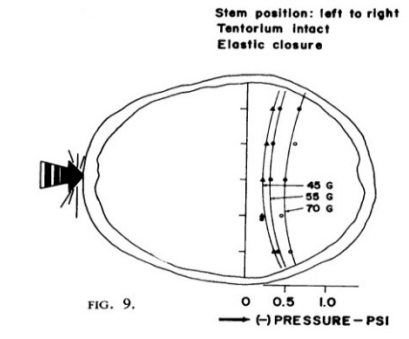


FIG. 9.

FIG. 8. Pressure distribution, with increasing magnitudes of acceleration, in the transverse axis with the falx and tentorium intact and a rigid closure over the foramen magnum.

FIG. 9. Pressure distribution, with increasing magnitudes of acceleration, in the transverse axis with the falx and tentorium in place and an elastic closure over the foramen magnum.

**Figure 5.23** The formation of the tensile ICP is greater against the interior skull surface and is greatest at the point opposite of impact. ICPs were measured using a fluid filled cadaver skull with either a rigid or elastic cap covering the foramen magnum. (Photo reproduced from Thomas et al. 1966. Experimental intracranial pressure gradients in the human skull. J. Neurol. Neurosurg. Psychiat. 29. 404.

## 5.8 Frequency response of the cadaver head to impact

The current data indicate that the loading of the incident shock wave on the surface of the skull will cause secondary intracranial pressure oscillations that are of higher frequency than experimental blunt impacts (Nahum et al. 1977; Stalnaker et al. 1977; Hardy 2007). This was demonstrated experimentally (Figure 5.20 and Figure 5.21). Due to the combination of the rise time of the shock front and the nature of the diffracted shock wave as it traverses the skull, additional modes of flexure may be excited.

Figure 5.24 describes the frequency response of the cadaver head for different rise times associated with impact. When the rise time of a blunt impact shortens, skull fracture can develop. Generally, highly localized forces are required to excite this response. The short rise times associated with a shock wave will subject the head to a wider band of excitation frequencies than what the head would be exposed to during a blunt impact. Aside from shorter rise times, the skull will experience diffracted loading. This includes the reflected pressure for regions normal to the shock wave propagation and regions parallel that experience loading amplitudes similar to the incident pressure magnitude. The combination of these factors may excite additional modes of skull flexure that would cause the ICP response to be different between a blunt impact and shock wave exposure.

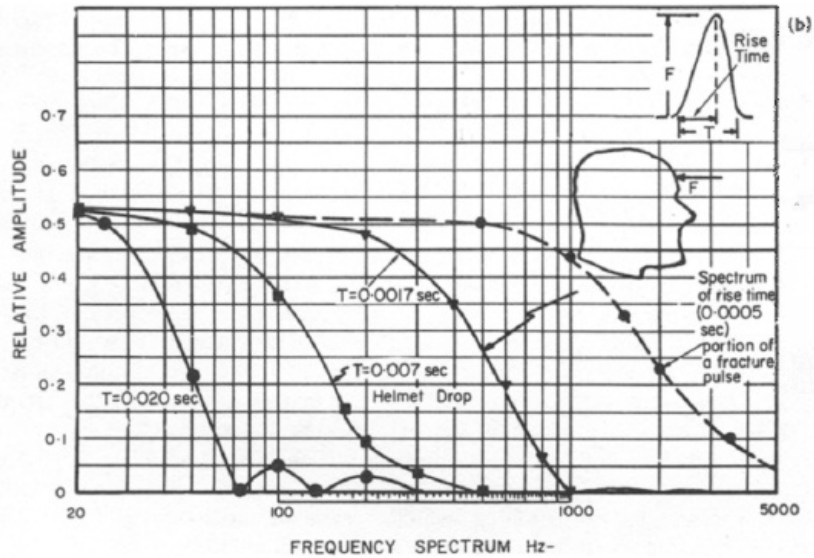


**Figure 5.24** The frequency response of the cadaver head during a frontal impact is dependent on the rise time of the initial event. As the rise time of the impact decreases, higher frequency content will be present. (Graphic taken from Gurjidan et al. 1970. Studies on mechanical impedance of the human skull: Preliminary report. J Biomech. 3; 239-247)

## 5.9 Hypothesis of response

Based on the collected data, a hypothesis of the response of the cadaver head when exposed to a shock wave can be made: The head is supported in the shock tube. The shock wave interacts with head. This interaction excites three observable modes of response. The region of the head exposed to the reflected pressure will undergo compression and the sides of the head go into tension. A series of larger amplitude oscillations resulting from this initial deformation will then dampen and return to baseline. At the same time, the second mode is excited that causes the bones to oscillate at a higher frequency at lower amplitude. The third response is a global compression of the head by the shock wave.

Due to the coupling between the skull and the brain via the meninges, the flexural modes taking place in the skull will cause the formation of dynamic pressure responses within the brain. The deformation of the skull caused by the reflected

pressure will drive the formation of the coup pressurization on the near-side of the brain. Contrecoup pressurization will form on the far-side as a result of out-bending of the bones. The damped oscillation axisymmetric (DOA) response mode, by alternating in tension and compression, will cause the formation of additional regions of positive and negative pressure within the brain. The high frequency low amplitude (HFLA) mode will transmit high frequency low amplitude oscillations into the brain. Additionally there will be a slight background positive pressurization, resulting from the quasi-steady compression.

### **5.10 Conclusion of Cadaver Testing**

The purpose of this chapter was to investigate if modes of skull flexure could be observed for the cadaver head during shock wave exposure and determine if these modes could be used to describe the resulting ICP response. Five cadaver heads (one frozen, five fresh) were exposed to shock waves at three intensities and four different orientations. Both intracranial pressure and skull strain were measured during the testing.

Three modes of skull flexure were observed in the strain and ICP data: The damped harmonic axisymmetric (DOA) mode, the high frequency low amplitude (HFLA) mode, and the quasi-steady compression (QSC) mode. The DOA and HFLA modes were both excited during the initial interaction of the shock wave with the skull. During this initial interaction, the region of the head exposed to the reflected pressure is compressed and the sides of the head go into tension. The back side of the head will also go into tension. This is expected to be a result of out-bending of the skull. Each

region will then oscillate and return to baseline. Frequencies at which the bones of the skull oscillate appear to be specific to the bone being measured.

The ICP response of the cadaver was dependent on the orientation in which the head was exposed to the shock wave. In the brain, nearest to the reflected pressure, a compressive phase ICP pulse would result, which is believed to be a result of compression of the bone to which it is coupled. On the contralateral side of the intracranial vault, a tensile phase ICP pulse would develop in the same time domain, which is believed to be a result of out-bending of the bone.

It could be argued that the magnitudes of the strain values for the cadaver may be too low to cause significant changes in intracranial pressure. In Chapter 3, it was hypothesized for the rat that the bones composing of the skull may be hinging about the suture lines. In this series of tests, all strain gages were adhered in locations that were not on suture lines. In future studies, measurement of skull strain about the suture lines will need to be undertaken to determine if hinging will occur in the human.

The skull is coupled to a pressurized system where changes in ICP can cause shifts in the cranial bones in cats at rest (Adams et al. 1992). Humans are not cats, but the cranial bones may not be entirely fused and further research should be undertaken to understand the exact nature of how sutures articulate in the adult human. If the bones composing the skull are responding semi-independent of each other, the hypothesis that the bones are oscillating at their own characteristic frequencies becomes more probable. To determine if entire cranial bones are oscillating during shock wave exposure, this author and colleagues have proposed the use of 3 dimensional laser displacement sensors to map cranial bone movement during shock wave exposure.

Such experiments are being considered at the Canadian Defense Research and Development Center in Suffield, Alberta, Canada.

Due to the large number of sensors that were lost in the study and small sample sizes, a large statistical analysis and corridors for the response of the cadaver head to shock wave exposure were not completed. Further studies are needed to build on these data, but the data does provide enough information to warrant these studies. The data show that the observed flexural modes of the human skull can be related to the observed ICP response, providing further evidence for the multi-modal skull flexure hypothesis.

## CHAPTER 6 IDENTIFICATION OF RELEVANT BIOMECHANICAL RESPONSES ACROSS SPECIES

### 6.1 Introduction

Three distinct species (rat, pig, and human) have been exposed to multiple shock waves in order to provide insight into the biomechanical responses that could be related to the multi-modal skull flexure hypothesis. Through this project, multiple modes of skull flexure occurring during shock wave exposure have been identified and related to ICP responses for each species tested. Responses across the three species will be compared to determine similarities and differences. Because physiological responses cannot be measured in cadavers, it needs to be determined that physiological responses resulting in animal models are appropriate for predicting or scaling injury to humans. For example, loading conditions to the rat brain may present specific injury patterns that would never occur in the human brain. It is possible that animal models may never be able to create pathologies that develop in humans and their pathological responses may be misleading for those studying injury in humans.

### 6.2 Relationships between the rat, pig, and cadaver

The shapes and sizes of the skulls differed between species (Figure 6.1). The human skull is more spherical in shape with a comparatively reduced muzzle length, with the largest of brain mass of the three species. The thickness of the human frontal bone was over times greater than the rat parietal bone Table 6.1. The pigs used in this study had skull thicknesses greater than what was observed in the human (frontal bone thickness was greater than 11 mm).

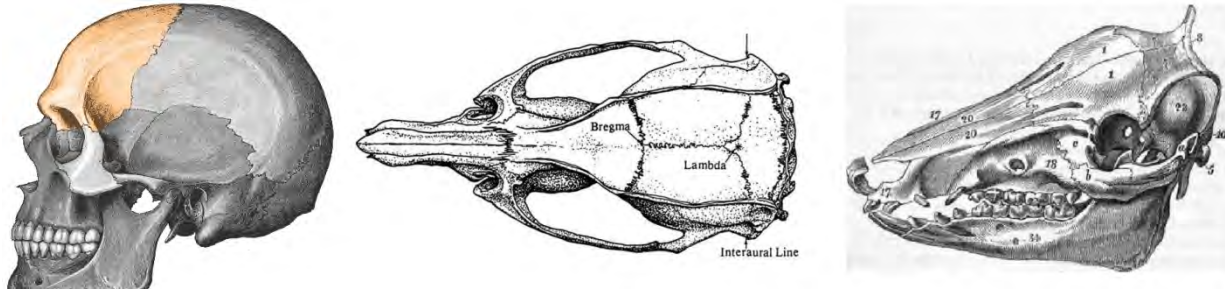


Figure 6.1 A side by side comparison of the different species that were tested in this project.

Table 6.1 Bone thickness measurements for the three species tested in this project. Human (frontal bone), Pig (frontal bone), and rat (parietal bone).

Species	Bone Thickness (mm)	Reference
Rat	$.630 \pm .06$	microCT results
Pig 3 month 5 month 7 month Tested	$4.2 \pm 0.6$ $8.7 \pm 3.2$ $11.9 \pm 2.6$ > 11 mm	Sun et al. 2002 Data
Human	$7 \pm 0.3$	Moreira - Gonzalez et al. 1963

A system will respond uniquely to the shape and duration of the excitation to which it is subjected (Misra et al. 1978). It was discussed prior that the frequency in which a system will oscillate following an excitation is dependent on mass and stiffness. Each system has a damping coefficient which determines how long the series of oscillations will exist. The transit time of the shock front across the skull surface is much shorter for the rat than both the pig and the cadaver (Table 6.2). The rat head was already engulfed by the shock wave by the time the shock front had traversed the frontal bone in the human.

The bones comprising the skull in the human (frontal, parietal, occipital) that are directly coupled to the brain are subjected to shock wave loading for a longer duration of time when compared to the pig. In Chapter 5, the net horizontal load on the cadaver during shock wave exposure was calculated using formulae designated for an arched surface. It was expected that these calculations would not be appropriate for geometries similar to the pig and the rat skulls, which are more conical. It can be assumed that objects with larger cross sectional areas will experience greater reflected pressures, assuming similar aerodynamics between the objects. For a front facing exposure, there is a larger percentage of surface area that is coupled to the brain in the cadaver when compared to the pig. Based on these observations, it can be hypothesized that the bones encasing the cadaver brain will be subjected to longer loading times and have a larger percentage of surface area subjected to reflected pressure than both the rat and the pig.

**Table 6.2 Shock front interaction times between different species. The skull lengths and braincases were measured from the specimens tested in this study.**

Species	Tissue	Distance (mm)	Travel Time ( $\mu$ s)
Rat	Skull	45	92
Porcine	Skull	260	531
Cadaver	Skull	180	367
Rat	Brain	25	51
Porcine	Brain	80	163
Cadaver	Brain	150	306

### **6.3 Biomechanical responses occurring across species during a front facing exposure**

Of the three species tested in this project, the rat demonstrated the most unique responses in both strain and ICP measurements. For both positions in which the ICP sensor was mounted in the rat brain, the overall ICP response was dominated by the

quasi-steady compression (QSC) mode of skull flexure. It was discussed prior, that the exaggerated QSC response was most likely the result of the compliance of the brain case, and specifically the superior brain case. Although the cadaver head and pig head ICP responses did have a contribution associated with the QSC mode, the effect was less significant. This may or may not have been an artifact of the head being sealed and detached from the body.

The strain and ICP responses were compared for each species at the low intensity for a front facing exposure. In Figure 6.2, the principal strain results indicated that the highest strains were observed within the first two milliseconds for all species. The responses will dampen out and return to baseline. Both the max and min principal strains were included for the pig and the cadaver because it was shown that both responses were important for describing the ICP response. Oscillations associated with the damped oscillation axisymmetric (DOA) response mode existed for a longer period of time for the cadaver when compared to the other species. The rats reported the greatest strain magnitudes and had the greatest levels of compression associated with the quasi-steady compression (QSC) mode.

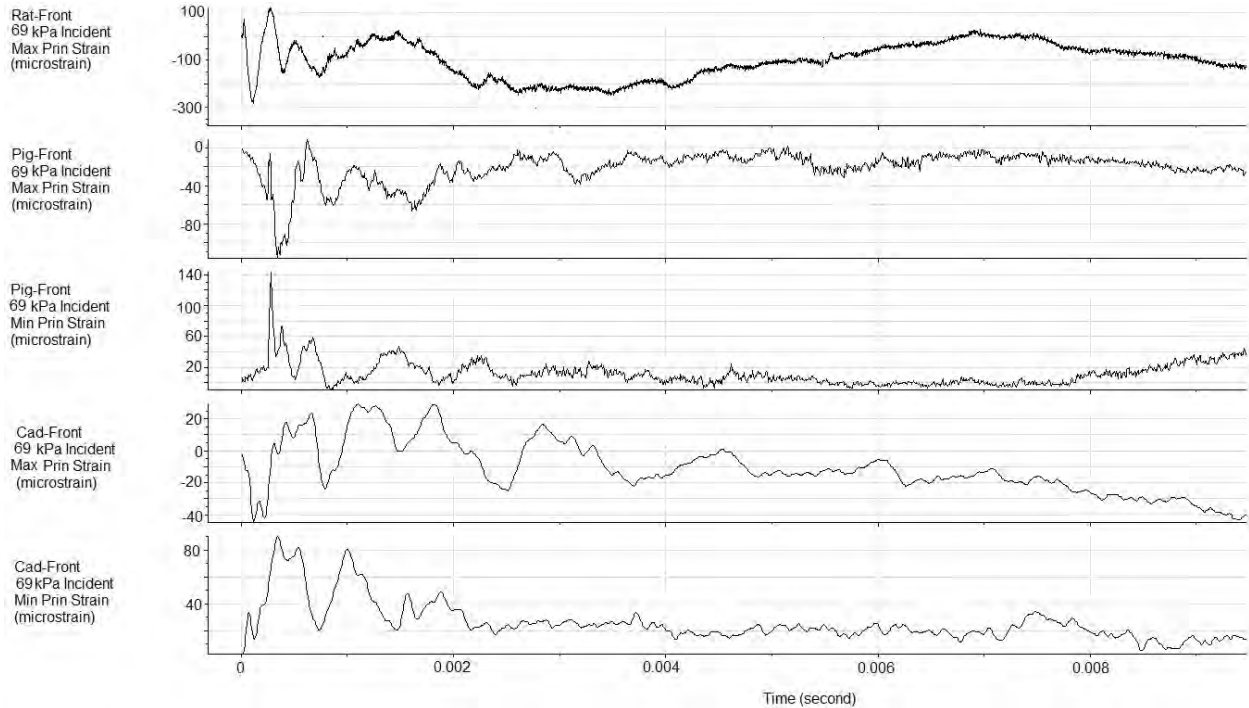


**Figure 6.2** The strain response for each of the species tested at the low pressure intensity.

The ICP response for each species was compared (Figure 6.3). The ICP responses resulting from the DOA, HFLA, and QSC modes of skull flexure were present in the data. The rat had the greatest QSC component and the HFLA waveforms were present in the cadaver and pig. The cadaver ICP profiles included a large pressure inversion that was not observed in the other species, and oscillations associated with the DOA mode that continued for the longest time. The cadaver also had the highest magnitude peak pressure.

To better observe the frequency content associated with the ICP profiles, pressure traces were separated out and plotted to amplitude range (Figure 6.4). The ICP signals were then filtered with a 500-7000 Hz band pass filter to remove content

associated with the QSC component to determine if similarities existed between the responses across specimens (Figure 6.5). The filtering demonstrated that the three species undergo a similar response shape. The response is an initial compression, then pressure inversion, followed by a series of oscillations. The response associated with the rat was of higher frequency and shorter duration than the pig and the cadaver. This response was expected to be the result of the DOA mode of skull flexure. HFLA frequency content was also observed for the cadaver and pig. The frequency associated with the DOA mode was compared between each species. The DOA frequency is significantly different between groups (\*  $p < 0.05$ ,  $p < 0.0001$ ) where the pressure response measured in the rat oscillated at the highest frequencies and the pressure response measured by the frontal sensor in the cadaver oscillated at the lowest frequencies (Table 6.3).

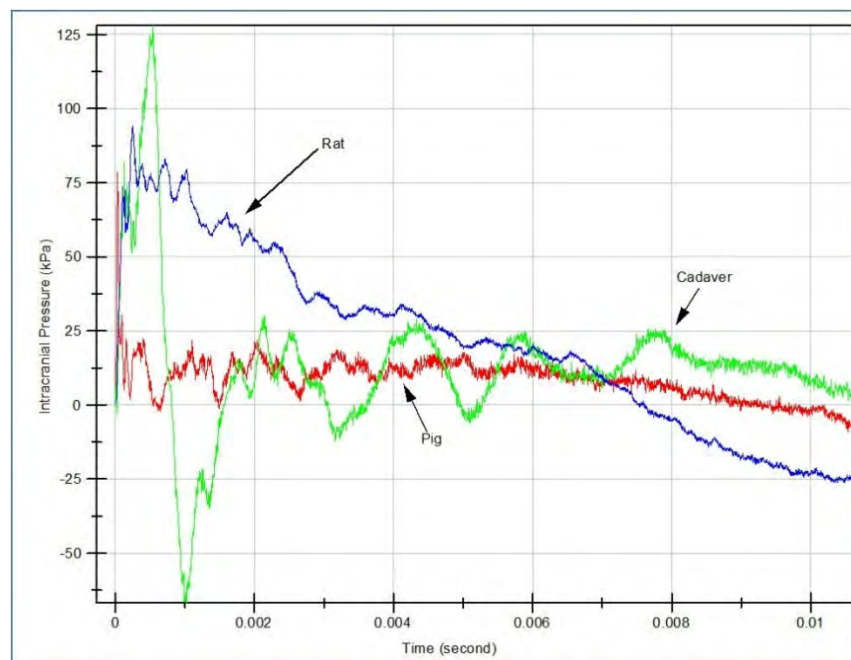
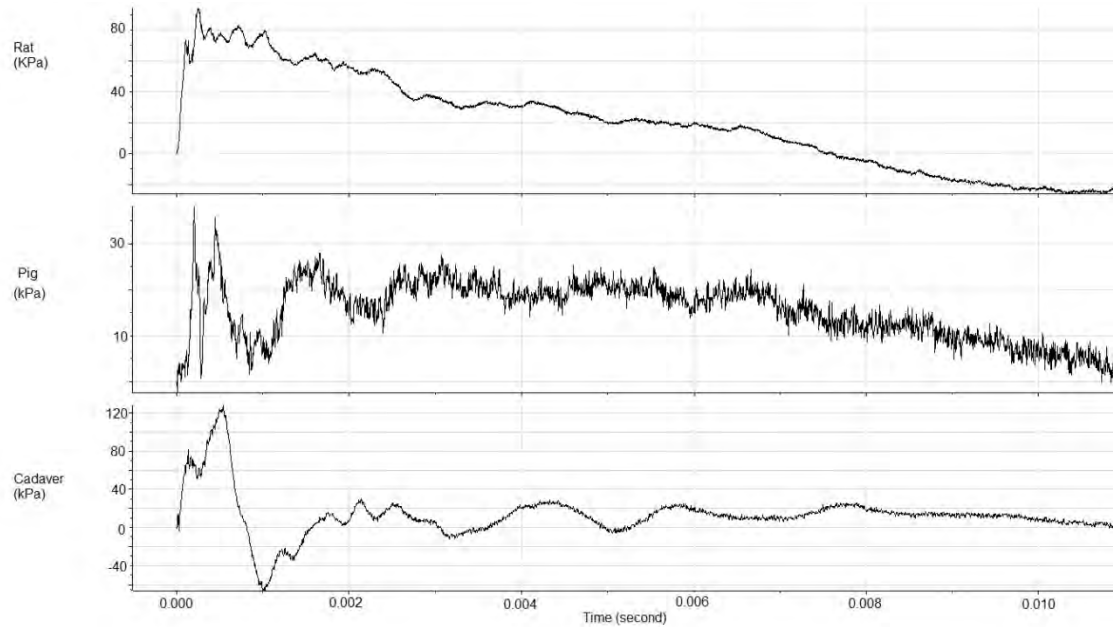
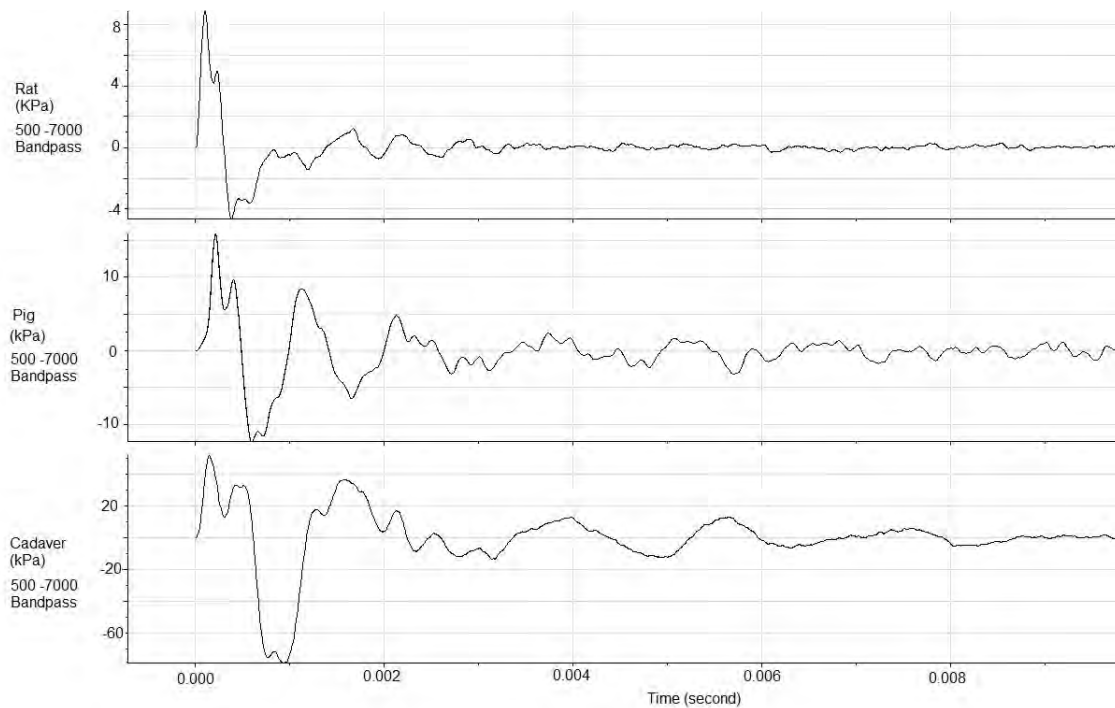


Figure 6.3 The ICP response for each species when exposed to a low intensity shock wave.



**Figure 6.4 Isolated ICP pressure profiles for each species during a front facing exposure. This was done so that frequency content was more observable.**



**Figure 6.5 Band pass filtering was applied to better observe the DOA waveform. When this filtering is applied, the DOA response in the rat became much more evident.**

**Table 6.3 The frequency of the DOA waveform was significantly different (\*  $p < 0.05$ ) between species.**

Species	N	Mean	Std. Dev.
Rat	16	5113	1499
Pig	8	1115	278
Human (frontal)	21	443	104

#### **6.4 ICP comparison between the pig and cadaver by orientation**

It had been demonstrated in prior chapters that the pig and cadaver ICP responses are highly dependent on orientation of the head relative to the incident shock wave and that this response may be related to skull flexure. The frequency of the oscillations associated with the DOA mode of skull flexure was higher for the pig when compared to the cadaver. In Figure 6.6, it was shown that the pressure responses associated with three identified modes of skull flexure were present in both species during a front facing exposure. In Figure 6.7, the ICP responses were compared for a side facing exposure. Similar characteristics are present for this exposure as well, except that the transient phase does not demonstrate as strong of a tensile component in the pig as it does in the cadaver. The pressure response between the species was provided for a back facing exposure (Figure 6.8). The transient negative phase in the cadaver was of greater amplitude than in the pig. The frequency of the transient phase in the pig was higher than that in the cadaver. In prior chapters a relationship between skull strain and ICP was described for each species. It can be hypothesized that the increased DOA frequencies are related to higher frequency oscillations of the bones composing the skull for the pig.

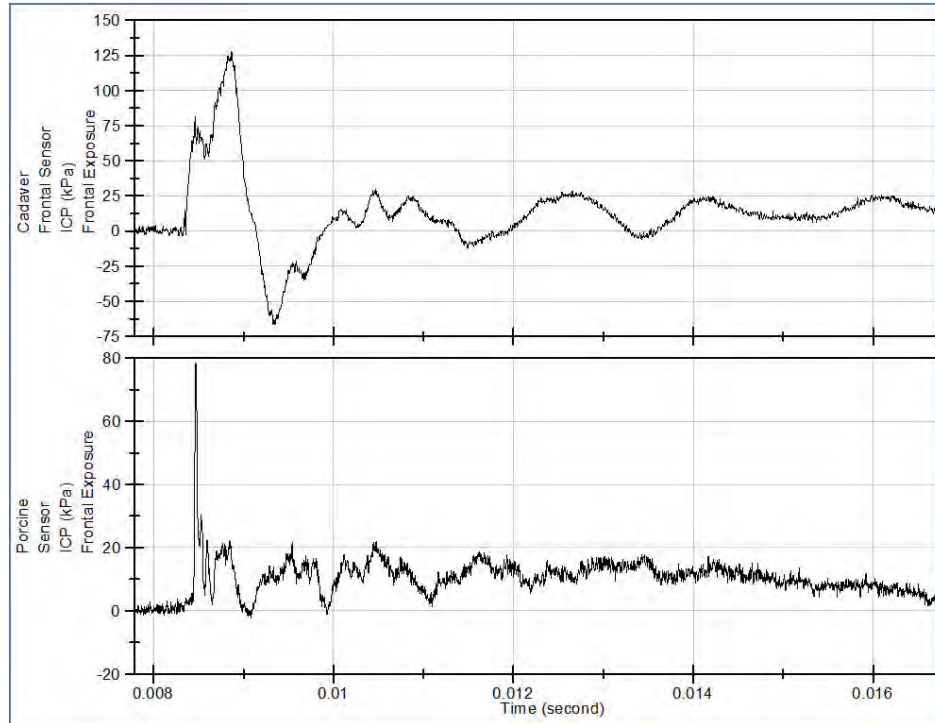


Figure 6.6 The ICP responses for the pig and cadaver when subjected to a shock wave during a face forward exposure.

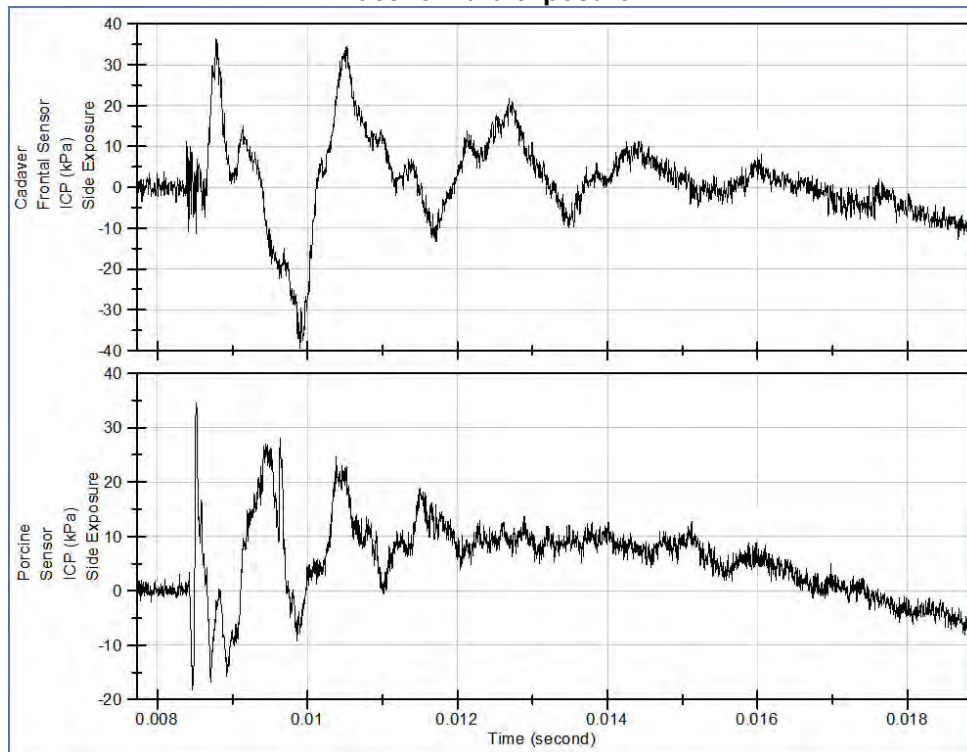


Figure 6.7 The ICP responses of the cadaver and pig when subjected to a side facing exposure.

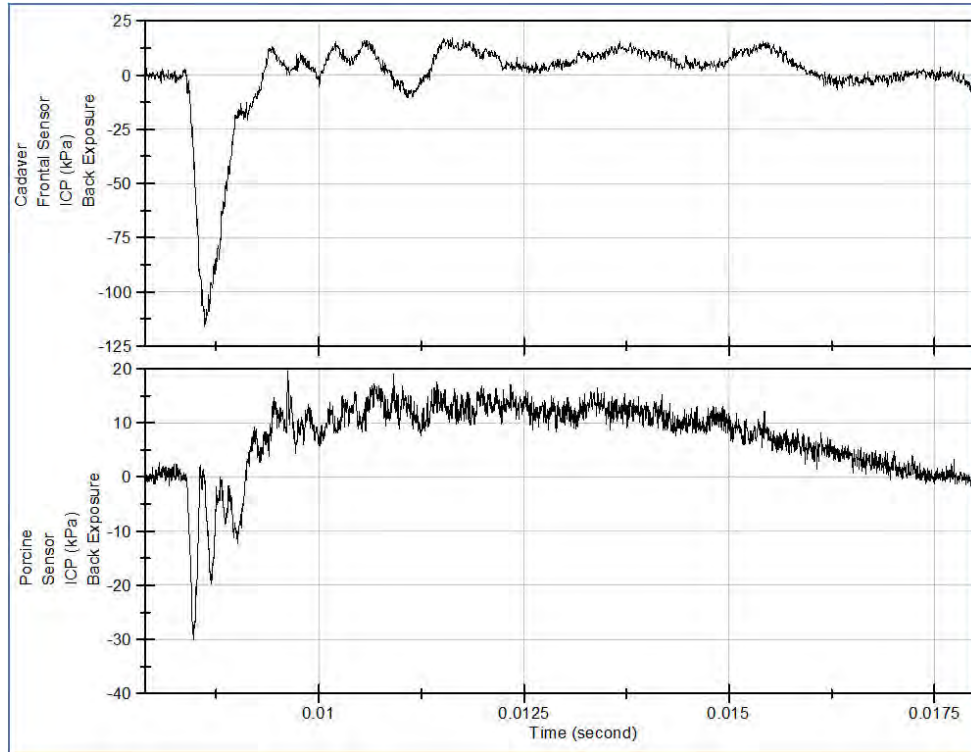


Figure 6.8 The ICP responses of the cadaver and pig when subjected to a back facing exposure.

## 6.5 Discussion of results

The skull flexure and subsequent ICP responses of the rat, pig head, and cadaver head were measured during interaction with a shock wave within a shock tube. Each of the different systems responds in a manner that is unique. The observed modes of skull flexure in this project provide a frame work in which to evaluate the responses between the three species.

The exaggerated ICP response in the rat was presumably the result of having a much thinner and flexible skull. The initial ICP inversion measured in the cadaver head was not observed to as great of an extent in the other species when comparing the unfiltered ICP responses. In chapter 5, it was shown that this pressure inversion was the result of the frontal bone “pulling” away from the brain case (as measured by the

max and min principal strains). It is hypothesized that this response would be the result of the combination of geometry of the system and the period of loading of the shock wave on the front of the head. The period of the initial ICP pulse was on the order of 1 ms. The front of the cadaver head is relatively flat and there is a larger percentage of bones directly coupled to the brain when compared to the other species tested. It is hypothesized that because of the flat surface and direct coupling to the brain, the frontal bone of the cadaver will experience higher magnitudes of reflected pressure across the surface. This loading will cause a larger amount of deformation that will be imparted to the brain, causing increased compressive pressure. When the bone “rebounds” (moves away from the brain), as a response to the compression, an increased tensile pressure will develop.

In the filtered ICP signals for the front facing specimens, a relationship does exist between the three species for the transient mode of response. The response consists of a rise in pressure, followed by an inversion and a damped series of oscillations. The rat, followed, by the pig, had higher frequencies than the human. Attempts were made to find a method in which to scale the responses of the species across each other, so that the frequency of the DOA oscillations in the rat ICP response would be related to the frequency of DOA oscillations in the cadaver ICP response. Simplistic methods such as calculating breathing mode frequency (Nayfeh and Arafat 2005) were attempted but considerably over predict the response. Currently simplified calculations have not been able to predict the relationship between species, but warrants future study. Finite element methods (FEM) may be the best option to determine how a relationship between the responses of each species once further experimental data can

be acquired to validate each model, so that model predicted responses correspond to the actual responses in specimens. However, biological material characterization and definition of boundary conditions need to be refined. It is also recommended that suture lines be incorporated into the model and assumptions such as a rigid skull should be avoided.

The comparison of ICP responses between the human and the pig by orientation was of interest because the measured signals were similar. The pig had higher frequencies of oscillation than the cadaver. The manner in which the pressure developed within the brain was shown to occur by different responses of skull flexure. For example, compressive pressure *increased* in the front and side orientations when the max and min principal strains moved in tension for the pig and compressive pressure *decreased* for the human when the max and min principal strains moved in tension when subjected to similar incident shock waves. The mechanisms for these responses were described in prior chapters. These results demonstrate that similar ICP responses could be developed from different methods of flexure.

Two points need to be made when comparing the ICP results. The first is that the comparisons between the pig and cadaver were only presented for one region of the brain (frontal lobe). It was shown for the cadaver that the ICP response was dependent on location. Data currently does not exist to determine if the pig responds in a similar manner to the human in all locations in the brain. It is expected that it would not, due to the geometry differences of both the skull and brain. In addition both the cadaver and pig were tested detached from the body. The PREVENT pig data, which was collected in vivo, showed a greater QSC component than the WSU pig data. Possible

explanations were provided for this difference in response in chapter 4. It is possible that a similar effect could be observed in the cadaver if the total body were included and pressurized during the testing. This should be addressed in future experiments in order to determine if a larger QSC component exists during full body cadaver testing.

## **6.6 CNS susceptibility to imparted pressure gradients**

It is important to determine the susceptibility of the CNS to each pressure response. Pathological responses of the CNS may be specific to a frequency within a pressure waveform. For example, the mean frequency of pressure oscillations associated with the DOA mode for the frontal bone of the cadaver and pig was 433 Hz and 1115 Hz respectively. Because the ratios of the described pressure responses are specific to the system being tested, it becomes much more difficult to scale injuries from specific species to the human until specific CNS tolerances can be determined.

A recent paper (VandeVord et al. 2011) investigates the cognitive and neuropathological responses of the rat resulting from shock wave exposure. The report indicated that at a specific band of pressures near 117 kPa, exaggerated neurotrauma resulted when compared to rats exposed to greater and lower magnitudes of incident shock waves. This range specific pathophysiological response was in agreement with the biomechanical responses reported in this study and does provide some evidence for a range-specific hypothesis of injury in the rat.

At this time it is recommended that scaling to the human based on injury tolerance values in animals be avoided until CNS susceptibility to specific waveforms can be determined. It needs to be re-emphasized that the intracranial pressure environment within a rat or pig is different than what the human brain will experience.

Once it is determined how the CNS is being damaged, interventions can be undertaken to treat these injuries. Post exposure therapies can be introduced that will mitigate secondary pathophysiological cascades. If cell susceptibility is found to result from a specific waveform, equipment can be designed that would prevent the mode of flexure that is inducing injury. It is still too early to determine what this technology would consist of, but this may be the most logical option if an injury mechanism is identified.

## 6.7 Discussion of hypotheses

Two hypotheses were proposed in chapter 1:

- **Hypothesis 1:** *Shock wave exposure will excite multiple modes of response of the skull and due to the coupling at the skull/brain interface, pressure gradients will be propagated into the intracranial contents.*
- **Hypothesis 2:** *Physical differences between species (such as thickness of the bones and geometry of the skull) will significantly affect the skull/brain biomechanical responses.*

The data presented allows for the acceptance of the first hypothesis. Multiple modes of skull flexure were identified for each species: The damped oscillation axisymmetric (DOA) response mode, the high frequency low amplitude (HFLA) response mode, and the quasi-steady compression (QSC) mode. The DOA mode results from the loading of the system where a series of large oscillations will result following an initial deformation. The manner in which this mode presents was provided for each species. The HFLA mode was best observed for the pig and the cadaver. For the cadaver, this mode was best observed in single channel strain profiles and resulted

from excitation of the bone being loaded by the shock wave. These frequencies could be over 1 kHz higher than the frequencies associated with the DOA mode. The QSC mode resulted from the external loading of the pressure wave. The mode created a global compression on the system.

These modes of skull flexure were shown to be related to the ICP response in each of the species. For the pig and the cadaver, the max and min principal strains were used to show how skull flexure could affect the ICP environment. This relationship was shown across orientations. Also, it was shown that when the brain becomes decoupled from the skull, lower pressure magnitudes develop, and the response shapes less resemble the strain responses of the skull. Because of this and other data presented in the dissertation, hypothesis 1 is accepted.

The pressure responses within the brain will be unique to the species subjected under similar loading conditions. The data provided in this chapter support this statement. The QSC component is hypothesized to be greater for the rat because of its thinner, more compliant skull. The frequencies of oscillation will also be specific to species. Frequencies are determined by mass and stiffness for an oscillating system. The manner in which modes present is also specific to species. For these reasons and the data presented throughout the dissertation, hypothesis 2 is accepted.

## 6.8 Conclusion

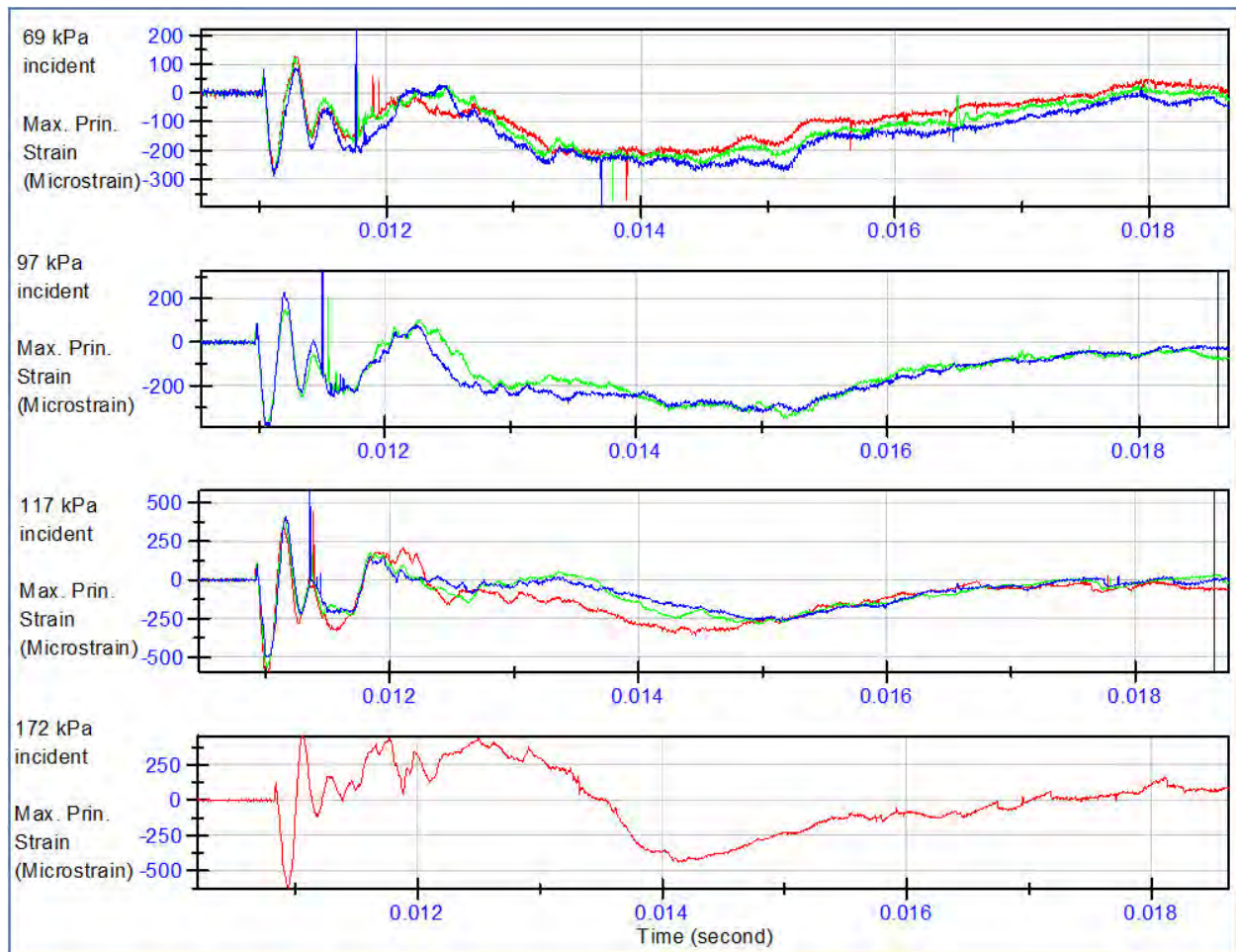
In conclusion, it was demonstrated that there are specific flexural modes occurring in the skull and can be related to ICP responses for a given species when subjected to a shock wave. This means that there is a combined effect of patterns in which the skull is flexing that is driving the formation of the ICP environment. It has also

been demonstrated that the pressure environment will also be somewhat localized, which further complicates the response.

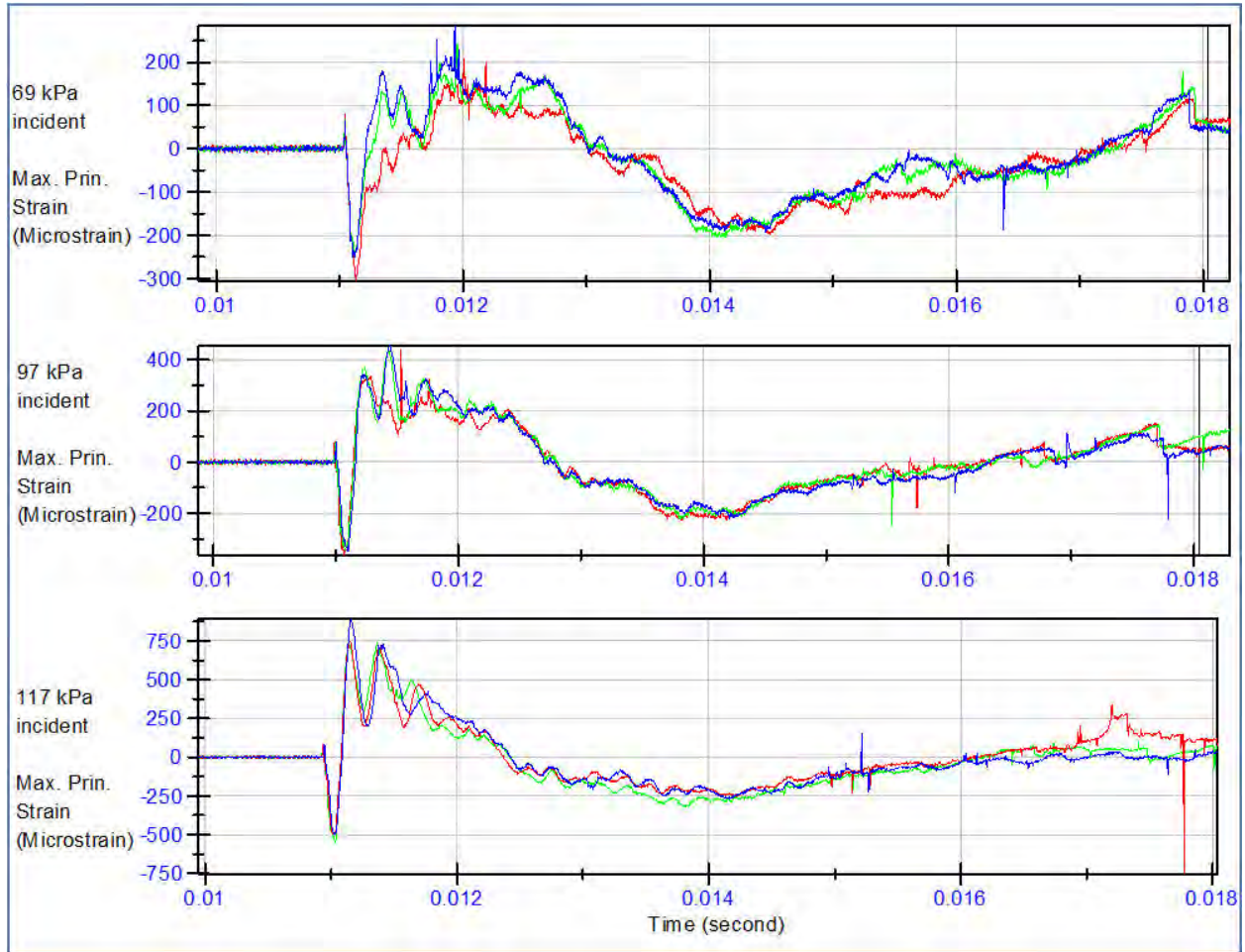
The manner in which these waveforms present is specific to the species, amplitude of the shock wave, and orientation of the head. Therefore, it is hypothesized that the injury response for a rat will be different than that of a pig under the same loading conditions.

This research provides a basis for the direction future research in this field will need to be pursued. Injury response data from testing with the rat should be closely examined as it responded the most uniquely of the three systems. The cadaver experienced pressure inversions and coup-contrecoup pressurization beyond that of the pig for the same incident shock wave intensity. Therefore, the response of the cadaver head will need to be further investigated to completely define the biomechanical responses that result from shock wave exposure. Those pressure waveforms will then need to be subjected to live CNS cells to determine which components are the most damaging. Finally, the cadaver will need to be investigated under a greater range of intensities to determine how the ICP response will change as a result of much higher shock wave amplitudes. A dose dependent response is probable along with a “sweet spot” where the most exaggerated neurotrauma would take place based on optimal excitation of the bones exposed to the shock wave.

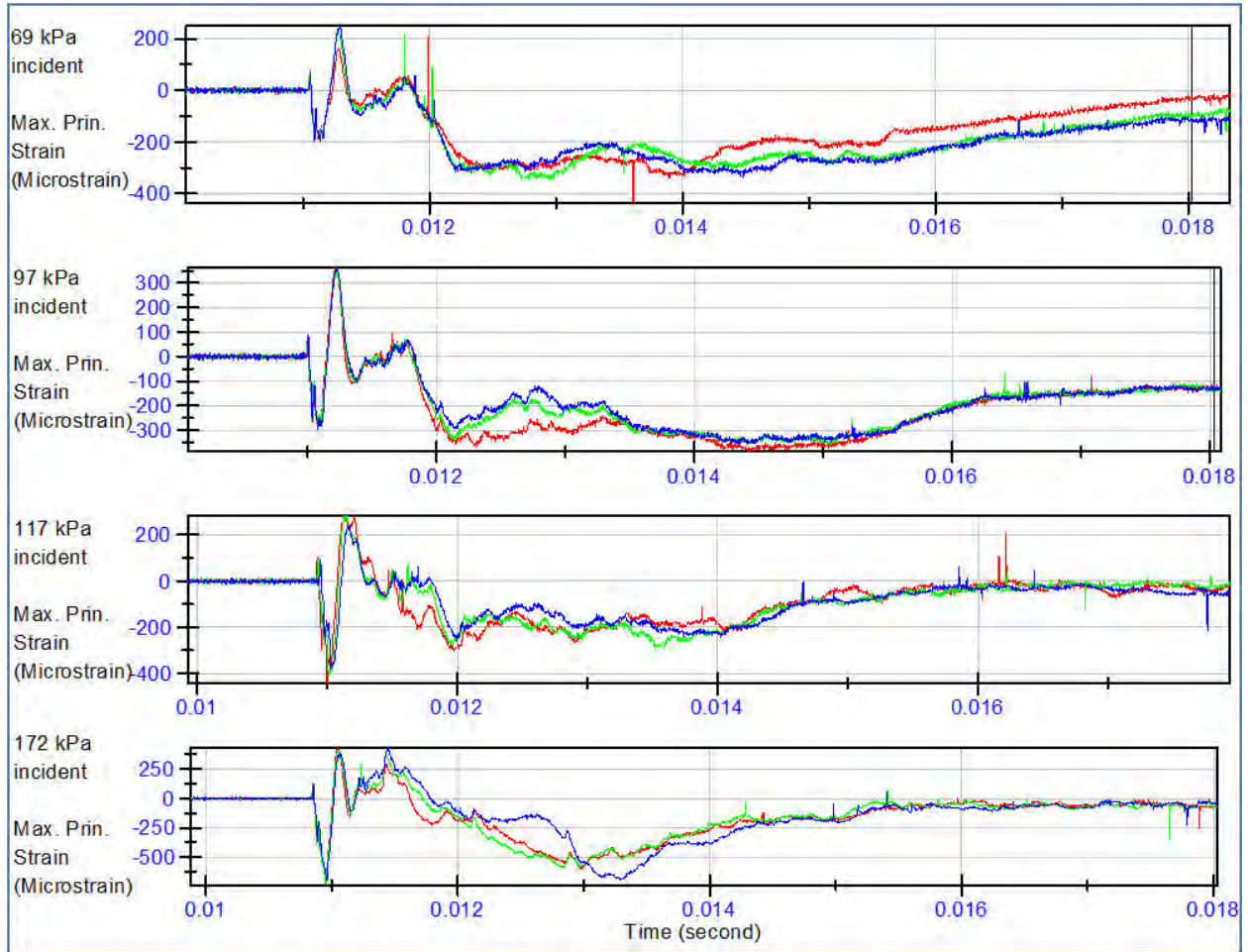
## APPENDIX A RAT DATA



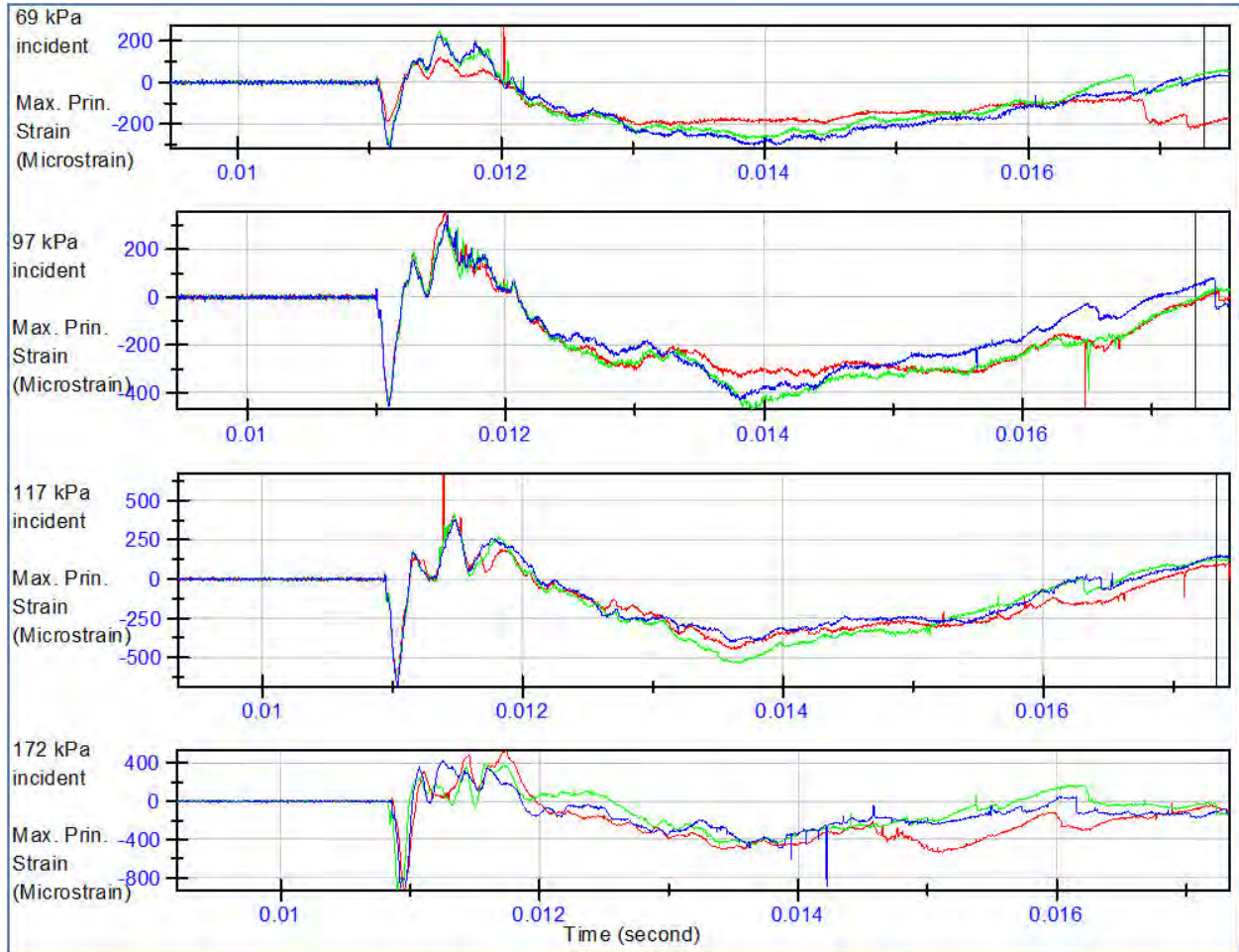
Strain response for a 247 gram rat.



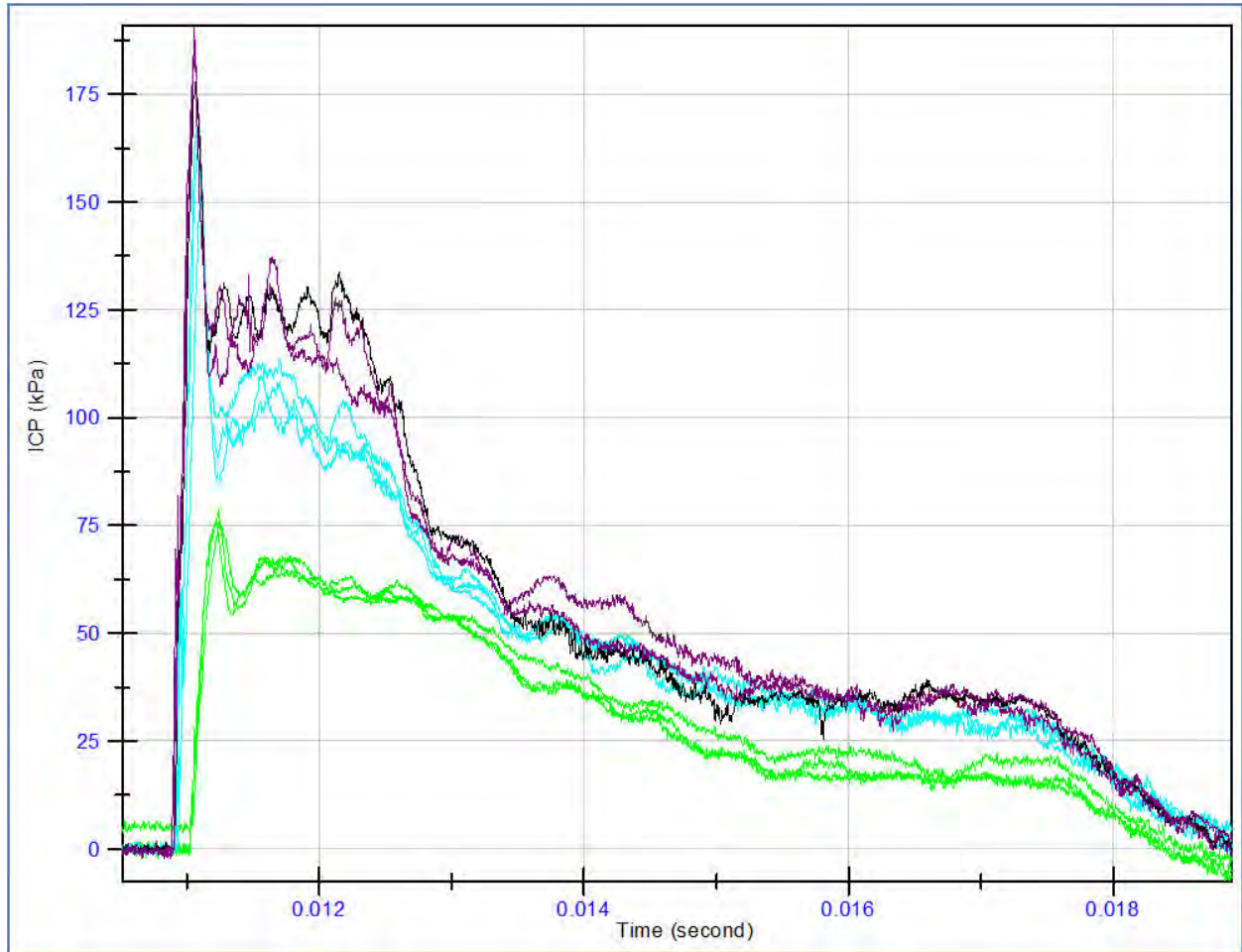
Strain response for a 266 gram rat.



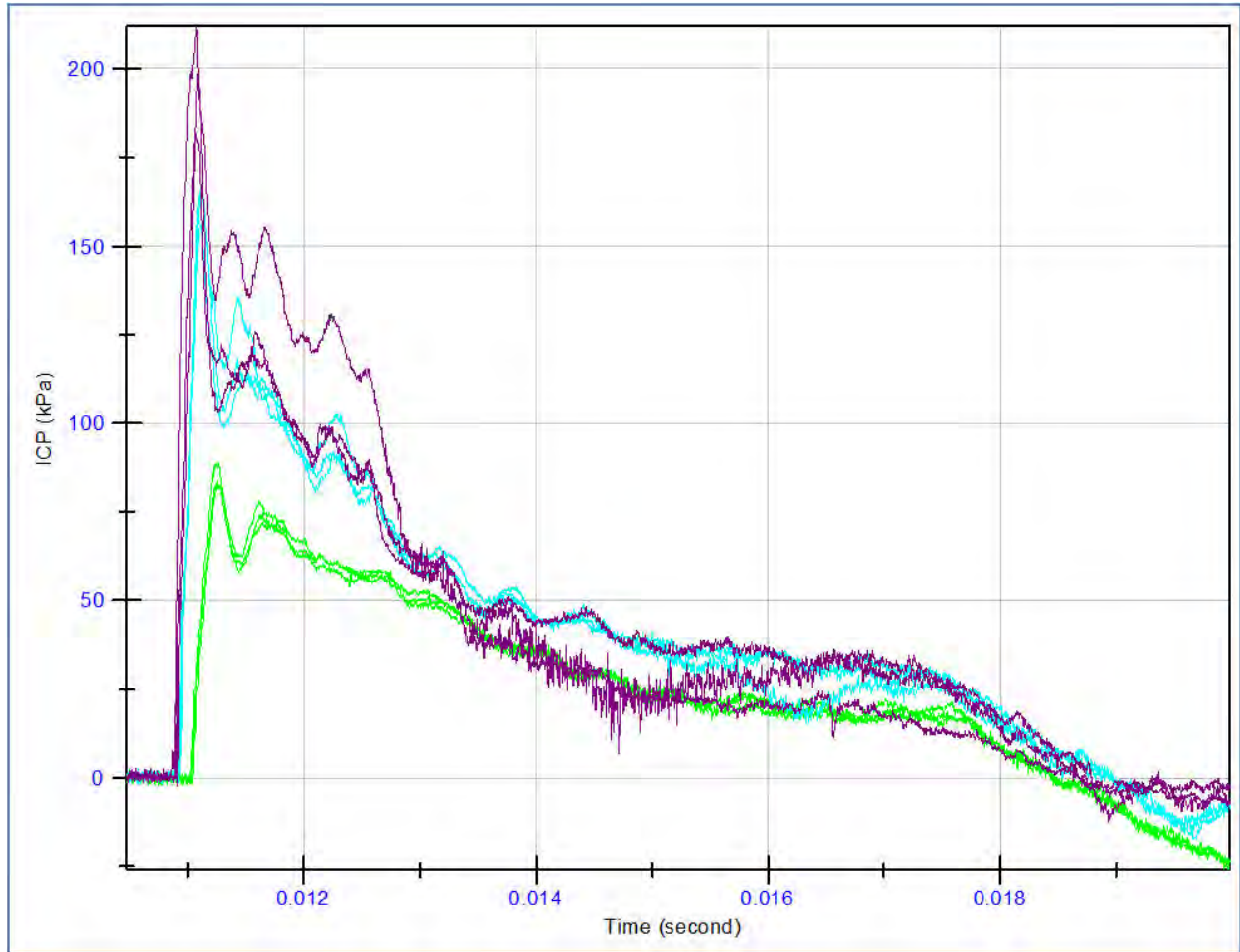
Strain response of a 262 gram rat.



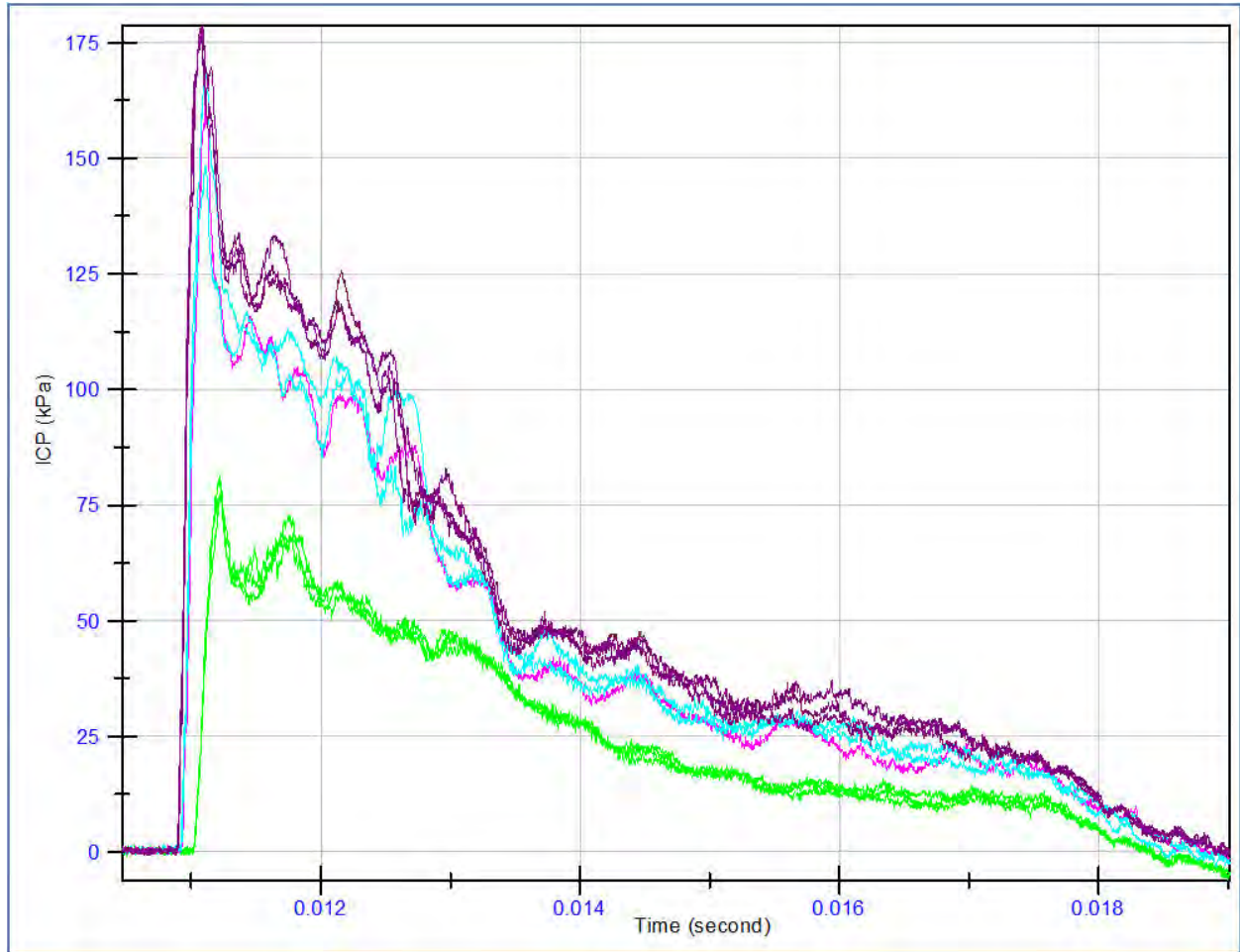
Strain response of a 246 gram rat.



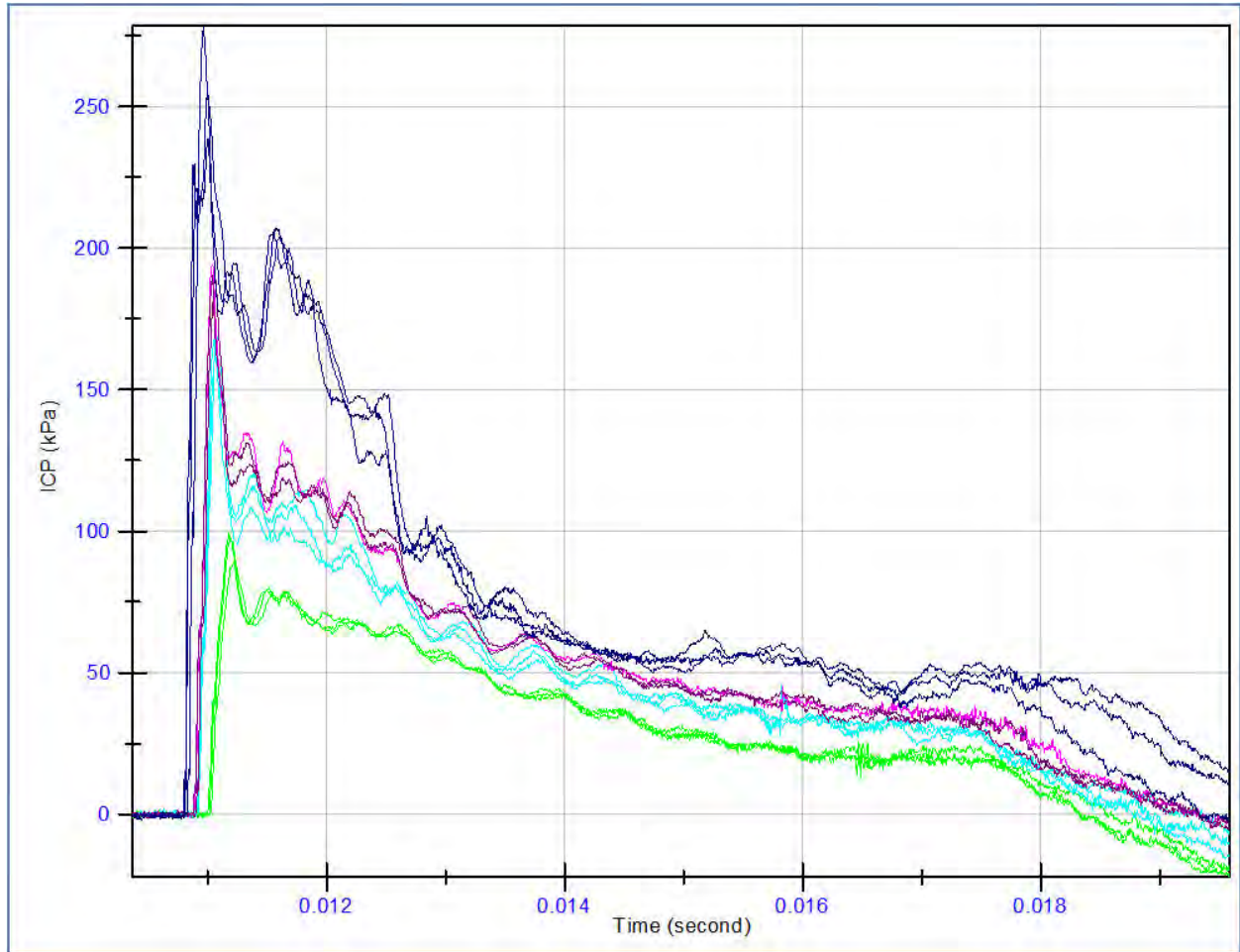
ICP response for Rat 2, 256 grams (IC Mount).



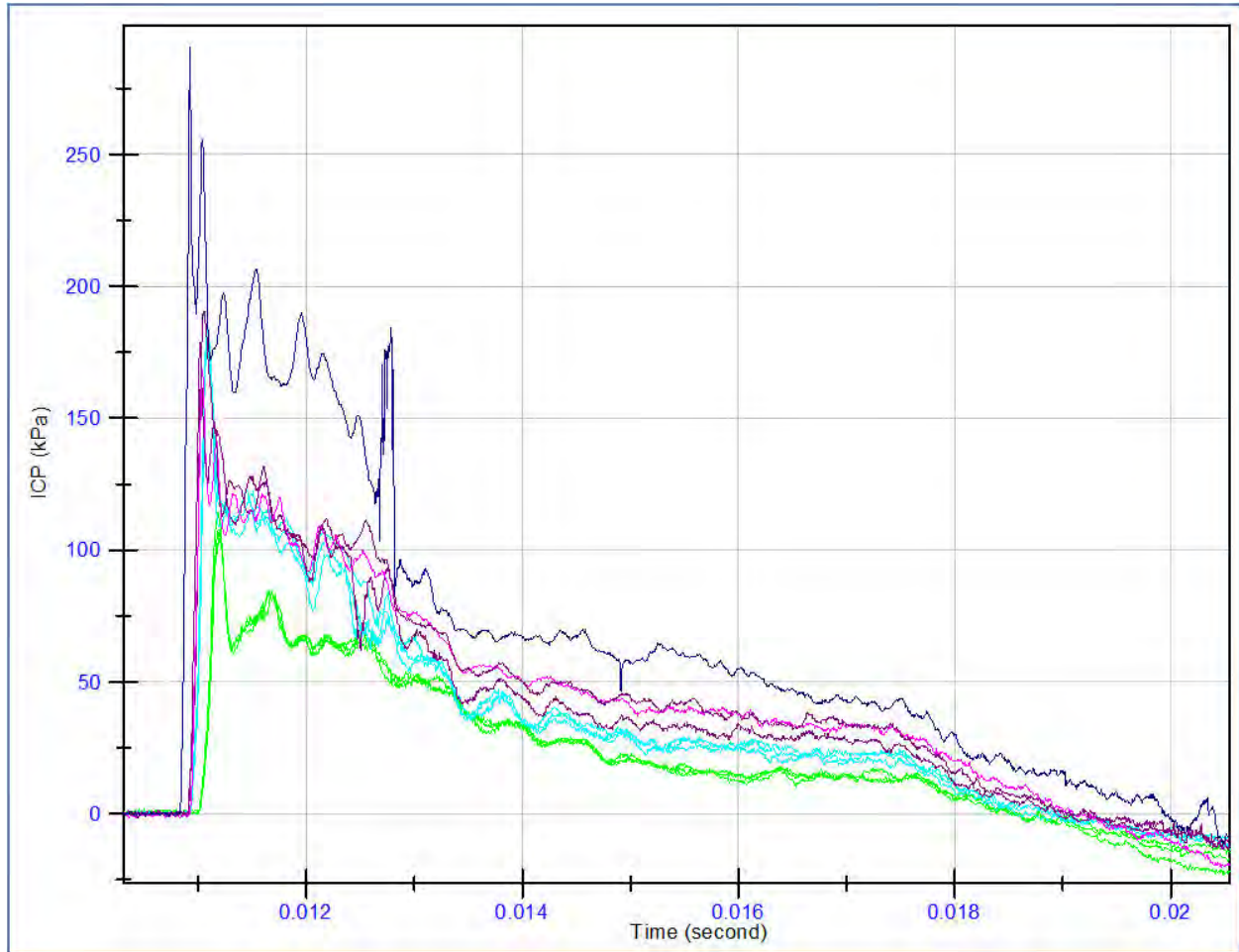
ICP response of a 368 gram rat (IC mount).



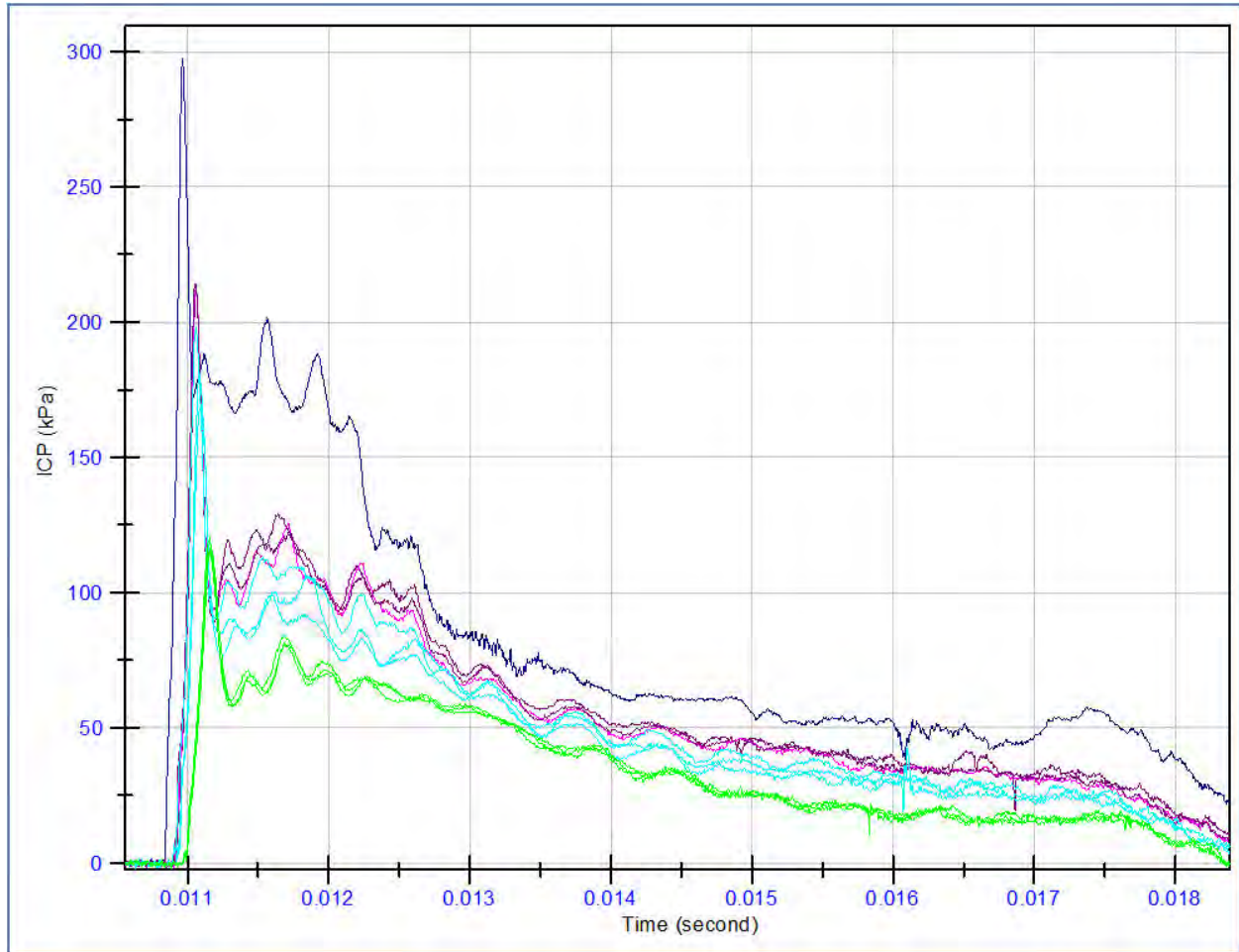
ICP response of a 369 gram rat (IC mount).



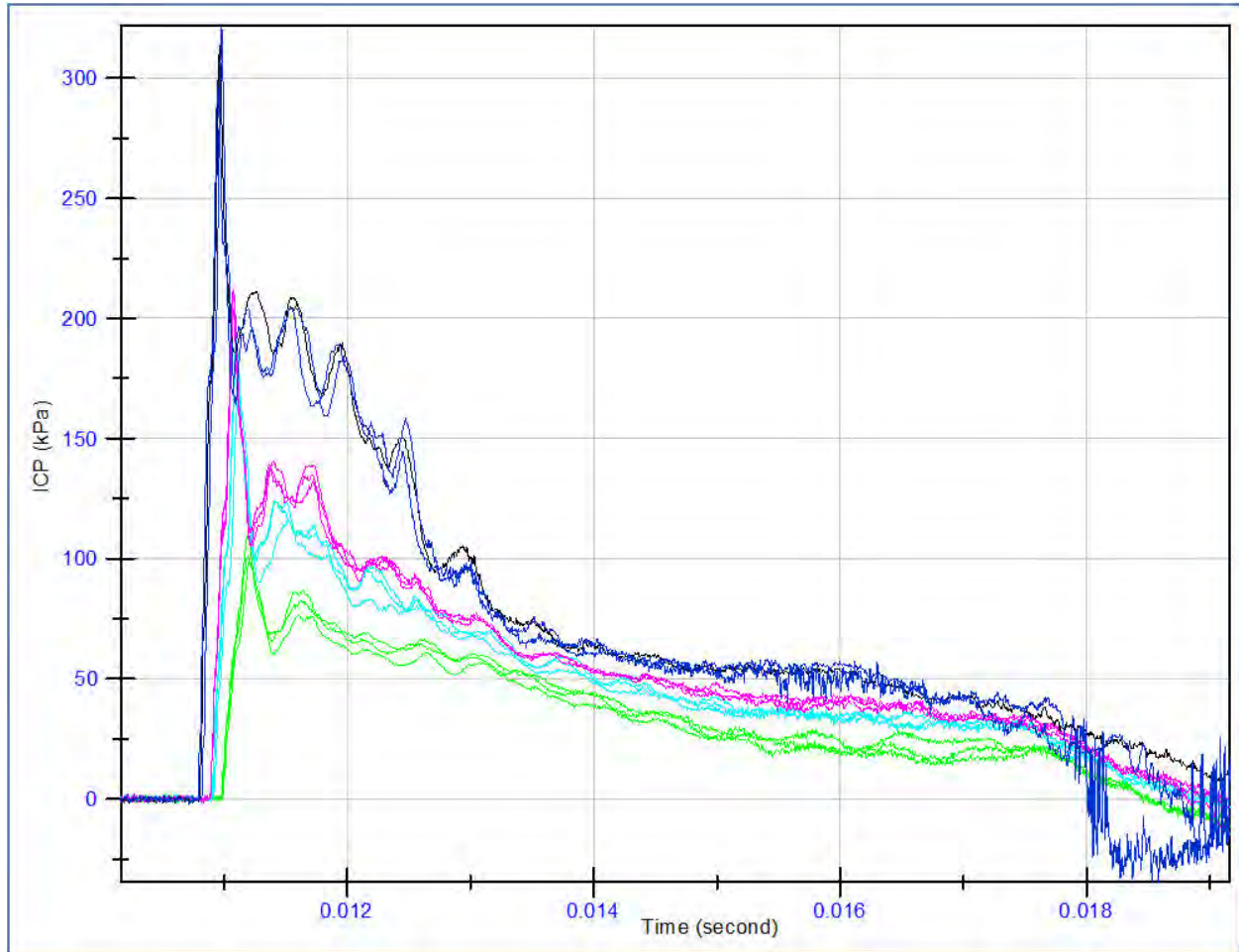
ICP response of a 200 gram rat (IC mount).



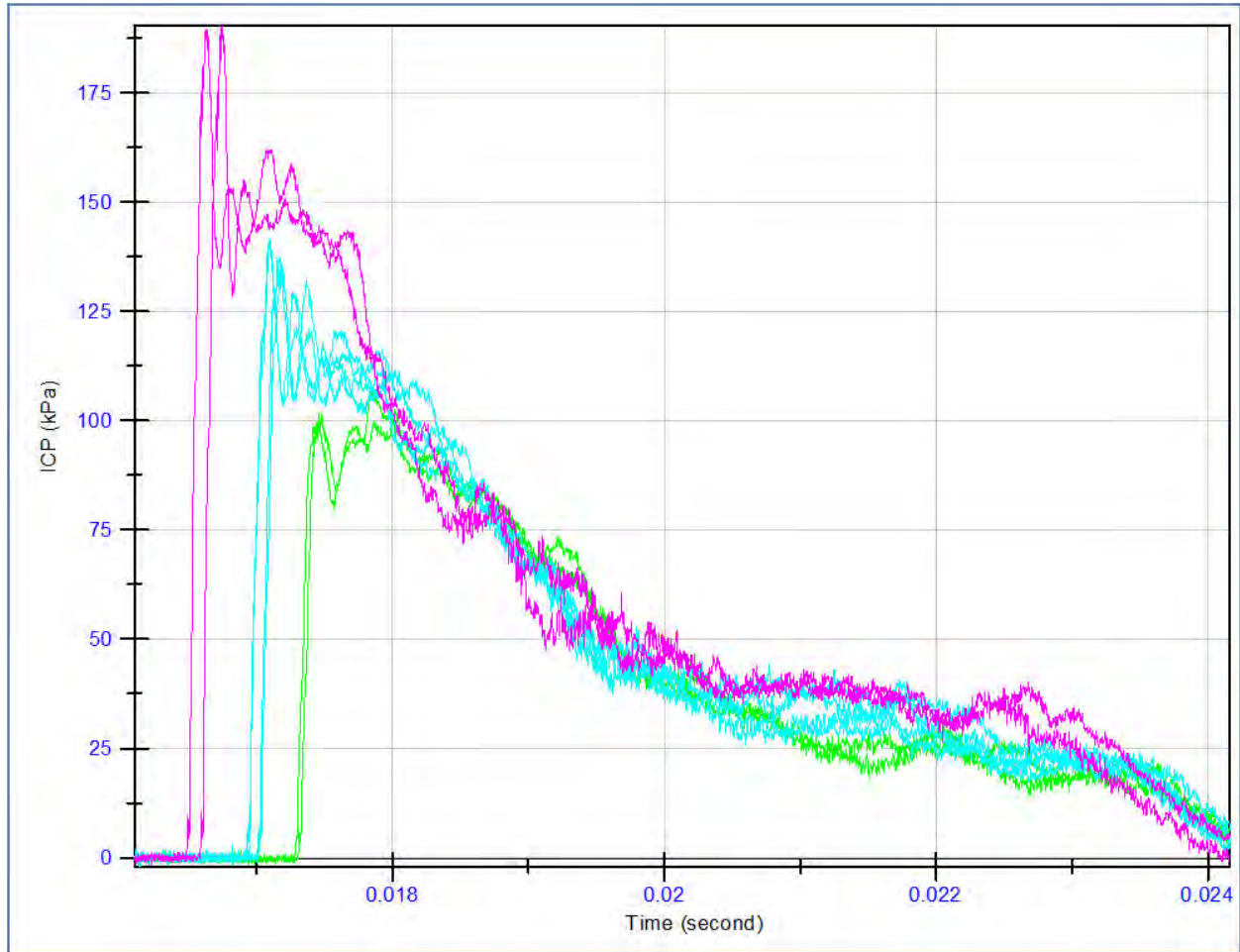
ICP response of a 301 gram rat (IC mount).



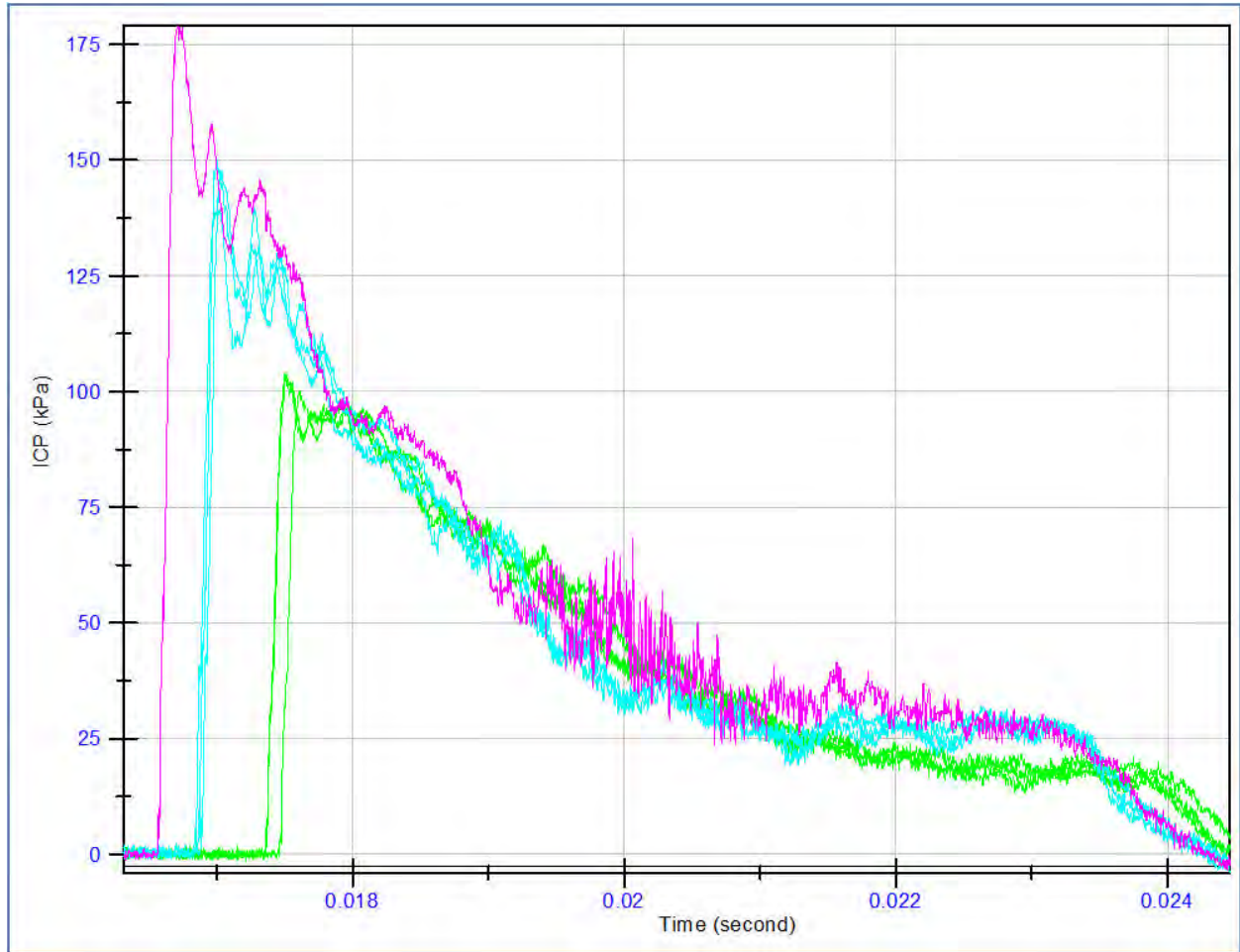
ICP response of a 273 gram rat (IC mount).



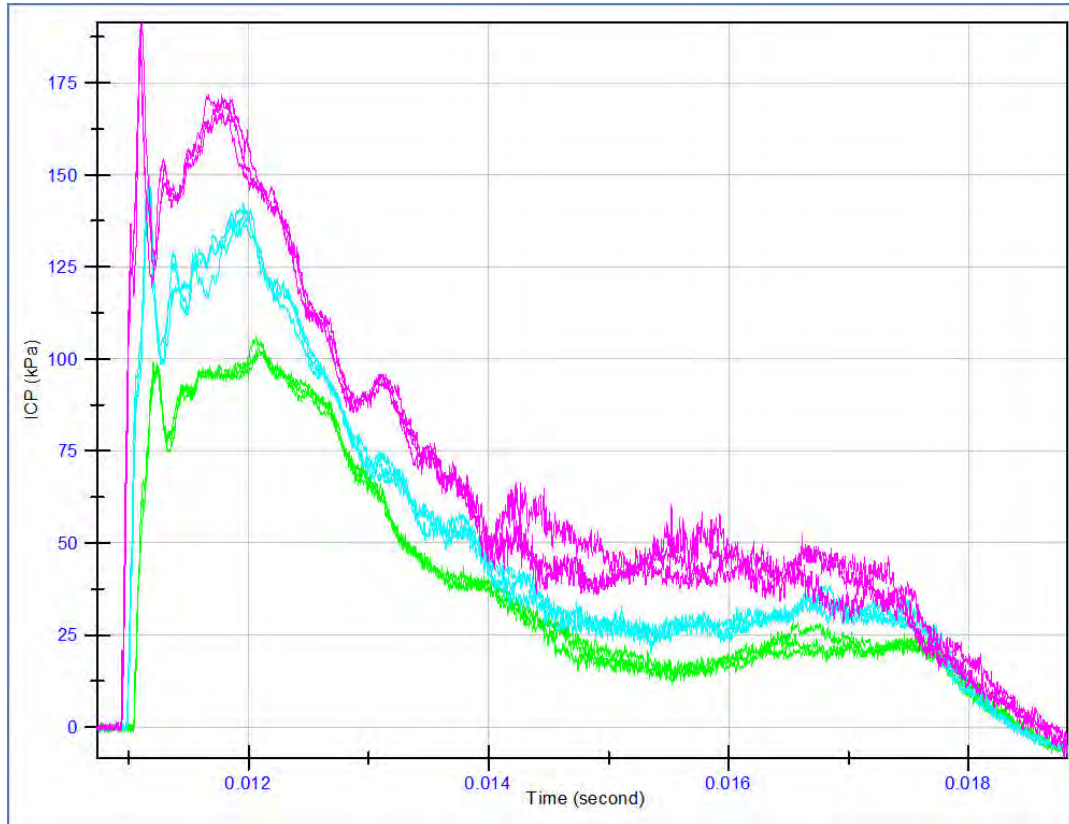
ICP response of a 437 gram rat (IC mount).



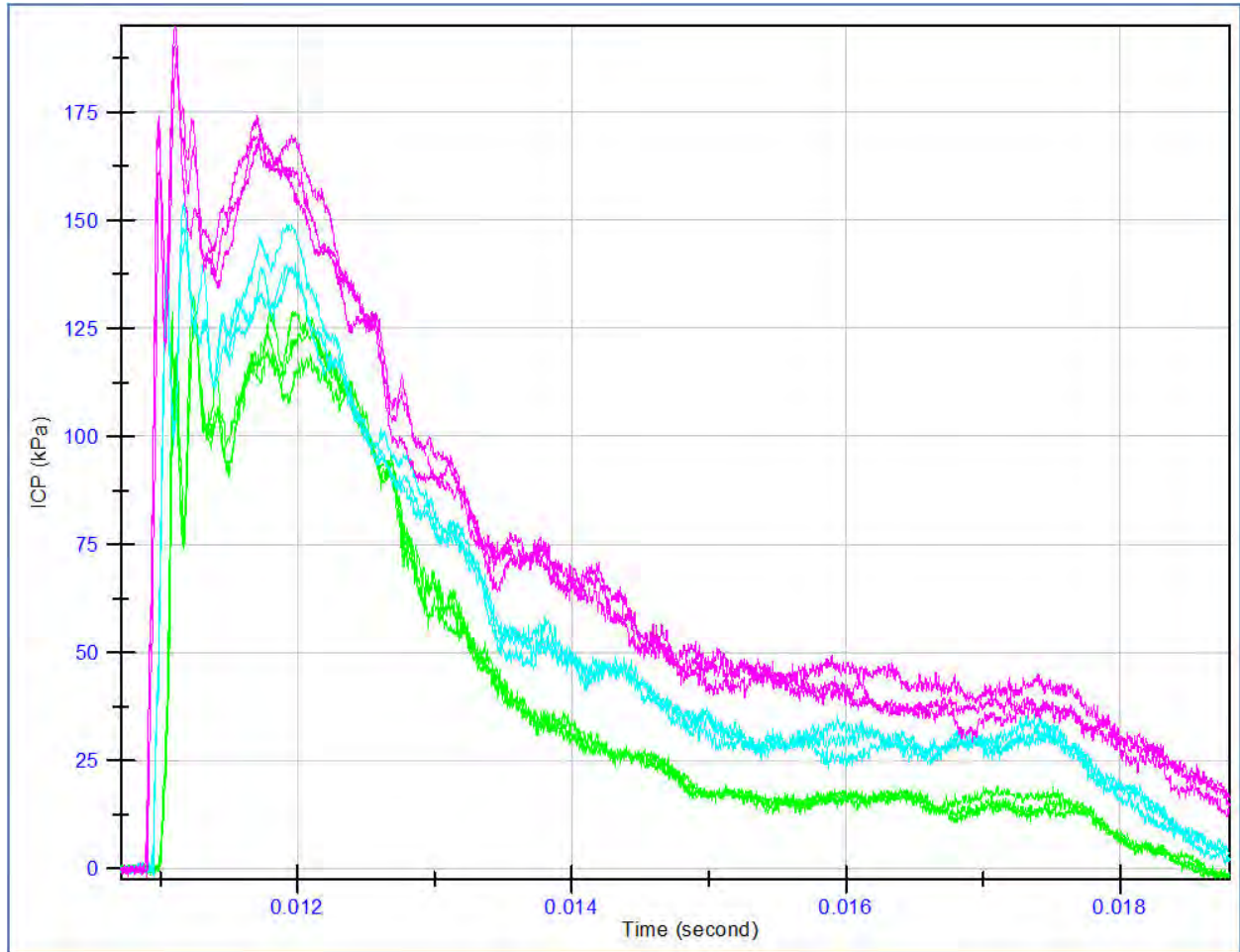
ICP response of 240 gram rat (IC mount).



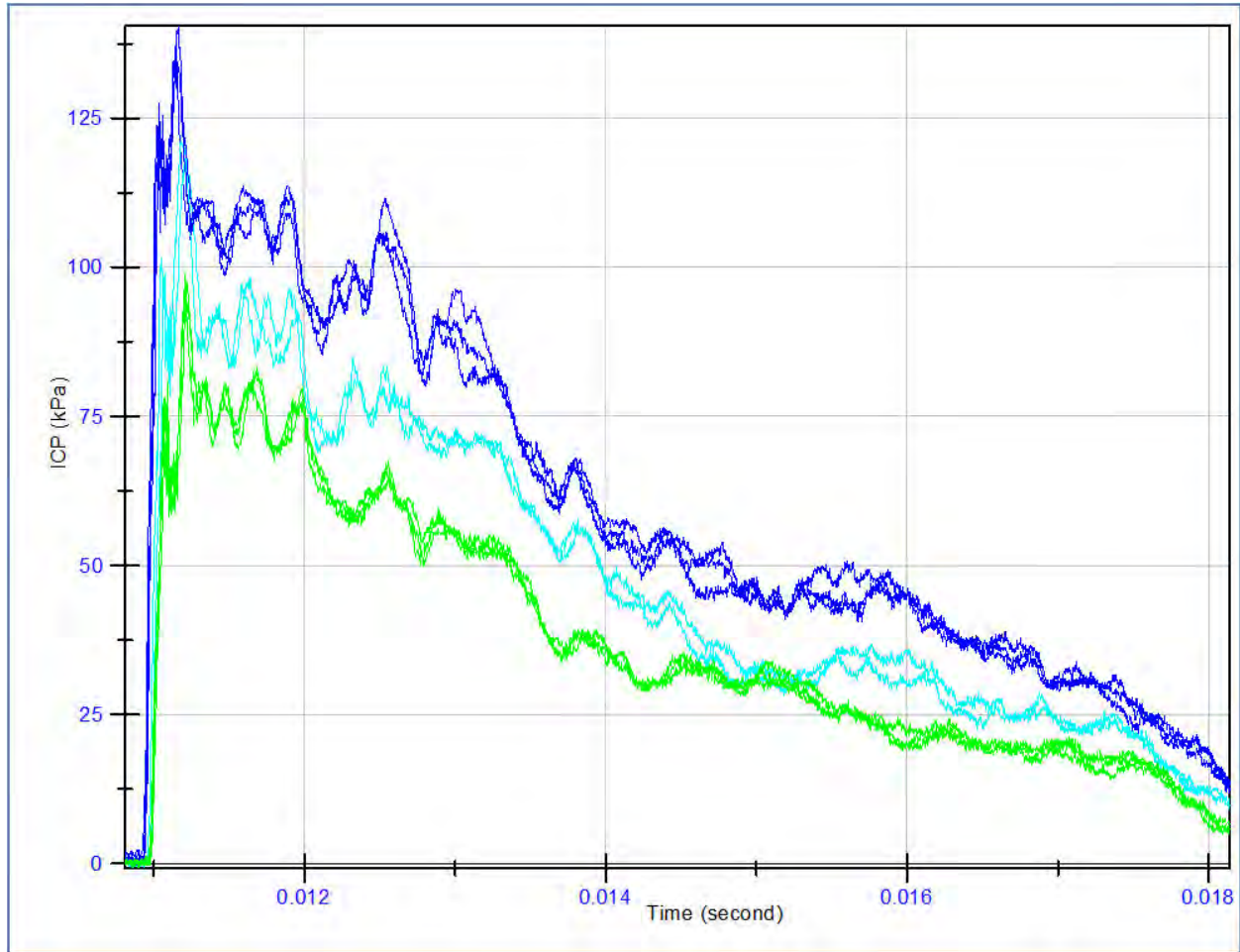
ICP response of 249 gram rat (IC mount).



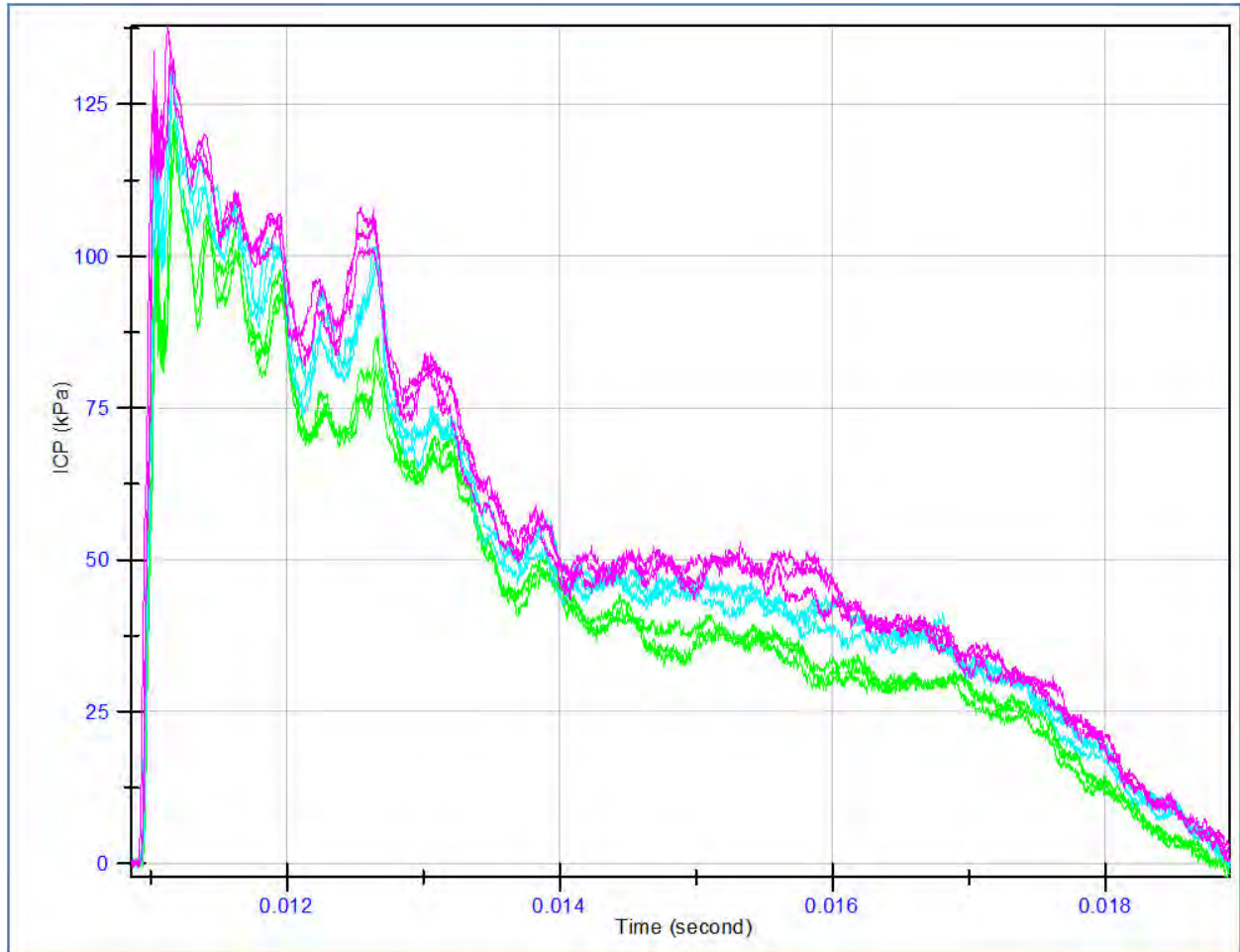
ICP response of a 239 gram rat (IC mount).



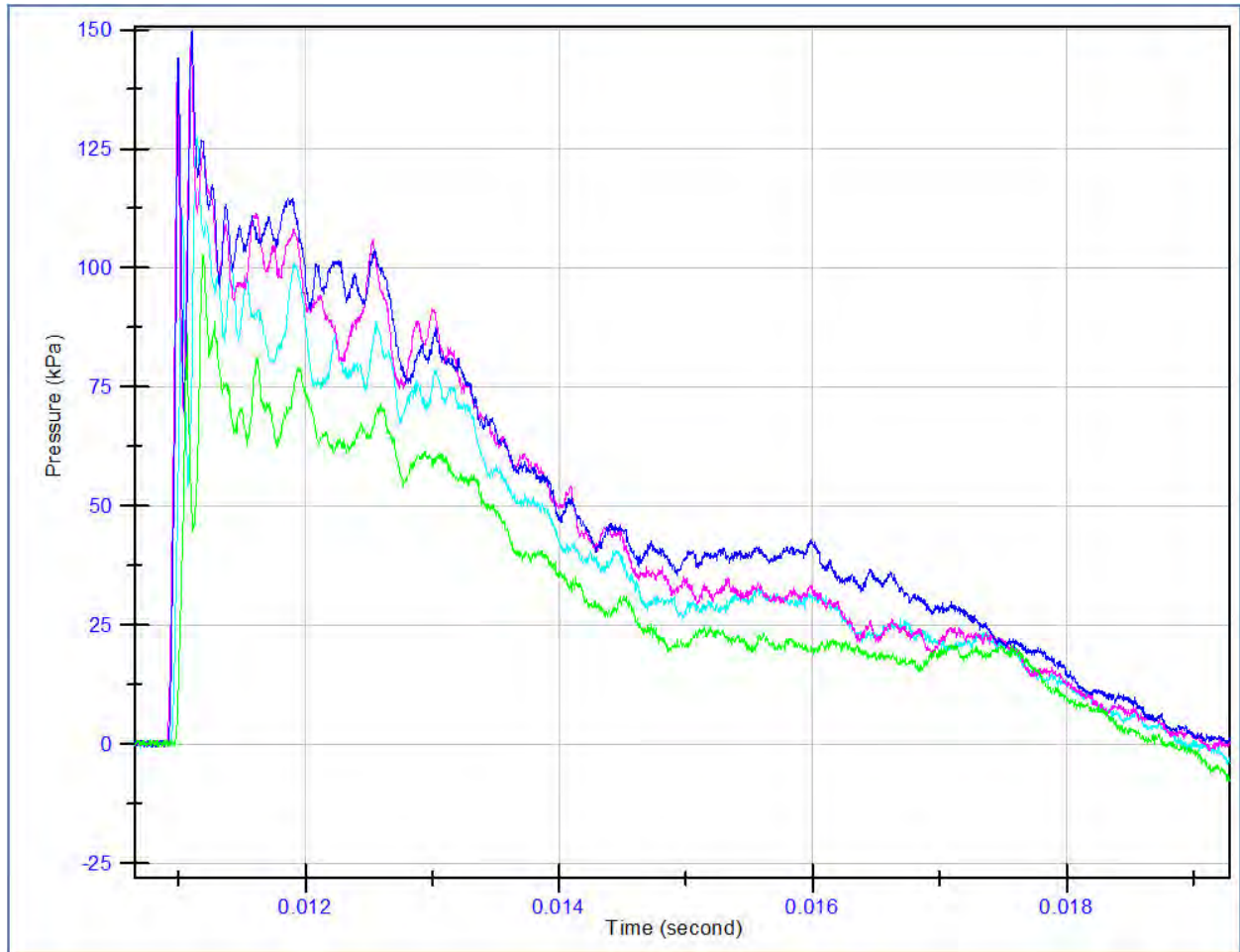
ICP response of a 244 gram rat (IC mount).



ICP response of a 264 gram rat (OIC mount).



ICP response of a 232 gram rat (OIC mount)



ICP response of a 238 gram rat (OIC mount).

## APPENDIX B PIG DATA

Nomenclature for this chapter: Pig # and orientation (front, side, back) - sensor (front, second front, occipital, temporal). P2F-T is Pig 2 for a front facing exposure and strain is measured by the temporal sensor.

Specimen	Sensor	Orientation	Intensity	ICP	Max P <sub>2</sub>	Min P <sub>2</sub>
Pig2	Frontal	Front	Low	5.5	102.2	63
Pig2	Frontal	Side	Low	5.56	210.9	61
Pig2	Frontal	Front	Low	9.254	91.38	79.27
Pig2	Frontal	Side	Low	5.4	80.59	76
Pig2	Frontal	Back	Low	3.83	78	82
Pig2	Frontal	Back	Low	3.83	86	76
Pig2	2 Frontal	Front	Low	5.5	157	146
Pig2	2 Frontal	Side	Low	5.56	357	193
Pig2	2 Frontal	Front	Low	9.254	94.3	149
Pig2	2 Frontal	Side	Low	5.4	470	269
Pig2	2 Frontal	Back	Low	3.83	191	131
Pig2	2 Frontal	Back	Low	3.83	189	139
Pig2	Temporal	Front	Low	5.5	61.54	36.6
Pig2	Temporal	Side	Low	5.56	104.7	57
Pig2	Temporal	Front	Low	9.254	33.7	47
Pig2	Temporal	Side	Low	5.4	36.2	57
Pig2	Temporal	Back	Low	3.83	80.5	43
Pig2	Temporal	Back	Low	3.83	82	45.4
Pig2	Occipital	Front	Low	5.5	200	782
Pig2	Occipital	Side	Low	5.56	161	1454
Pig2	Occipital	Front	Low	9.254	166	646
Pig2	Occipital	Side	Low	5.4	171	1351
Pig2	Occipital	Back	Low	3.83	310	1271
Pig2	Occipital	Back	Low	3.83	344	1266

Strain and ICP peak for Pig 2

Specimen	Sensor	Orientation	Intensity	ICP	Max P <sub>2</sub>	Min P <sub>2</sub>
Pig1	Frontal	Front	GF1F	0.845	107	152
Pig1	Frontal	Side	GF1S	1.4	75	110
Pig1	Frontal	Back	GF1B	1.5	85	100
Pig1	Frontal	Front	GF1FB	4.77	153	229
Pig1	Frontal	Side	GF1SB	2.54	132	215
Pig1	Frontal	Front	LF1F	1	116	174
Pig1	Frontal	Side	LF1S	1.5	90.2	102
Pig1	Frontal	Back	LF1B	1.3	83	112
Pig1	Frontal	Front	PICP	1	104	120
Pig1	2 Frontal	Front	GF1F	0.845	587	1460
Pig1	2 Frontal	Side	GF1S	1.4	800	1900
Pig1	2 Frontal	Back	GF1B	1.5	600	1200
Pig1	2 Frontal	Front	GF1FB	4.77	787	1900
Pig1	2 Frontal	Side	GF1SB	2.54	904	1970
Pig1	2 Frontal	Front	LF1F	1	586	1200
Pig1	2 Frontal	Side	LF1S	1.5	924	1900
Pig1	2 Frontal	Back	LF1B	1.3	524	1130
Pig1	2 Frontal	Front	PICP	1	600	1100
Pig1	Temporal	Front	GF1F	0.845	156	93
Pig1	Temporal	Side	GF1S	1.4	135	61
Pig1	Temporal	Back	GF1B	1.5	90	93
Pig1	Temporal	Front	GF1FB	4.77	302	166
Pig1	Temporal	Side	GF1SB	2.54	215	81
Pig1	Temporal	Front	LF1F	1	152	77
Pig1	Temporal	Side	LF1S	1.5	136	62
Pig1	Temporal	Back	LF1B	1.3	81	103
Pig1	Temporal	Front	PICP	1	174	59
Pig1	Occipital	Front	GF1F	0.845	271	206
Pig1	Occipital	Side	GF1S	1.4	420	255
Pig1	Occipital	Back	GF1B	1.5	236	259
Pig1	Occipital	Front	GF1FB	4.77	439	314
Pig1	Occipital	Side	GF1SB	2.54	418	364
Pig1	Occipital	Front	LF1F	1	328	240
Pig1	Occipital	Side	LF1S	1.5	291	201
Pig1	Occipital	Back	LF1B	1.3	271	327
Pig1	Occipital	Front	PICP	1	346	255

Strain and ICP peak for Pig 1

Specimen	Sensor	Orientation	Intensity	ICP	Max P <sub>2</sub>	Min P <sub>2</sub>
Pig3	Frontal	Front	Low	7.2	835	387
Pig3	Frontal	Side	Low	5.7	807	309
Pig3	Frontal	Back	Low	4.05	495	253
Pig3	Frontal	Front	Low	7.4	676	348
Pig3	Frontal	Front	Low	5.97	778	365
Pig3	Frontal	Side	Low	5.53	666	234
Pig3	Frontal	Side	Low	5.45	543	257
Pig3	Frontal	Back	Low	4.8	464	255
Pig3	Frontal	Back	Low	4.25	432	230
Pig3	Frontal	Front	High	10.7	1283	629
Pig3	Frontal	Side	High	9.2	1144	460
Pig3	Frontal	Back	High	7.7	732	458
Pig3	2 Frontal	Front	Low	7.2	96	59
Pig3	2 Frontal	Side	Low	5.7	94	88
Pig3	2 Frontal	Back	Low	4.05	134	104
Pig3	2 Frontal	Front	Low	7.4	101	57
Pig3	2 Frontal	Front	Low	5.97	95	44
Pig3	2 Frontal	Side	Low	5.53	84	95
Pig3	2 Frontal	Side	Low	5.45	135	100
Pig3	2 Frontal	Back	Low	4.8	117	88
Pig3	2 Frontal	Back	Low	4.25	124	92
Pig3	2 Frontal	Front	High	10.7	160	87
Pig3	2 Frontal	Side	High	9.2	113	193
Pig3	2 Frontal	Back	High	7.7	195	163
Pig3	Temporal	Front	Low	7.2	62	97
Pig3	Temporal	Side	Low	5.7	57	182
Pig3	Temporal	Back	Low	4.05	98	98
Pig3	Temporal	Front	Low	7.4	82	82
Pig3	Temporal	Front	Low	5.97	59	98
Pig3	Temporal	Side	Low	5.53	53	171
Pig3	Temporal	Side	Low	5.45	57	205
Pig3	Temporal	Back	Low	4.8	92	95
Pig3	Temporal	Back	Low	4.25	101	92
Pig3	Temporal	Front	High	10.7	723	700
Pig3	Temporal	Side	High	9.2	89	322
Pig3	Temporal	Back	High	7.7	182	175
Pig3	Occipital	Front	Low	7.2	167	88
Pig3	Occipital	Side	Low	5.7	116	61
Pig3	Occipital	Back	Low	4.05	195	108
Pig3	Occipital	Front	Low	7.4	127	58
Pig3	Occipital	Front	Low	5.97	170	74
Pig3	Occipital	Side	Low	5.53	110	59
Pig3	Occipital	Side	Low	5.45	108	50
Pig3	Occipital	Back	Low	4.8	189	88
Pig3	Occipital	Back	Low	4.25	190	104
Pig3	Occipital	Front	High	10.7	249	98.3
Pig3	Occipital	Side	High	9.2	226	92
Pig3	Occipital	Back	High	7.7	269	190

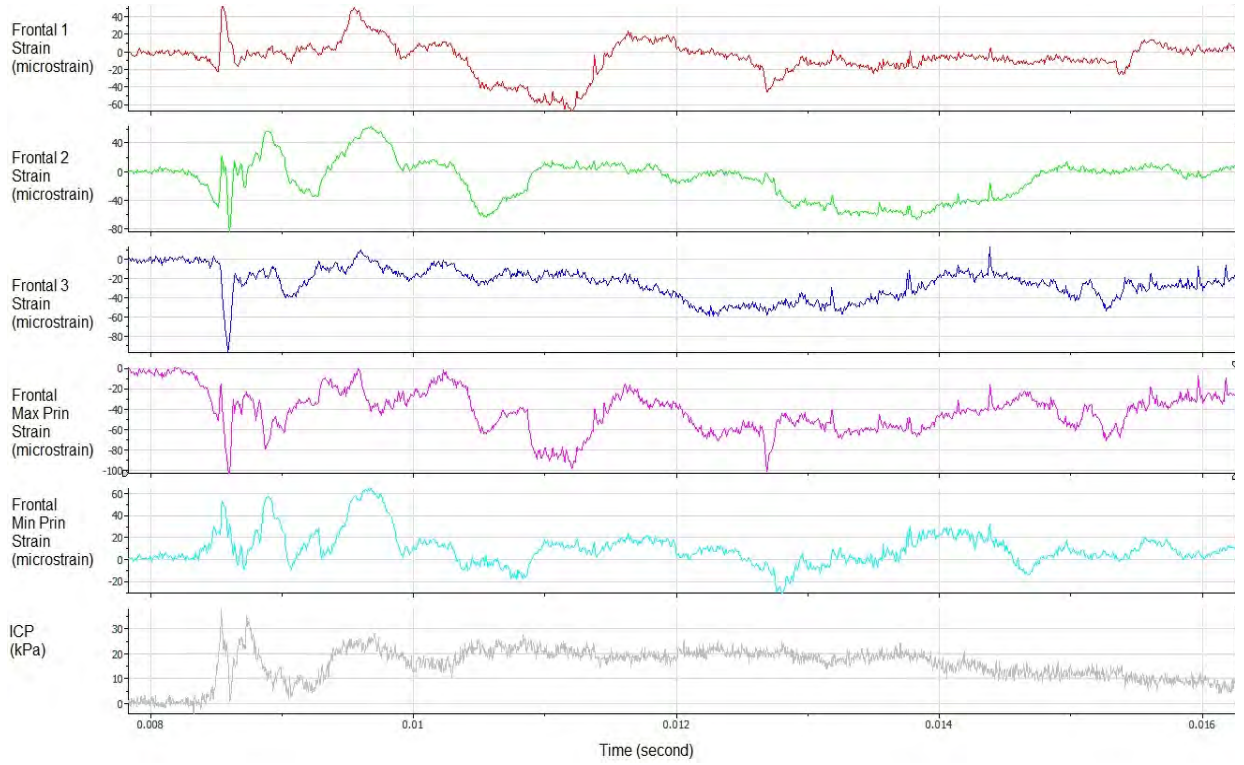
Strain and ICP peak for Pig 3

Specimen	Sensor	Orientation	Intensity	ICP	Max P <sub>2</sub>	Min P <sub>2</sub>
Pig4	Frontal	Front	Low	5.9	130	93
Pig4	Frontal	Side	Low	5.1	161	101
Pig4	Frontal	Back	Low	5.3	121	92.2
Pig4	Frontal	Front	Low	5.8	131	106
Pig4	Frontal	Front	Low	6.1	136	103
Pig4	Frontal	Side	Low	5	152	77
Pig4	Frontal	Side	Low	5.4	171	90
Pig4	Frontal	Back	Low	5.6	105	93
Pig4	Frontal	Side	High	6.7	236	209
Pig4	Frontal	Back	High	7.1	162	159
Pig4	2 Frontal	Front	Low	5.9	135	237
Pig4	2 Frontal	Side	Low	5.1	332	513
Pig4	2 Frontal	Back	Low	5.3	148	173
Pig4	2 Frontal	Front	Low	5.8	139	205
Pig4	2 Frontal	Front	Low	6.1	148	207
Pig4	2 Frontal	Side	Low	5	319	816
Pig4	2 Frontal	Side	Low	5.4	472	385
Pig4	2 Frontal	Back	Low	5.6	108	150
Pig4	2 Frontal	Side	High	6.7	421	1200
Pig4	2 Frontal	Back	High	7.1	173	1200
Pig4	Temporal	Front	Low	5.9	208	167
Pig4	Temporal	Side	Low	5.1	430	256
Pig4	Temporal	Back	Low	5.3	443	260
Pig4	Temporal	Front	Low	5.8	235	167
Pig4	Temporal	Front	Low	6.1	231	198
Pig4	Temporal	Side	Low	5	439	246
Pig4	Temporal	Side	Low	5.4	353	204
Pig4	Temporal	Back	Low	5.6	467	246
Pig4	Temporal	Side	High	6.7	729	488
Pig4	Temporal	Back	High	7.1	388	421
Pig4	Occipital	Front	Low	5.9	198	83
Pig4	Occipital	Side	Low	5.1	156	43
Pig4	Occipital	Back	Low	5.3	167	107
Pig4	Occipital	Front	Low	5.8	198	84
Pig4	Occipital	Front	Low	6.1	202	87
Pig4	Occipital	Side	Low	5	129	34
Pig4	Occipital	Side	Low	5.4	138	32
Pig4	Occipital	Back	Low	5.6	163.5	97
Pig4	Occipital	Side	High	6.7	269	74
Pig4	Occipital	Back	High	7.1	227	185

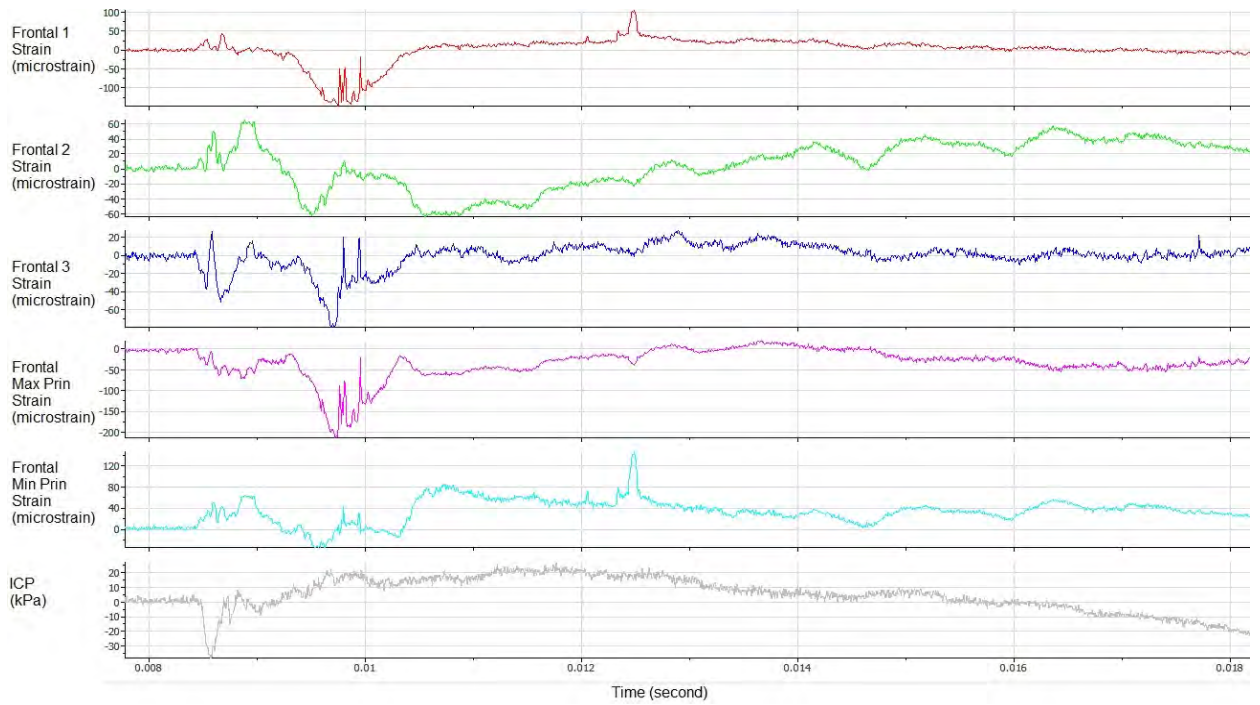
Strain and ICP peak for Pig 4

Specimen	Sensor	Orientation	Intensity	ICP	Max P <sub>2</sub>	Min P <sub>2</sub>
Pig5	Frontal	Side	Low	5	290	64
Pig5	Frontal	Back	Low	3.9	152	120
Pig5	Frontal	Front	Low	11.4	116	144
Pig5	Frontal	Back	Low	3.9	159	118
Pig5	Frontal	Side	Low	3.3	161	76
Pig5	Frontal	Back	Low	5	133	93
Pig5	Frontal	Front	Low	9	125	153
Pig5	Frontal	Front	High	14.8	232	304
Pig5	Frontal	Side	High	3.9	239	143
Pig5	Frontal	Back	High	5.8	364	195
Pig5	2 Frontal	Side	Low	4.9	147	69
Pig5	2 Frontal	Back	Low	4	75	107
Pig5	2 Frontal	Front	Low	11.3	59	106
Pig5	2 Frontal	Back	Low	4.5	76	106
Pig5	2 Frontal	Side	Low	3.3	79	79
Pig5	2 Frontal	Back	Low	4.4	61	93
Pig5	2 Frontal	Front	Low	9	46	100
Pig5	2 Frontal	Front	High	14.8	95	193
Pig5	2 Frontal	Side	High	4.4	155	143
Pig5	2 Frontal	Back	High	5.7	234	267
Pig5	Temporal	Side	Low	4.9	200	214
Pig5	Temporal	Back	Low	4	75	73
Pig5	Temporal	Front	Low	11.3	55	64
Pig5	Temporal	Back	Low	4.5	66	16
Pig5	Temporal	Side	Low	3.3	96	95
Pig5	Temporal	Back	Low	4.4	65	21
Pig5	Temporal	Front	Low	9	50	60
Pig5	Temporal	Front	High	14.8	80	120
Pig5	Temporal	Side	High	4.4	58	94
Pig5	Temporal	Back	High	5.7	119	31
Pig5	Occipital	Side	Low	4.9	172	55
Pig5	Occipital	Back	Low	4	161	119
Pig5	Occipital	Front	Low	11.3	179	83
Pig5	Occipital	Back	Low	4.5	152	121
Pig5	Occipital	Side	Low	3.3	126	27
Pig5	Occipital	Back	Low	4.4	117	159
Pig5	Occipital	Front	Low	9	156	86
Pig5	Occipital	Front	High	14.8	317	123
Pig5	Occipital	Side	High	4.4	244	69
Pig5	Occipital	Back	High	5.7	146	281

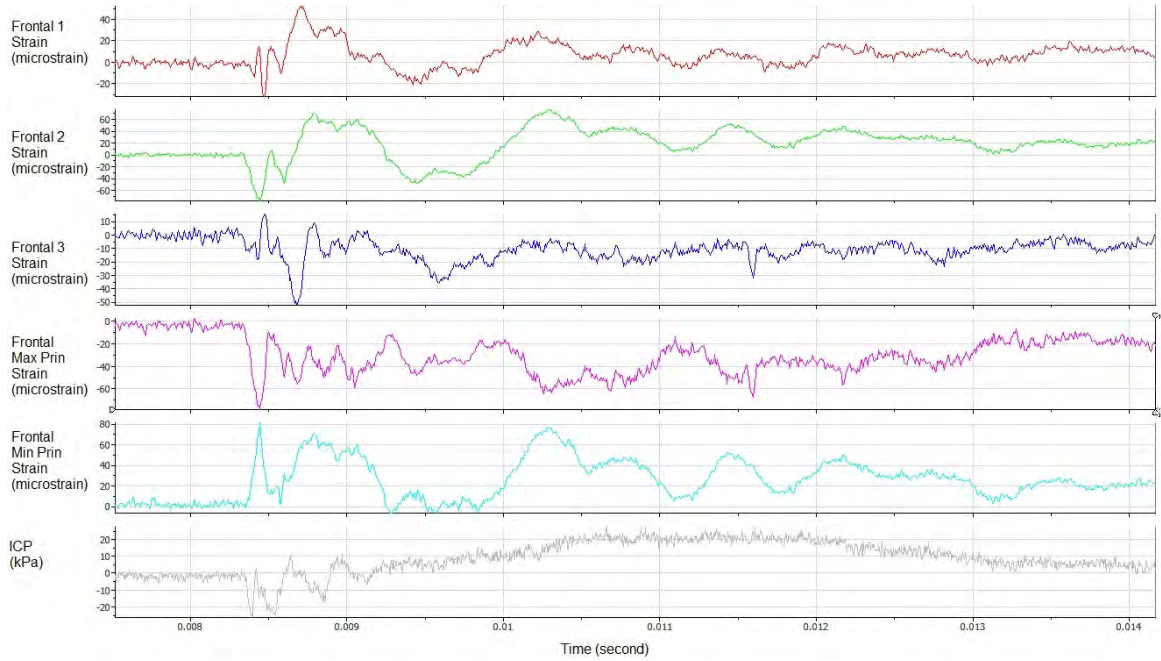
Strain and ICP peak for Pig 5



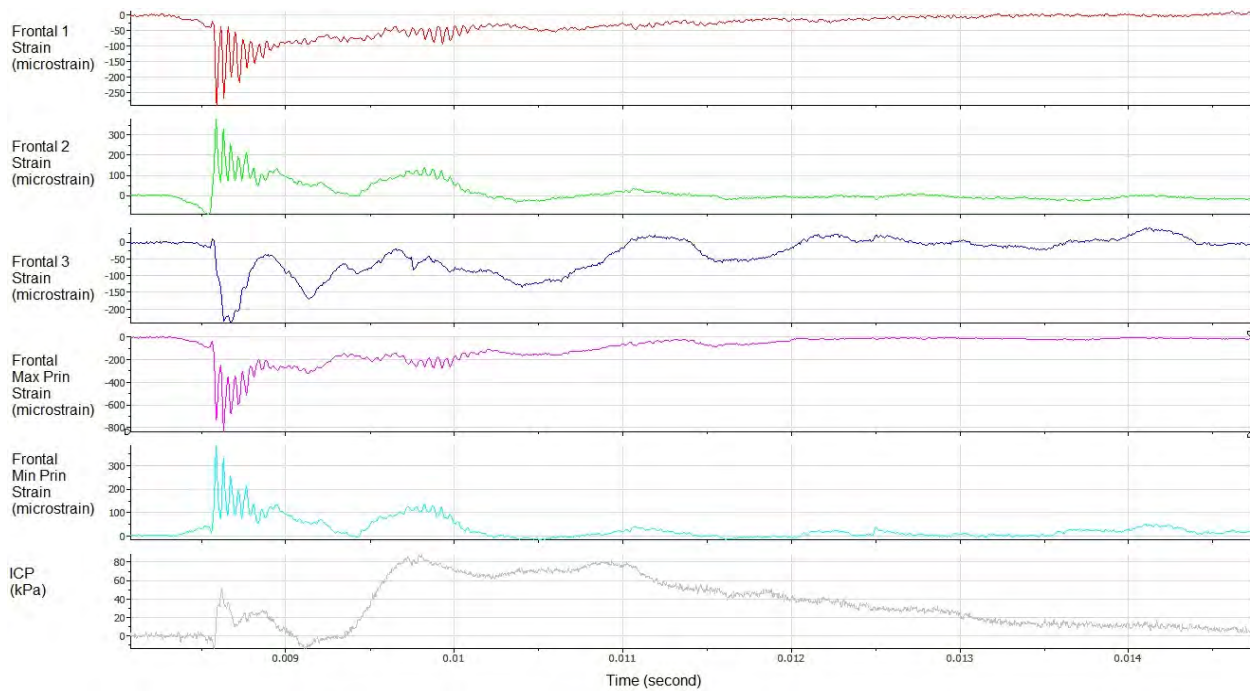
P2F-F



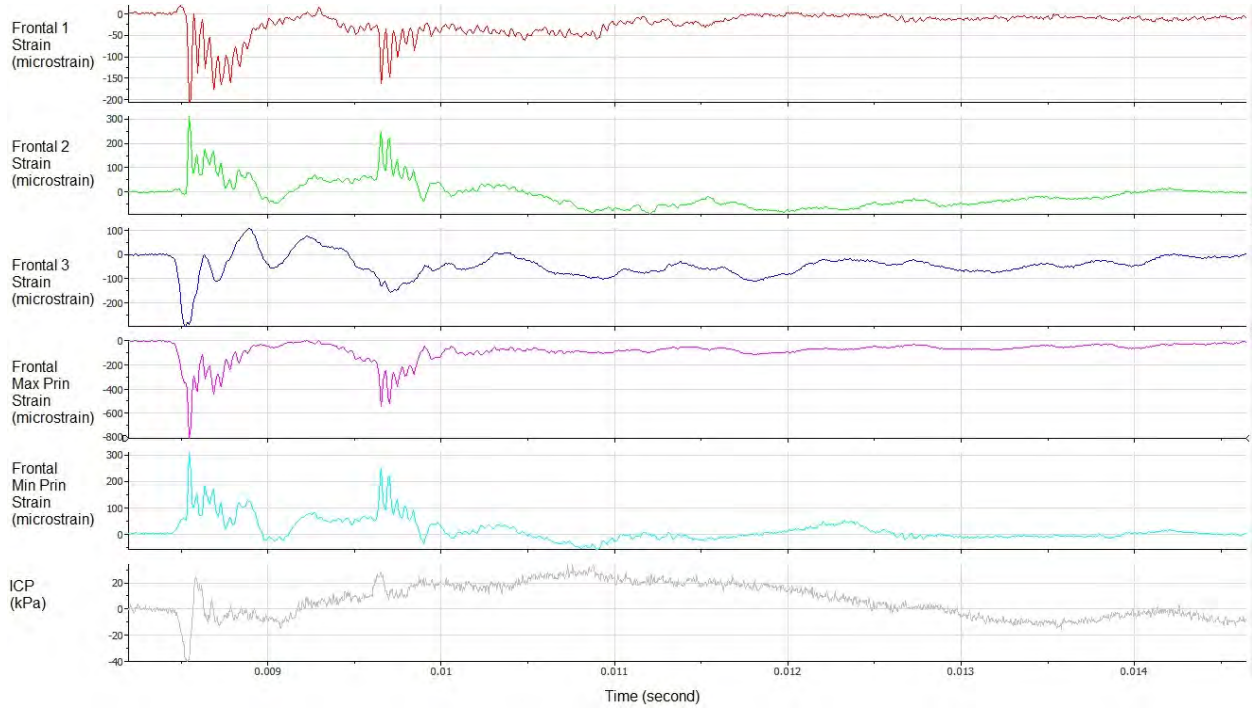
P2S-F



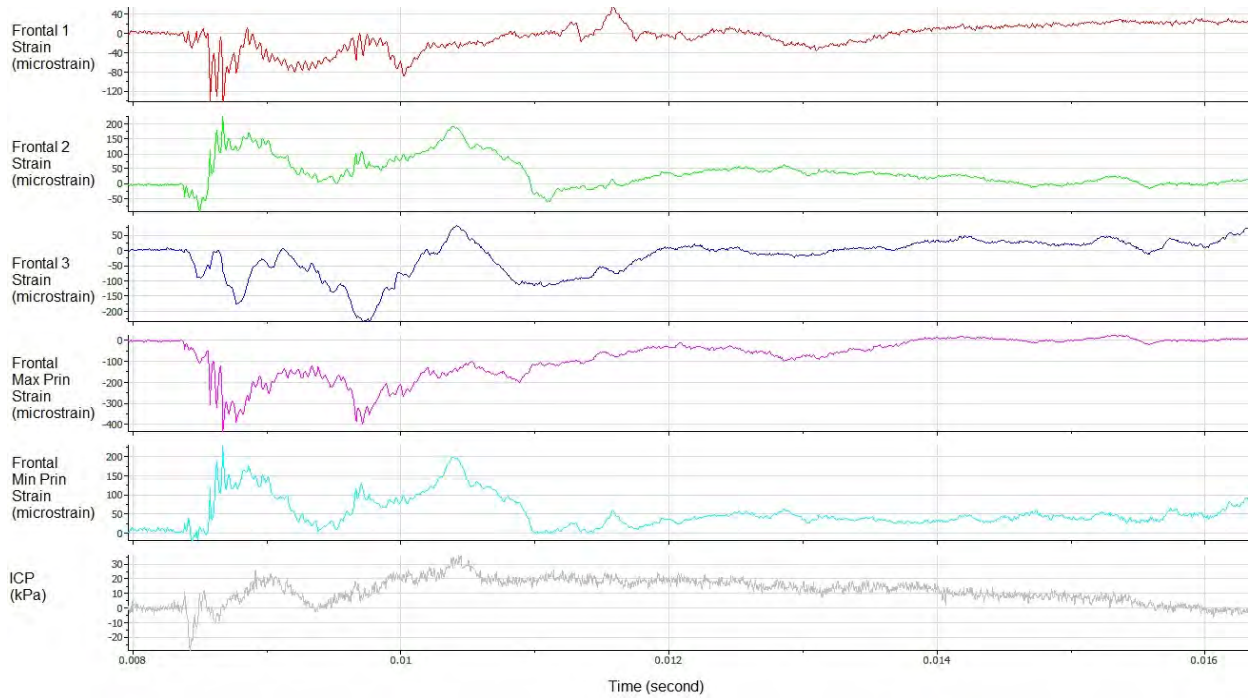
P2B-F



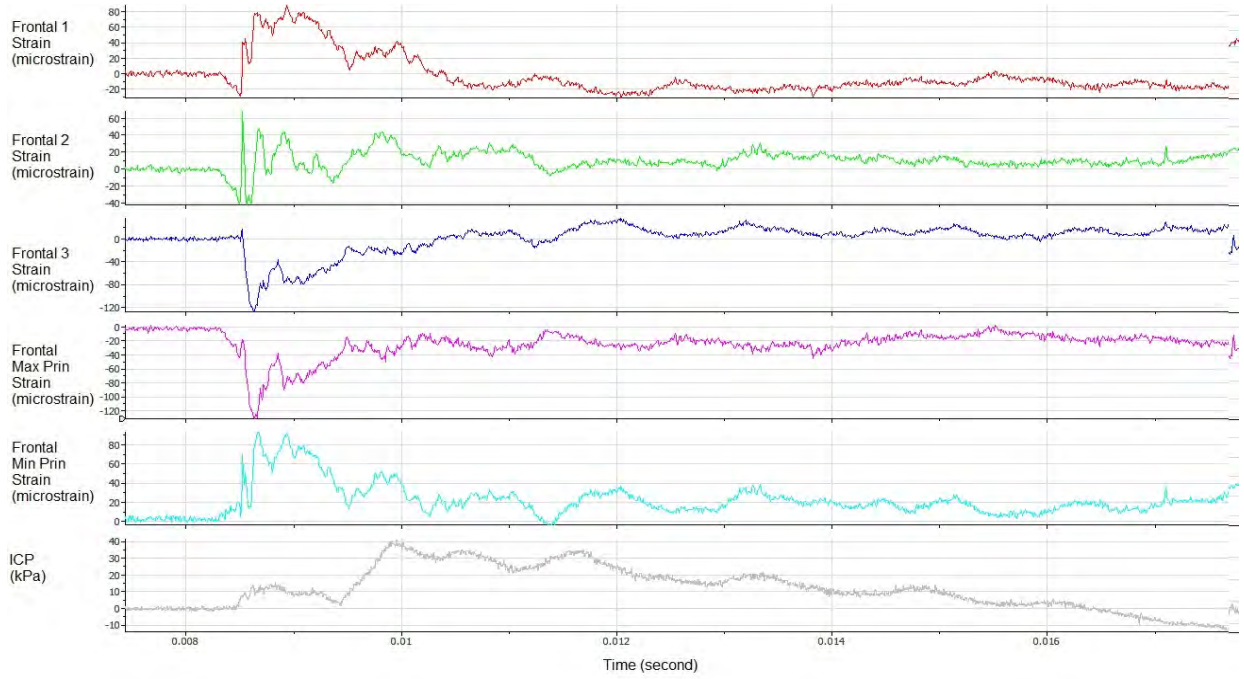
P3F-F



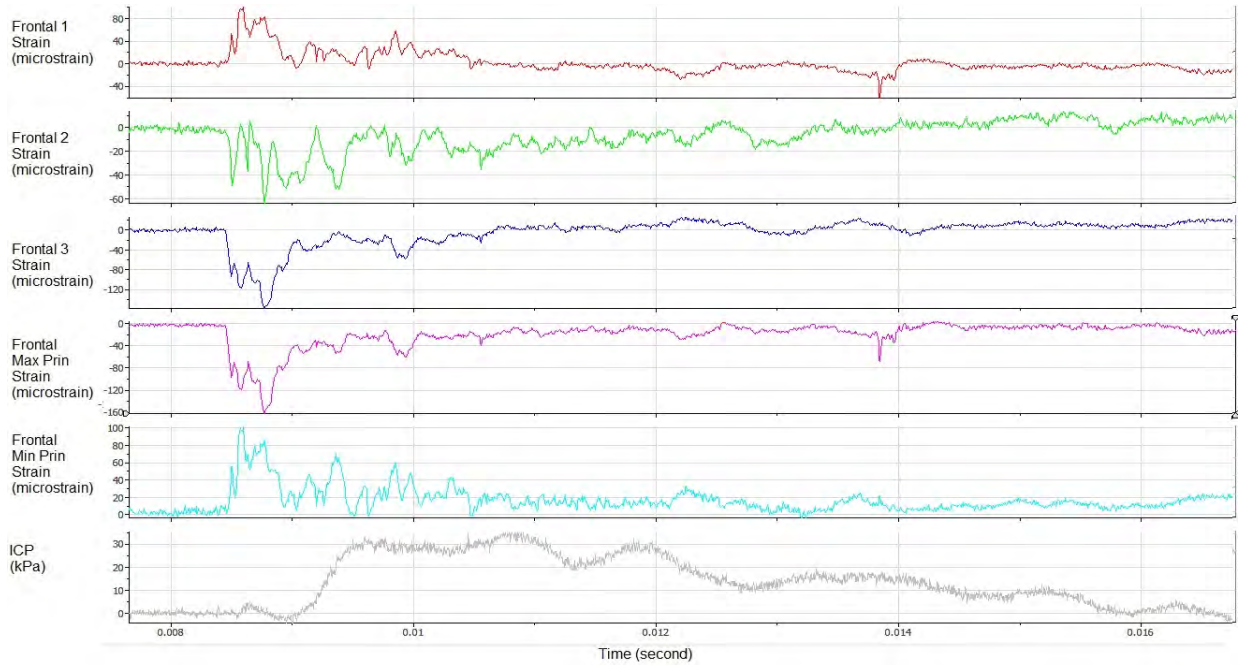
P3S-F



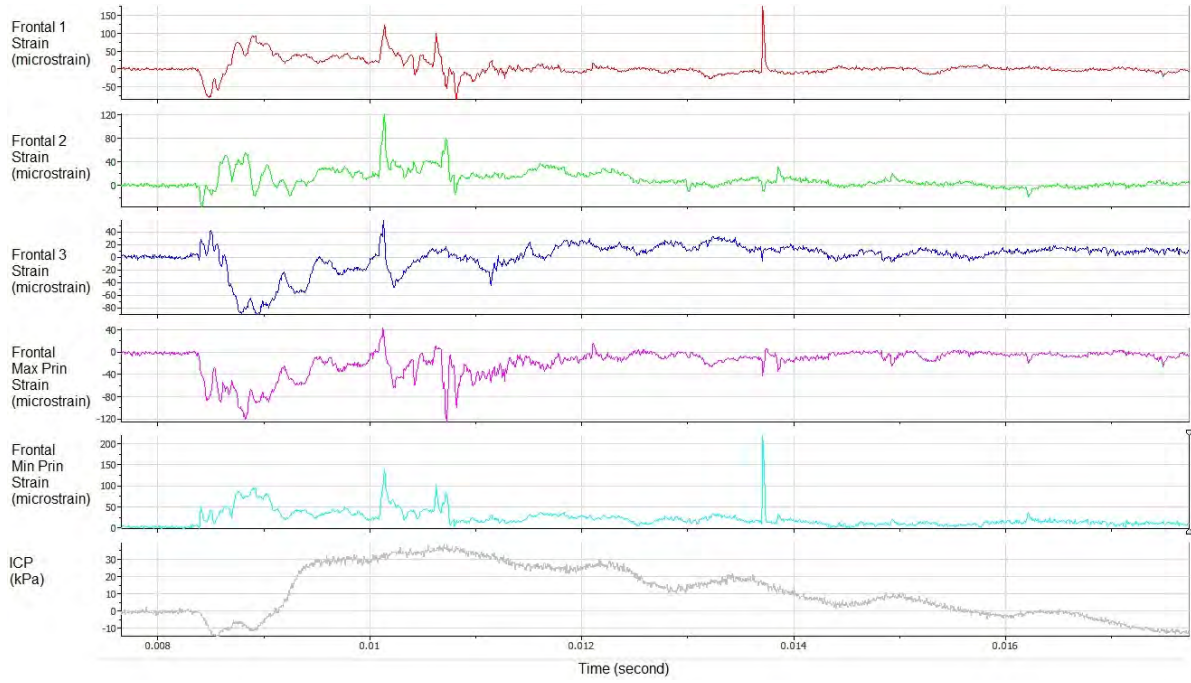
P3B-F



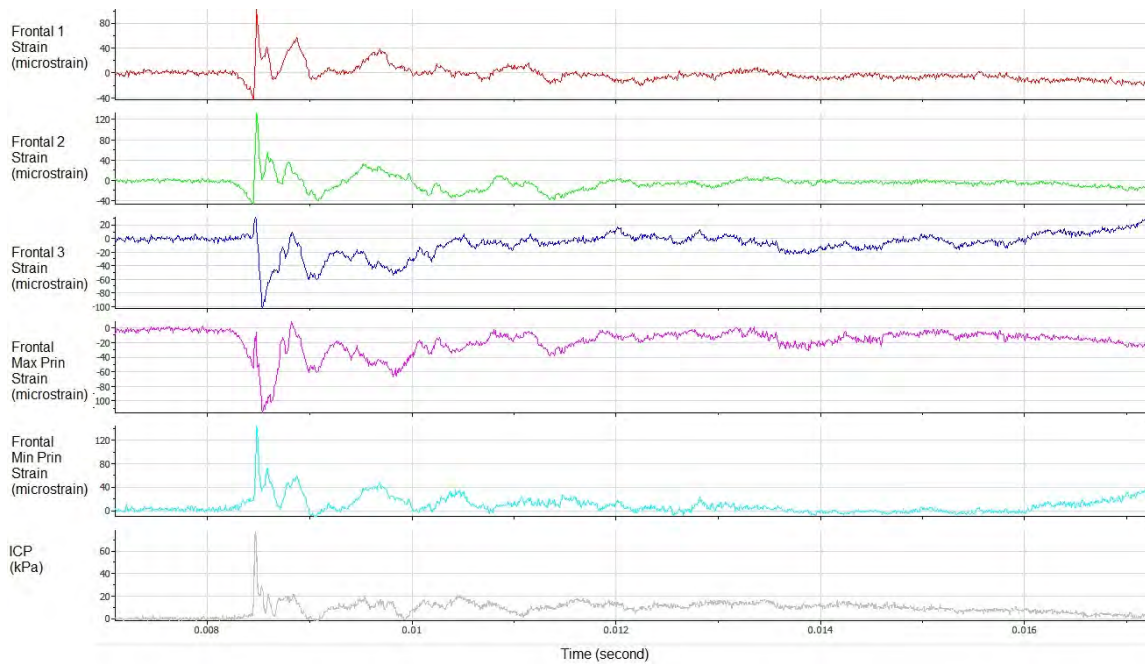
P4F-F



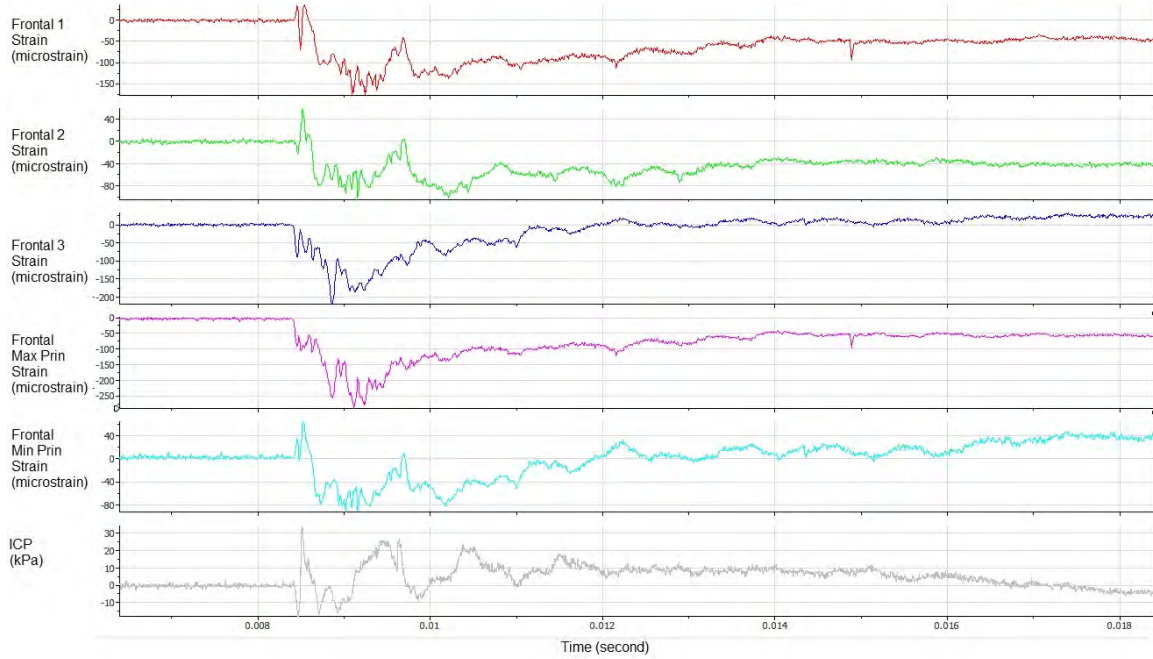
P4S-F



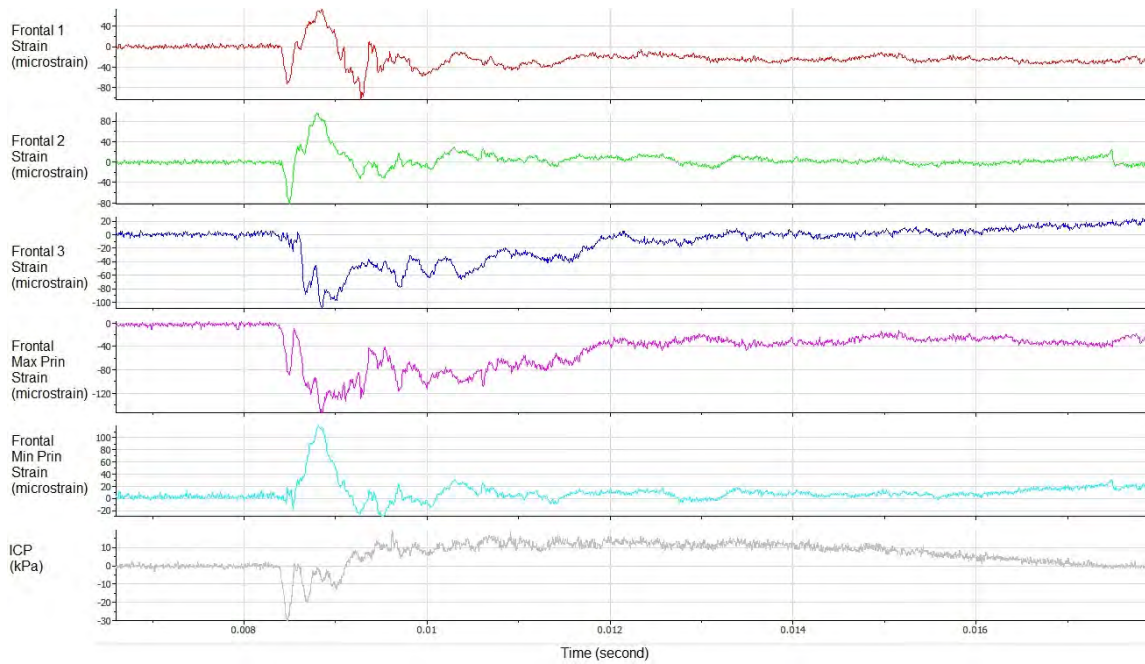
P4B-F



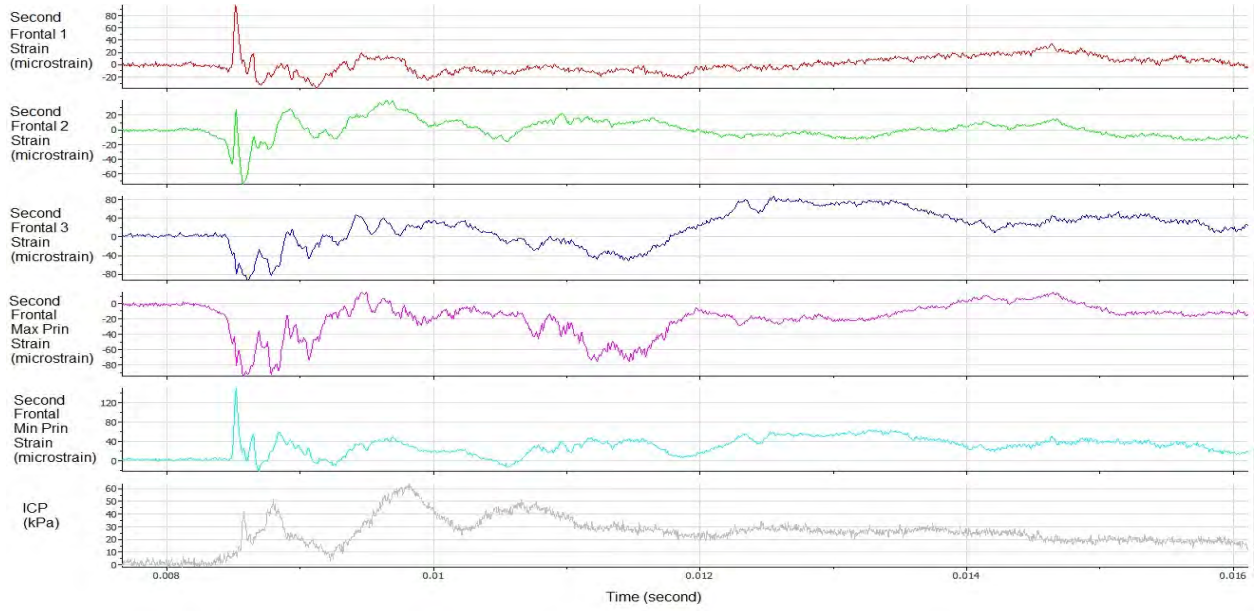
P5F-F



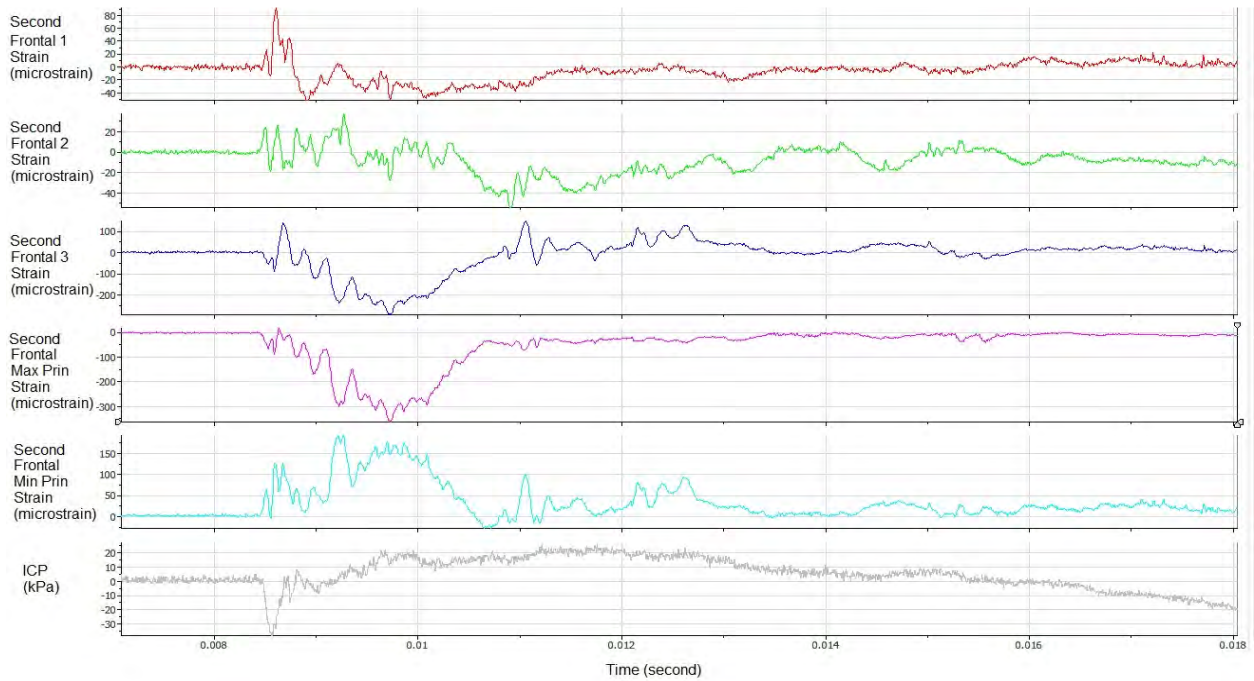
P5S-F



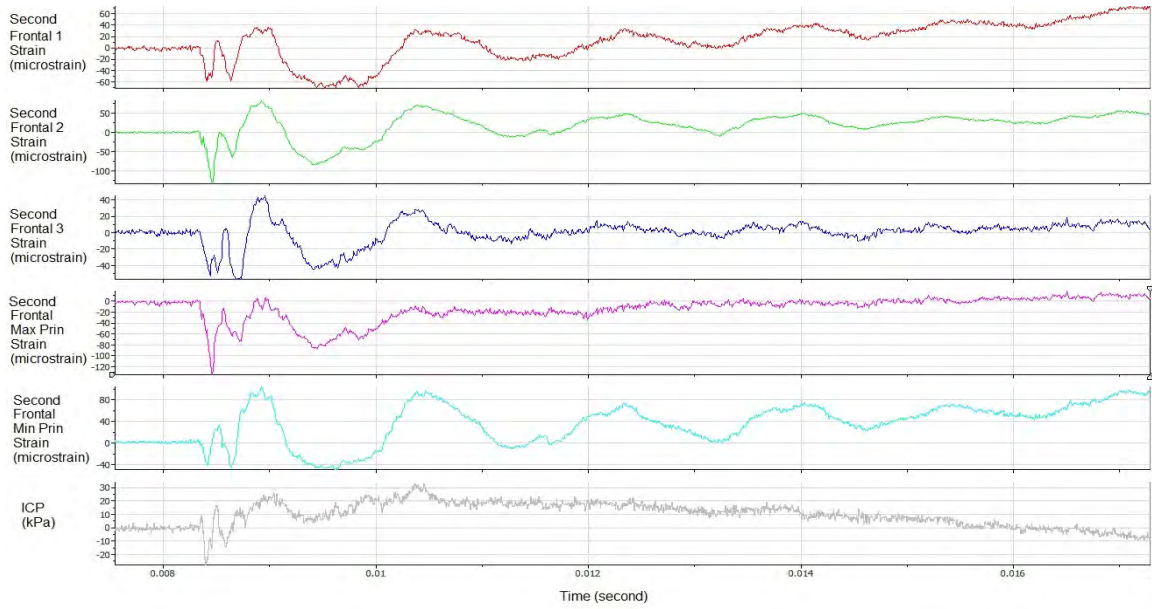
P5B-F



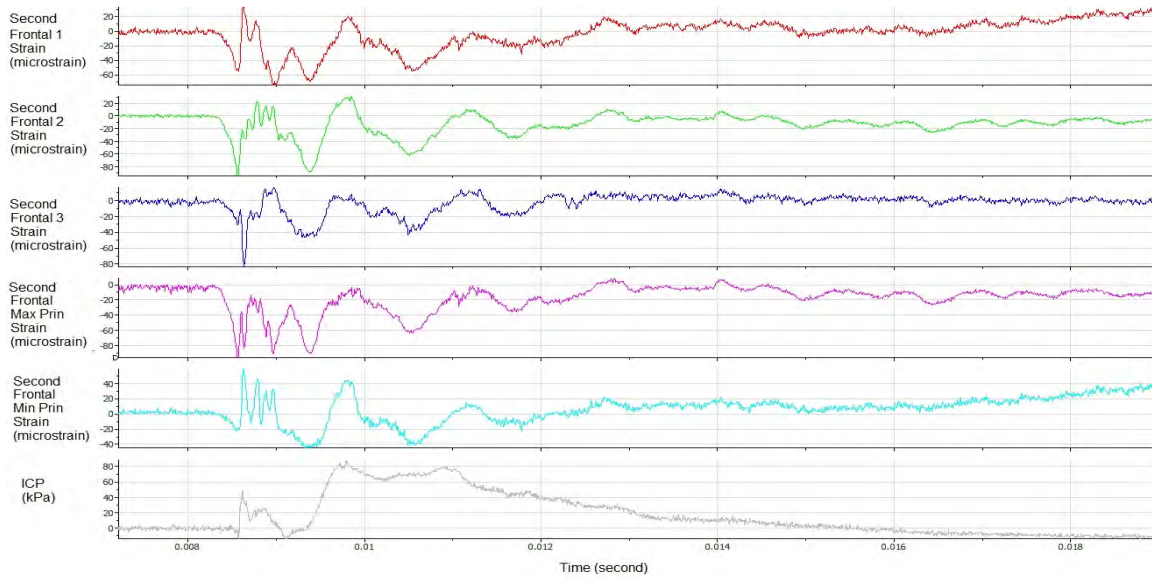
P2F-2F



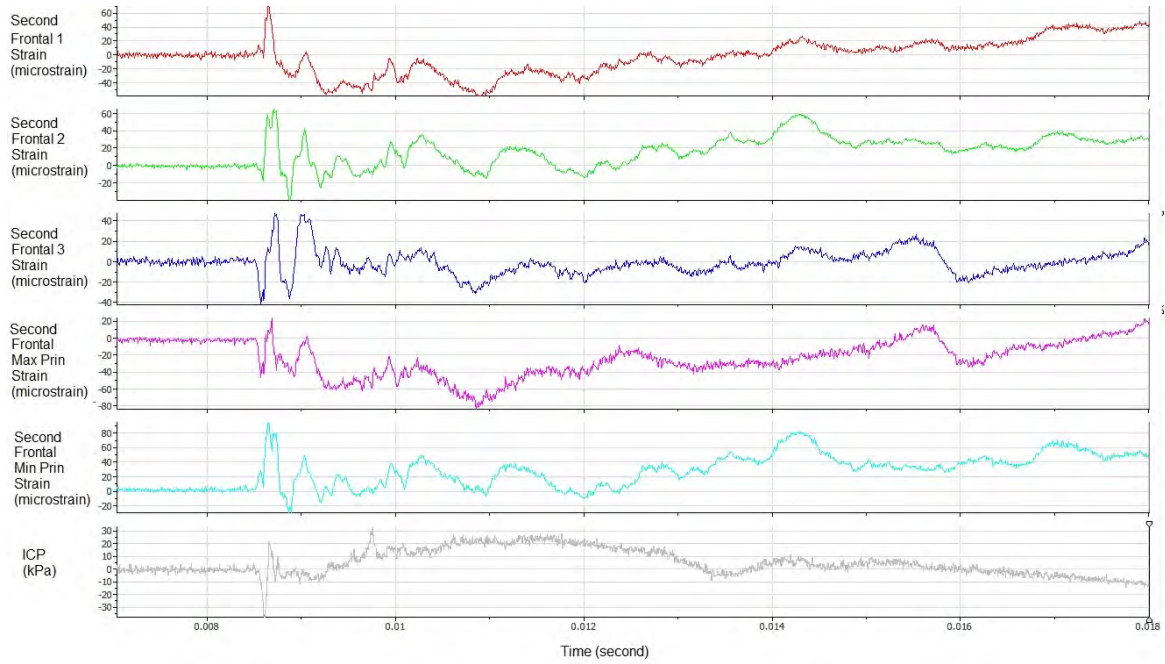
P2S-2F



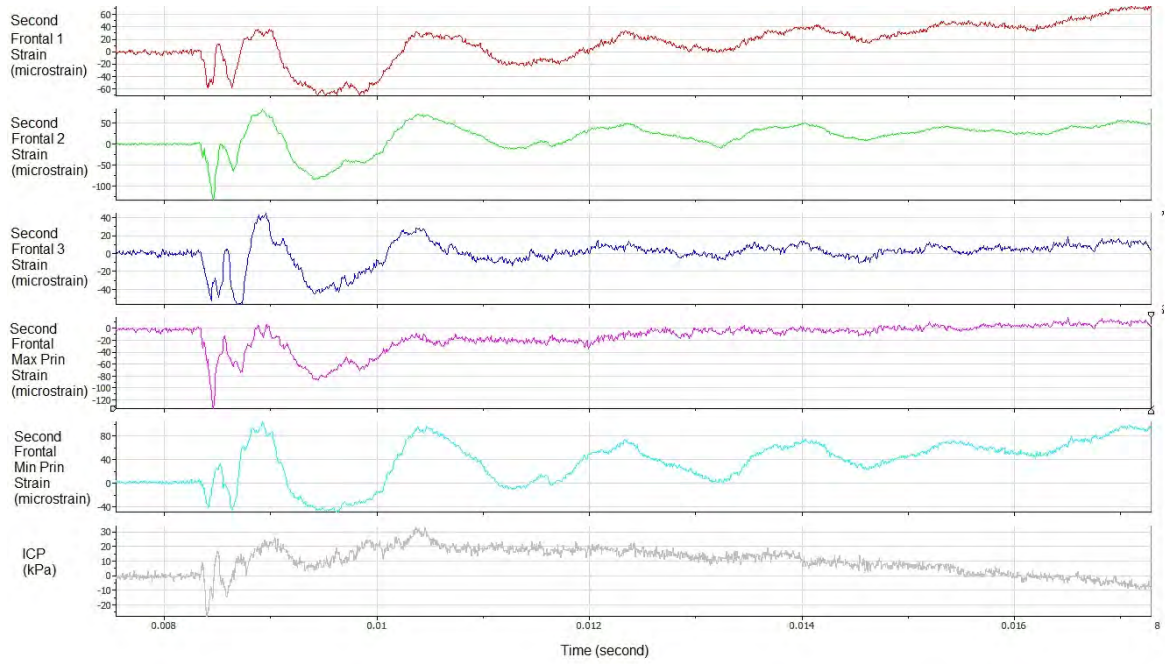
### P2B-2F



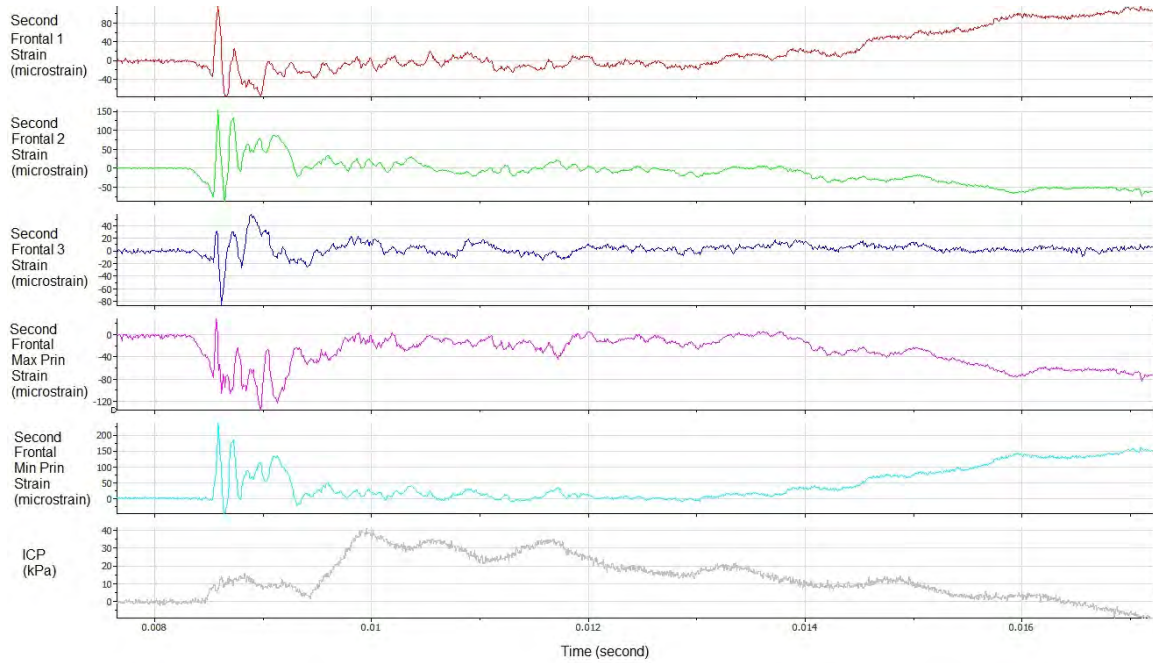
### P3F-2F



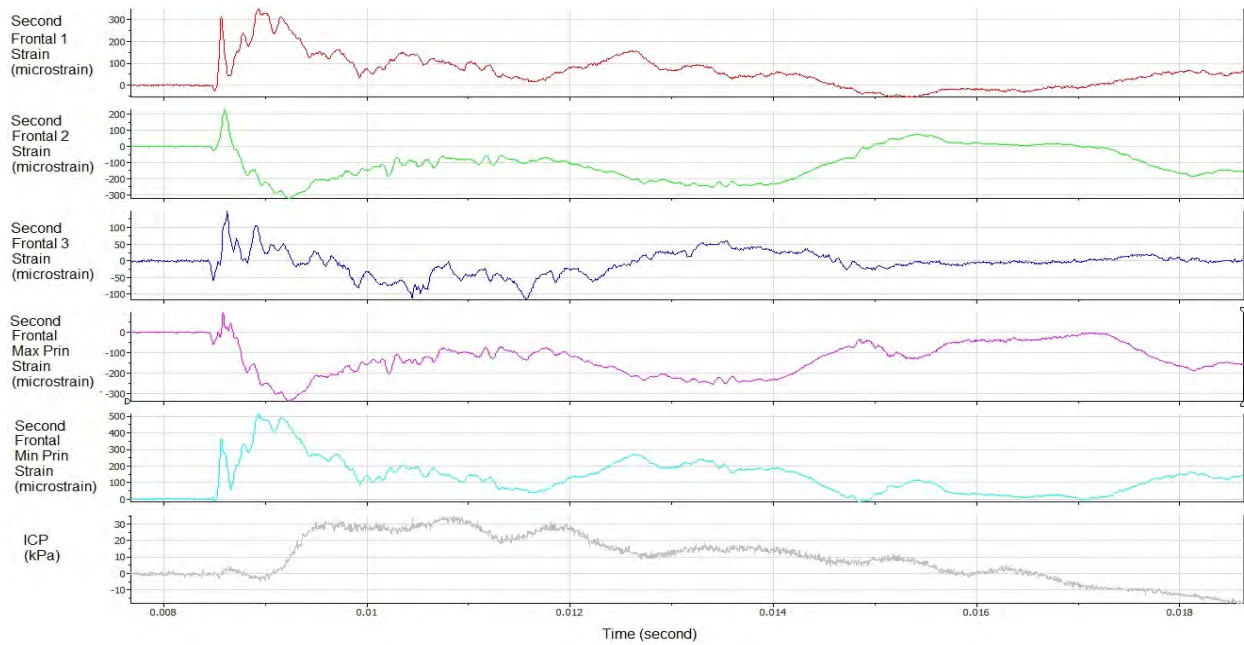
P3B-2F



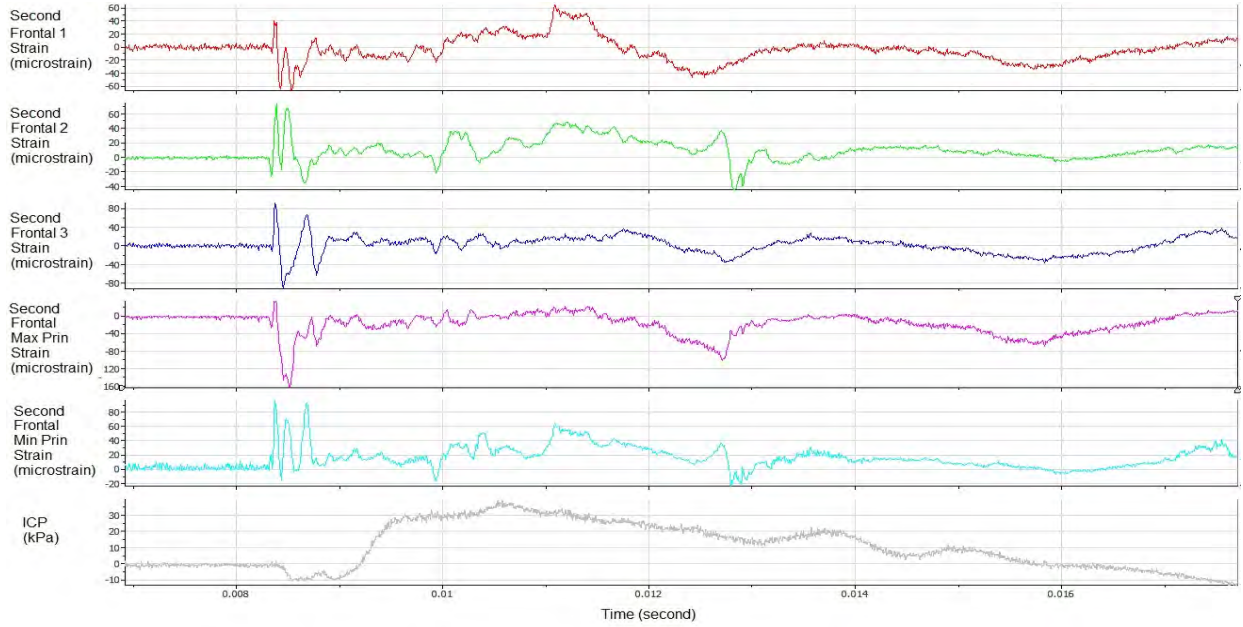
P3B-2F



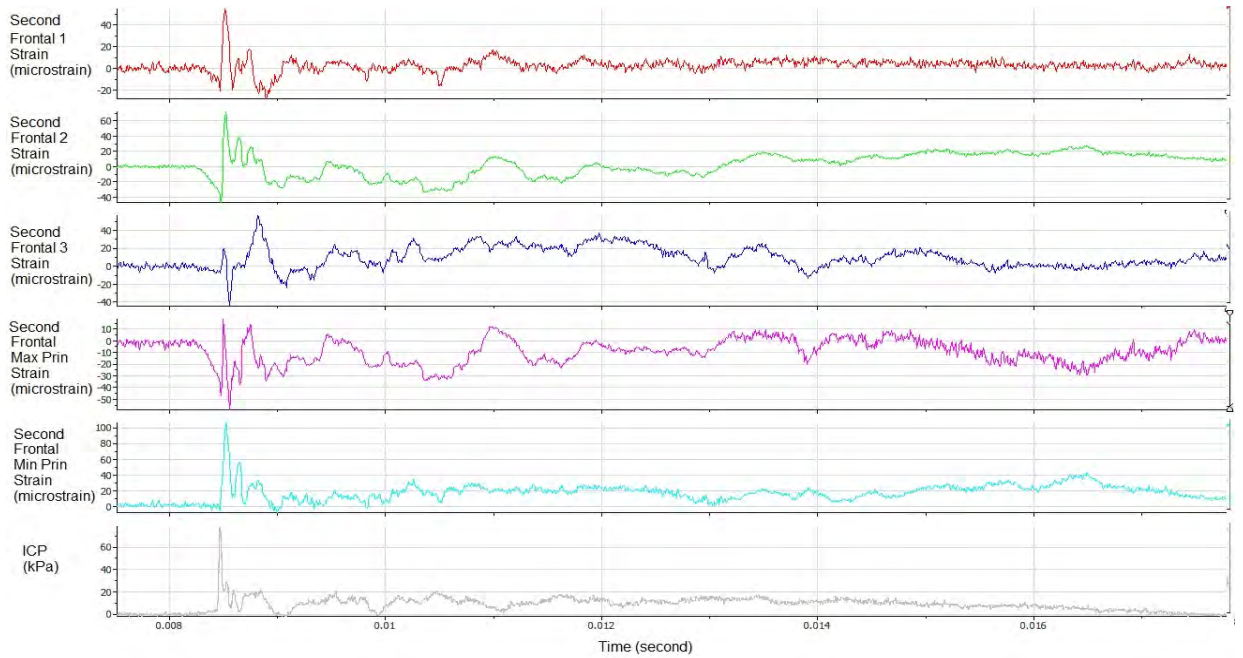
P4F-2F



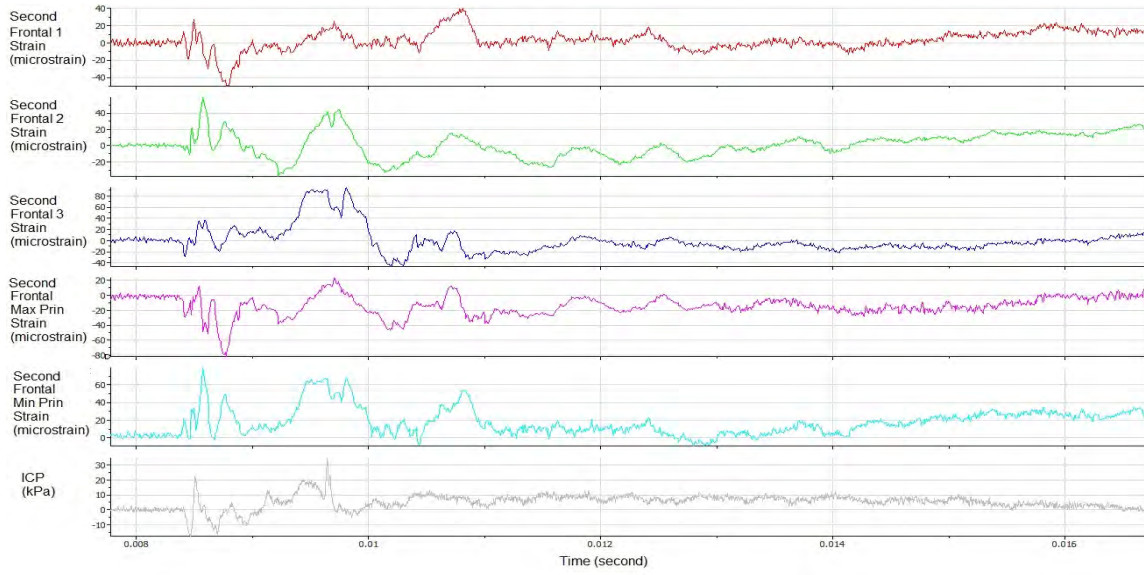
P4S-2F



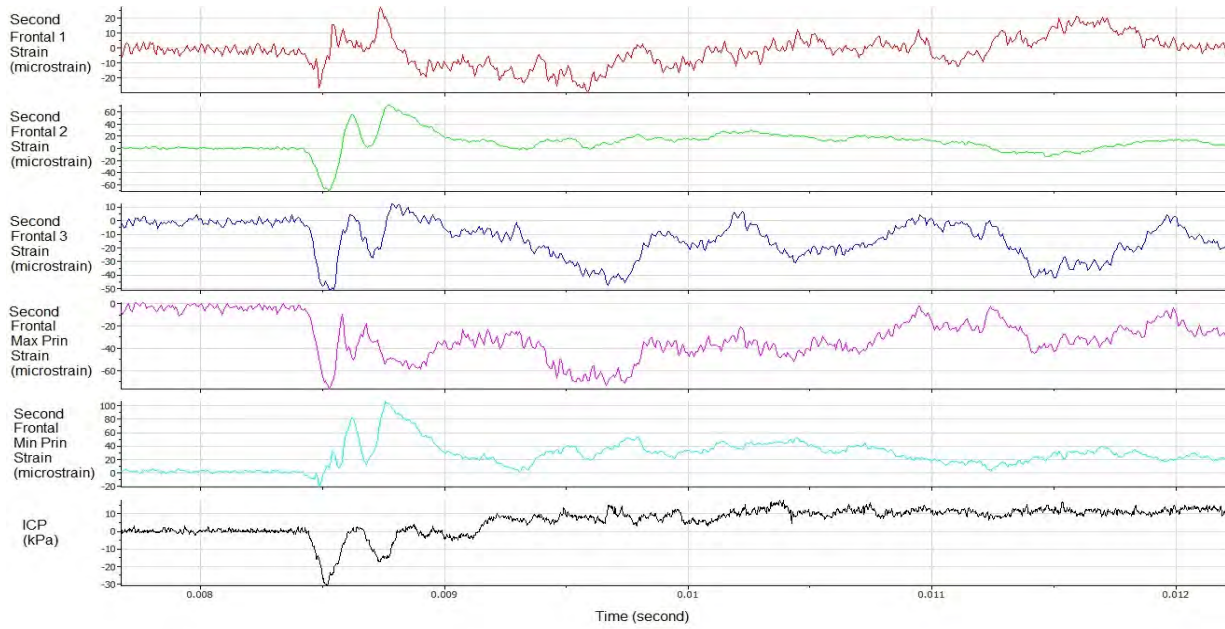
P4B-2F



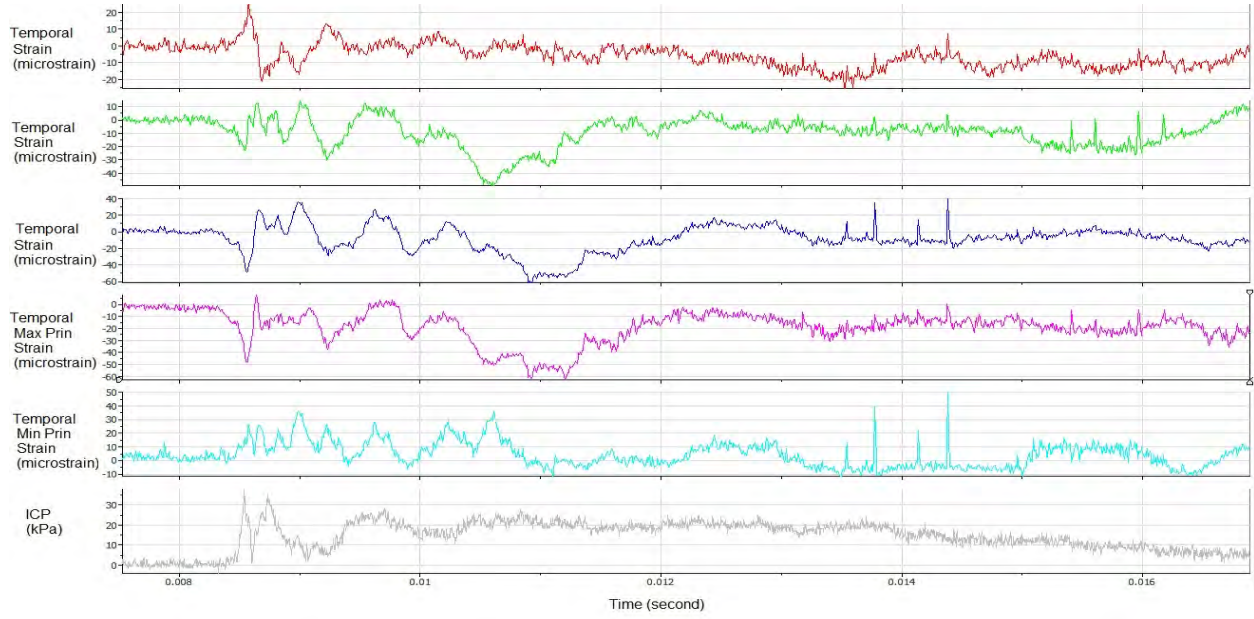
P5F-2F



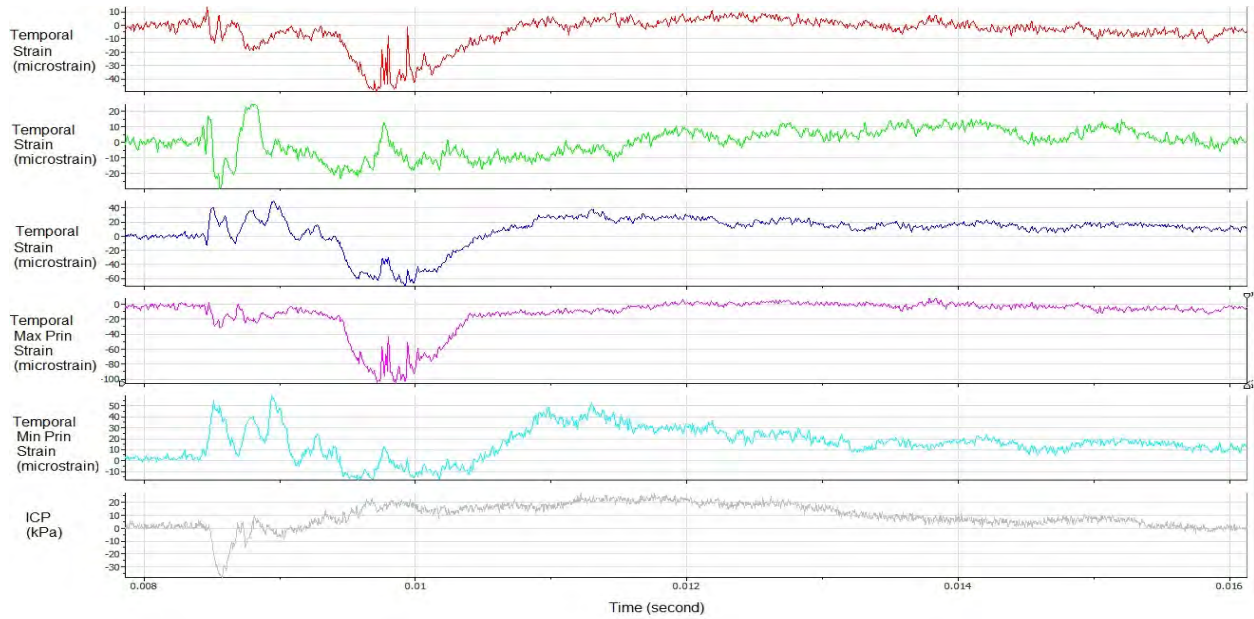
P5S-2F



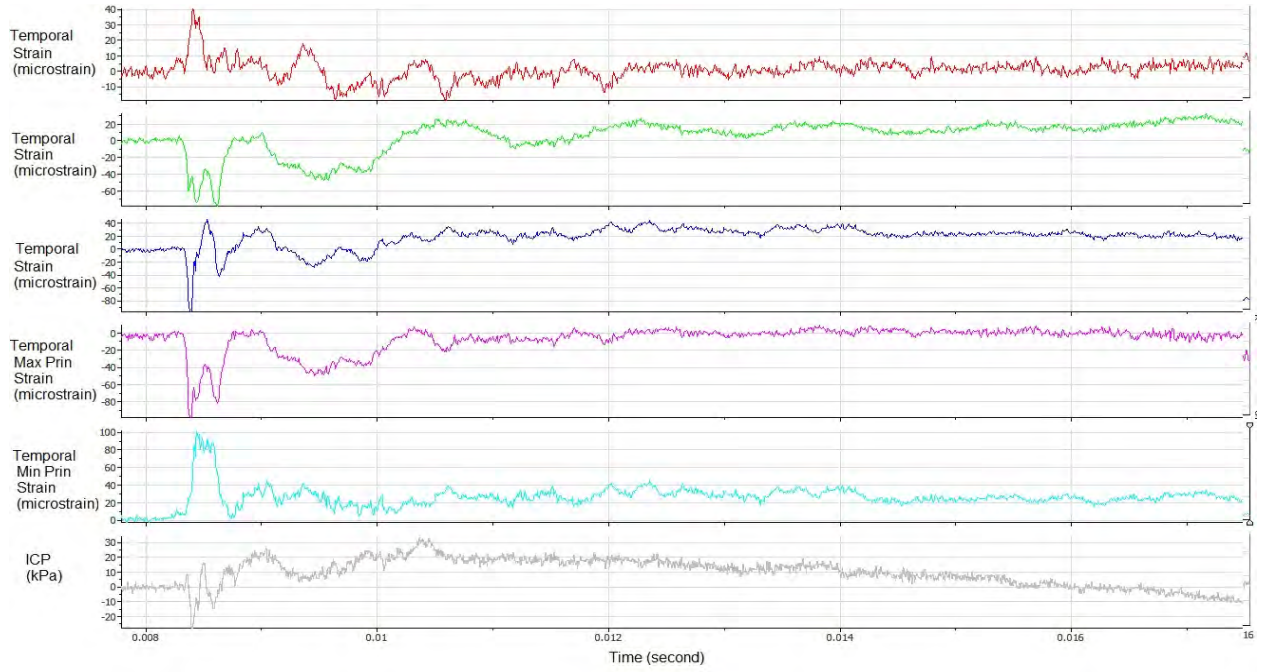
P5B-2F



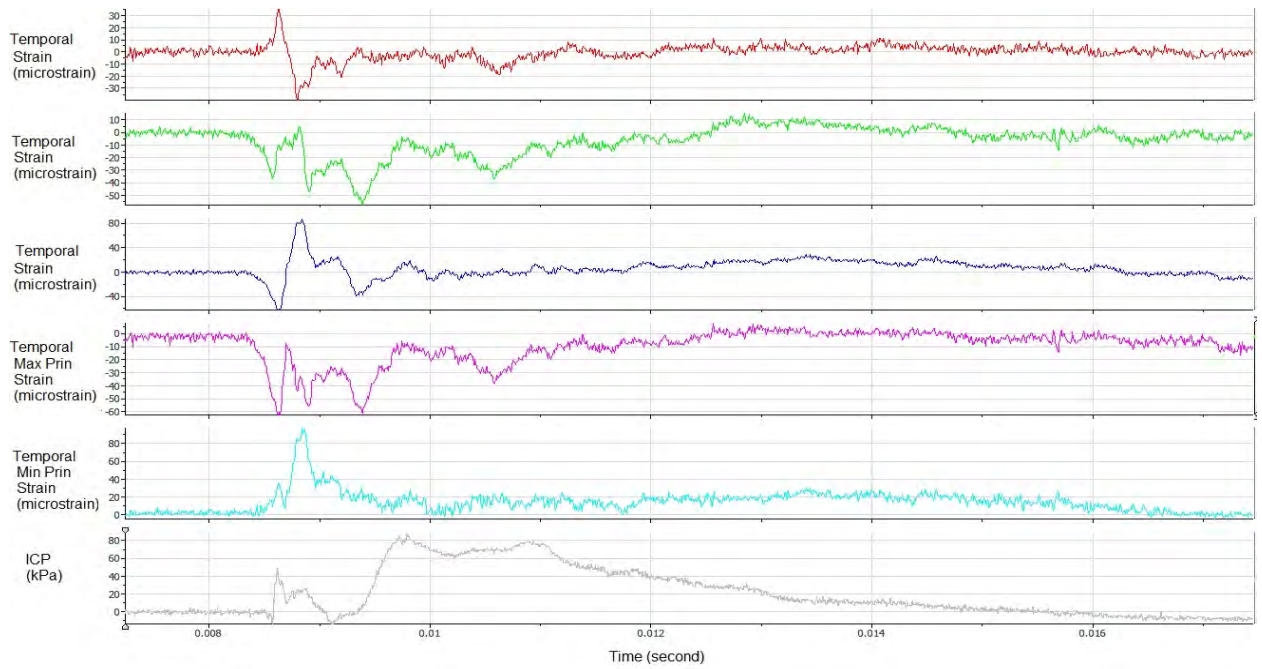
P2F-T



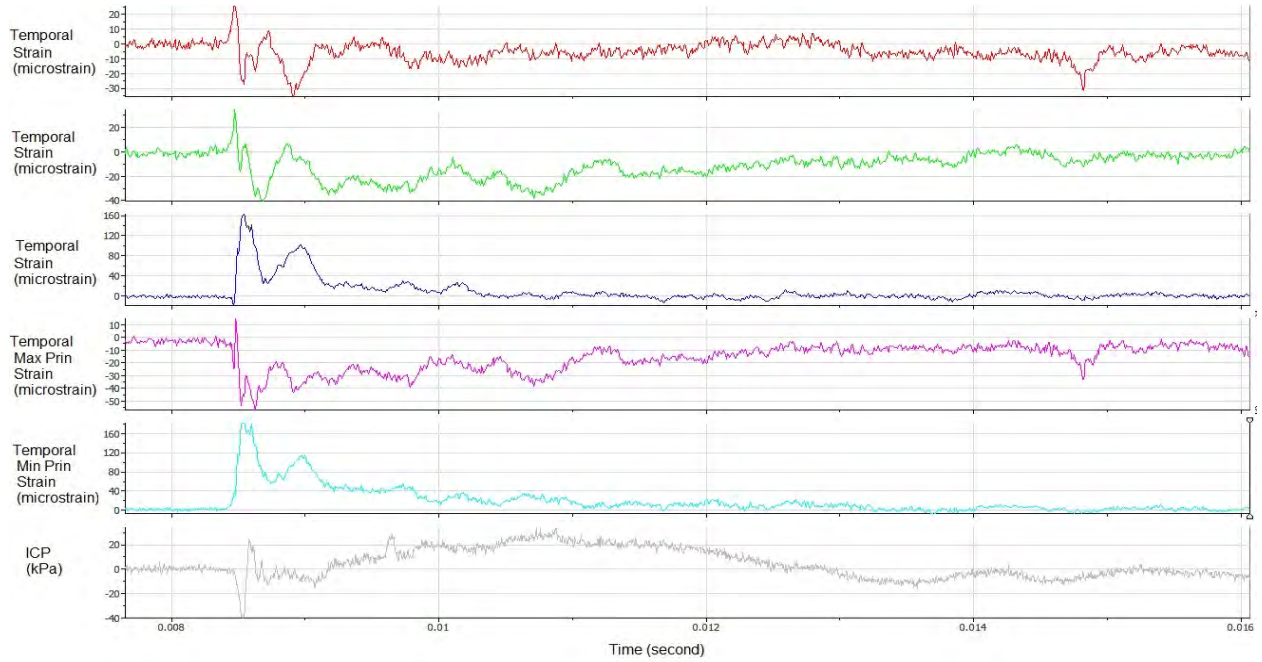
P2S-T



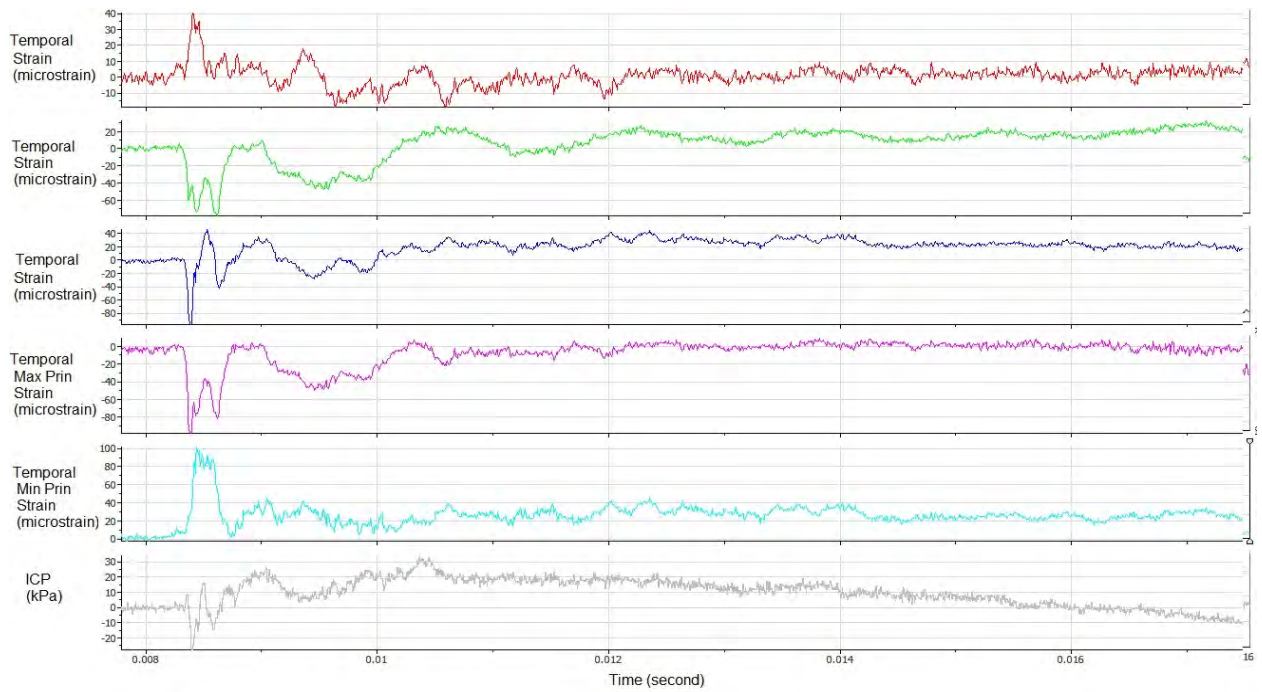
P2B-T



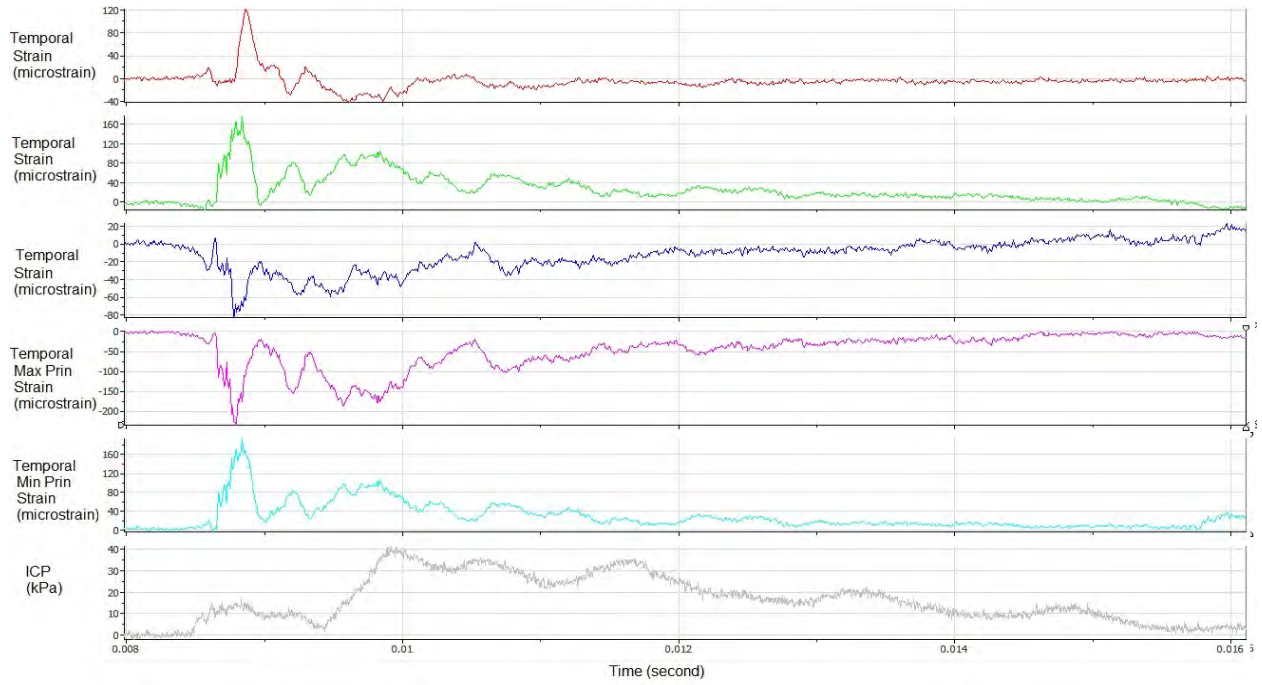
P3F-T



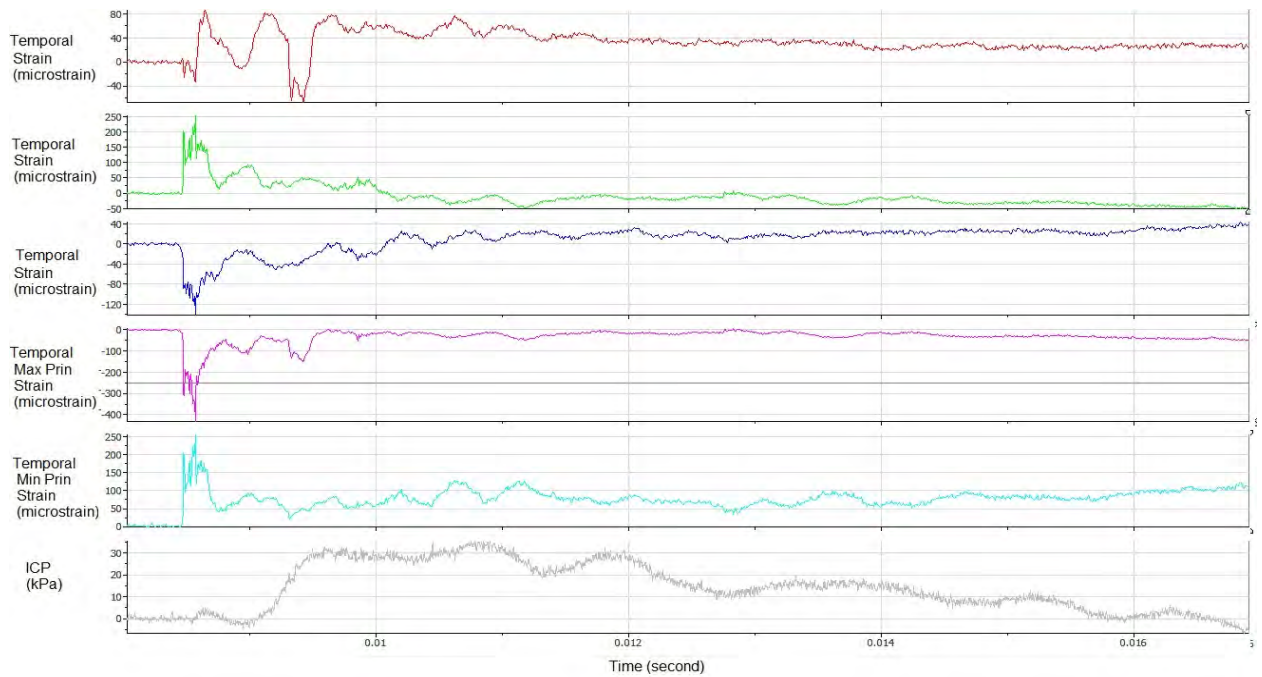
P3S-T



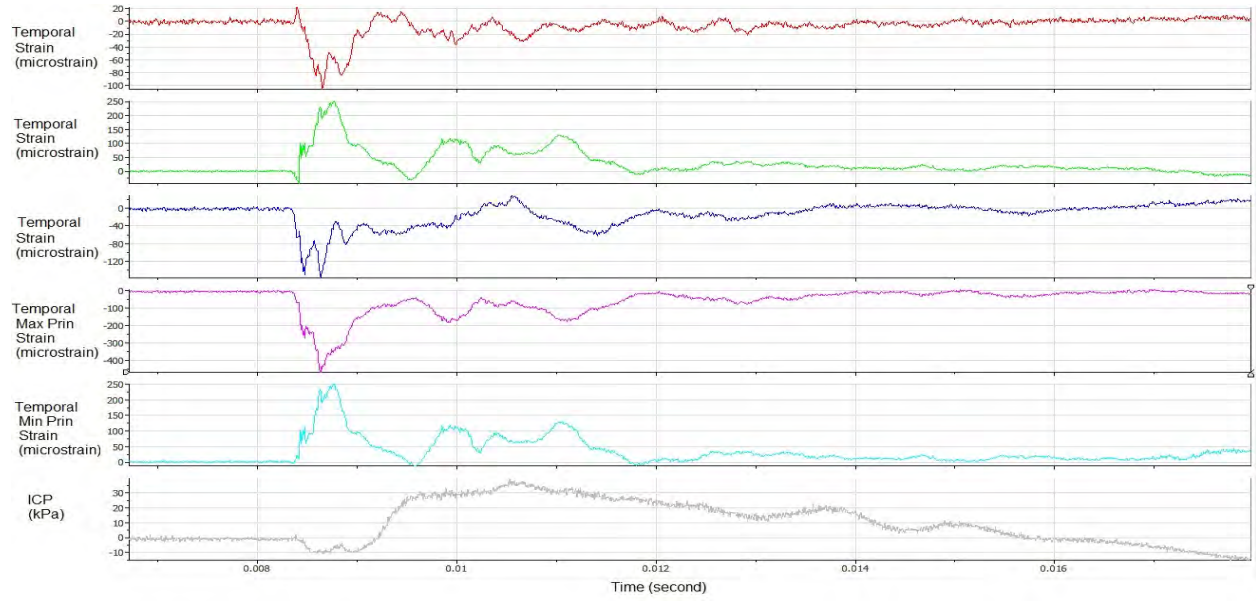
P3B-T



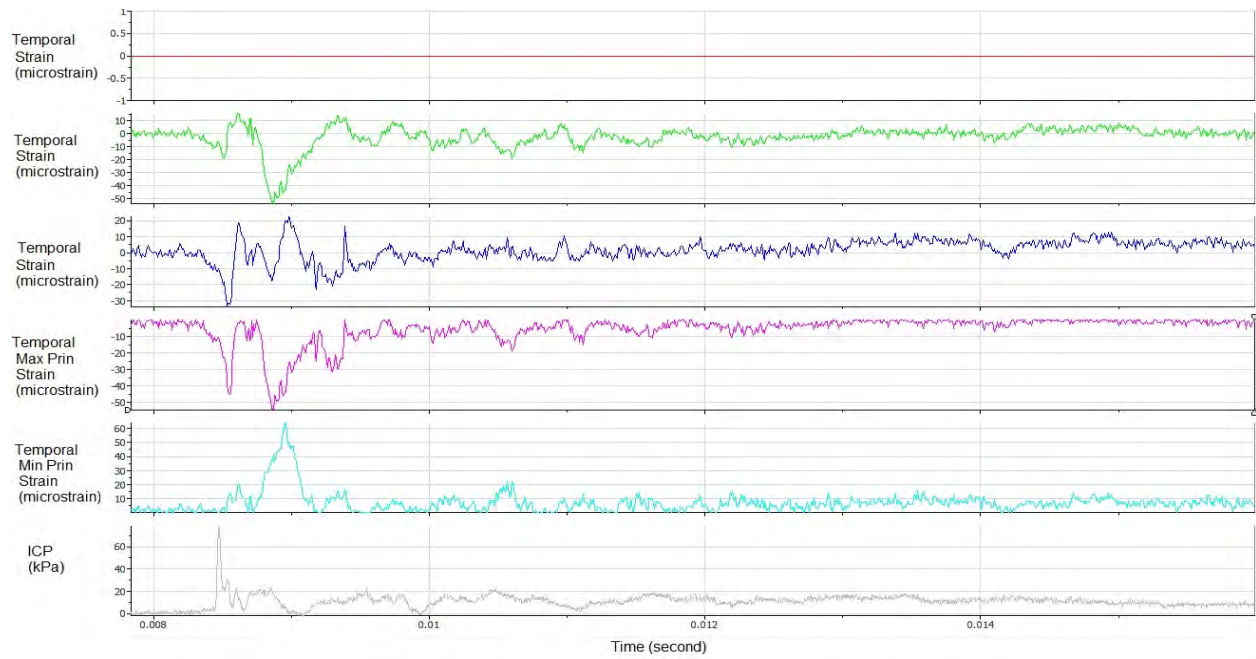
P4F-T



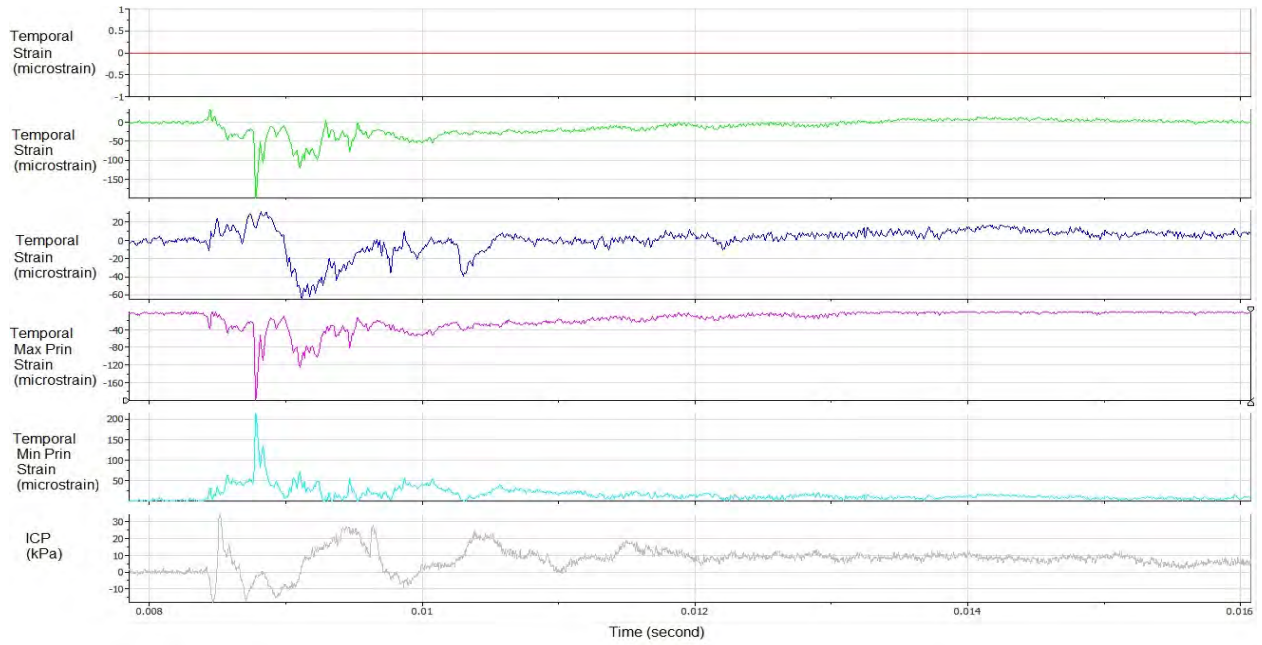
P4S-T



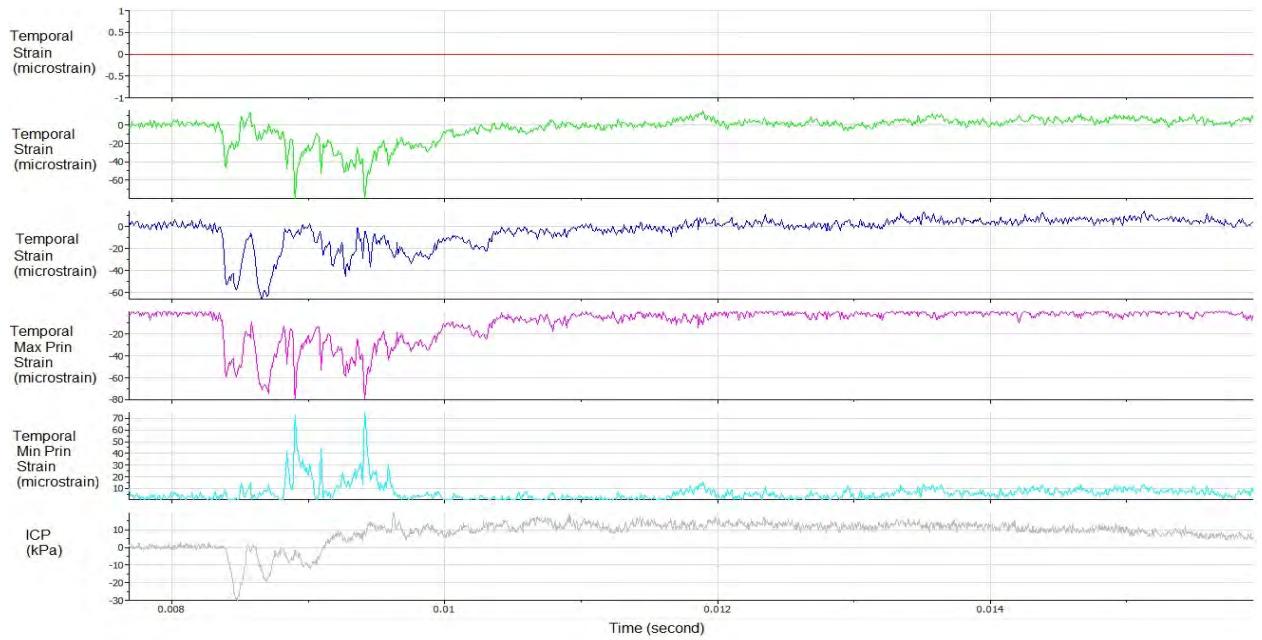
P4B-T



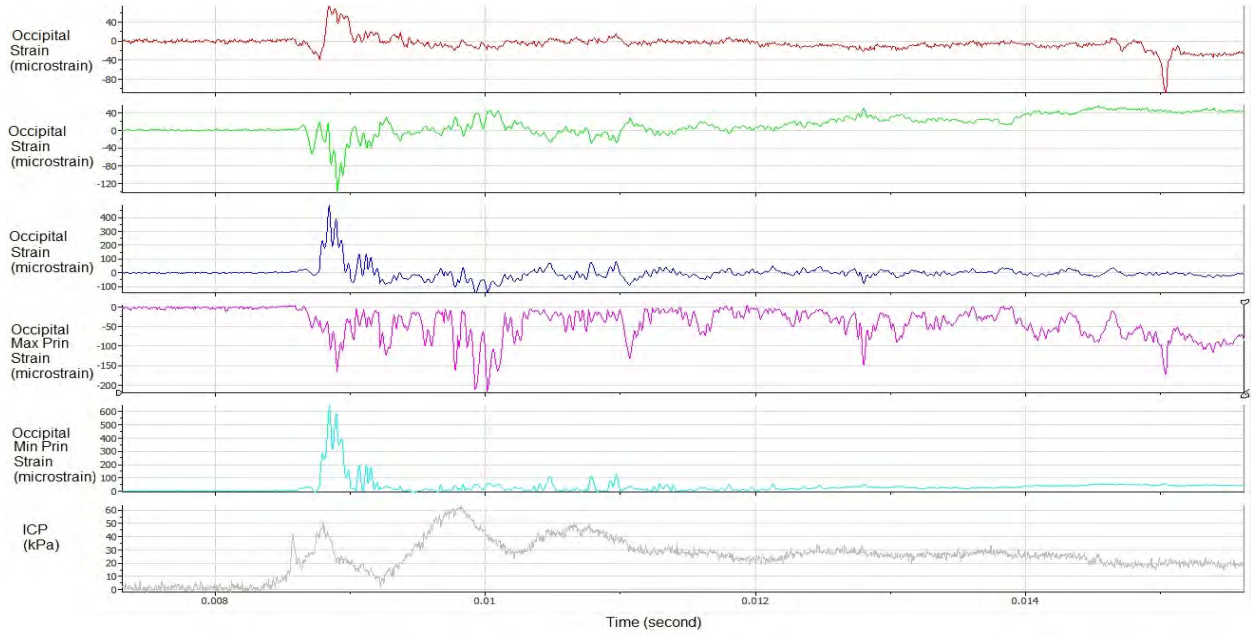
P5F-T



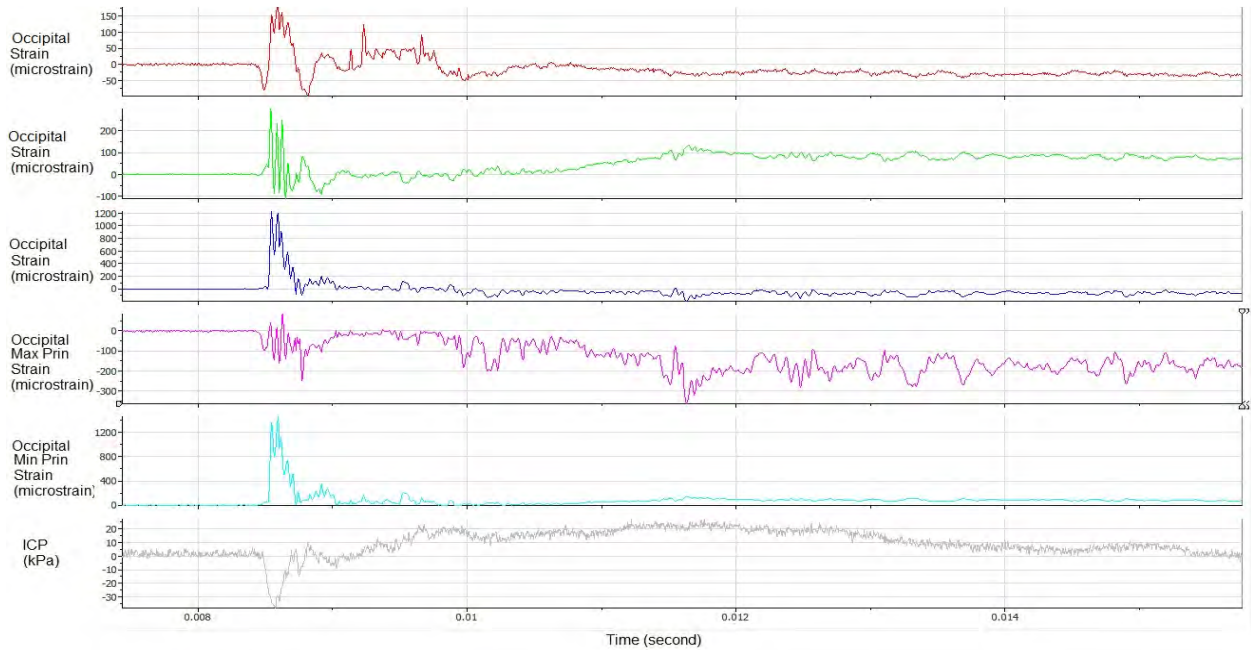
P5S-T



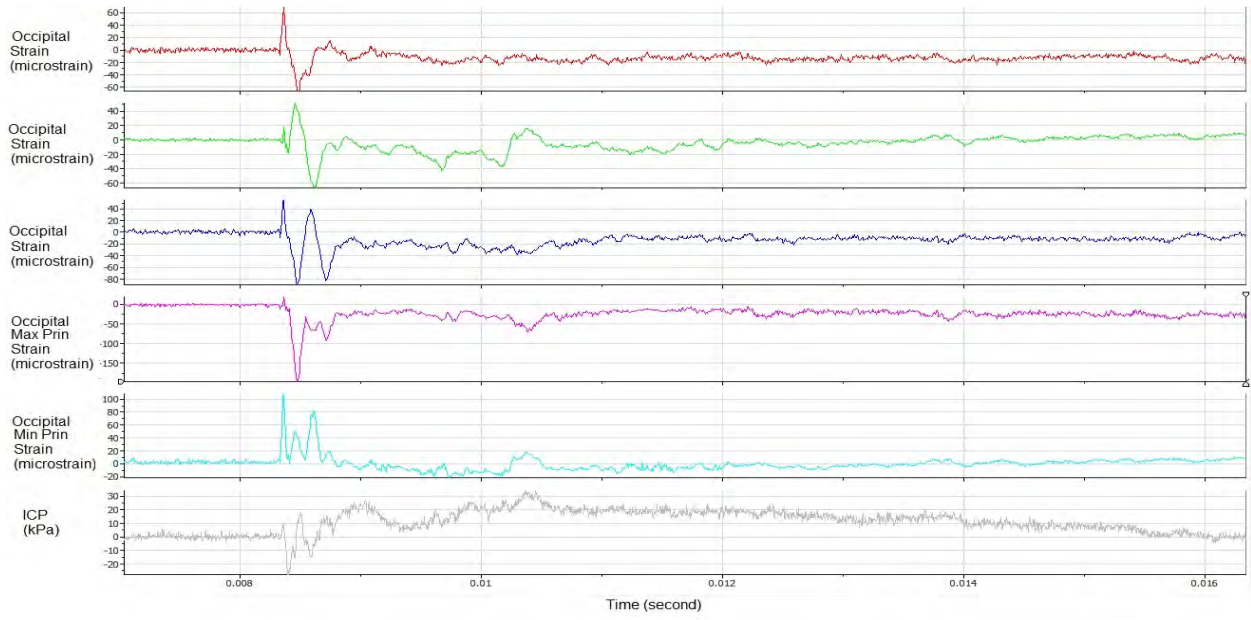
P5B-T



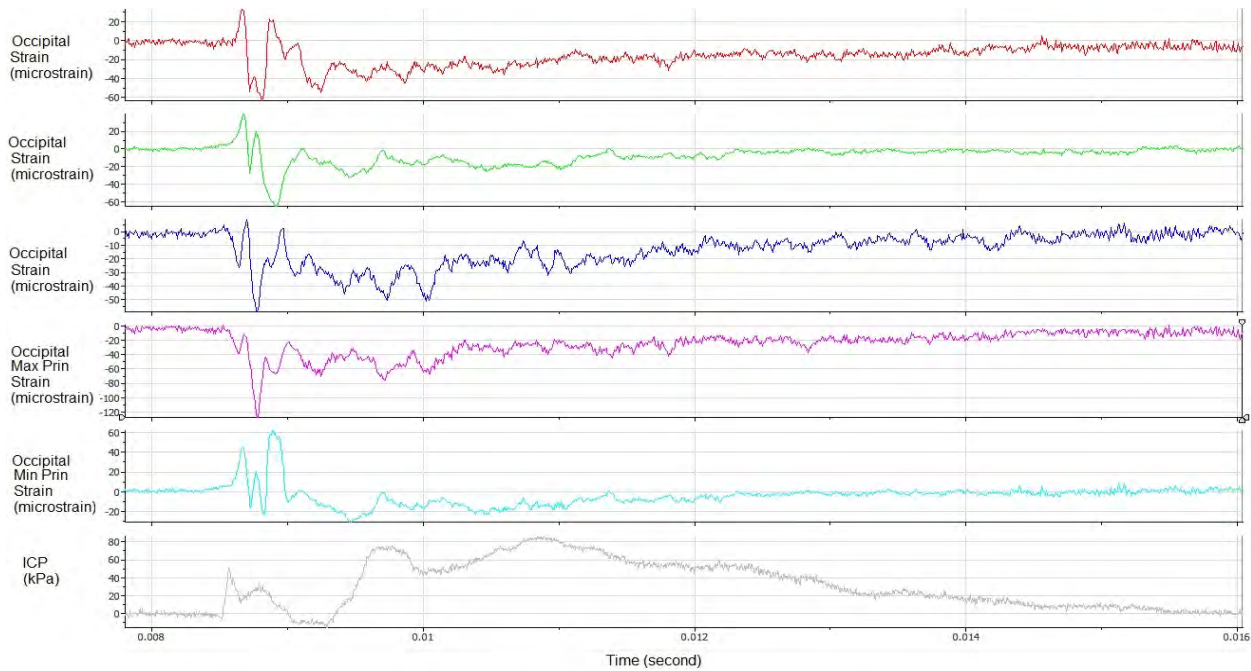
P2F-O



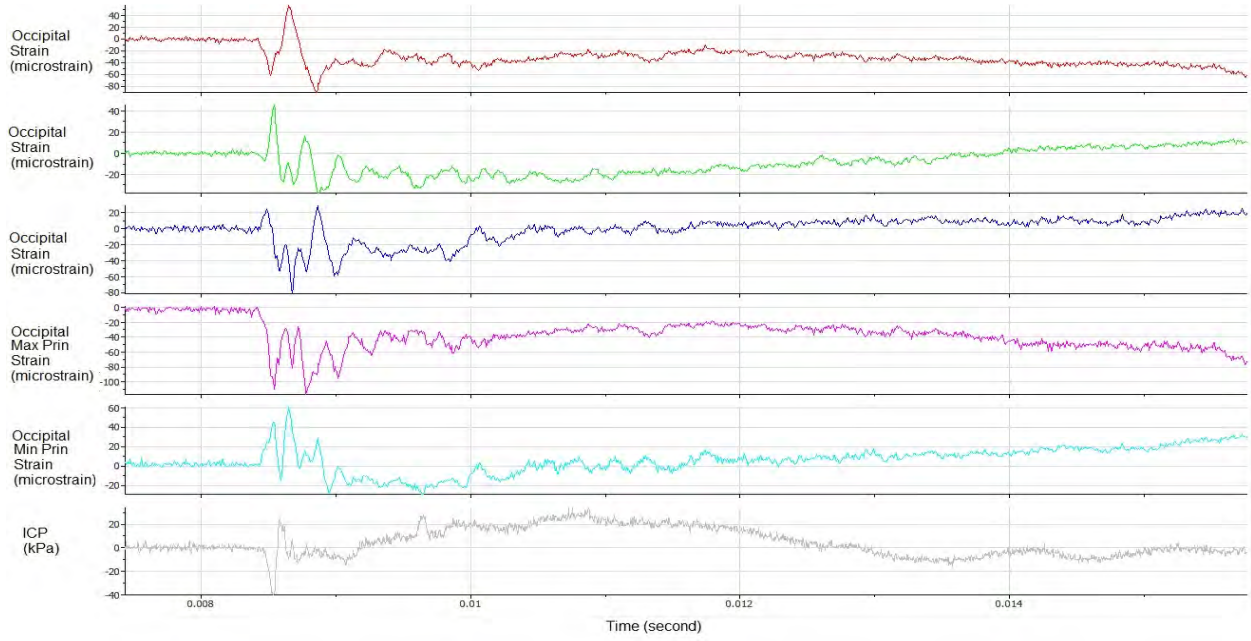
P2S-O



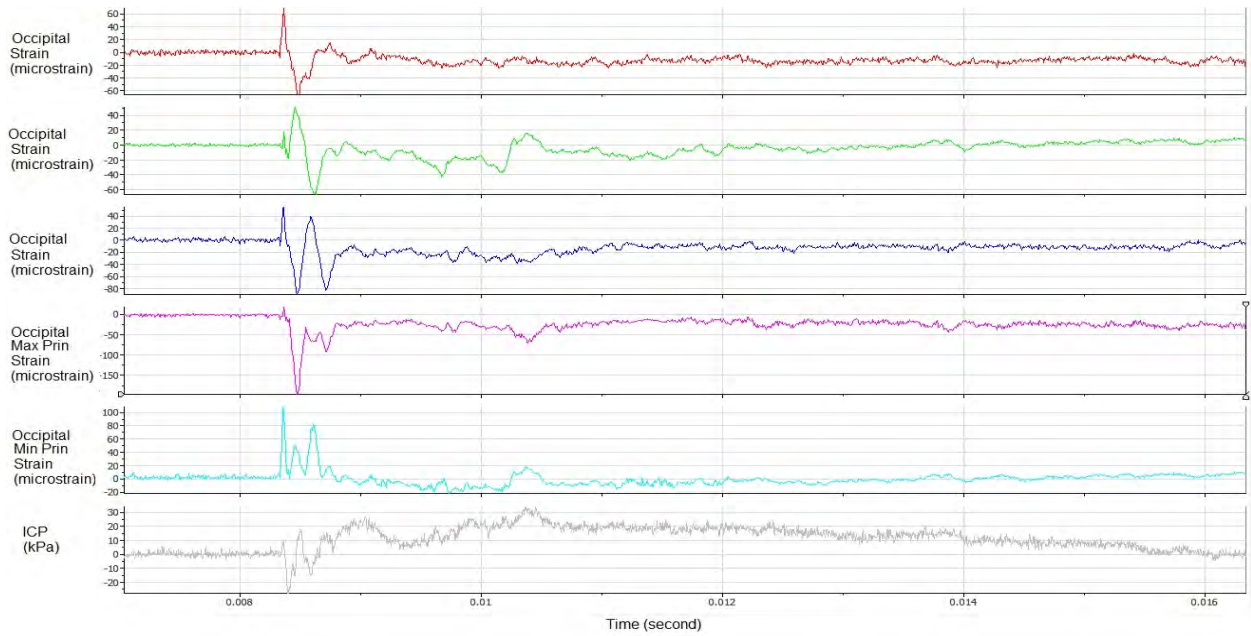
P2B-O



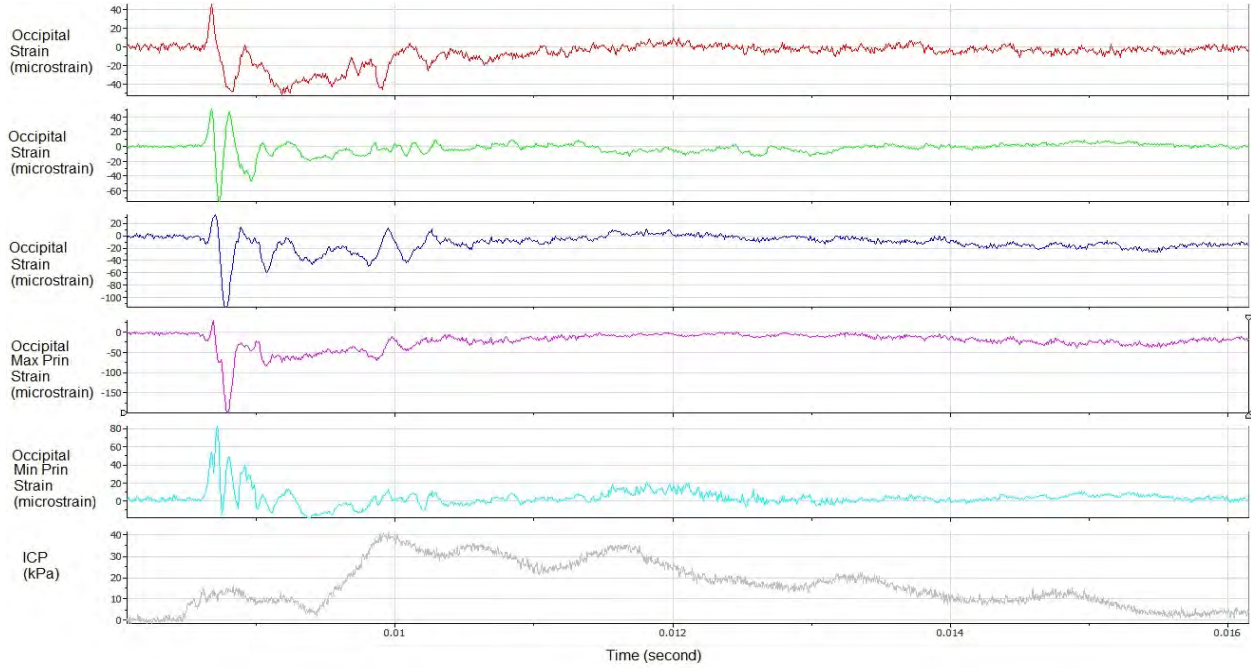
P3F-O



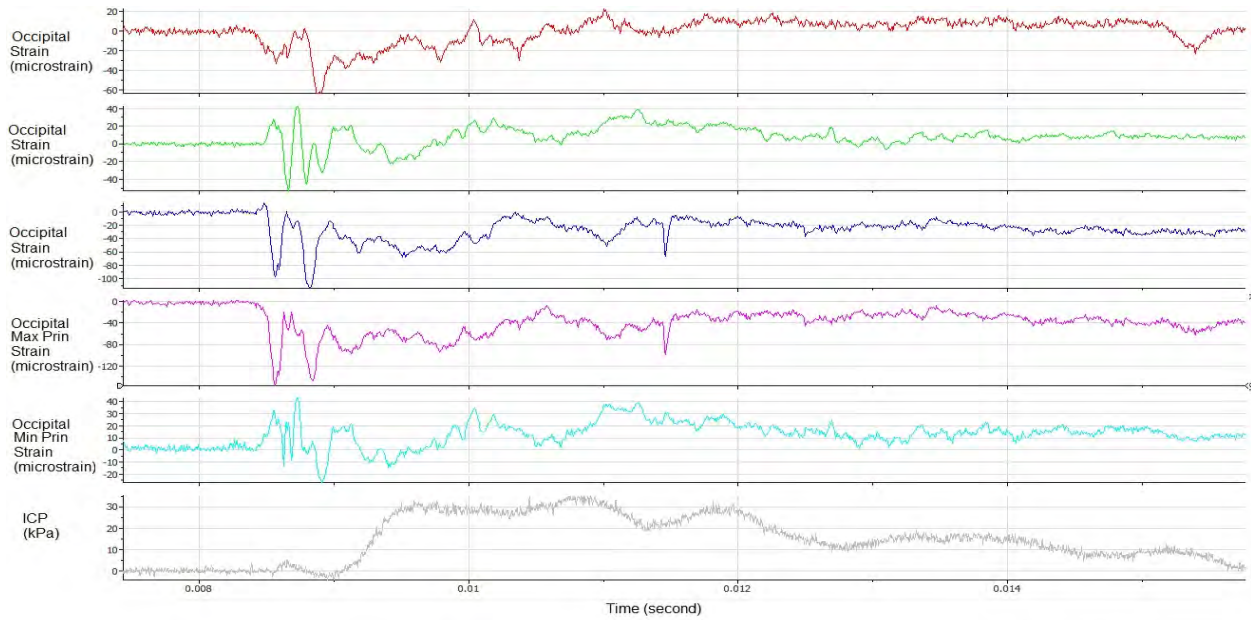
P3S-O



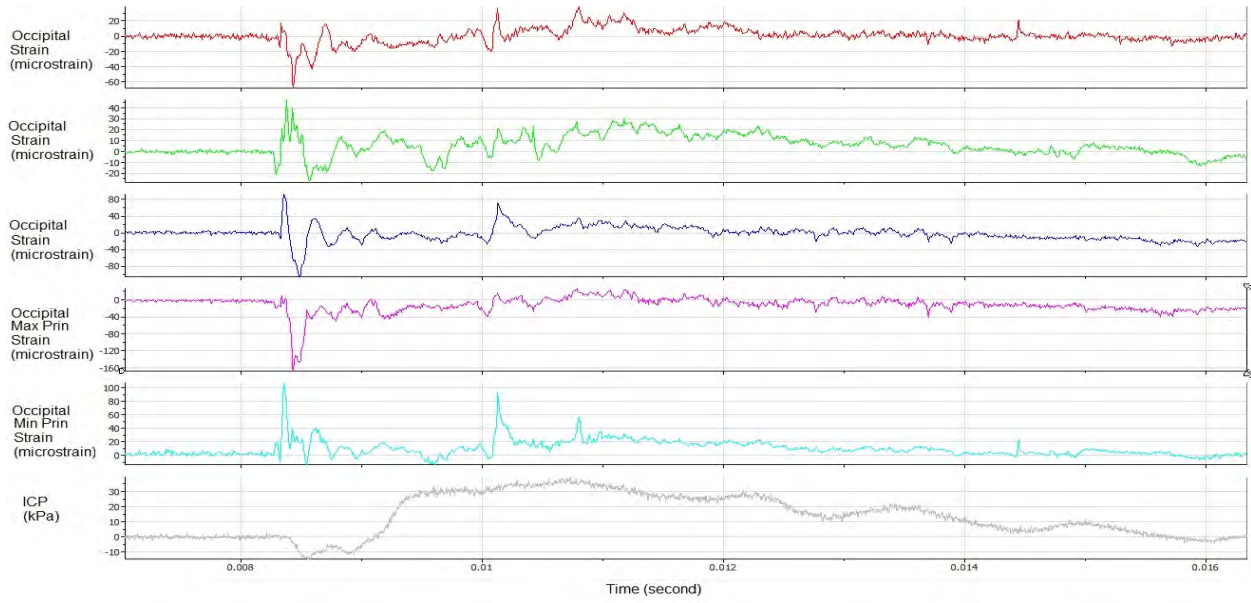
P3B-O



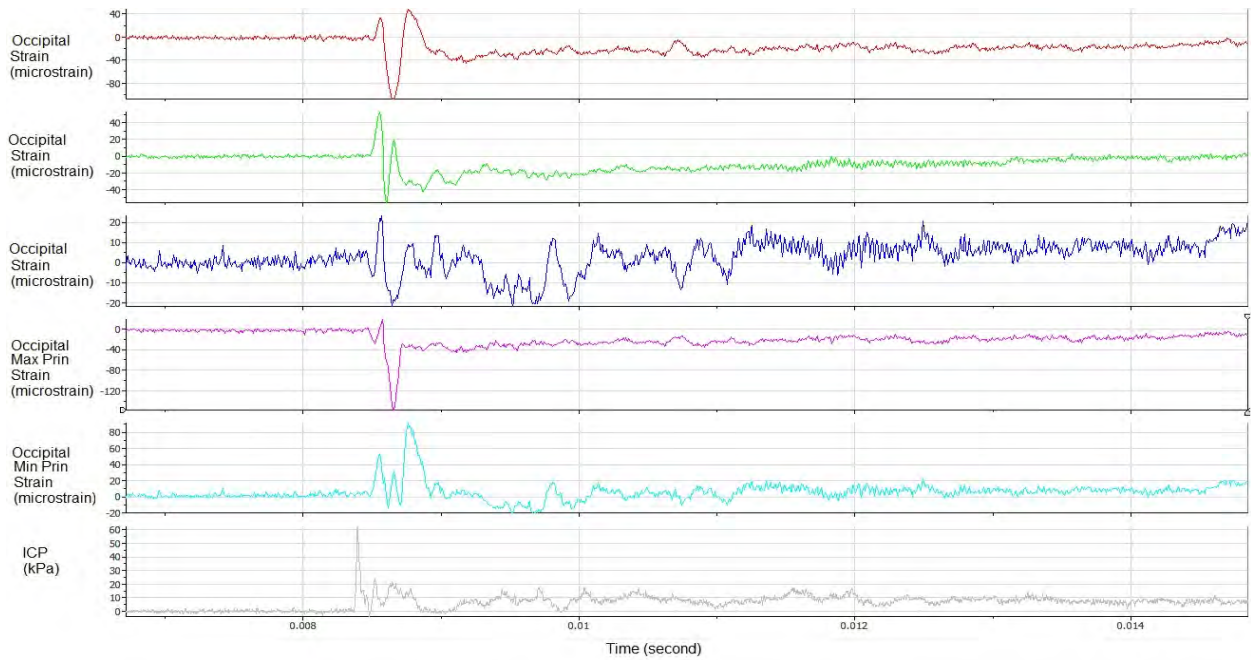
P4F-O



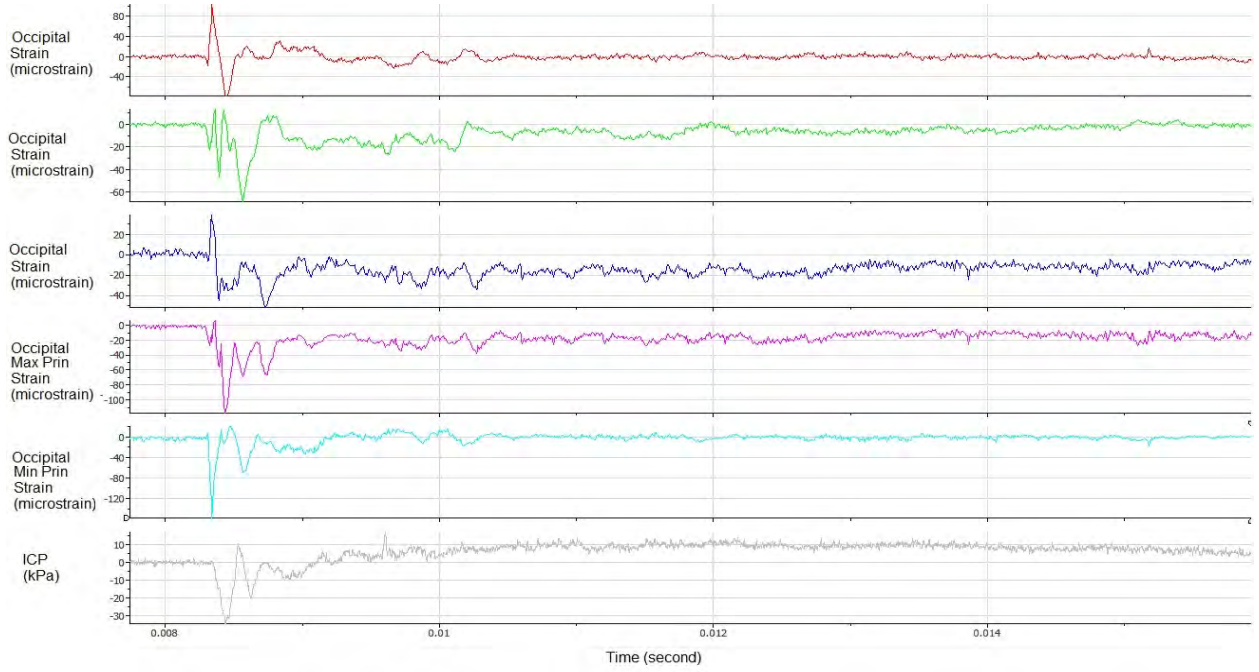
P4S-O



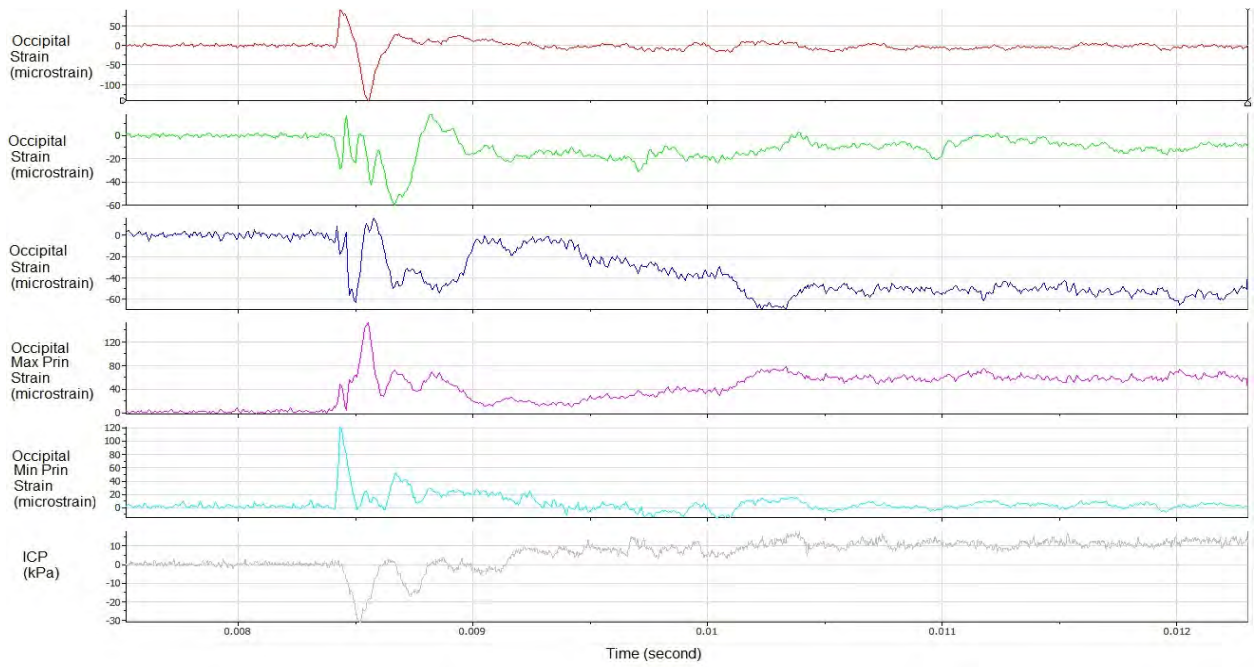
P4B-O



P5F-O



P5S-O



P5B-O

## APPENDIX C CADAVER DATA

Nomenclature for series: Specimen # and orientation (front, left, right, back) - sensor (frontal, temporal, zygomatic, parietal, occipital) C2F-F is cadaver 2 during a front facing exposure with strain being measured by the frontal rosette strain gages.

Cadaver	UM	33655							
Position	Intensity	Frontal 1	Frontal 2	Frontal3	Frontal Max Prin.	Occipital 1	Occipital 2	Occipital 3	Occipital Max Prin.
Front	Low	80	96	48	69	40	38	205	76
Side	Low	100	139	92	38	40	231	424	334
Back	Low	70	84	60	38	25	164	497	545
Side	Low	88	115	86	55	26	136	397	456
Front	Low	34	101	72	89	34	72	140	x
Front	Med	80	132	70	x	55	50	129	x
Side	Med	112	140	96	117	x	72	448	x
Back	Med	100	100	60	44	x	x	498	x
Side	Med	100	164	114	110	x	x	568	x
Front	Med	60	122	92	106	x	x	129	x
Front	High	94	226	161	199	x	x	x	x
Side	High	194	235	183	171	x	x	x	x
Back	High	87	145	91	x	x	x	x	x
Side	High	107	146	129	x	x	x	x	x
Front	High	90	200	89	x	x	x	x	x

Position	Intensity	Zygo 1	Zygo 2	Zygo 3	Zygo Max Prin	Temporal 1	Temporal 2	Temporal 3	Temporal Max Prin.
Front	Low	200	x	341	x	130	194	x	x
Side	Low	500	x	x	x	200	350	x	x
Back	Low	300	x	x	x	100	200	x	x
Side	Low	500	x	x	x	169	229	x	x
Front	Low	378	x	x	x	95	174	x	x
Front	Med	356	x	x	x	174	221	x	x
Side	Med	200	x	x	x	200	297	x	x
Back	Med	400	x	x	x	108	200	x	x
Side	Med	500	x	x	x	282	x	x	x
Front	Med	200	x	x	x	100	280	x	x
Front	High	164	x	x	x	174	374	x	x
Side	High	x	x	x	x	350	x	x	x
Back	High	x	x	x	x	150	x	x	x
Side	High	x	x	x	x	263	x	x	x
Front	High	x	x	x	x	146	x	x	x

Position	Intensity	Parietal 1	Parietal 2	Parietal 3	Parietal Max Prin.
Front	Low	56	78	71	80
Side	Low	37	62	38	50
Back	Low	60	55	51	74
Side	Low	45	56	45	55
Front	Low	x	60	x	x
Front	Med	x	x	x	x
Side	Med	x	x	x	x
Back	Med	x	x	x	x
Side	Med	x	x	x	x
Front	Med	x	x	x	x
Front	High	x	x	x	x
Side	High	x	x	x	x
Back	High	x	x	x	x
Side	High	x	x	x	x
Front	High	x	x	x	x

### Strain Response for Cadaver 5

Cadaver	UM	33652							
Position	Intensity	Frontal 1	Frontal 2	Frontal3	Frontal Max Prin.	Occipital 1	Occipital 2	Occipital 3	Occipital Max Prin.
Front	Low	30	20	45	47	325	323	275	518
Side	Low	45	x	27	x	962	649	231	664
Back	Low	38	50	x	x	703	646	377	758
Side	Low	20	29	x	x	354	479	269	626
Front	Low	43	26	46	59	353	365	312	621
Front	Med	47	31	43	57	420	403	373	679
Side	Med	60	70	42	40	879	856	483	1011
Back	Med	41	51	33	54	1200	787	237	808
Side	Med	41	33	41	58	509	420	389	729
Front	Med	60	51	63	91	734	537	500	931
Front	High	51	59	33	63	1190	1166	355	1233
Side	High	65	79	52	48	1120	887	572	985
Back	High	48	20	63	41	342	690	496	942
Side	High	61	45	x	x	689	491	462	911
Front	High	79	108	67	61	1080	997	580	858

Position	Intensity	Zygo 1	Zygo 2	Zygo 3	Zygo Max Prin	Temporal 1	Temporal 2	Temporal 3	Temporal Max Prin.
Front	Low	574	250	863	1244	73	27	154	166
Side	Low	548	337	687	1029	142	105	261	312
Back	Low	350	167	366	646	70	32	116	134
Side	Low	460	189	354	632	127	53	133	170
Front	Low	556	678	661	766	63	42	127	138
Front	Med	667	658	904	1271	101	50	163	179
Side	Med	508	224	x	x	86	35	153	169
Back	Med	795	x	1607	x	181	160	317	370
Side	Med	879	x	x	x	110	47	137	153
Front	Med	1168	2337	1290	2336	144	66	156.5	172
Front	High	1298	x	2302	x	249	206	x	755
Side	High	587	x	x	x	97	80	313	319
Back	High	632	x	x	x	156	248	310	331
Side	High	x	x	x	x	409	202	203	320
Front	High	x	x	x	x	106	57	294	323

Position	Intensity	Parietal 1	Parietal 2	Parietal 3	Parietal Max Prin.
Front	Low	42	136	49	136
Side	Low	30	146	65	139
Back	Low	50	188	54	190
Side	Low	37	168	38	170
Front	Low	57	142	51	144
Front	Med	45	160	65	160
Side	Med	86	200	81	207
Back	Med	75	150	89	176
Side	Med	52	176	38	180
Front	Med	78	220	46	220
Front	High	92	248	96	268
Side	High	x	278	91	x
Back	High	83	198	65	201
Side	High	227	190	85	228
Front	High	152	284	115	285

#### Strain Response for Cadaver 4

Cadaver	WSU	509							
Position	Intensity	Frontal 1	Frontal 2	Frontal 3	Frontal Max Prin.	Occipital 1	Occipital 2	Occipital 3	Occipital Max Prin.
Front	Low	93	83	178	103	155	368	101	622
Side	Low	97	129	105	146	77	402	117	549
Back	Low	108	284	64	240	103	269	96	398
Front	Low	98	51	59	126	149	333	84	569
Front	Med	112	99	71	113	178	367	92	680
Side	Med	75	119	78	133	90	237	127	433
Back	Med	124	252	67	236	142	547	185	852
Side	Med	120	226	51	231	112	317	149	544
Front	Med	101	217	38	218	163	344	144	650
Front	High	146	369	88	174	220	398	174	884
Side	High	134	219	72	222	99	408	72	576
Back	High	x	x	x	x	291	568	217	1068
Side	High	x	x	x	x	94	304	132	518
Front	High	x	x	x	x	x	483	147	621

Position	Intensity	Zygo 1	Zygo 2	Zygo 3	Zygo Max Prin	Temporal 1	Temporal 2	Temporal 3	Temporal Max Prin.
Front	Low	x	x	x	x	x	x	x	x
Side	Low	x	x	x	x	x	x	x	x
Back	Low	x	x	x	x	x	x	x	x
Front	Low	x	x	x	x	x	x	x	x
Front	Med	x	x	x	x	x	x	x	x
Side	Med	x	x	x	x	x	x	x	x
Back	Med	x	x	x	x	x	x	x	x
Side	Med	x	x	x	x	x	x	x	x
Front	Med	x	x	x	x	x	x	x	x
Front	High	x	x	x	x	x	x	x	x
Side	High	x	x	x	x	x	x	x	x
Back	High	x	x	x	x	x	x	x	x
Side	High	x	x	x	x	x	x	x	x
Front	High	x	x	x	x	x	x	x	x

Position	Intensity	Parietal 1	Parietal 2	Parietal 3	Parietal Max Prin.
Front	Low	113	x	x	x
Side	Low	95	x	x	x
Back	Low	107	x	x	x
Front	Low	86	x	x	x
Front	Med	110	x	x	x
Side	Med	107	x	x	x
Back	Med	98	x	x	x
Side	Med	108	x	x	x
Front	Med	116	x	x	x
Front	High	101	x	x	x
Side	High	114	x	x	x
Back	High	152	x	x	x
Side	High	122	x	x	x
Front	High	106	x	x	x

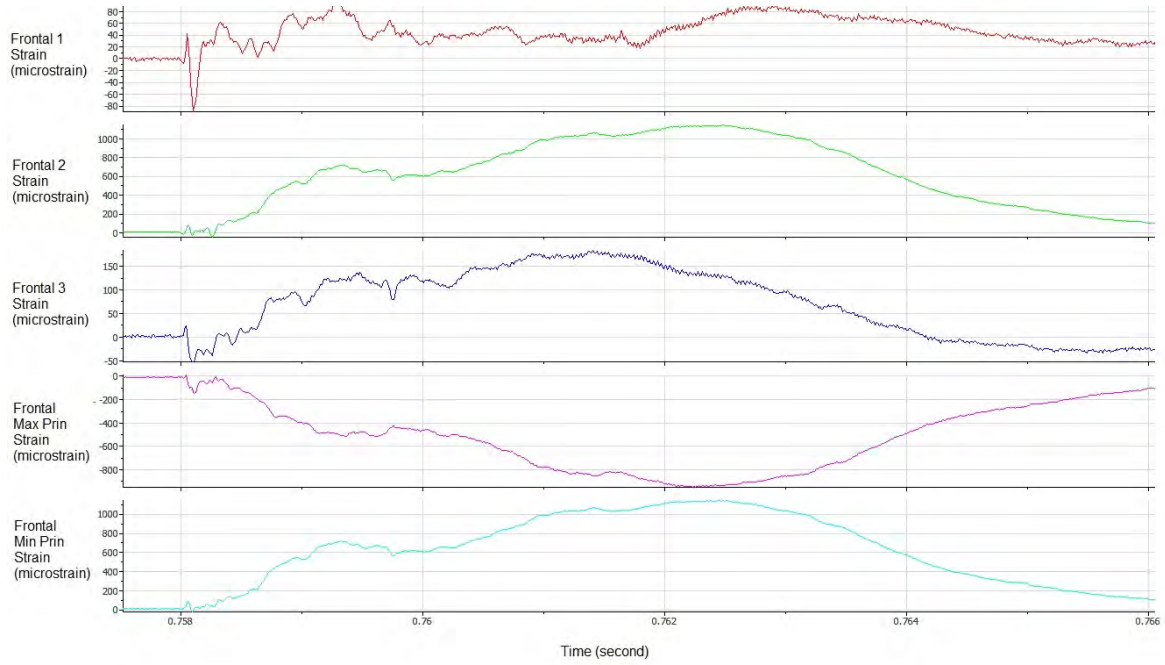
Strain response for Cadaver 2

Cadaver	WSU	510							
Position	Intensity	Frontal 1	Frontal 2	Frontal 3	Frontal Max Prin.	Occipital 1	Occipital 2	Occipital 3	Occipital Max Prin.
Front	Low	119	95	136	169	x	73	41	x
Side	Low	112	118	103	105	x	125	75	x
Back	Low	73	64	41	95	x	26	37	x
Front	Low	106	82	128	157	x	61	48	x
Front	Med	143	116	145	192	x	35	52	x
Side	Med	198	116	112	241	x	44	151	x
Back	Med	100	107	118	95	x	32	x	x
Side	Med	35	88	78	13	x	26	x	x
Front	Med	149	116	147	183	x	39	x	x
Front	High	228	197	230	279	x	50	x	x
Side	High	102	158	139	157	x	32	x	x
Back	High	137	164	161	137	x	37	x	x
Side	High	119	112	105	119	x	43	x	x
Front	High	202	160	205	255	x	48	x	x

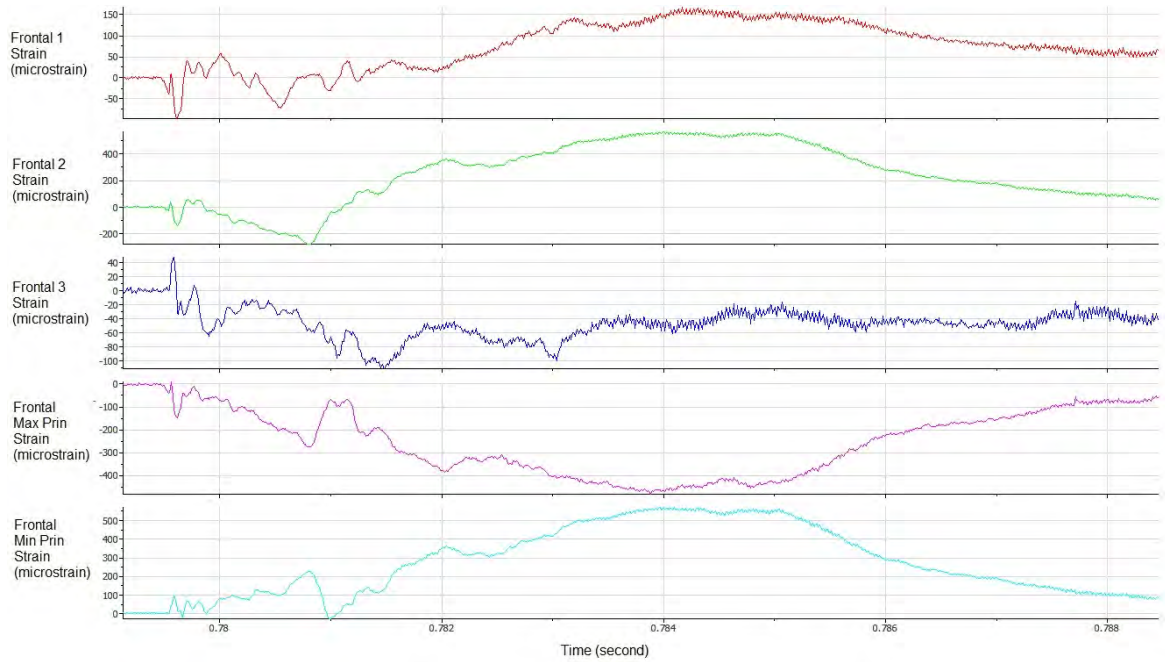
Position	Intensity	Zygo 1	Zygo 2	Zygo 3	Zygo Max Prin.	Temporal 1	Temporal 2	Temporal 3	Temporal Max Prin.
Front	Low	747	649	247	696	234	237	x	x
Side	Low	523	121	50	574	182	276	x	x
Back	Low	433	112	106	500	360	313	x	x
Front	Low	852	381	210	938	176	x	x	x
Front	Med	603	487	175	817	256	x	x	x
Side	Med	505	723	288	910	x	x	x	x
Back	Med	321	126	114	424	240	x	x	x
Side	Med	685	323	149	417	470	x	x	x
Front	Med	431	439	186	619	228	x	x	x
Front	High	568	592	415	1042	345	x	x	x
Side	High	1195	1042	507	1111	631	x	x	x
Back	High	240	310	210	665	310	x	x	x
Side	High	523	400	244	424	561	x	x	x
Front	High	949	613	671	386	272	x	x	x

Position	Intensity	Parietal 1	Parietal 2	Parietal 3	Parietal Max Prin.
Front	Low	104	x	98	
Side	Low	115	68	83	144
Back	Low	109	153	86	152
Front	Low	79	134	99	129
Front	Med	143	123	168	135
Side	Med	112	153	88	151
Back	Med	139	102	90	141
Side	Med	117	197	82	196
Front	Med	128	90	106	156
Front	High	162	x	134	x
Side	High	80	x	68	x
Back	High	187	171	114	192
Side	High	145	x	112	x
Front	High	157	x	132	x

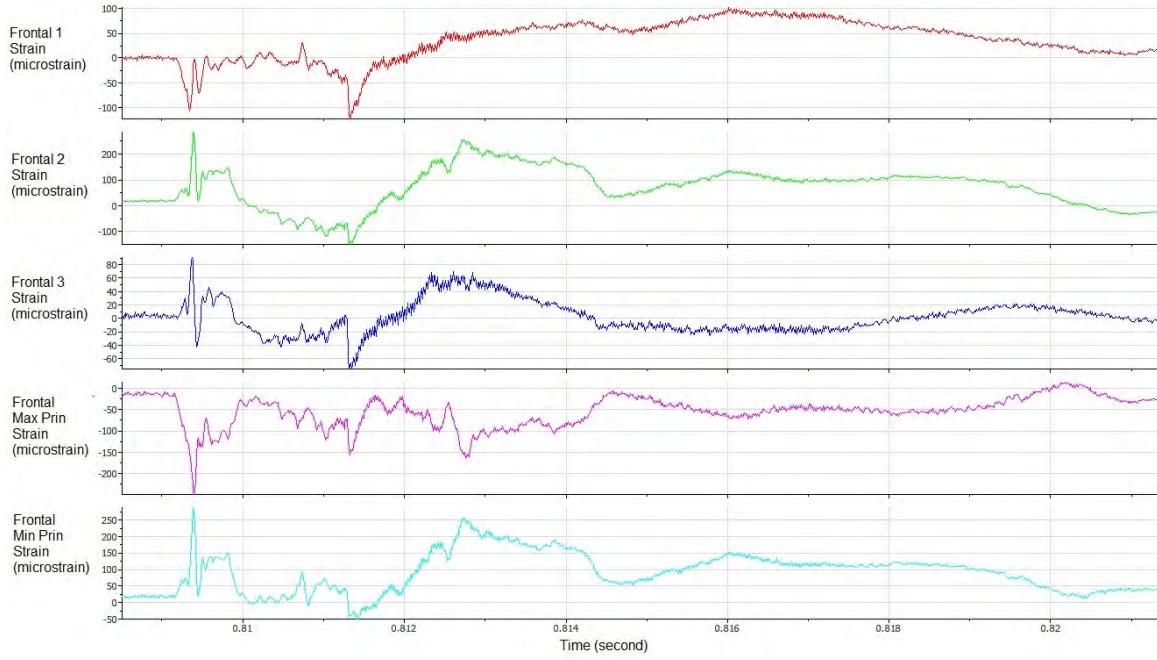
Strain response for Cadaver 3



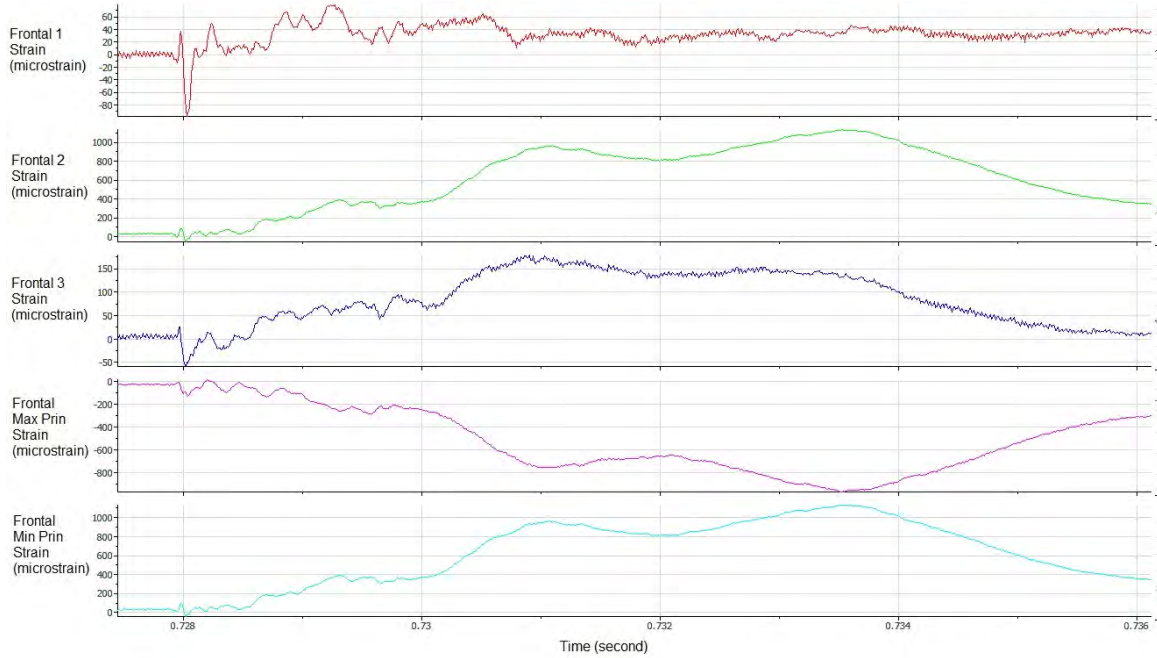
C2F-F



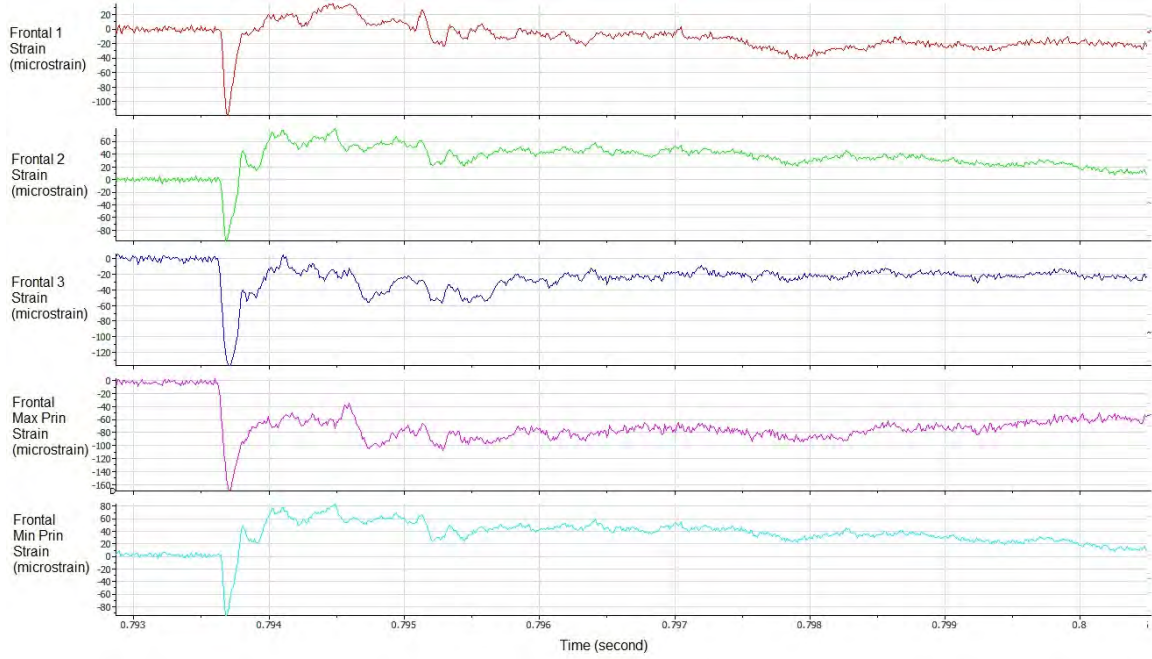
C2L-F



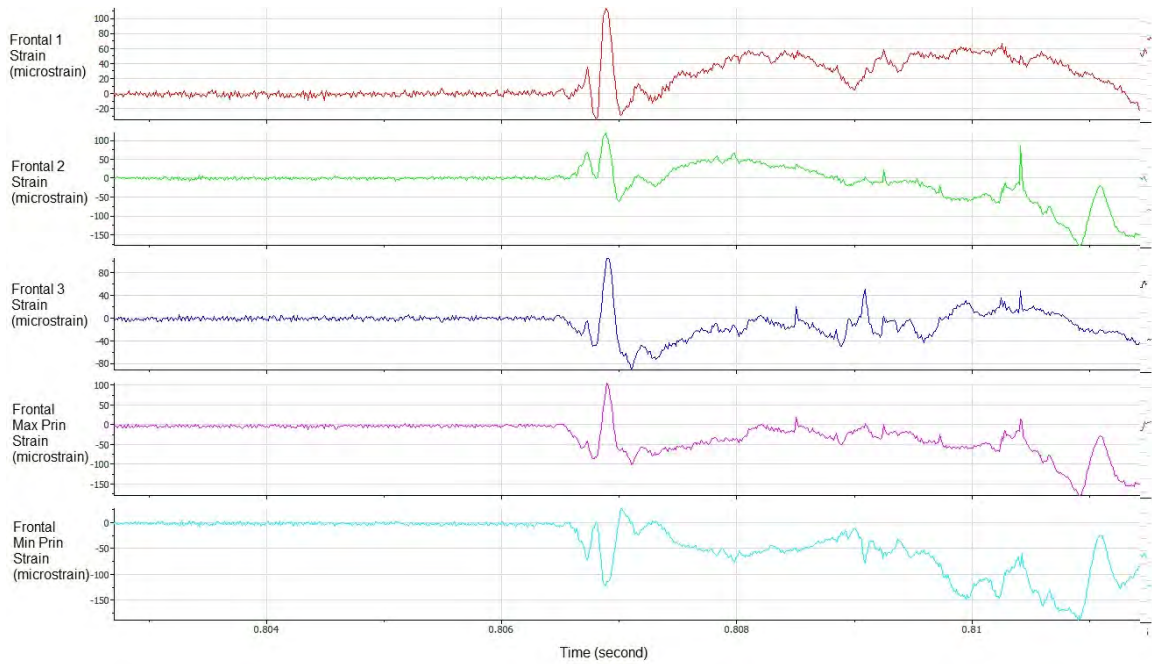
C2B-F



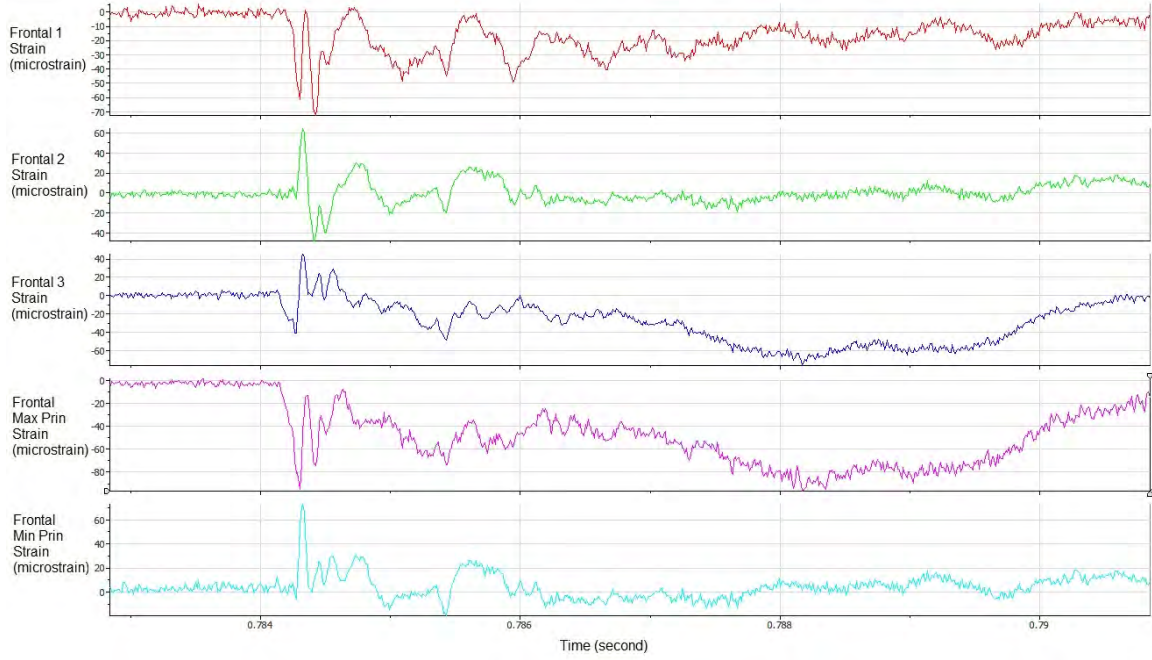
C2R-F



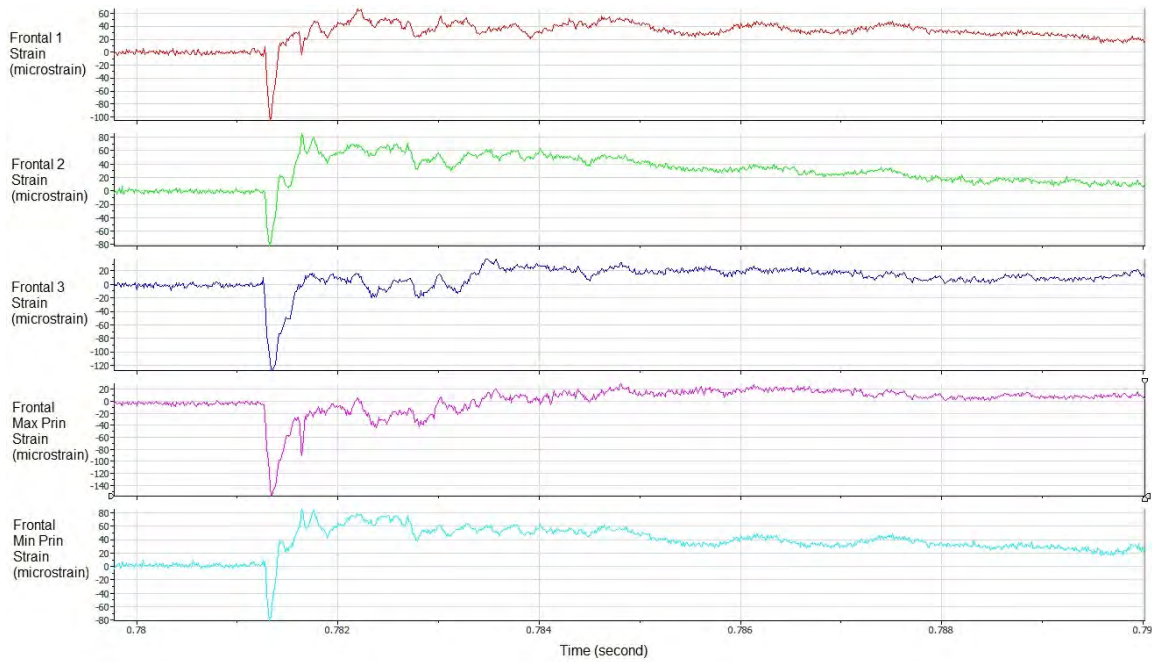
C3F-F



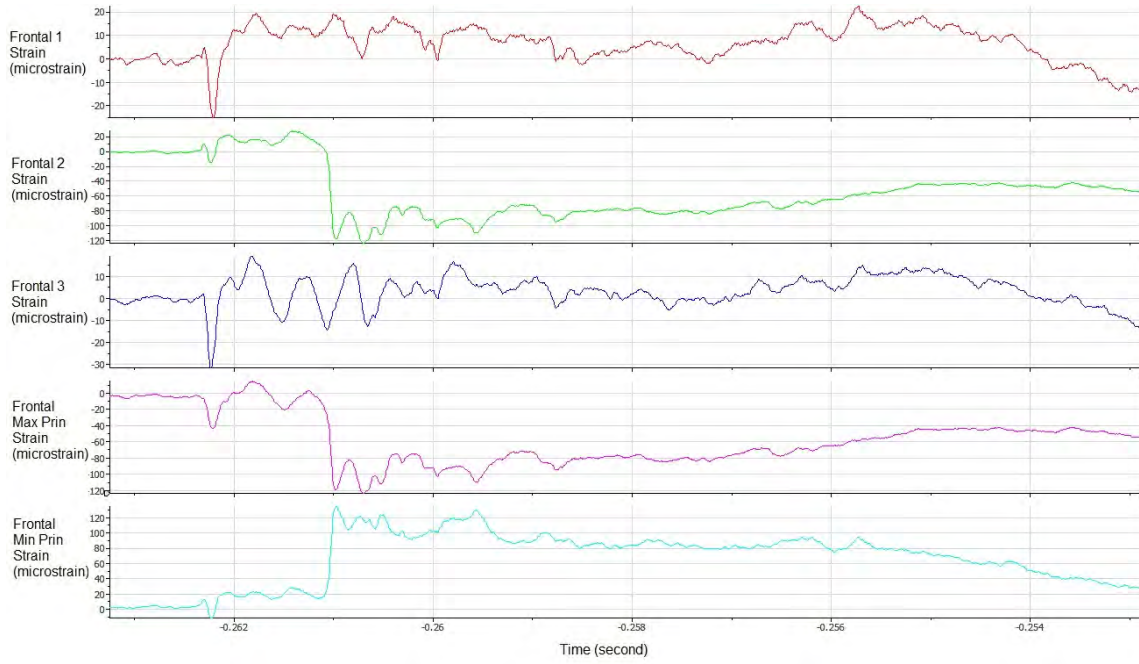
C3L



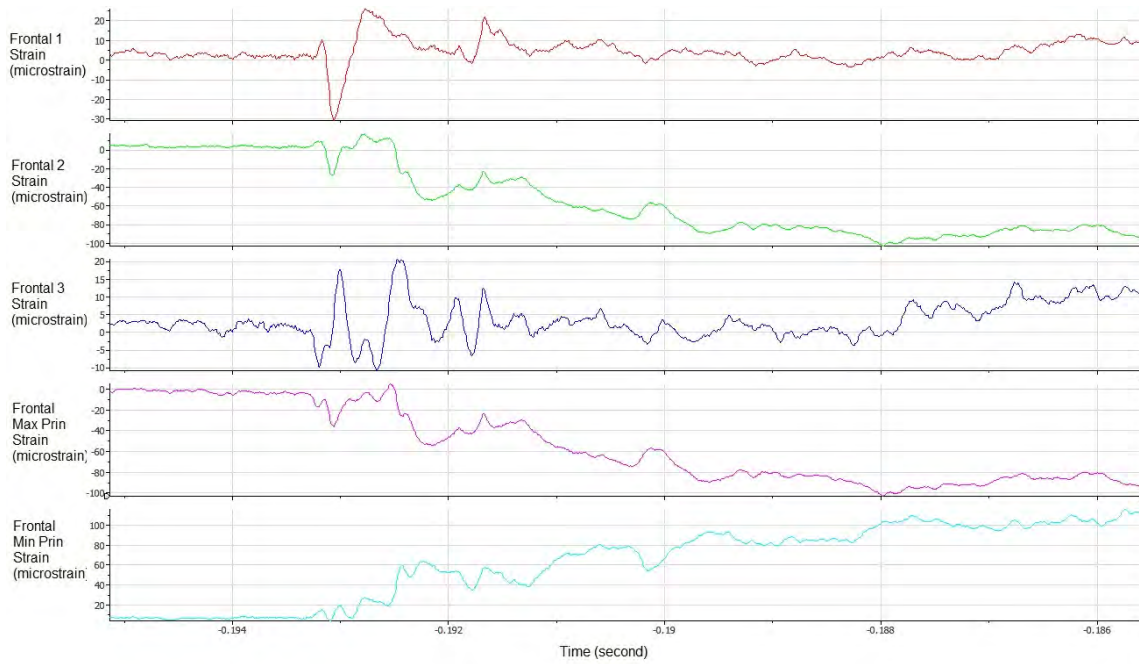
C3B-F



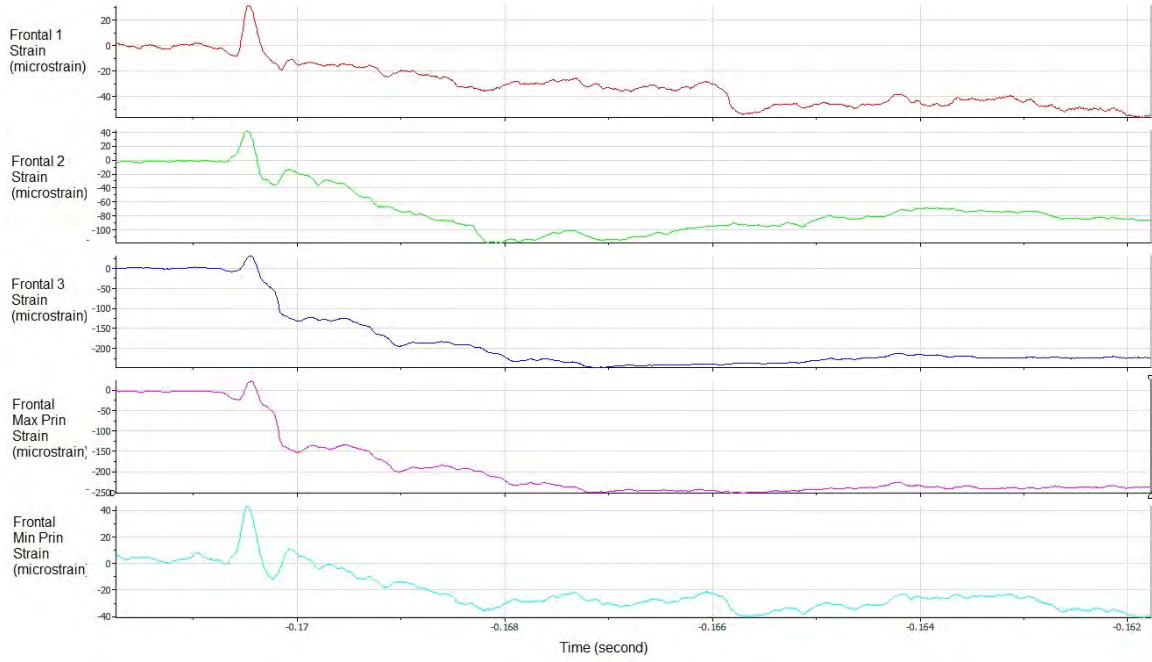
C3R-F



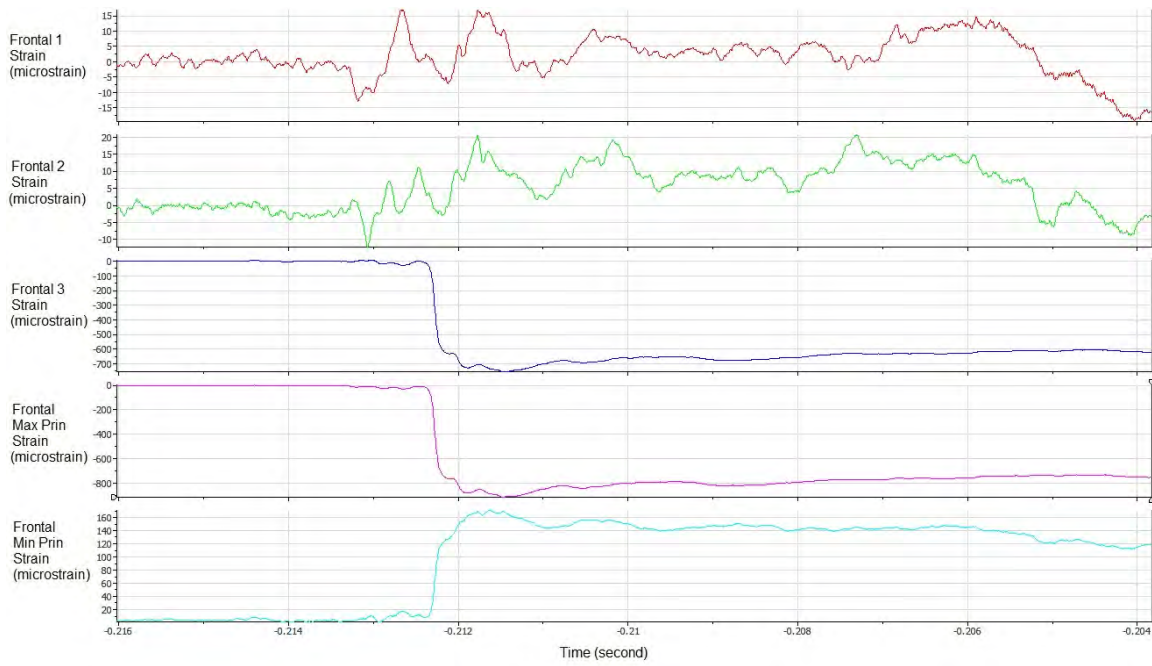
C4F-F



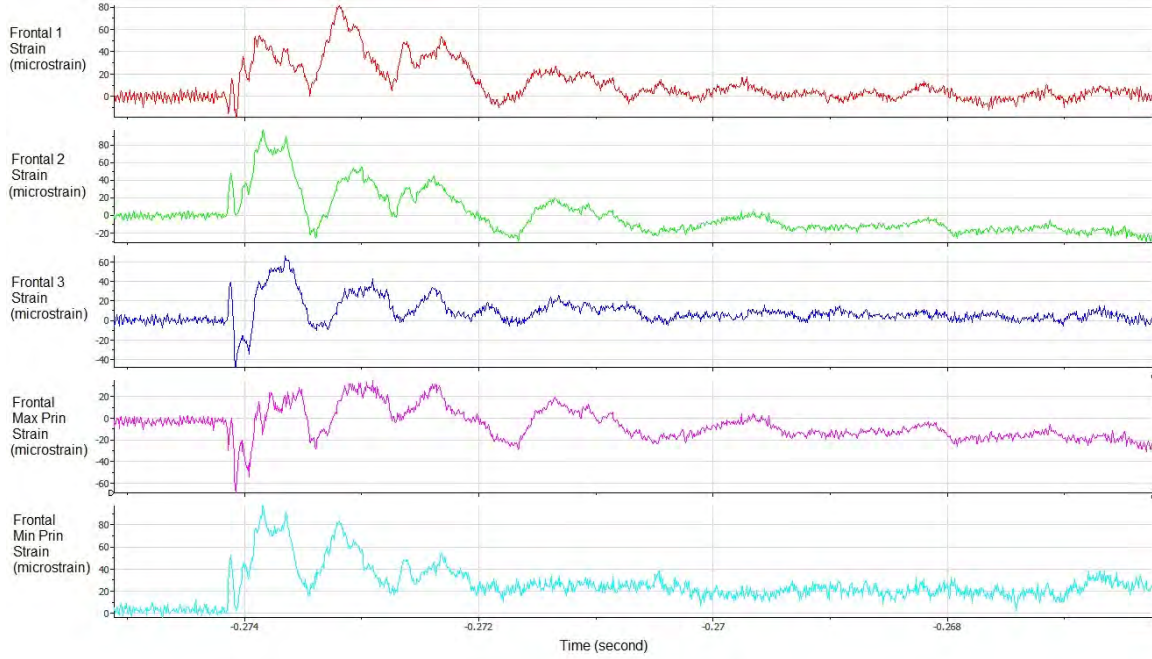
C4L-F



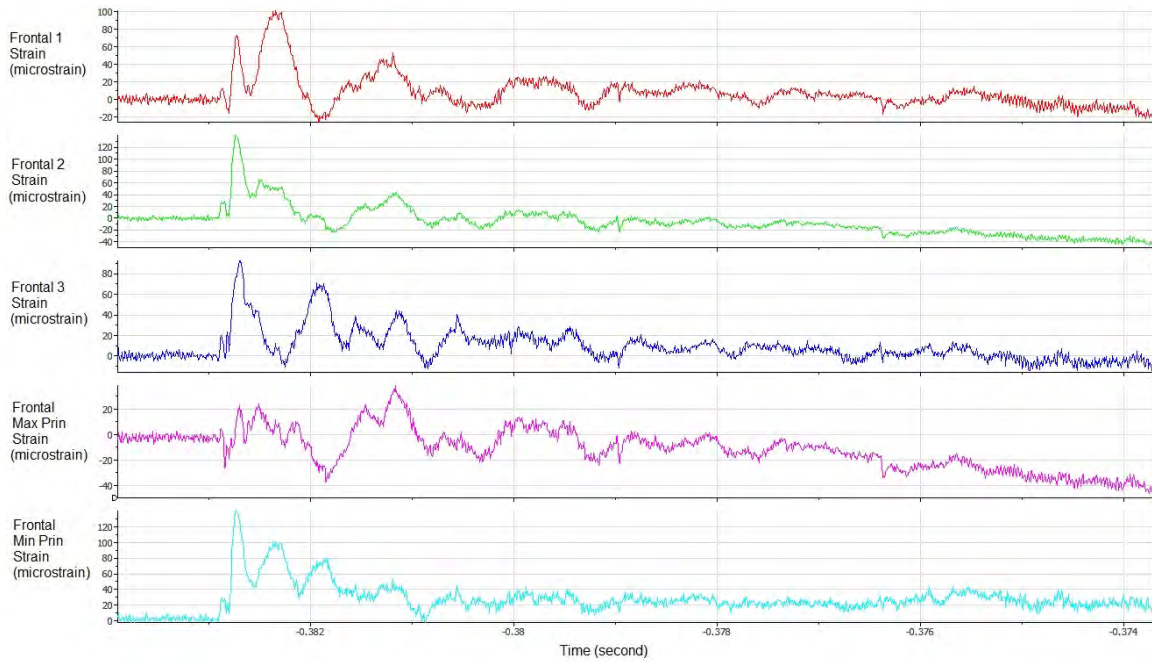
C4B-F



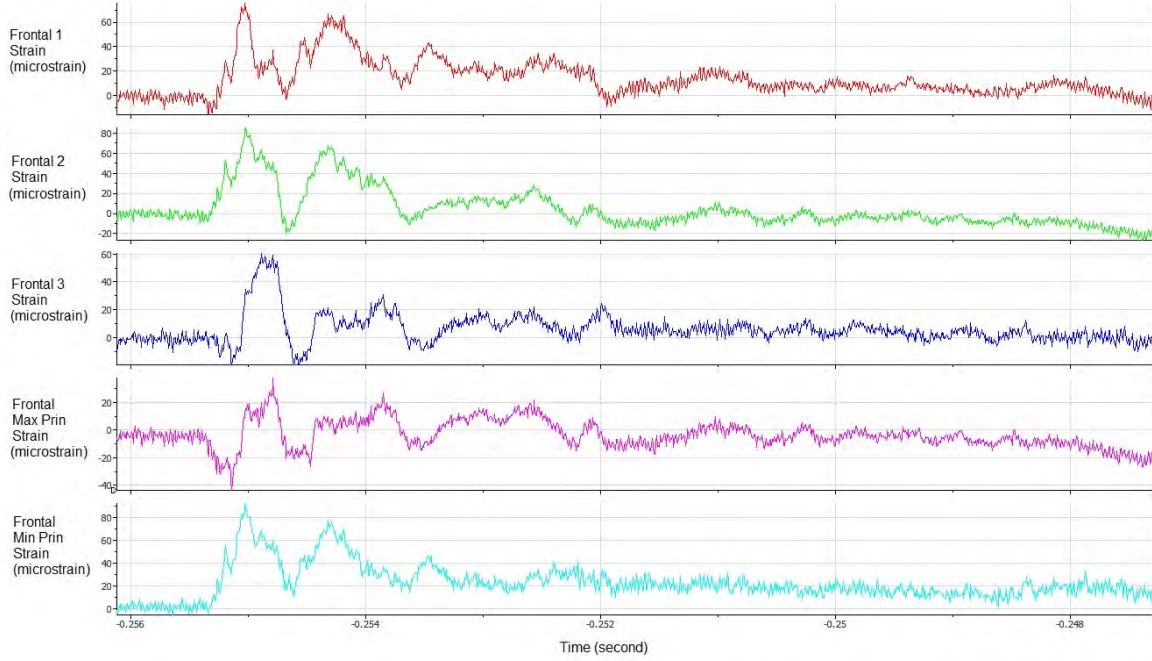
C4R-F



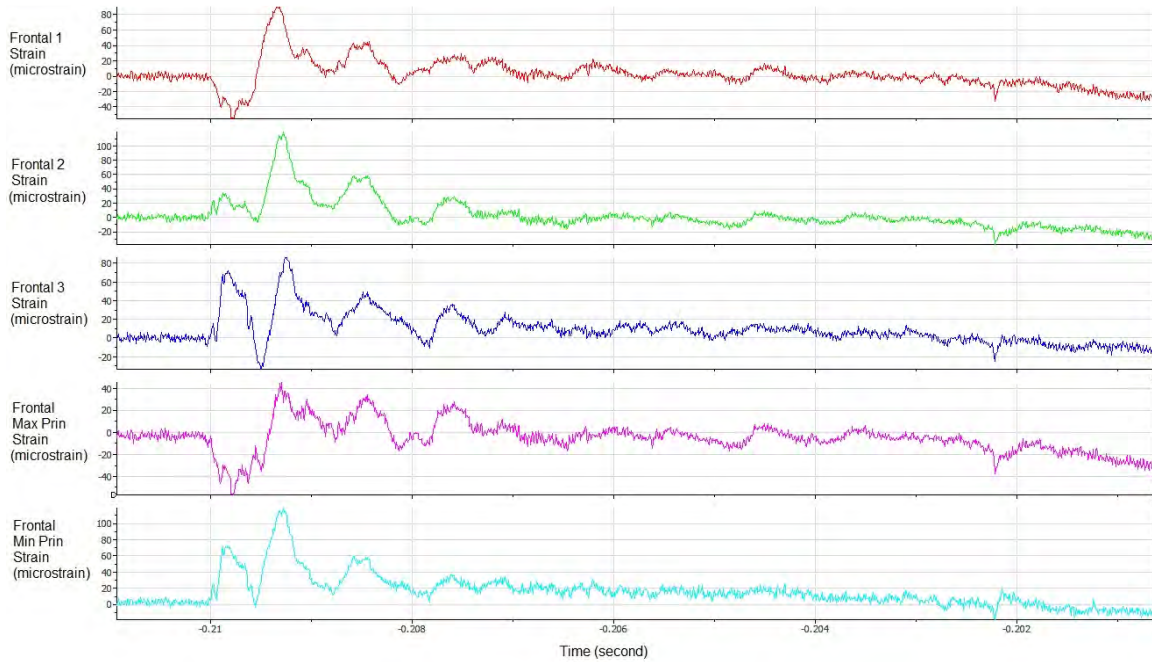
C5F-F



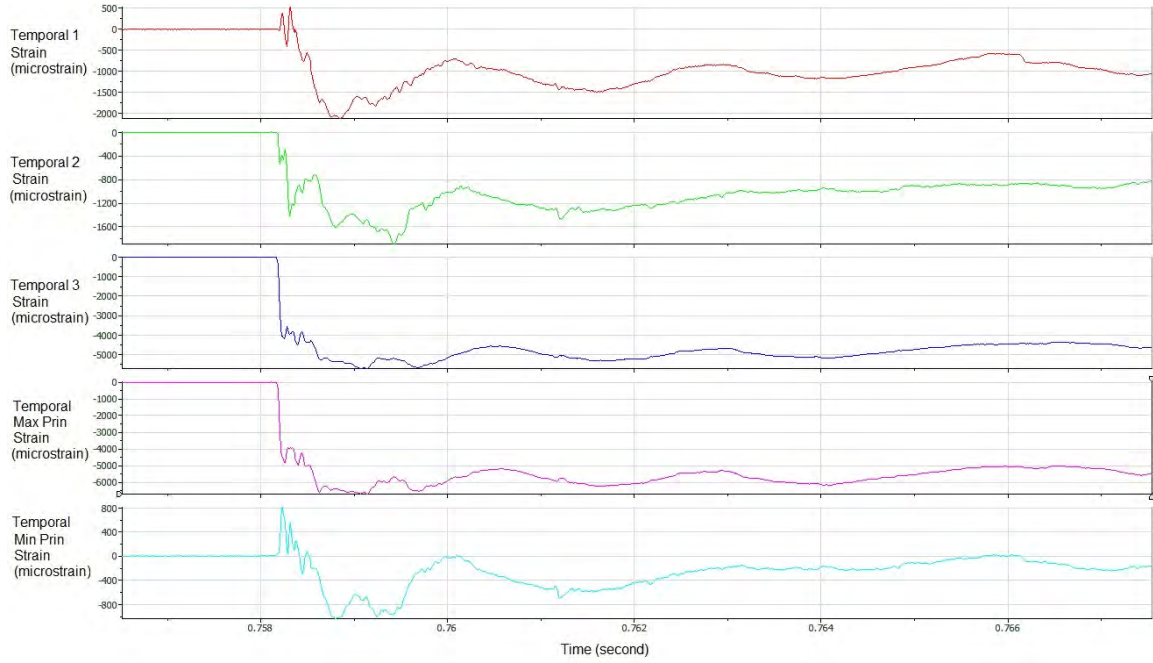
C5L-F



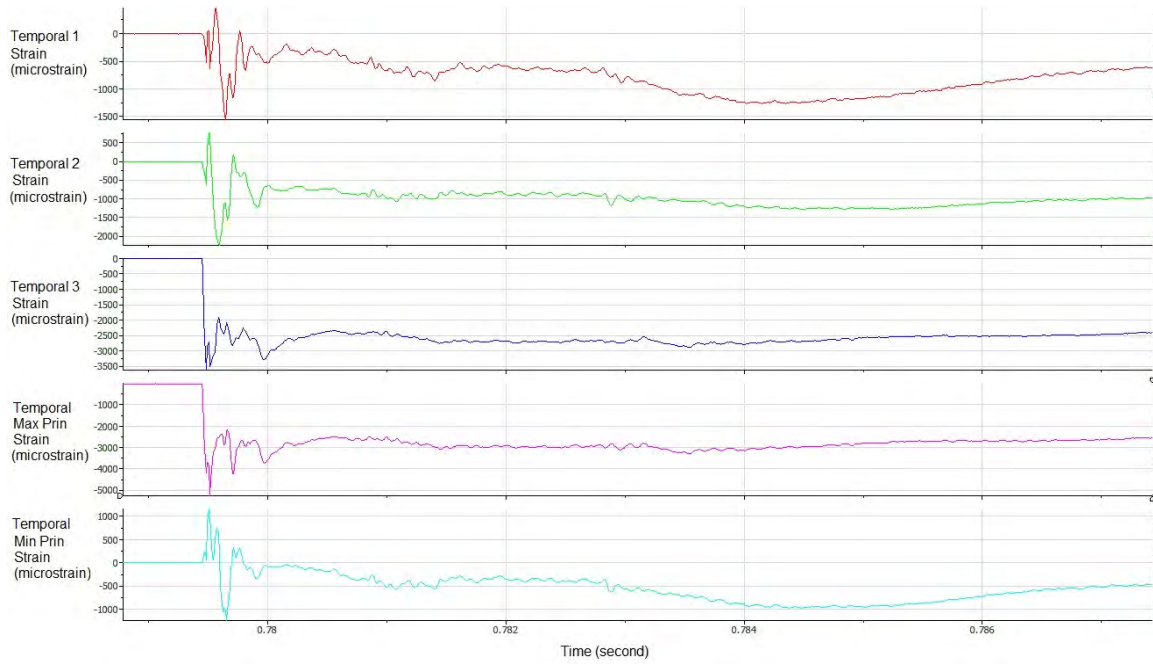
C5B-F



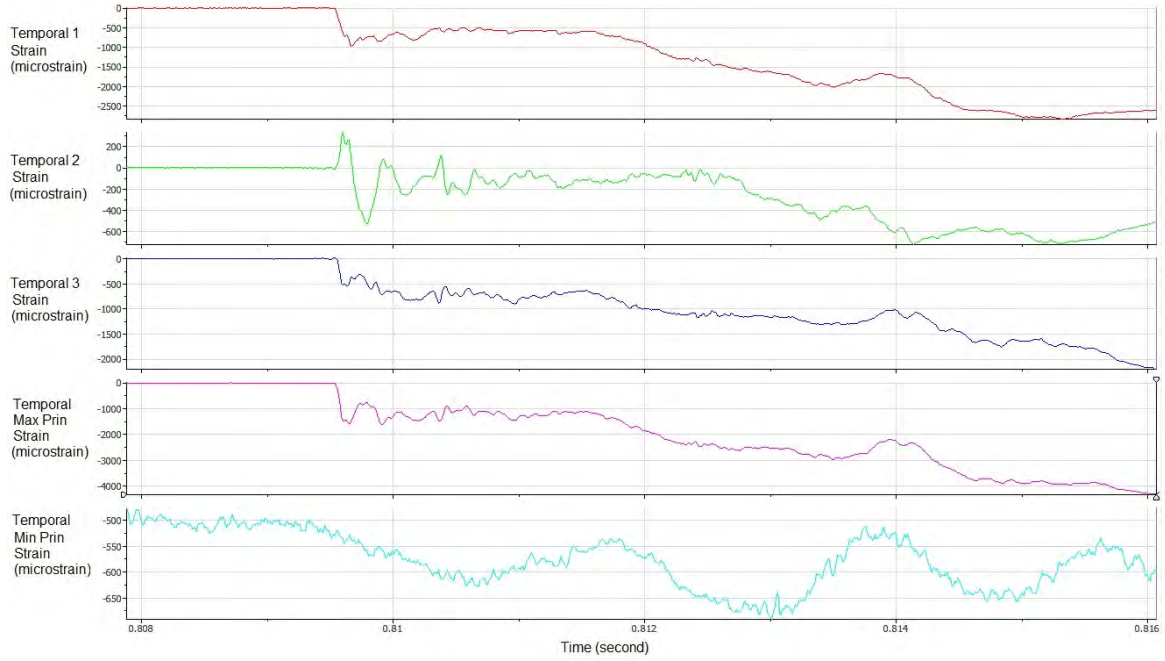
C5R-F



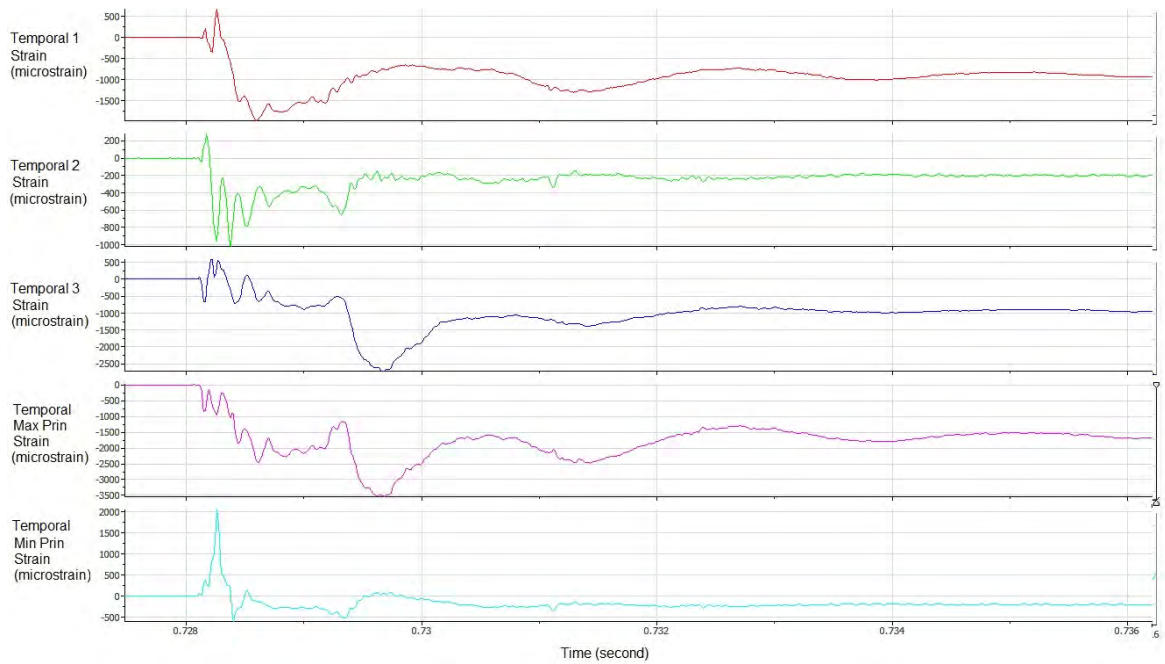
### C2F-T



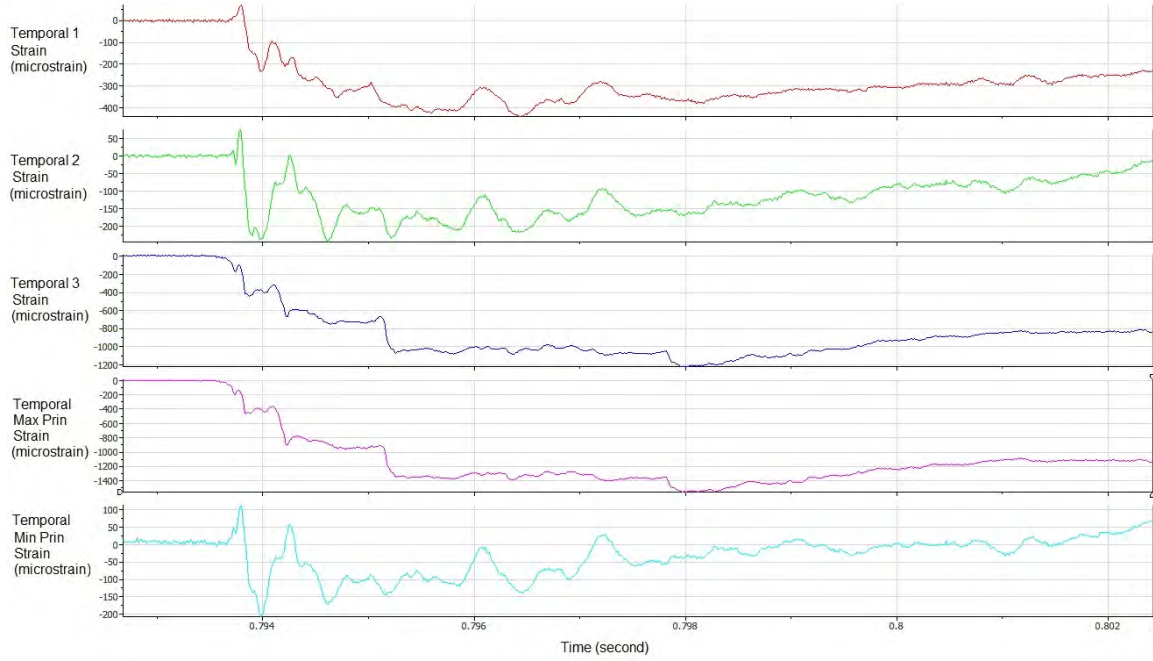
### C2L-T



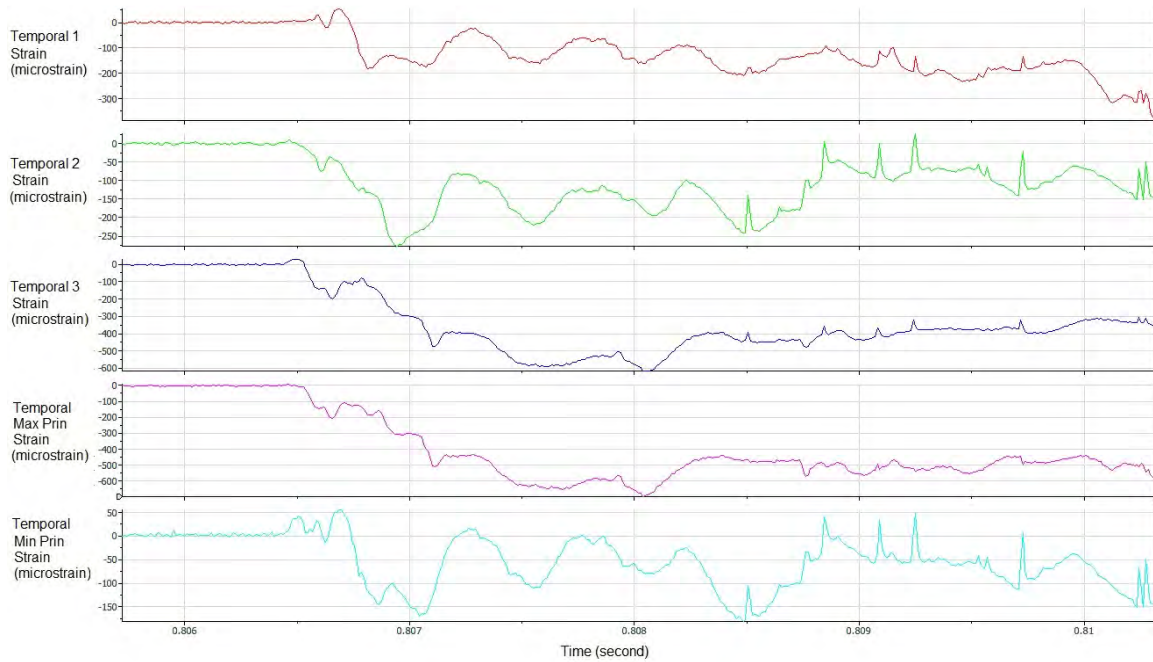
C2B-T



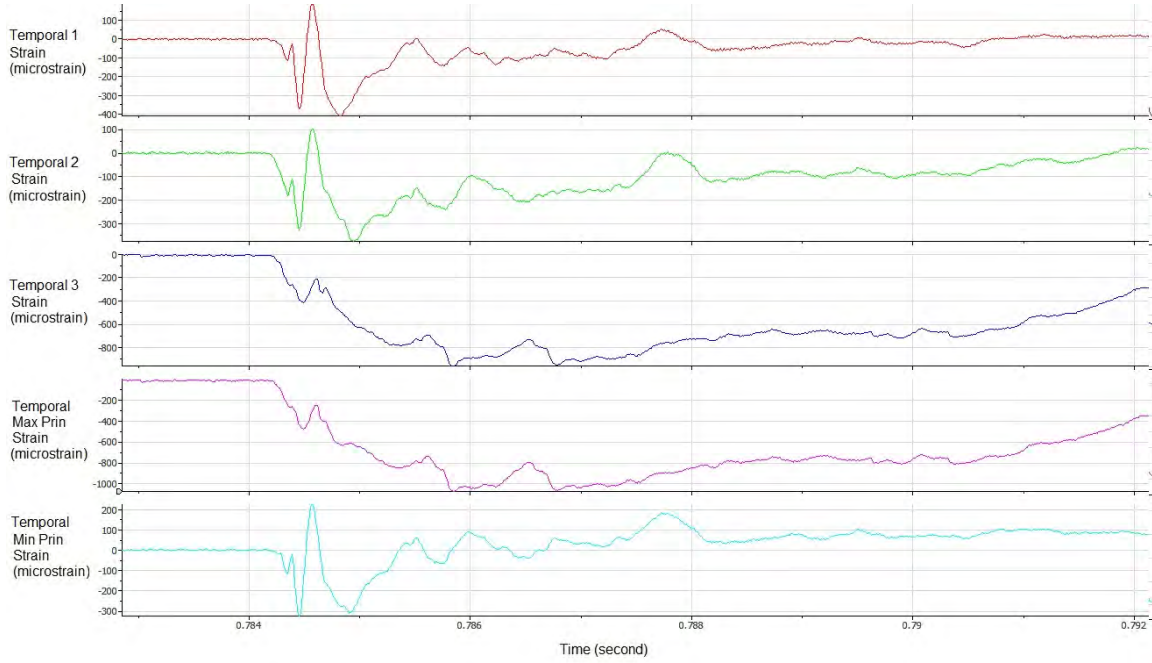
C2R-T



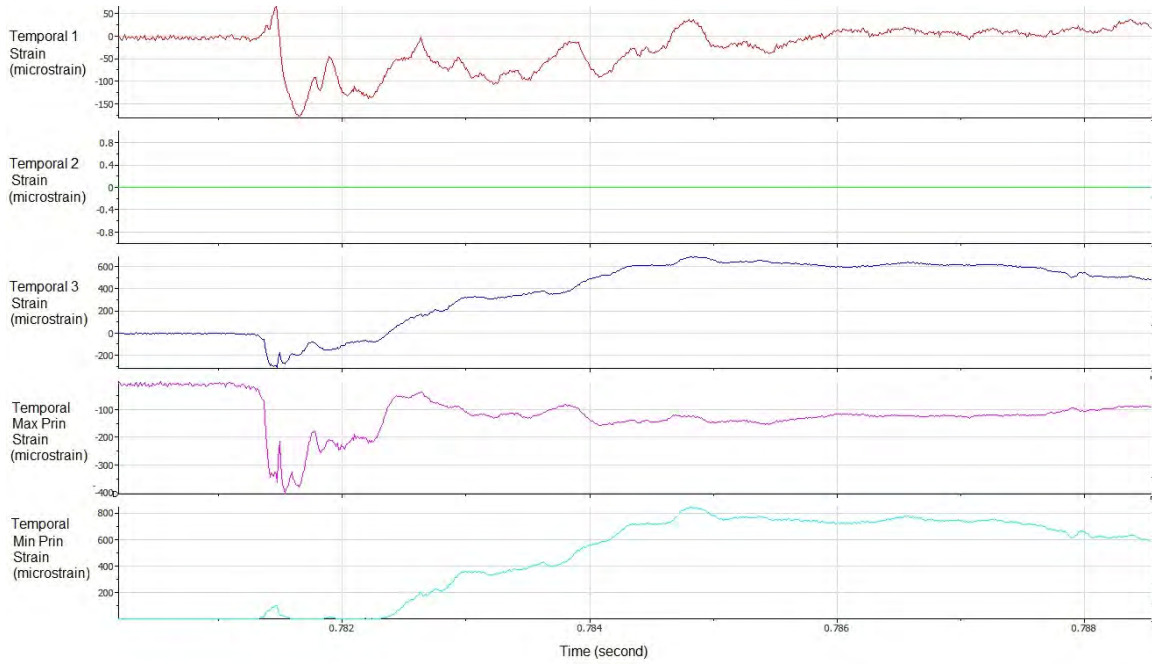
C3F-T



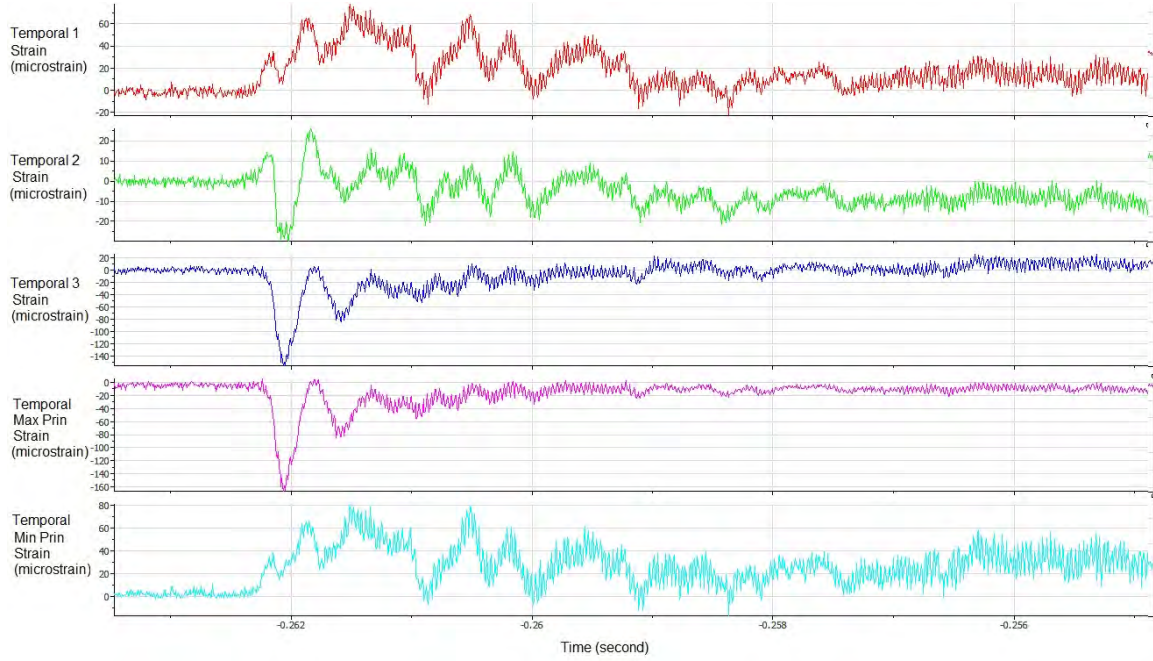
C3L-T



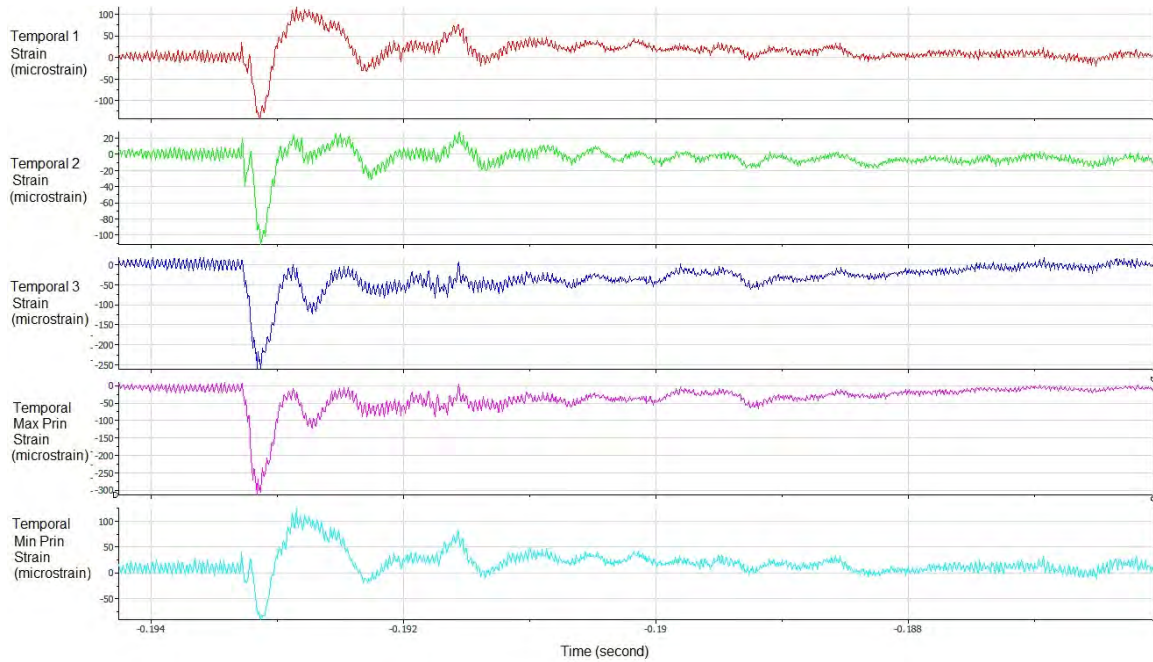
C3B-T



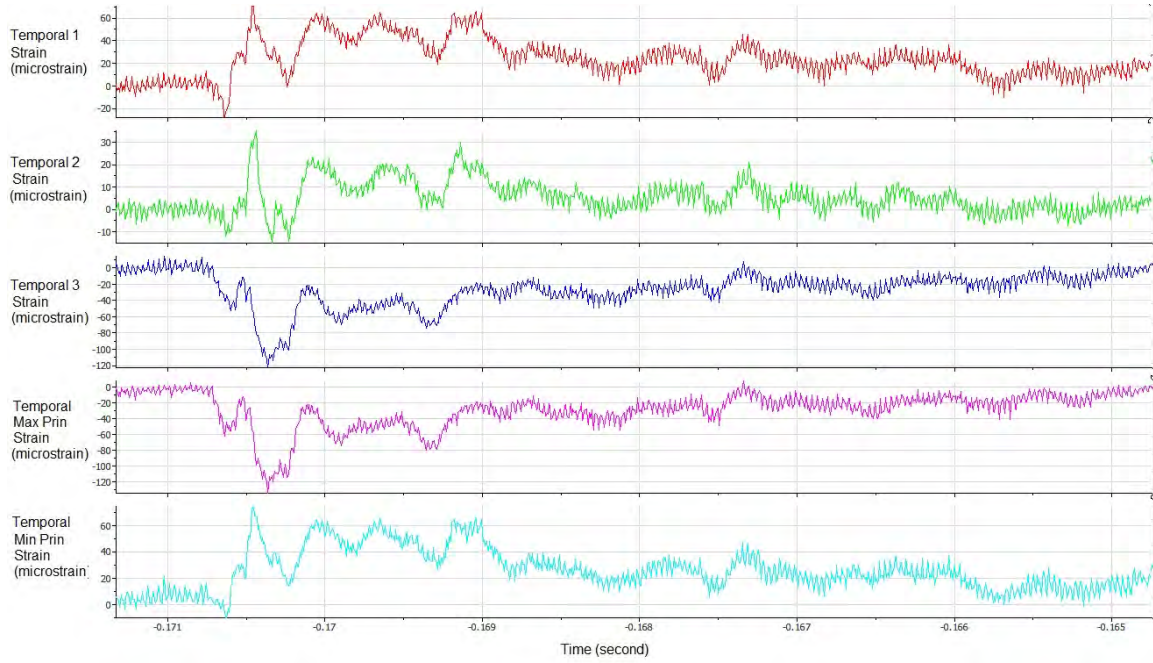
C3R-T



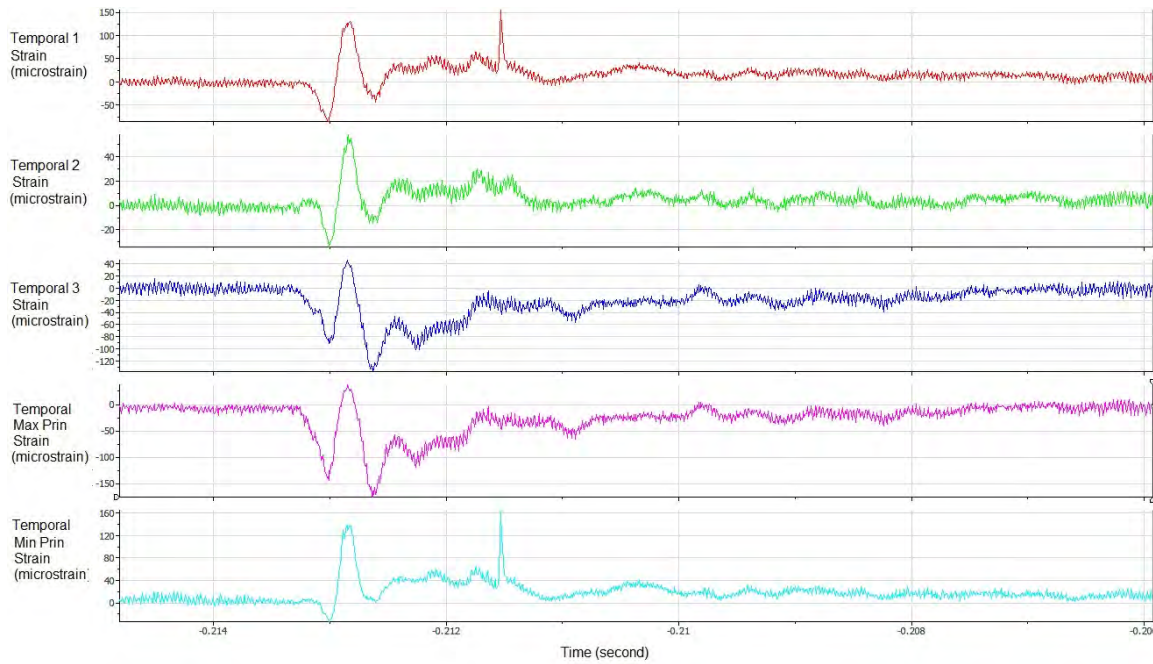
C4F-T



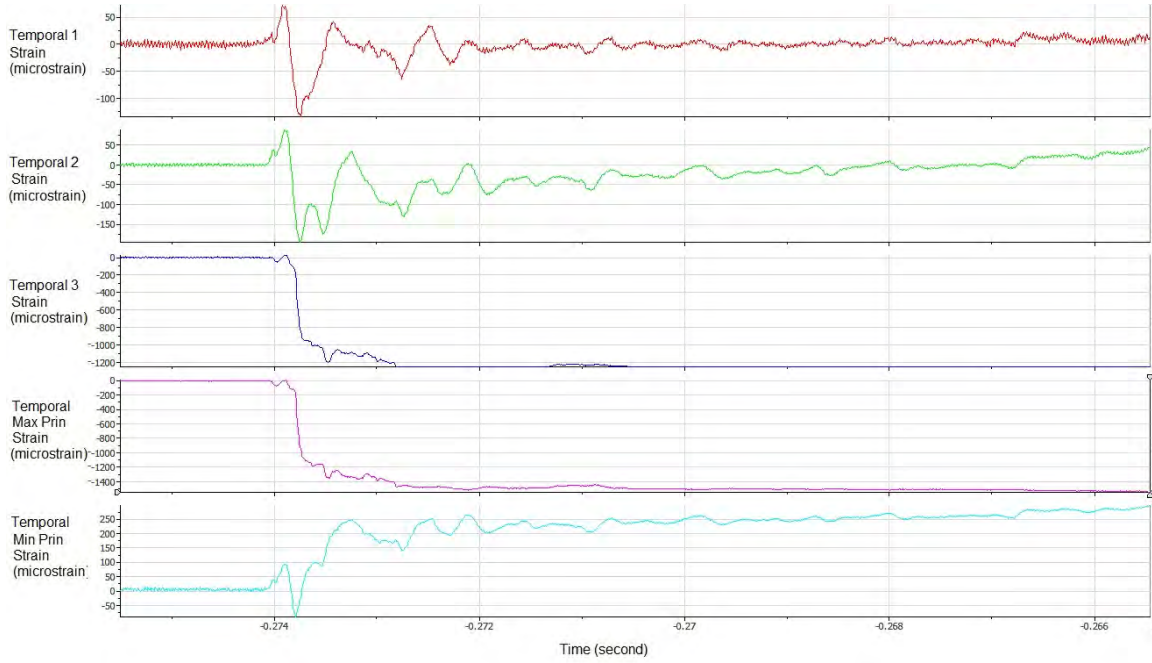
C4L-T



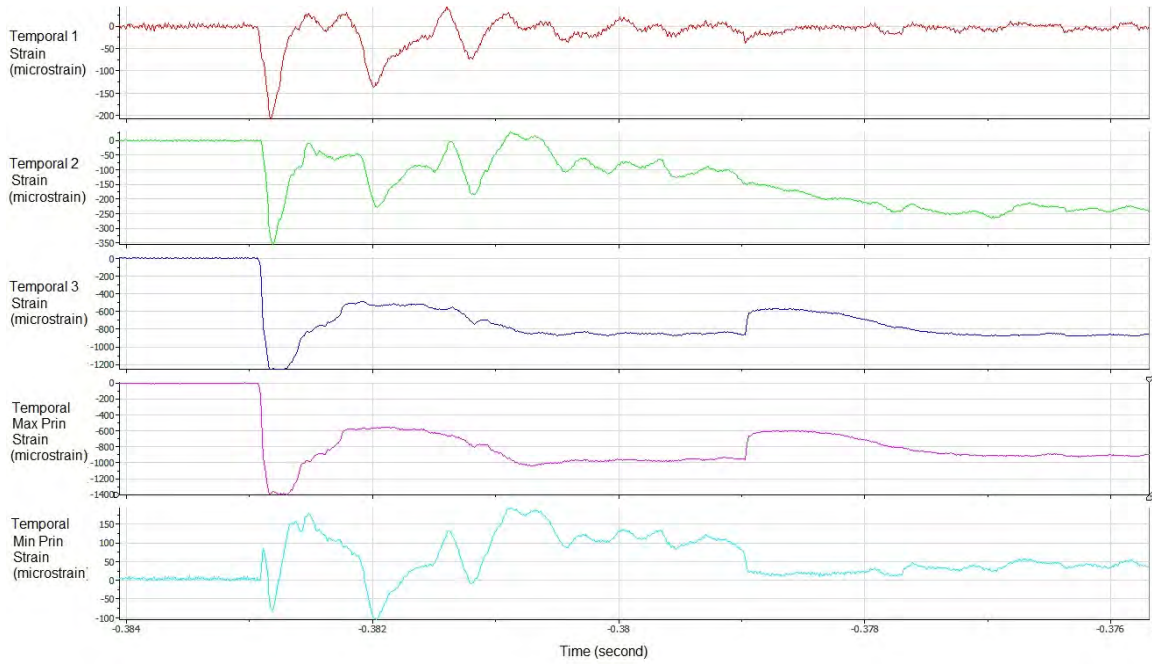
C4B-T



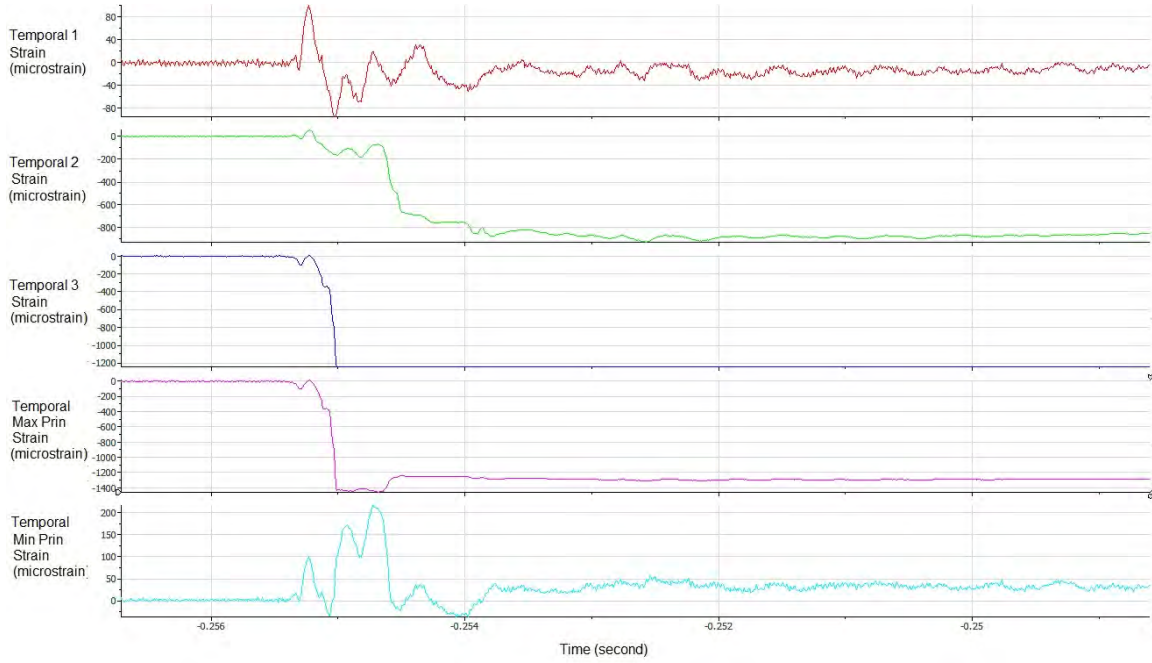
C4R-T



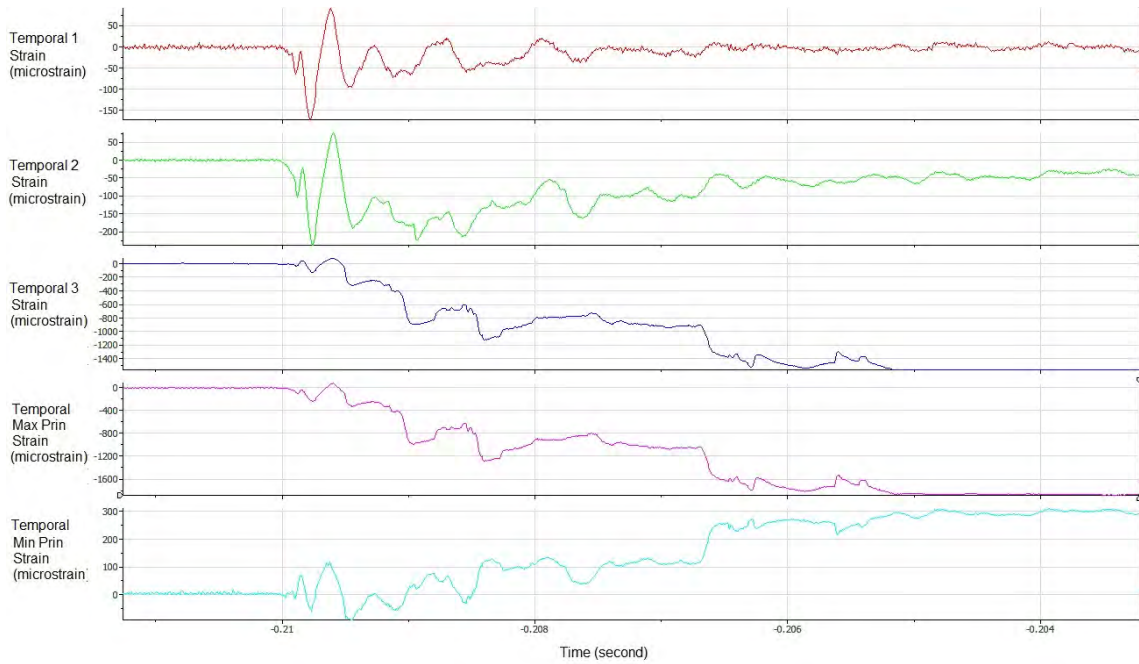
### C5F-T



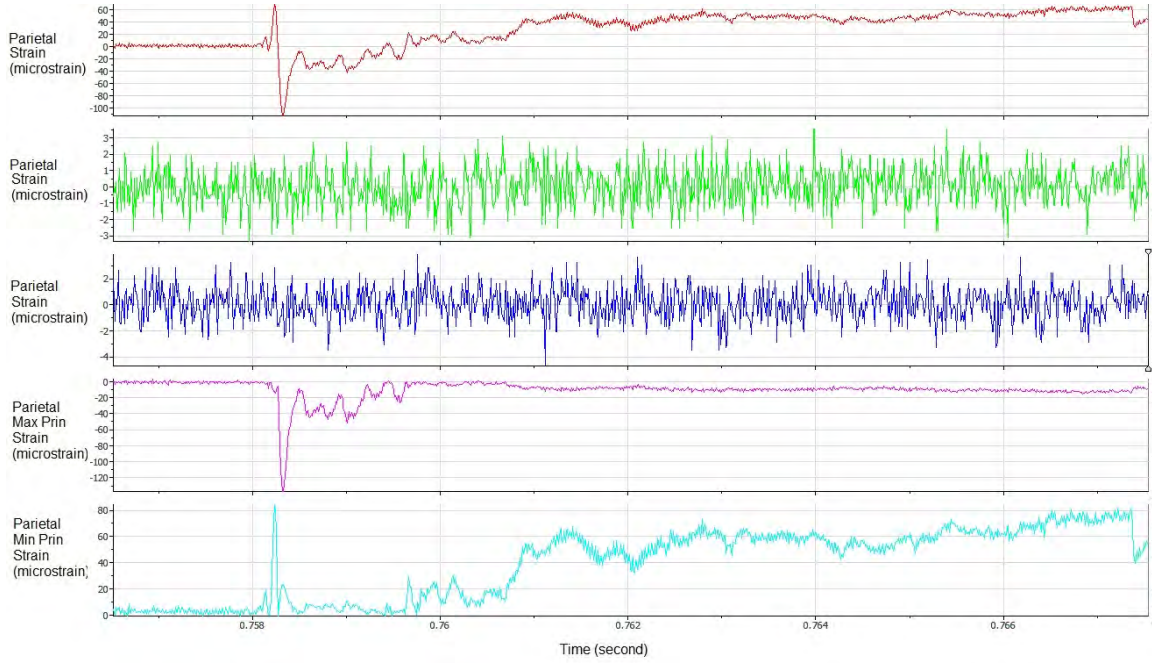
### C5L-T



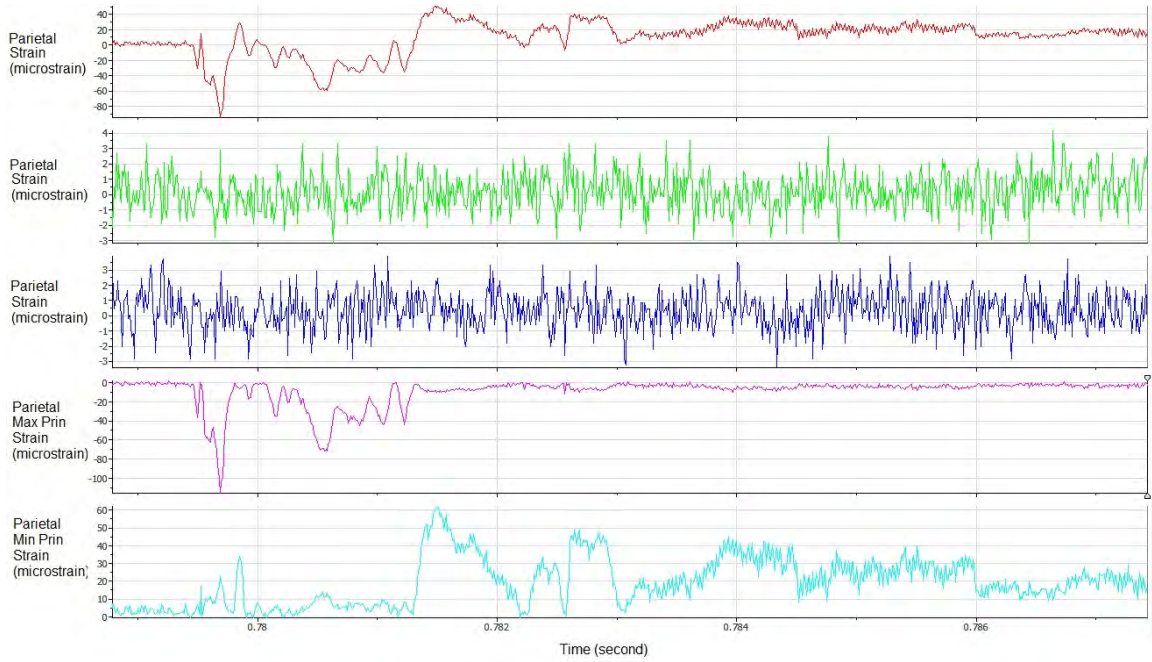
C5B-T



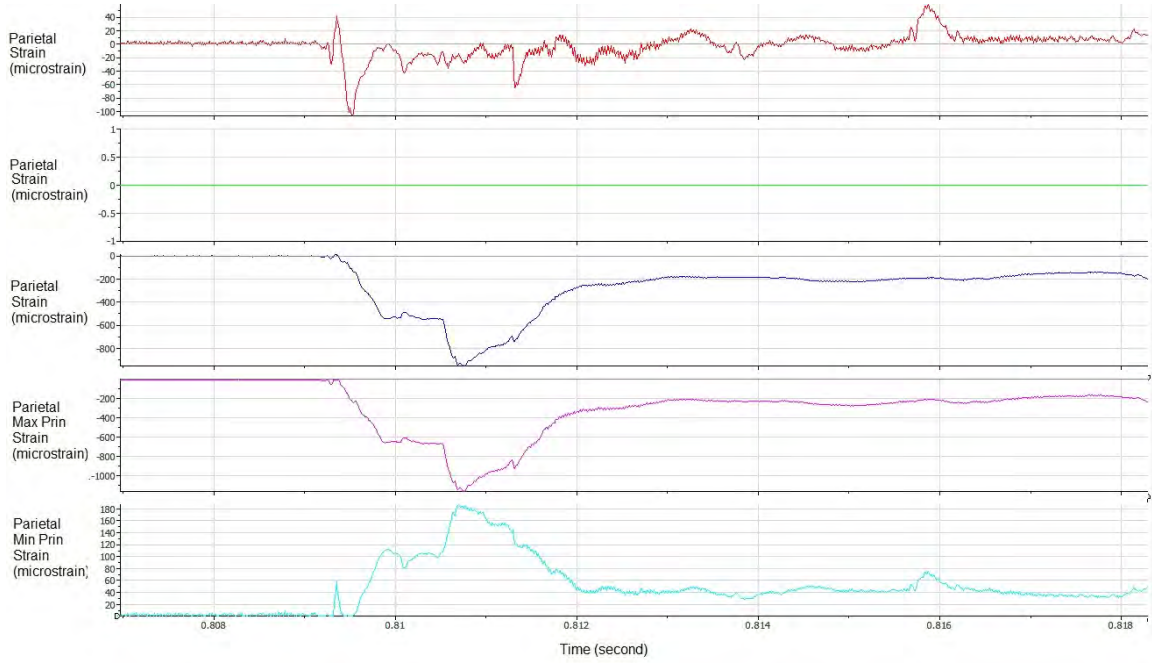
C5R-T



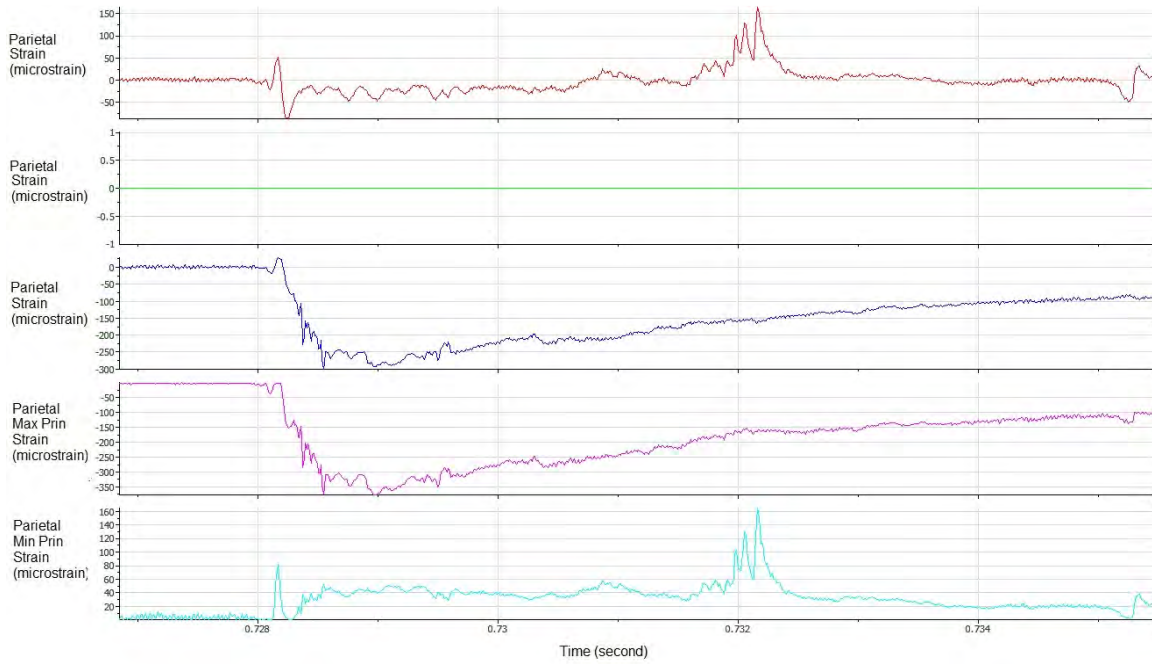
C2F-P



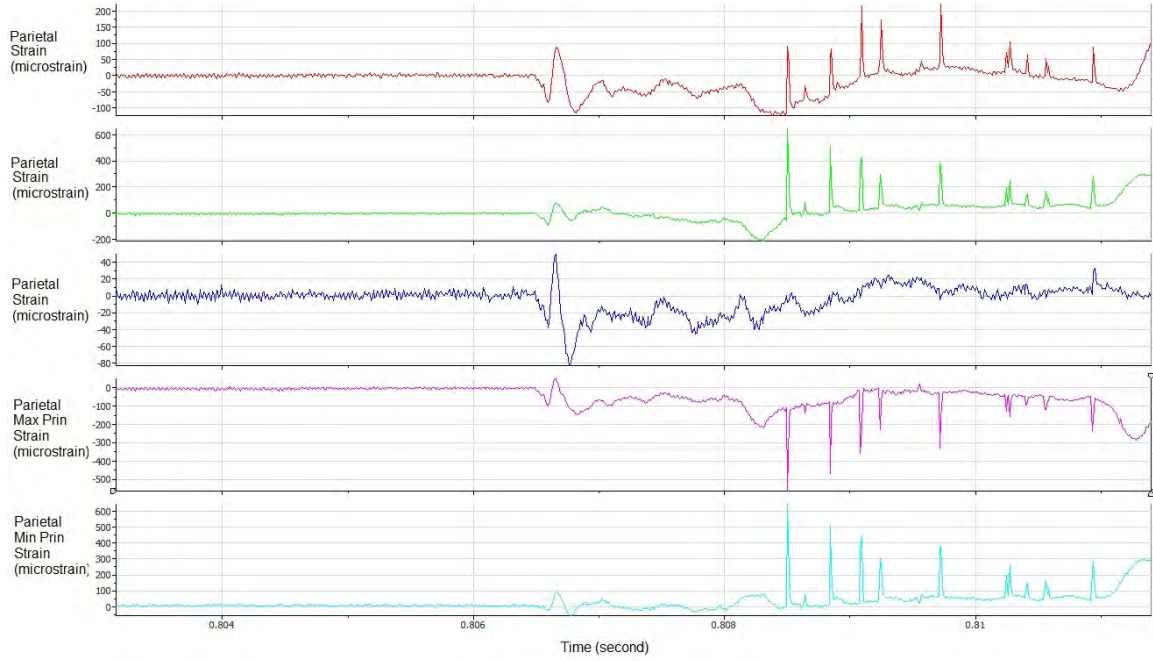
C2L-P



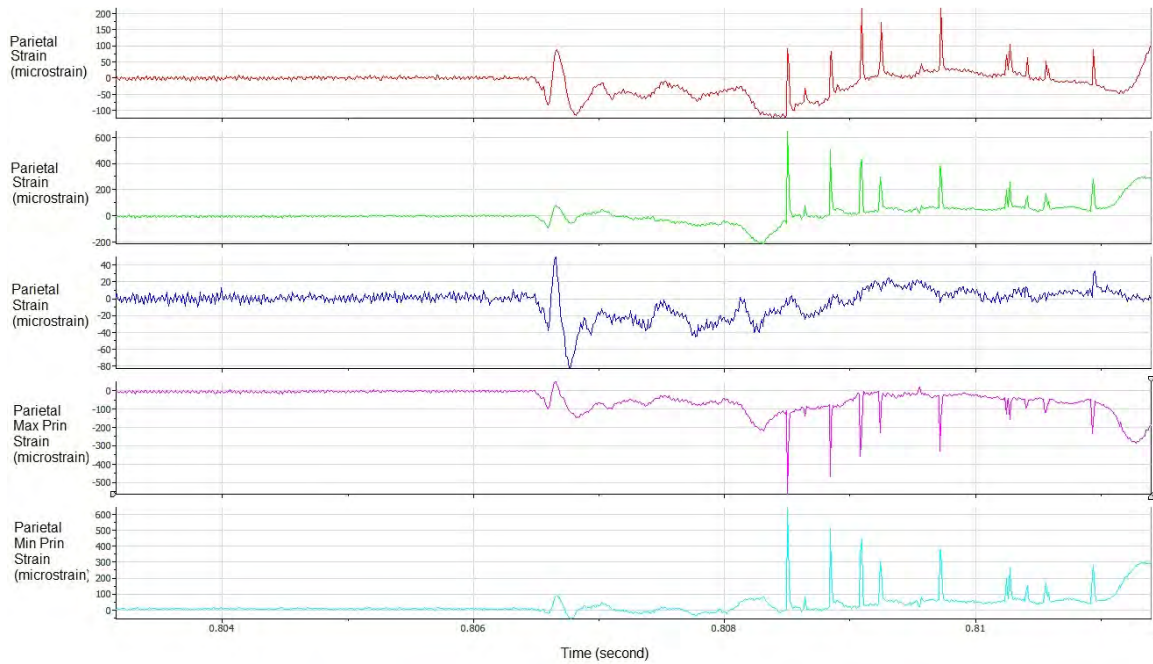
C2B-P



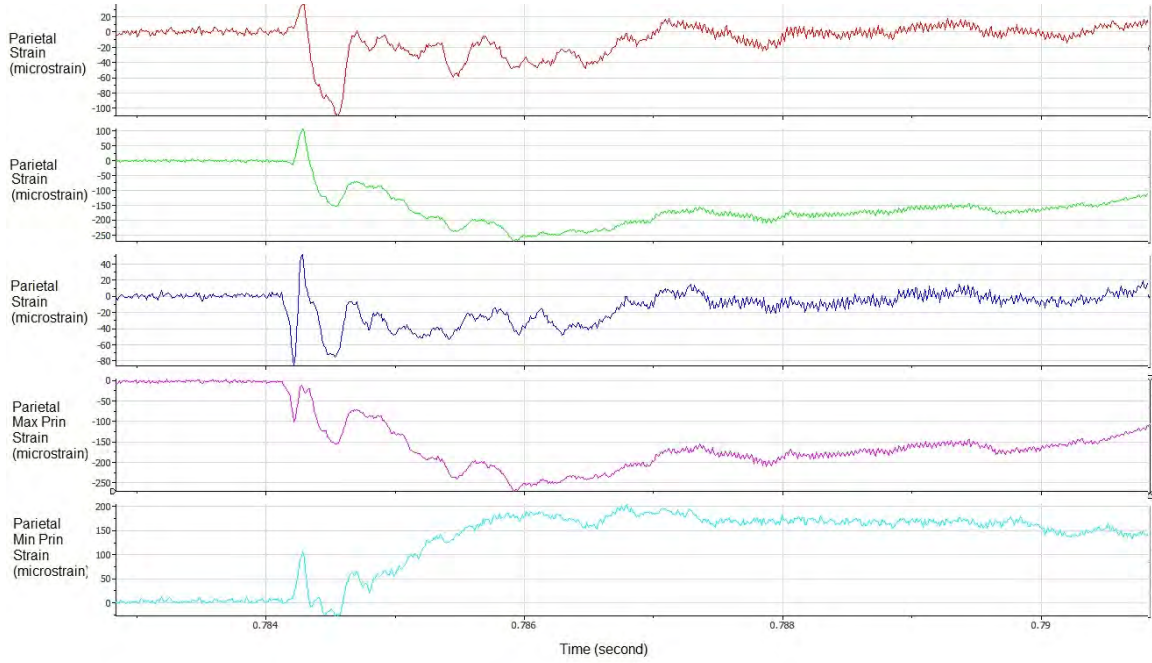
C2R-P



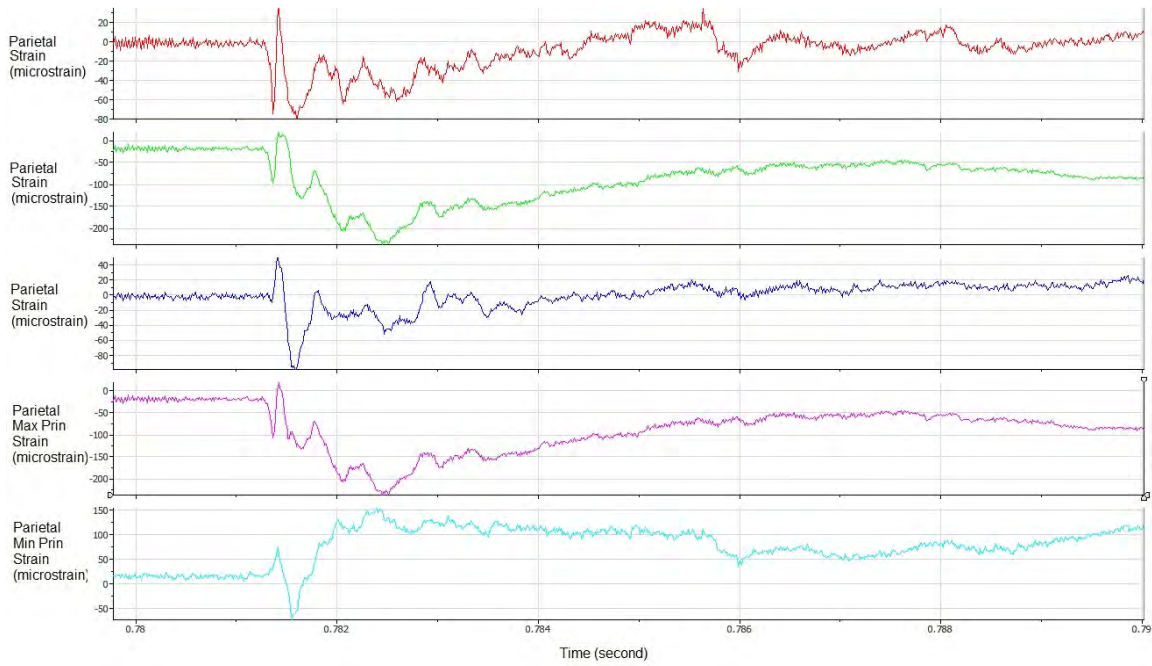
C3F-P



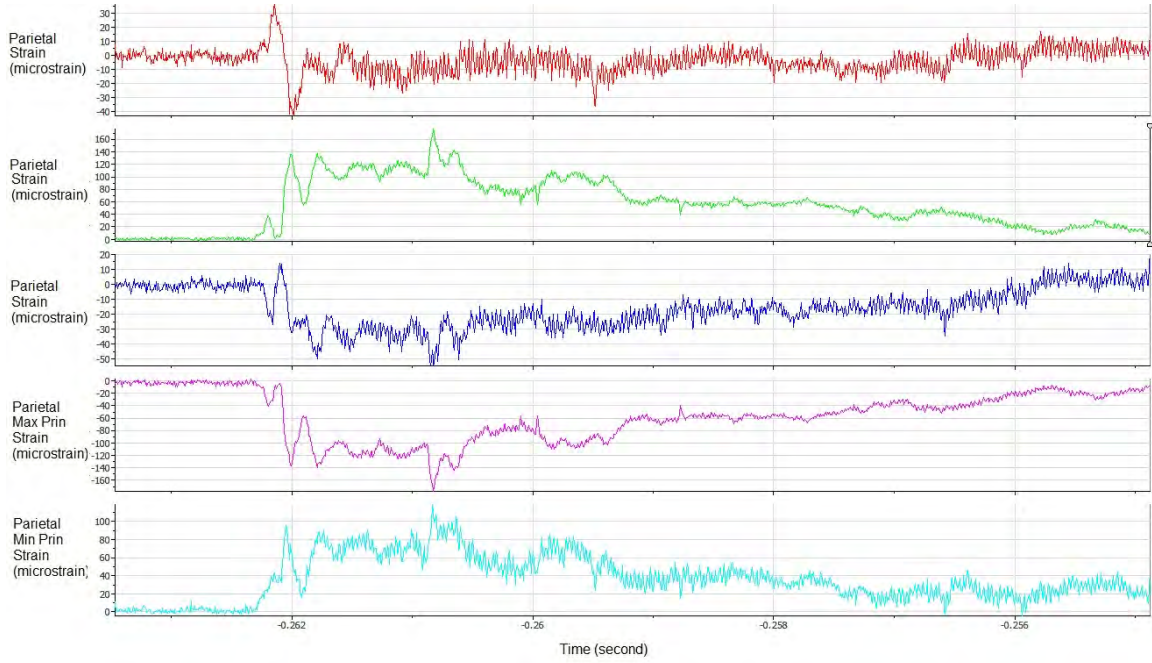
C3L-P



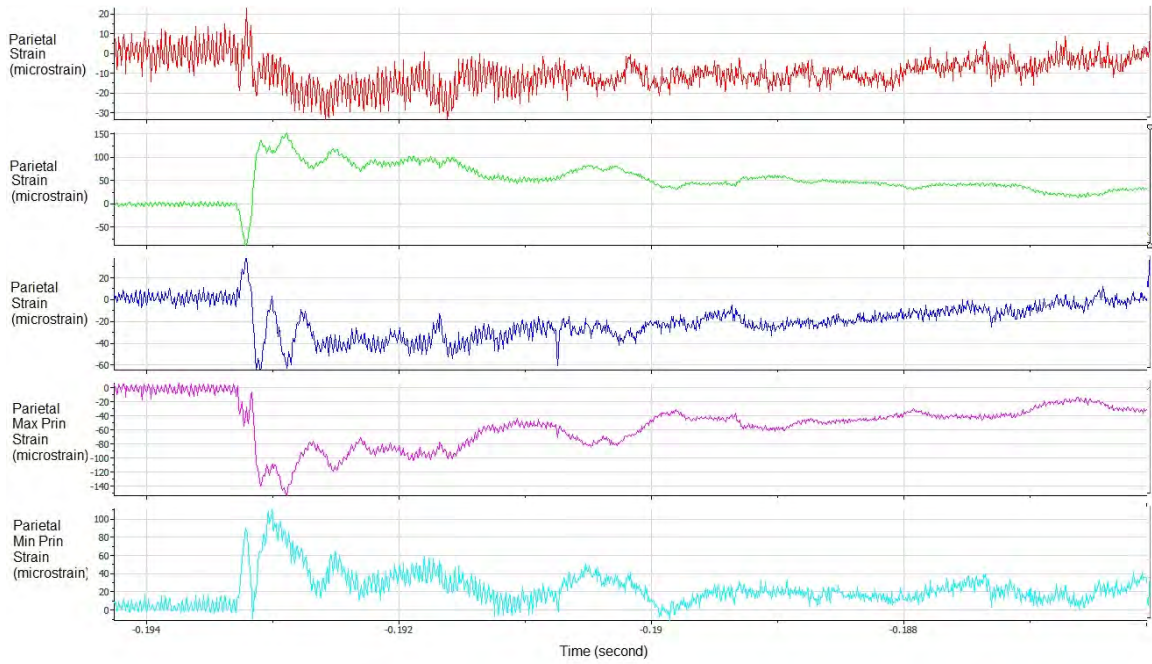
C3B-P



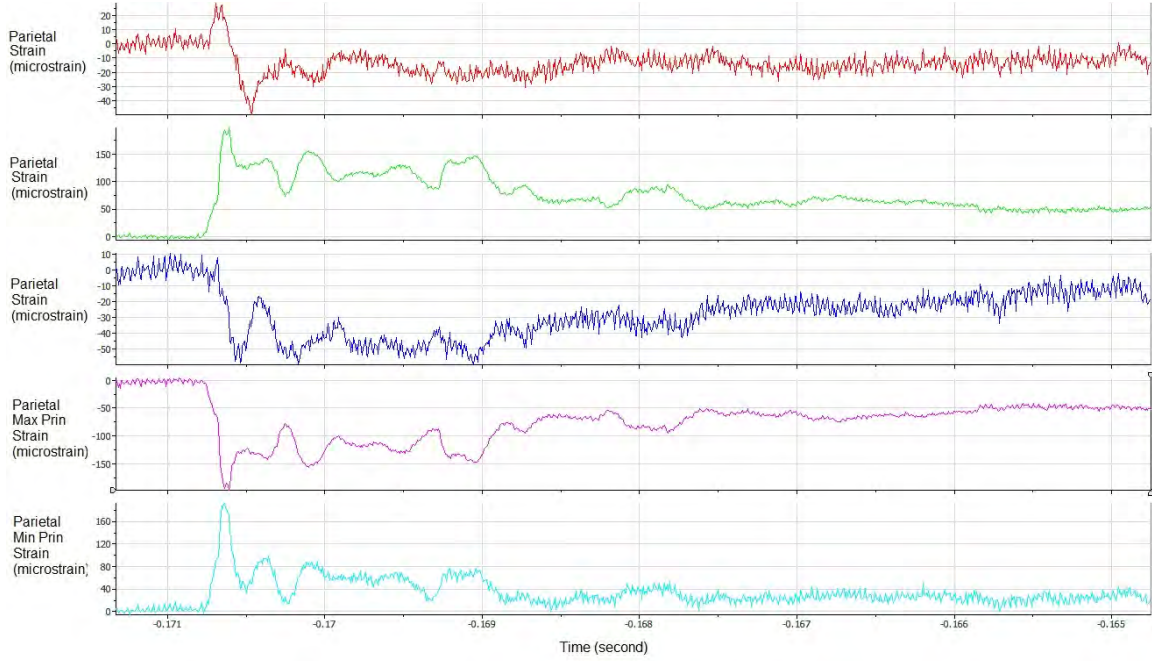
C3R-P



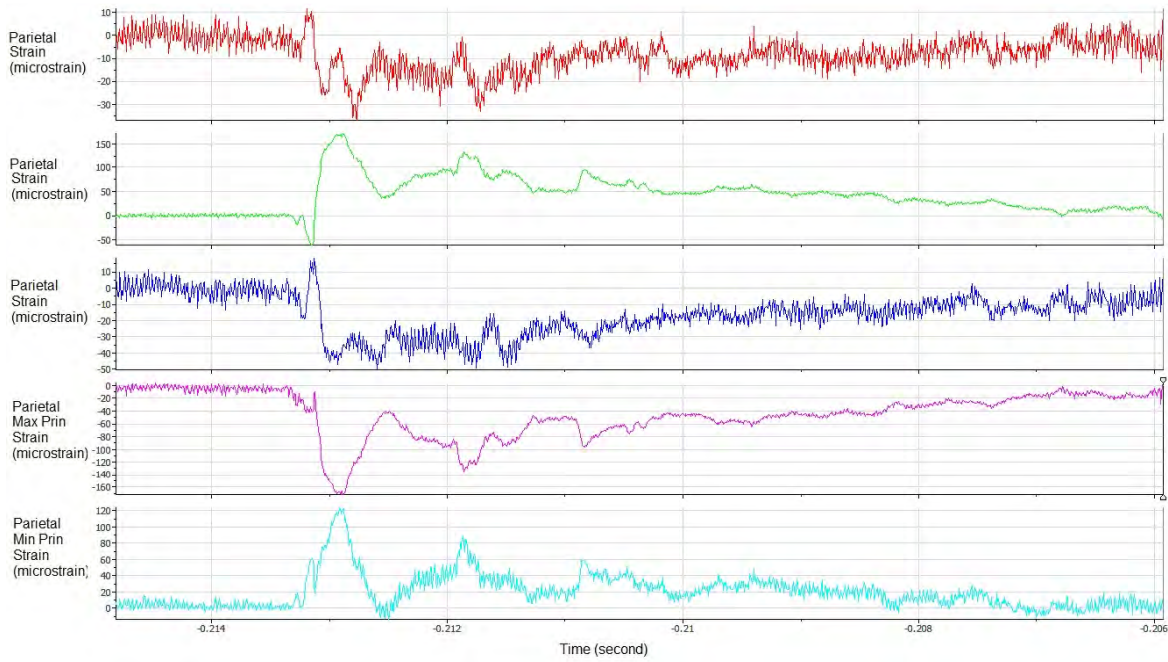
C4F-P



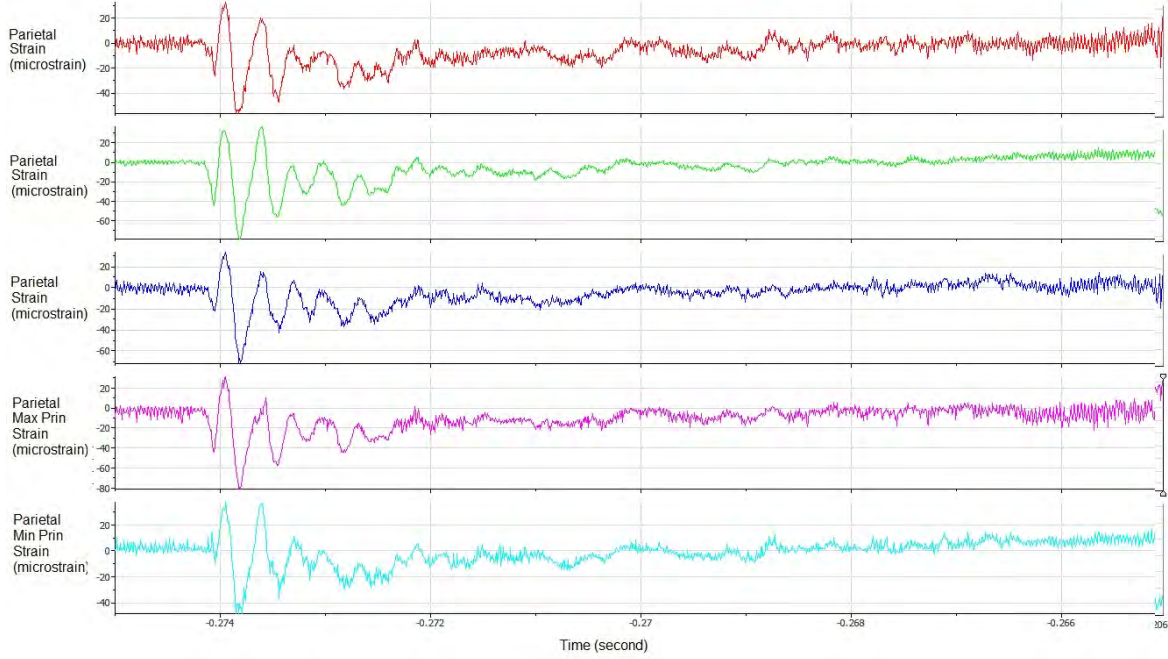
C4L-P



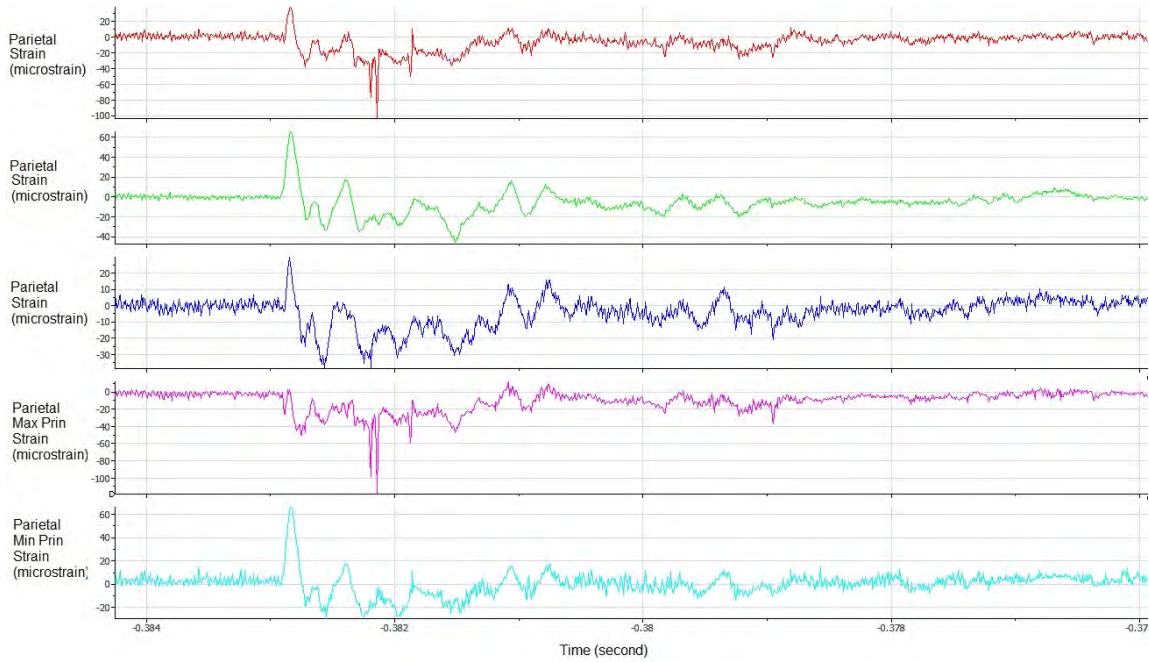
C4B-P



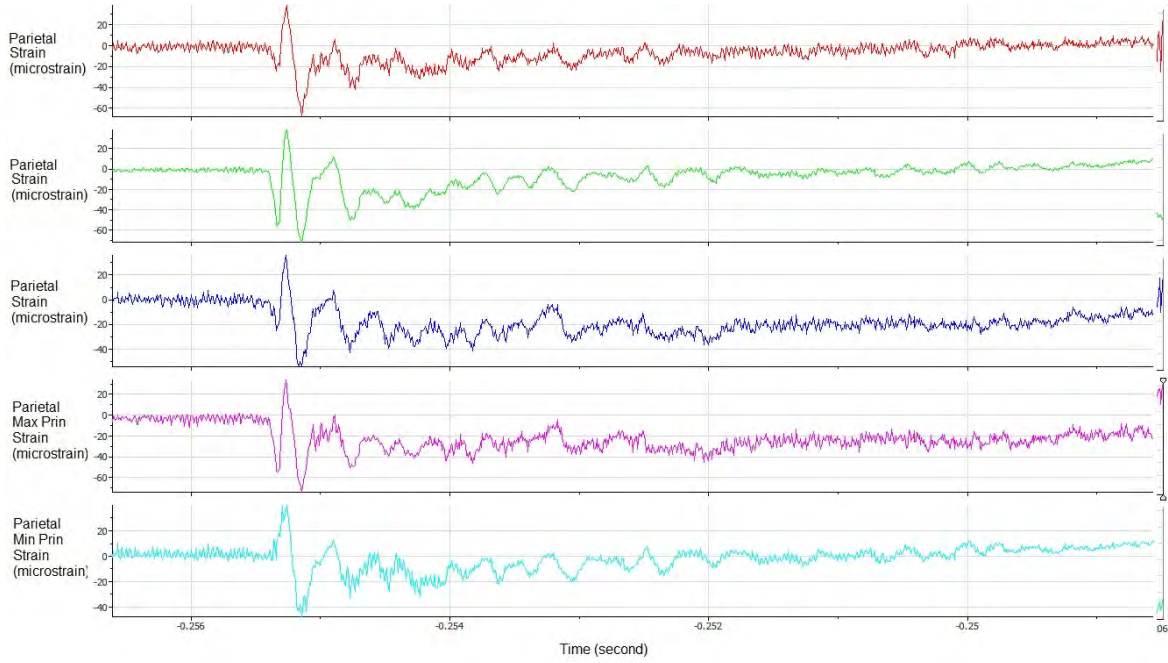
C4R-P



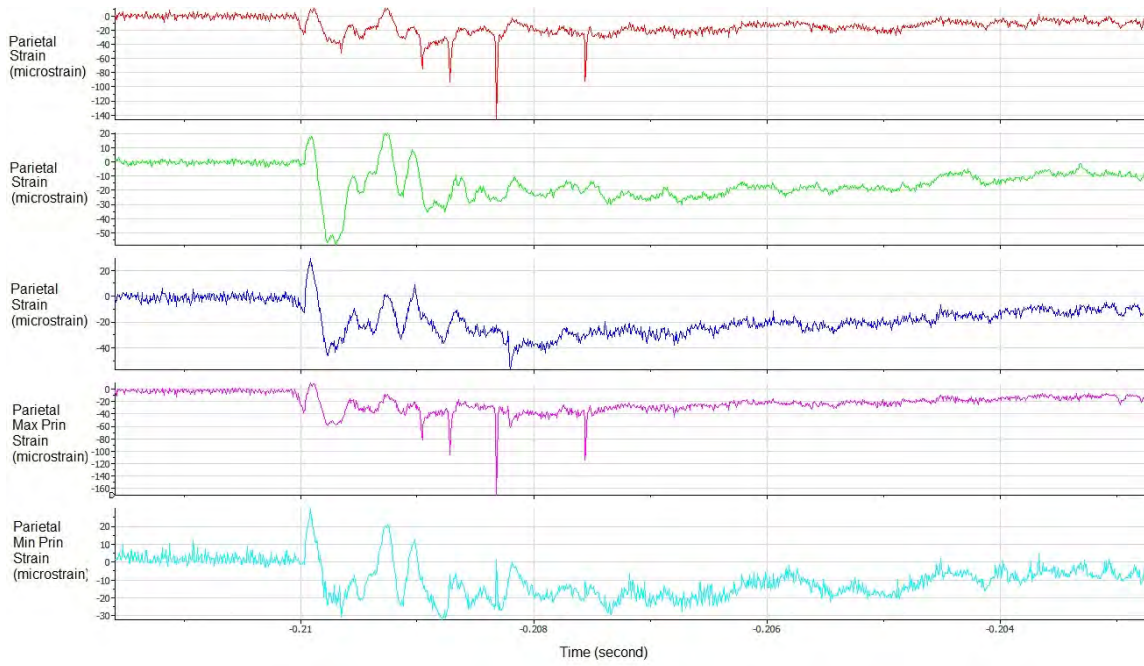
C5F-P



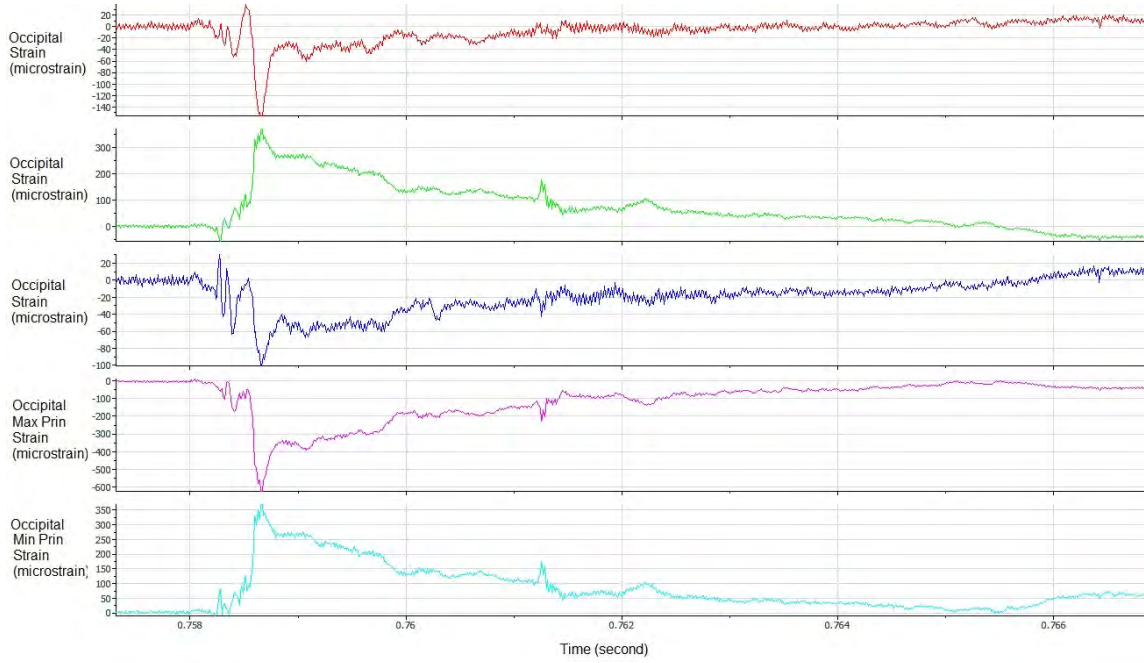
C5L-P



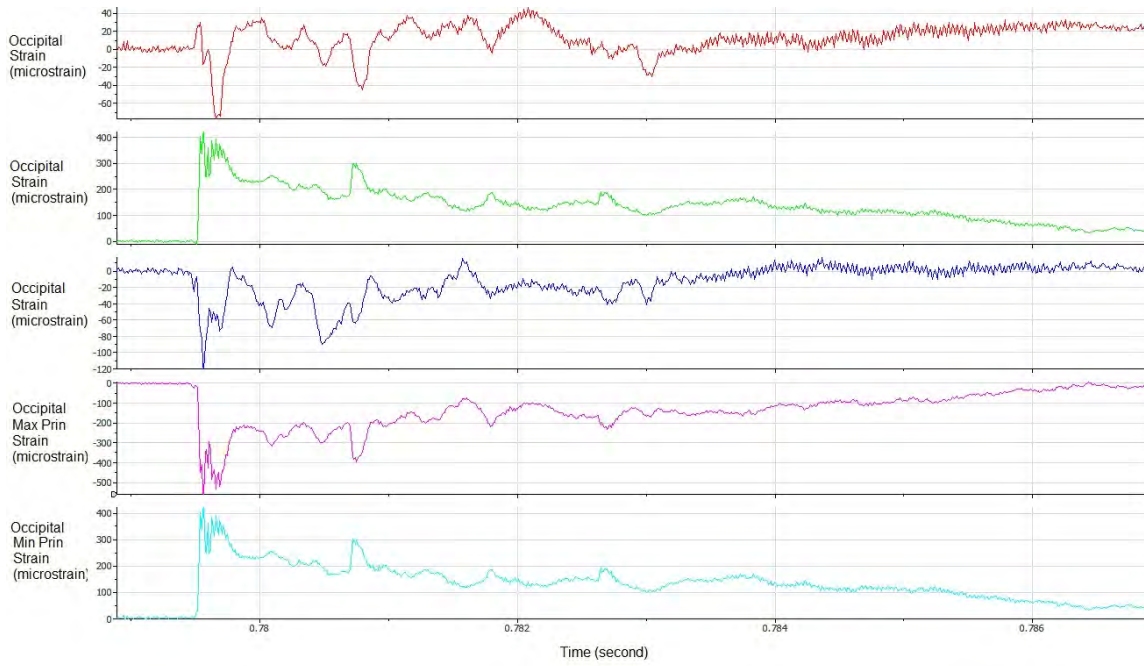
C5B-P



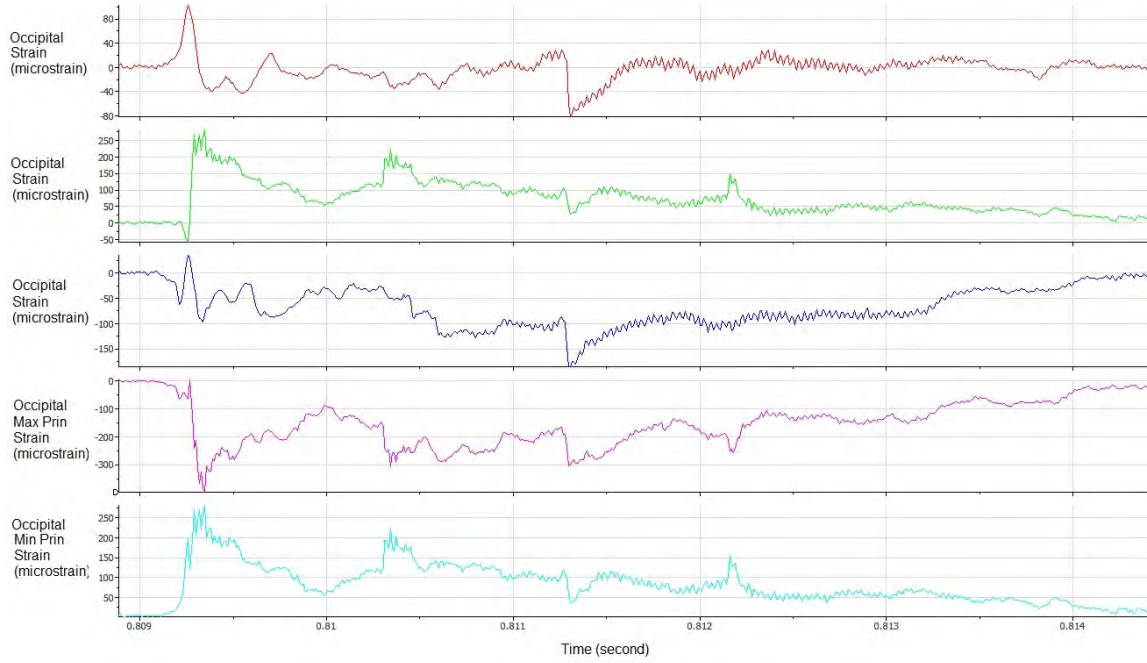
C5R-P



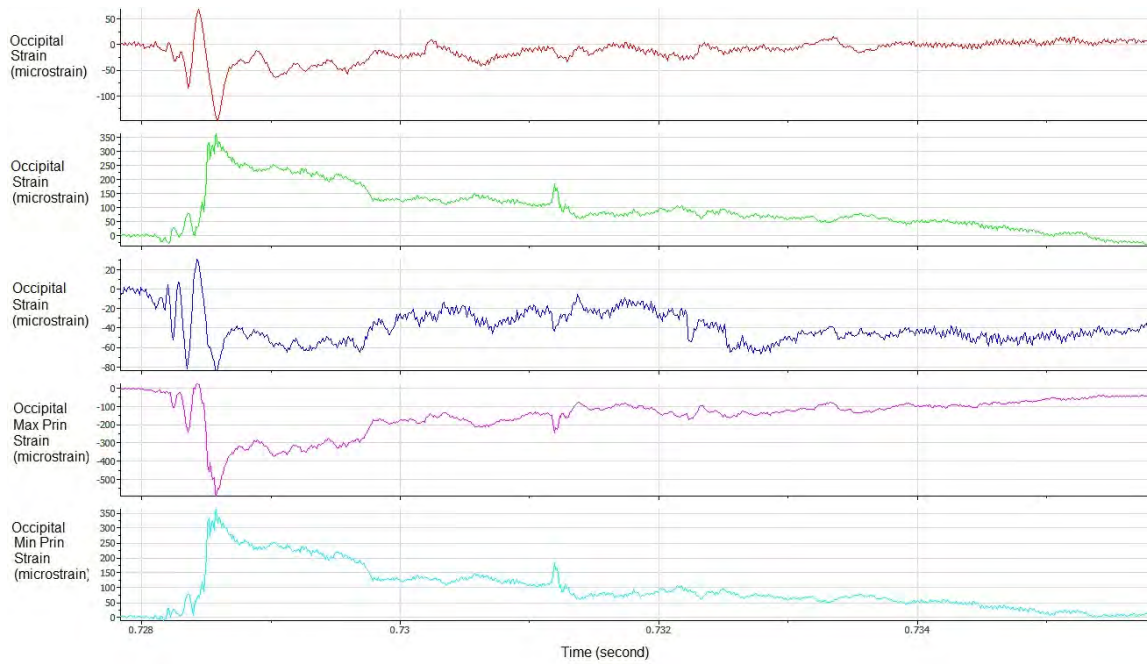
C2F-O



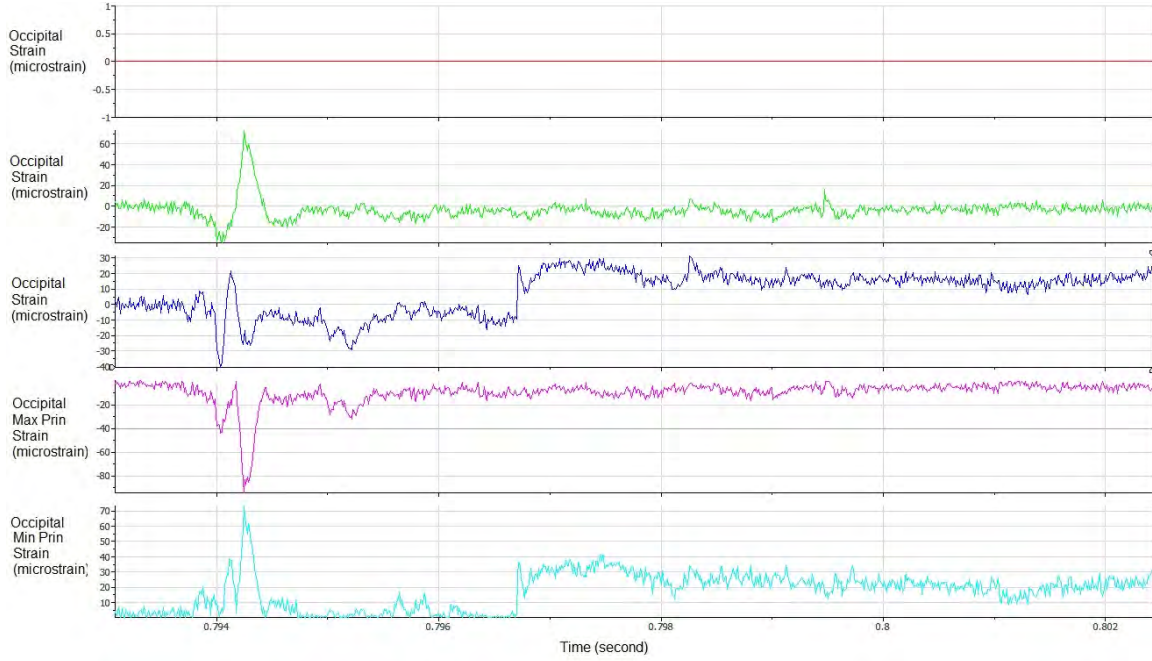
C2L-O



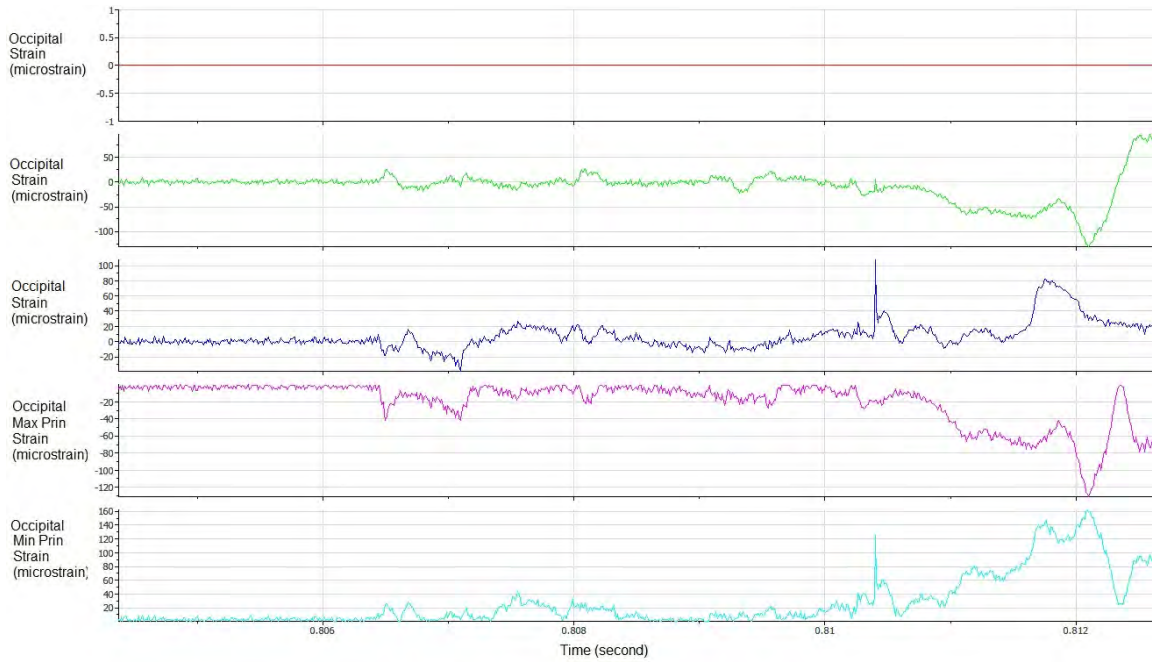
C2B-O



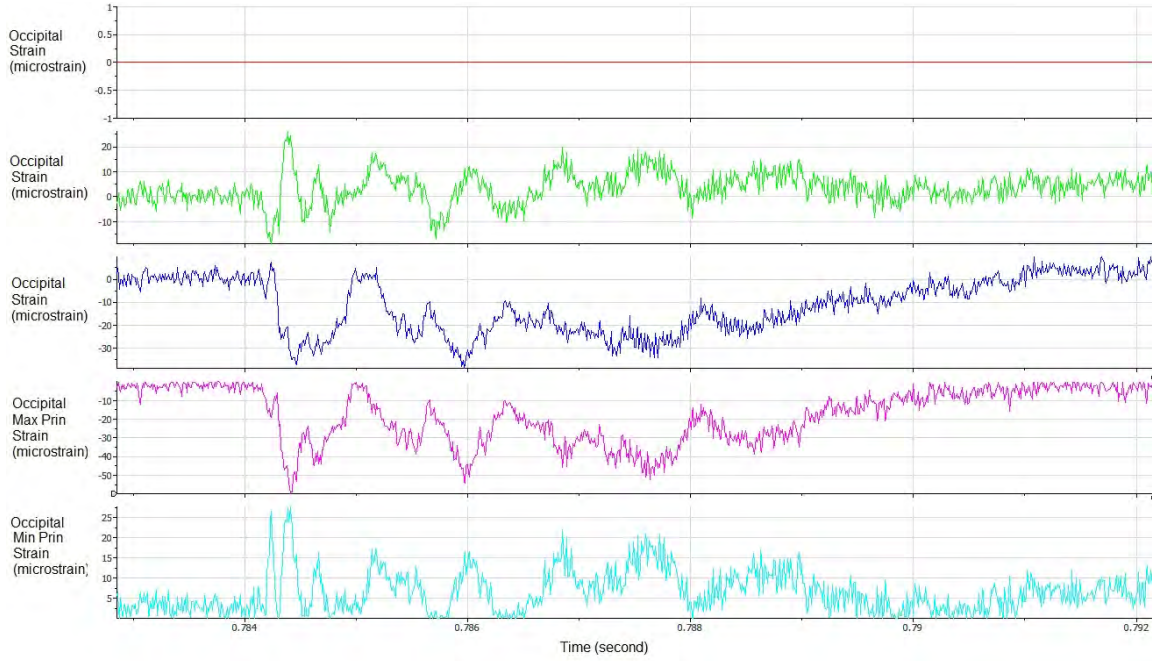
C2R-O



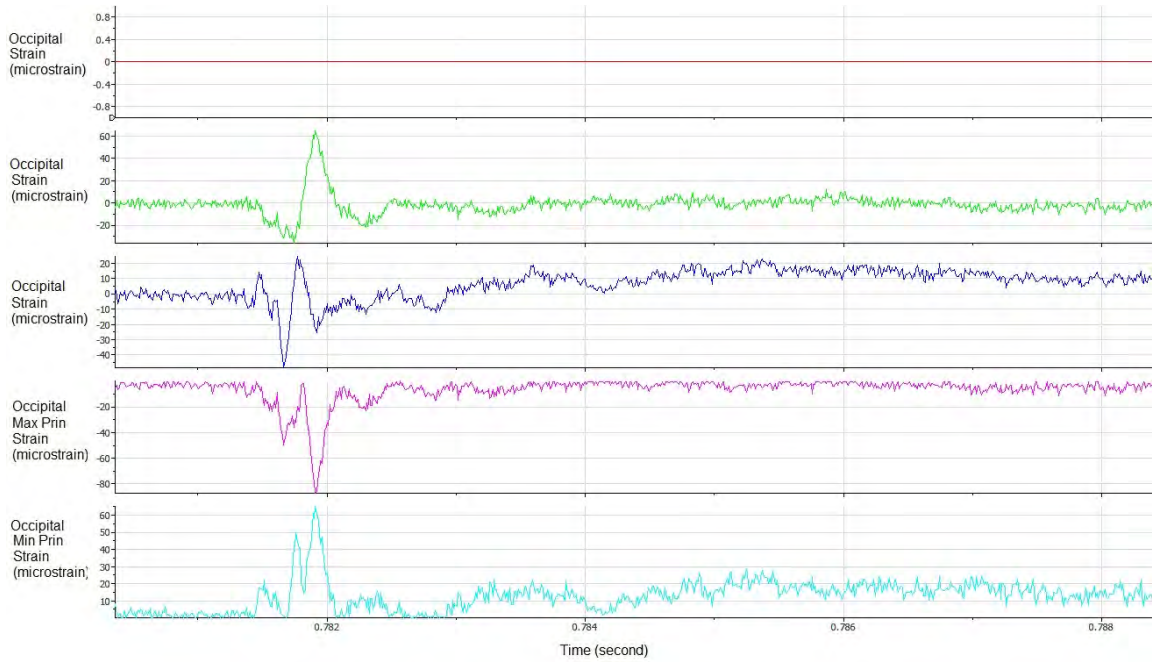
C3F-O



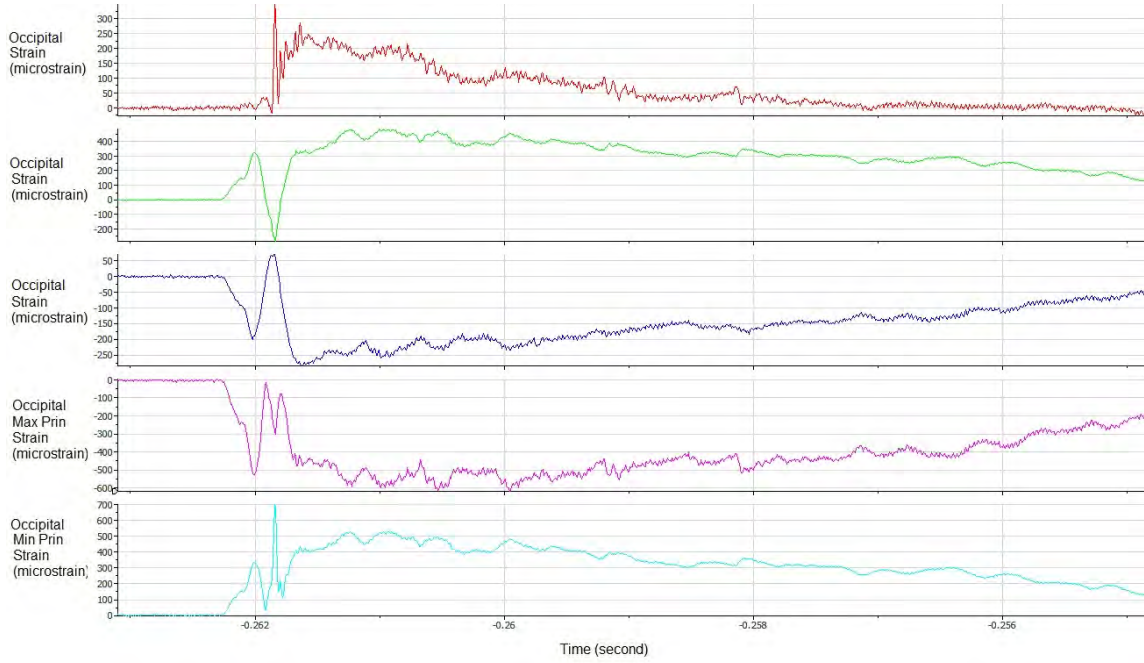
C3L-O



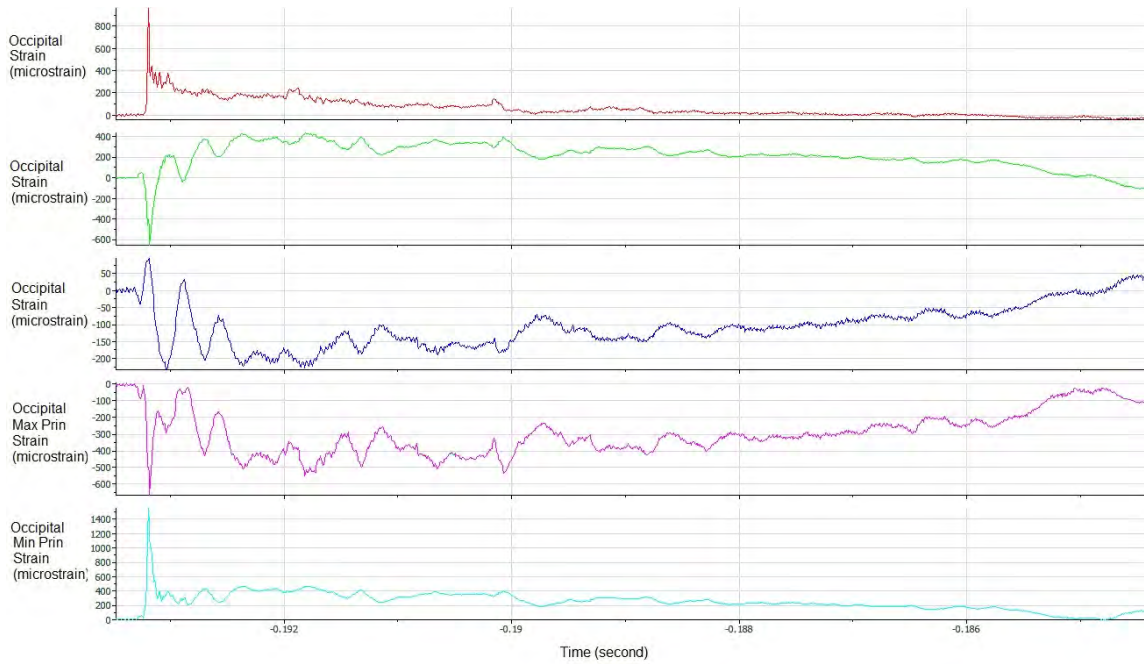
C3B-O



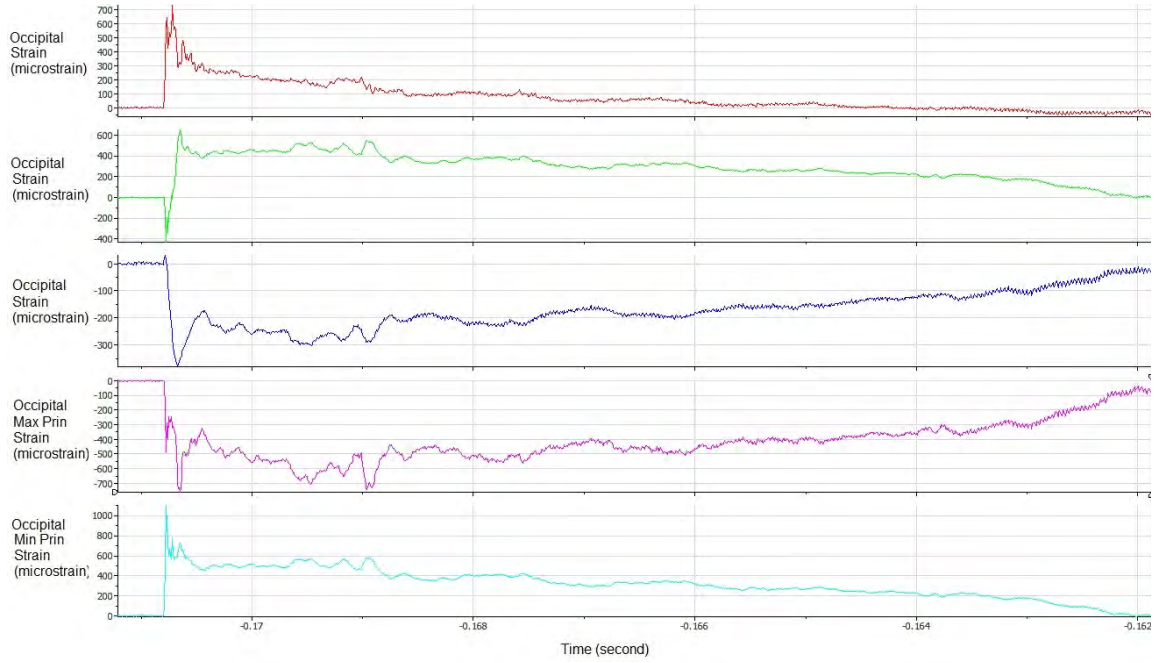
C3R-O



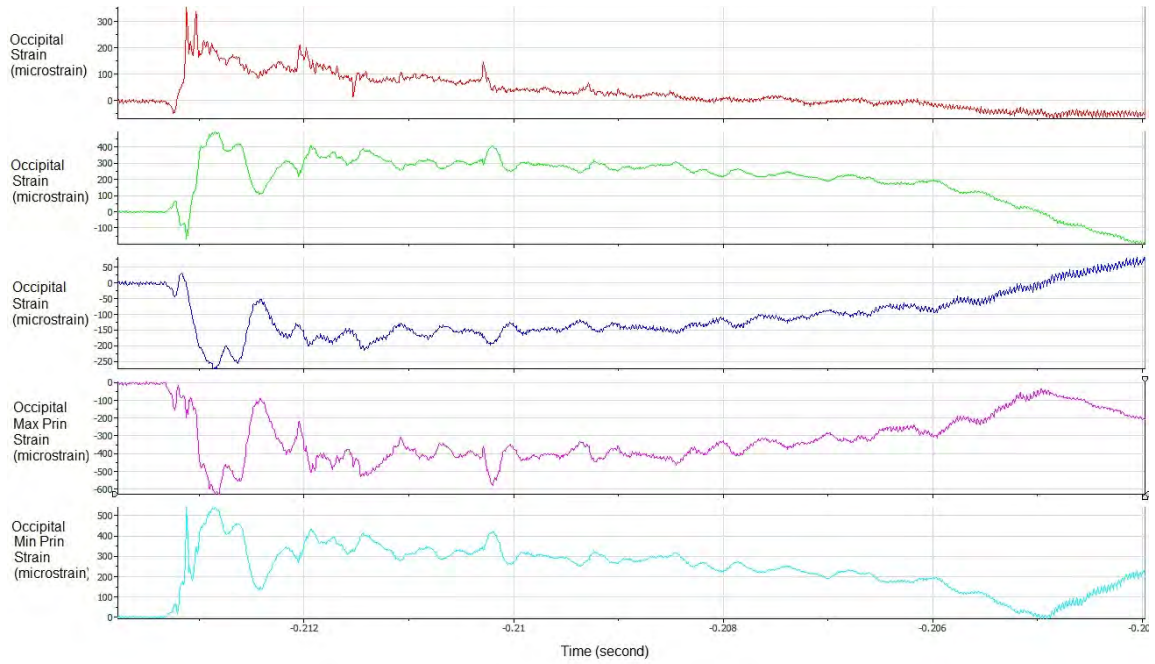
C4F-O



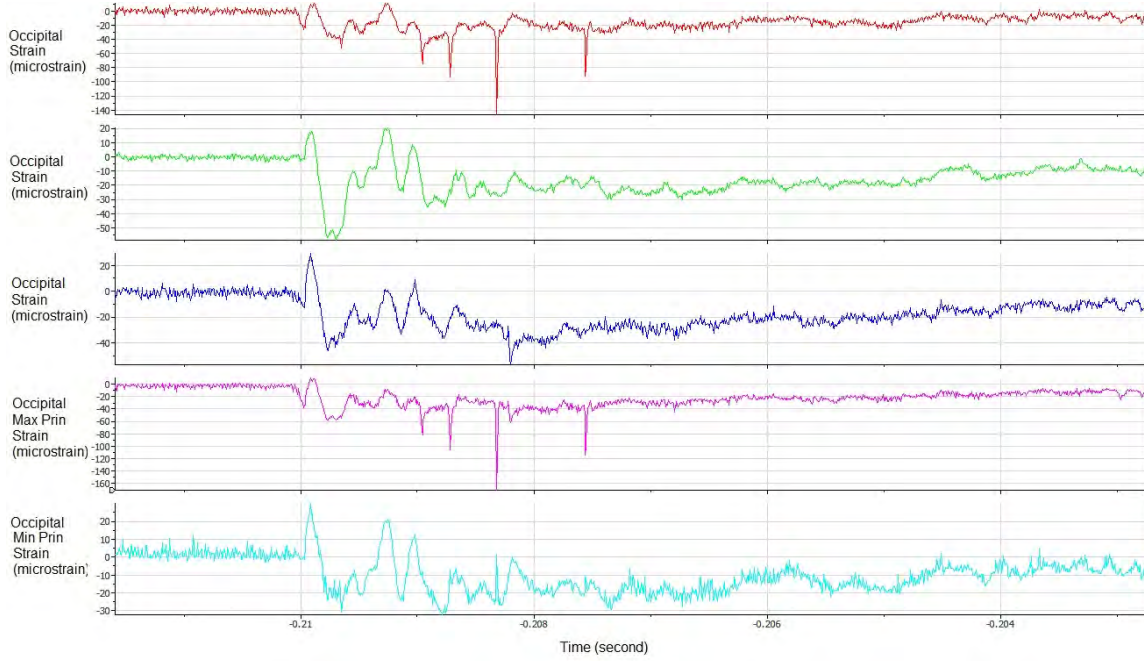
C4L-O



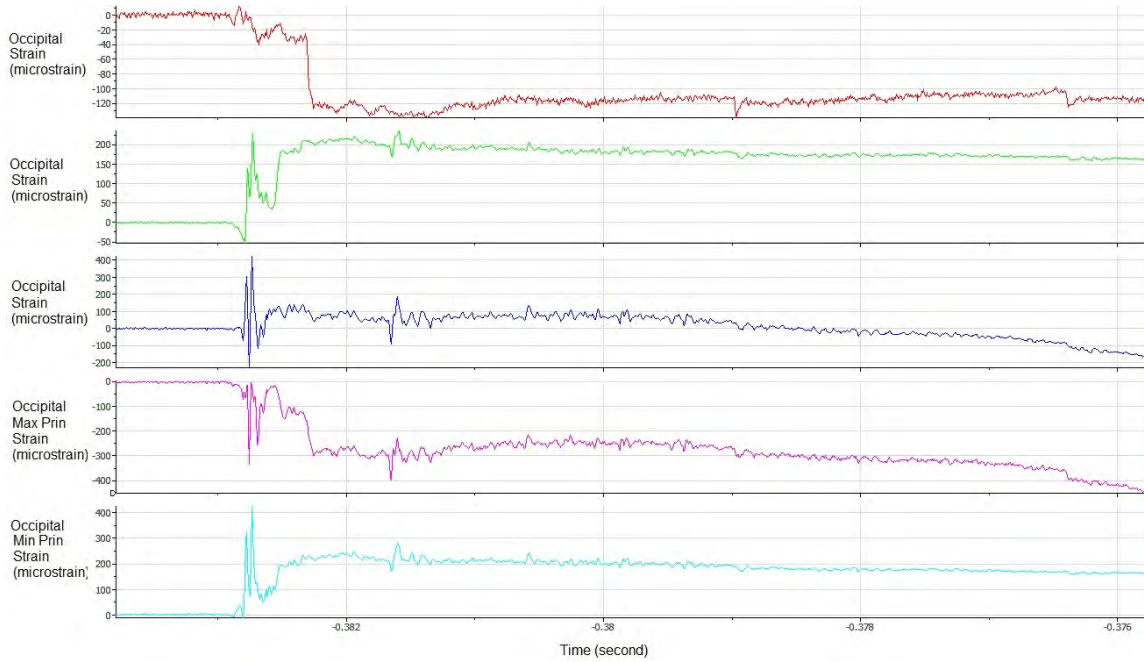
C4B-O



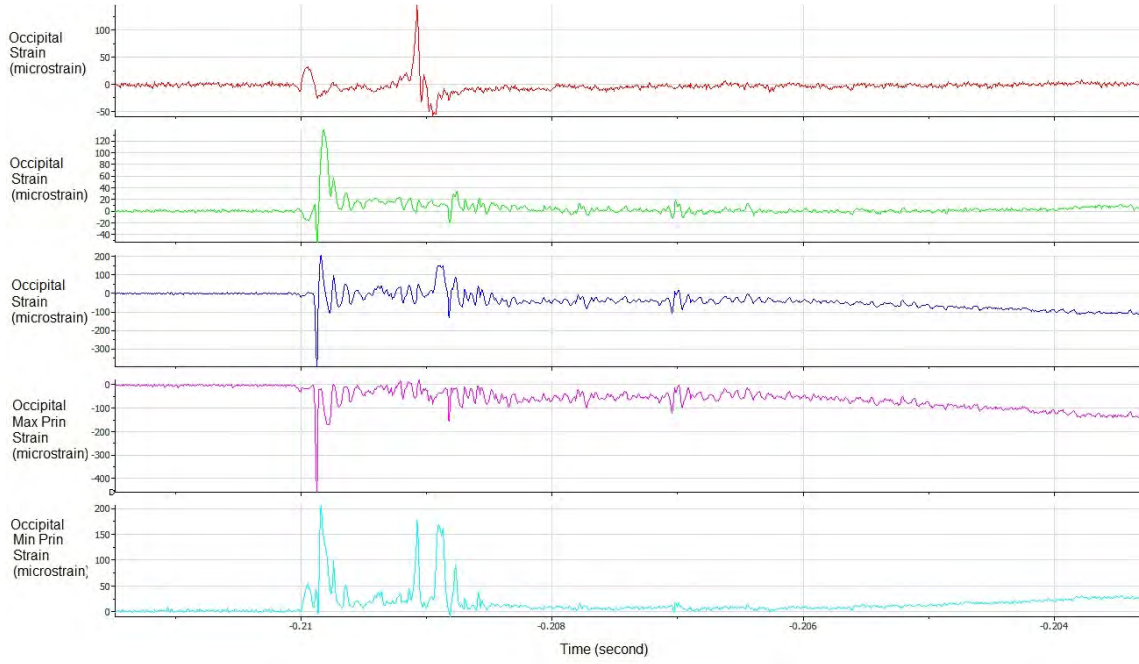
C4R-O



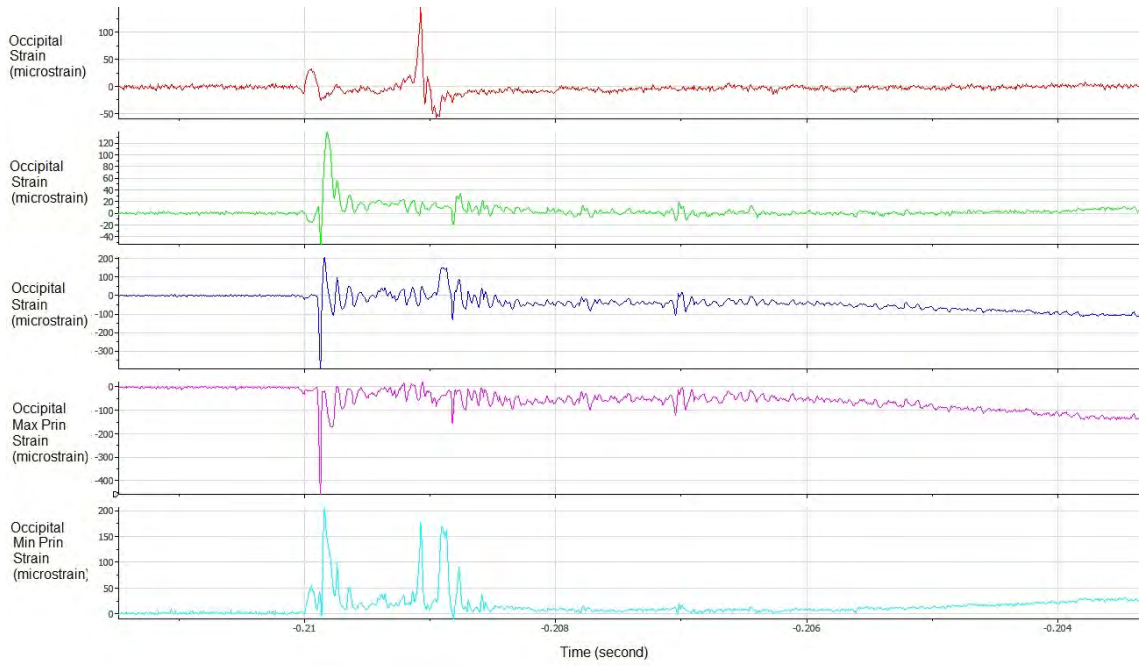
C5F-O



C5L-O



C5B-O



C5R-O

**REFERENCES**

- Adams, T., Heisey, R. S., Smith, M. C. and Briner, B. J., 1992. Parietal bone mobility in the anesthetized cat. *J Am Osteopath Assoc* 92, 599-600, 603-510, 615-522.
- Alley, M. D., Schimizza, B. R. and Son, S. F., 2010. Experimental modeling of explosive blast-related traumatic brain injuries. *Neuroimage*
- Bauman, R. A., Elsayed, N., Petras, J. M. and Widholm, J., 1997. Exposure to sublethal blast overpressure reduces the food intake and exercise performance of rats. *Toxicology* 121, 65-79.
- Bauman, R. A., Ling, G. S., Tong, L., Januszkiewicz, A., Agoston, D., Delanerolle, N., Kim, J., Ritzel, D., Bell, R., Ecklund, J. M., Armonda, R., Bandak, F. and Parks, S., 2009. An introductory characterization of a combat-casualty-care relevant swine model of closed head injury resulting from exposure to explosive blast. *J Neurotrauma*
- Bird, S. M. and Fairweather, C. B., 2007. Military fatality rates (by cause) in Afghanistan and Iraq: a measure of hostilities. *Int J Epidemiol* 36, 841-846.
- Bolander, R., Mathie, B., Bir, C., Ritzel, D. and VandeVord, P., 2011. Skull flexure as a contributing factor in the mechanism of injury in the rat when exposed to a shock wave. *Annals of Biomedical Engineering (In Process)*,
- Bowman, R. M. 1966. Investigation of shock front topography in shock tubes. Mechanical Engineering. Pasadena, California Institute of Technology. Doctor of Philosophy, 216.
- Cernak, I., 2005. Animal models of head trauma. *NeuroRx* 2, 410-422.

- Cernak, I., Savic, J., Malicevic, Z., Zunic, G., Radosevic, P. and Ivanovic, I., 1996. Leukotrienes in the pathogenesis of pulmonary blast injury. *J Trauma* 40, S148-151.
- Cernak, I., Savic, J., Malicevic, Z., Zunic, G., Radosevic, P., Ivanovic, I. and Davidovic, L., 1996. Involvement of the central nervous system in the general response to pulmonary blast injury. *J Trauma* 40, S100-104.
- Cernak, I., Vink, R., Zapple, D. N., Cruz, M. I., Ahmed, F., Chang, T., Fricke, S. T. and Faden, A. I., 2004. The pathobiology of moderate diffuse traumatic brain injury as identified using a new experimental model of injury in rats. *Neurobiol Dis* 17, 29-43.
- Cernak, I., Wang, Z., Jiang, J., Bian, X. and Savic, J., 2001. Cognitive deficits following blast injury-induced neurotrauma: possible involvement of nitric oxide. *Brain Inj* 15, 593-612.
- Cernak, I., Wang, Z., Jiang, J., Bian, X. and Savic, J., 2001. Ultrastructural and functional characteristics of blast injury-induced neurotrauma. *J Trauma* 50, 695-706.
- Chafi, M. S., Karami, G. and Ziejewski, M., 2009. Biomechanical Assessment of Brain Dynamic Responses Due to Blast Pressure Waves. *Ann Biomed Eng*
- Chafi, M. S., Karami, G. and Ziejewski, M., 2010. Biomechanical assessment of brain dynamic responses due to blast pressure waves. *Ann Biomed Eng* 38, 490-504.
- Chavko, M., Koller, W. A., Prusaczyk, W. K. and McCarron, R. M., 2007. Measurement of blast wave by a miniature fiber optic pressure transducer in the rat brain. *J Neurosci Methods* 159, 277-281.

- Clemedson, C. and Criborn, C., 1955. Mechanical response of different parts of a living body to a high explosive shock wave impact. *Am. J. Physiol.* 181, 471-476.
- Clemedson, C. J., 1957. Respiratory and circulatory vagal reflexes in rabbits exposed to high explosive shock waves. *Am J Physiol* 190, 467-472.
- Clemedson, C. J. and Nelson, A., 1957. The effects of a high explosive blast in mice with radiation injury. *Acta radiol* 47, 79-85.
- Command, N. F. E. 1986. Blast Resistant Structures. Short and Long Duration Blast loads, Structural Analysis and Design. Alexandria.
- Cooper, G. J. and Taylor, D. E., 1989. Biophysics of impact injury to the chest and abdomen. *J R Army Med Corps* 135, 58-67.
- Courtney, A. C. and Courtney, M. W., 2009. A thoracic mechanism of mild traumatic brain injury due to blast pressure waves. *Med Hypotheses* 72, 76-83.
- Courtney, M. W. and Courtney, A. C., 2010. Working toward exposure thresholds for blast-induced traumatic brain injury: Thoracic and acceleration mechanisms. *Neuroimage*
- Engin, A., 1969. The axisymmetric response of a fluid -filled spherical shell to a local radial impulse- A model for head injury. *J Biomechanics* 2, 325-341.
- Engin, A. and Liu, Y., 1970. Axisymmetric response of a fluid-filled spherical shell in free vibrations. *J Biomechanics* 3, 11-22.
- Finkel, M. F., 2006. The neurological consequences of explosives. *J Neurol Sci* 249, 63-67.
- Frykberg, E., 2002. Medical management of disasters and mass casualties from terrorist bombings: how can we cope? *Journal of Trauma* 53, 201-212.

- Gefen, A., Gefen, N., Zhu, Q., Raghupathi, R. and Margulies, S. S., 2003. Age-dependent changes in material properties of the brain and braincase of the rat. *J Neurotrauma* 20, 1163-1177.
- Glasstone, S. and Dolan, P. 1977. The effects of nuclear weapons. Air blast loading, DOD and ERDA.
- Gujidan, E., Roberts, V. and Thomas, L., 1966. Tolerance Curves of Acceleration and Intracranial pressure and protective index in experimental head injury. *Journal of Trauma* 6, 600-604.
- Halliday, D., Resnick, R. and Walker, J., 2005. *Fundamentals of Physics*. 1,
- Hardy, W. 2007. Response of the Human Cadaver Head to Impact. Biomedical Engineering. Detroit, Wayne State University. Doctor of Philosophy, 318.
- Ho, A. M., 2002. A simple conceptual model of primary pulmonary blast injury. *Med Hypotheses* 59, 611-613.
- Hoge, C. W., McGurk, D., Thomas, J. L., Cox, A. L., Engel, C. C. and Castro, C. A., 2008. Mild traumatic brain injury in U.S. Soldiers returning from Iraq. *N Engl J Med* 358, 453-463.
- Iakovlev, S., 2006. External shock loading on a submerged fluid-filled cylindrical shell. *Journal of Fluid Mechanics* 22, 997-1028.
- Iakovlev, S., 2007. Submerged fluid filled cylindrical shell subjected to a shock wave: fluid structure interaction effects. *Journal of Fluid and Structures* 23, 117-142.
- Katz, E., Ofek, B., Adler, J., Abramowitz, H. B. and Krausz, M. M., 1989. Primary blast injury after a bomb explosion in a civilian bus. *Ann Surg* 209, 484-488.
- Kinney, G. F., Ed. (1962). Explosive Shocks in Air. New York, Springer- Verlag.

- Kluger, Y., Nimrod, A., Biderman, P., Mayo, A. and Sorkin, P., 2007. The quinary pattern of blast injury. *Am J Disaster Med* 2, 21-25.
- Kwon, Y. and Fox, P., 1993. Under water shock response of a cylinder subjected to a side-on explosion. *Computers and Structures* 48, 637-646.
- Lamanna, G., Ed. (1996). Shock Tube.
- Leonardi, A. 2011. An investigation of the biomechanical response from shock wave loading to the head. Biomedical Engineering. Detroit, Wayne State University. Doctor of Philosophy.
- Leonardi, A., Bir, C., Ritzel, D. and VandeVord, P., 2011. Intracranial pressure increases during exposure to a shock wave. . *J Neurotrauma* 28, 85-94.
- Lighthall, J. and Anderson, T. (1994). In: The neurobiology of central nervous system trauma. New York/ Oxford.
- Lynnerup, N., Astrup, J. and Sejrsen, B., 2005. Thickness of the human cranial dipole in relation to age, sex, and general body build. *Head and face medicine*
- Mao, J., Pace, E., Peirozynski, P., Kou, Z., Shen, Y., VandeVord, P., Haacke, E., Zhang, X. and Zhang, J., 2011. Blast induced tinnitus and hearing loss in rats: Behavioral and imaging assays. *J Neurotrauma* epub ahead of print,
- McGinn, M. J., Kelley, B. J., Akinyi, L., Oli, M. W., Liu, M. C., Hayes, R. L., Wang, K. K. and Povlishock, J. T., 2009. Biochemical, structural, and biomarker evidence for calpain-mediated cytoskeletal change after diffuse brain injury uncomplicated by contusion. *J Neuropathol Exp Neurol* 68, 241-249.
- McMilian, R. 2004. Shock tube investigation of pressure and ion sensors used in pulse detonation engine research, Wright Patterson Air Force Base. Master of Science.

- Mediavilla Varas, J., Philippens, M., Meijer, S. R., van den Berg, A. C., Sibma, P. C., van Bree, J. L. and de Vries, D. V., 2011. Physics of IED Blast Shock Tube Simulations for mTBI Research. *Front Neurol* 2, 58.
- Mellor, S. G. and Cooper, G. J., 1989. Analysis of 828 servicemen killed or injured by explosion in Northern Ireland 1970-84: the Hostile Action Casualty System. *Br J Surg* 76, 1006-1010.
- Misra, J., Hartung, C. and Mahrenholtz, O., 1978. Stresses in a Human Skull Due to Pulse Loading. *Ingenieur-Archiv* 47, 329-337.
- Moore, D. F., Jerusalem, A., Nyein, M., Noels, L., Jaffee, M. S. and Radovitzky, R. A., 2009. Computational biology - modeling of primary blast effects on the central nervous system. *Neuroimage* 47 Suppl 2, T10-20.
- Moreira-Gonzalez, A., 1963. Calvarial thickness and its relation to cranial bone harvest. *Plastic and reconstructive surgery* 117, 1964-1971.
- Moss, W. C., King, M. J. and Blackman, E. G., 2008. Skull Flexure from Blast Waves: A new Mechanism for Brain Injury with implications for helmet design. LLNL-JRNL-405130-Draft
- Mott, F., 1916. On the effects of high explosives upon the central nervous system. *Lancet* 187, 331-338.
- Nahum, A., Smith, R. and Ward, C., 1977. Intracranial pressure dynamics during head impact. *Proc 21st Stapp Car Crash Conference* 337-366.
- Nayfeh, A. and Arafat, H., 2005. Axisymmetric vibrations of closed spherical shells: Equations of motion and bifurcation analysis. *Structural controls and health monitoring* 13, 388-416.

- Owens, B. D., Kragh, J. F., Jr., Wenke, J. C., Macaitis, J., Wade, C. E. and Holcomb, J. B., 2008. Combat wounds in operation Iraqi Freedom and operation Enduring Freedom. *J Trauma* 64, 295-299.
- Phillips, Y. Y., 1986. Primary blast injuries. *Ann Emerg Med* 15, 1446-1450.
- Ritzel, D., Parks, S., Roseveare, J., Rude, G. and Sawyer, T., 2011. Experimental Blast Simulation for Injury Studies. NATO Human Factors associated with blast meeting
- Romba, J. and Martin, P., 1961. The propagation of air shock waves on a biophysical model. DA Project 5B9520001
- Ruff, R. L., Ruff, S. S. and Wang, X. F., 2008. Headaches among Operation Iraqi Freedom/Operation Enduring Freedom veterans with mild traumatic brain injury associated with exposures to explosions. *J Rehabil Res Dev* 45, 941-952.
- Saljo, A., Arrhen, F., Bolouri, H., Mayorga, M. and Hamberger, A., 2008. Neuropathology and pressure in the pig brain resulting from low-impulse noise exposure. *J Neurotrauma* 25, 1397-1406.
- Saljo, A., Bao, F., Haglid, K. G. and Hansson, H. A., 2000. Blast exposure causes redistribution of phosphorylated neurofilament subunits in neurons of the adult rat brain. *J Neurotrauma* 17, 719-726.
- Saljo, A., Svensson, B., Mayorga, M., Hamberger, A. and Bolouri, H., 2009. Low levels of blast raises intracranial pressure and impairs cognitive function in rats. *J Neurotrauma*
- Sayer, N. A., Chiros, C. E., Sigford, B., Scott, S., Clothier, B., Pickett, T. and Lew, H. L., 2008. Characteristics and rehabilitation outcomes among patients with blast and

- other injuries sustained during the Global War on Terror. *Arch Phys Med Rehabil* 89, 163-170.
- Stalnaker, R., Melvin, J., Husholtz, G., Alem, N. and Benson, J., 1977. Head Impact response. *Proc 21st Stapp Car Crash Conference* 303-335.
- Sun, Z., Lee, E. and Herring, S., 2004. Cranial Sutures and Bones: Growth and Fusion in Relation of Masticatory Strain. *The anatomical record part A* 276A, 150-161.
- Taylor, P. and Ford, C., 2009. Simulation of blast-induced early time intracranial wave physics leading to traumatic brain injury. *Journal of Biomechanics* 131, 061007.
- Thomas, L., Roberts, V. and Gujidan, E., 1966. Experimental intercranial pressure gradients in the human skull. *N Neurol. Neurosurg. Psychiat.*, 29, 404.
- Turegano-Fuentes, F., Caba-Doussoux, P., Jover-Navalon, J. M., Martin-Perez, E., Fernandez-Luengas, D., Diez-Valladares, L., Perez-Diaz, D., Yuste-Garcia, P., Guadalajara Labajo, H., Rios-Blanco, R., Hernando-Trancho, F., Garcia-Moreno Nisa, F., Sanz-Sanchez, M., Garcia-Fuentes, C., Martinez-Virto, A., Leon-Baltasar, J. L. and Vazquez-Estevez, J., 2008. Injury patterns from major urban terrorist bombings in trains: the Madrid experience. *World J Surg* 32, 1168-1175.
- Van Boven, R. W., Harrington, G. S., Hackney, D. B., Ebel, A., Gauger, G., Bremner, J. D., D'Esposito, M., Detre, J. A., Haacke, E. M., Jack, C. R., Jr., Jagust, W. J., Le Bihan, D., Mathis, C. A., Mueller, S., Mukherjee, P., Schuff, N., Chen, A. and Weiner, M. W., 2009. Advances in neuroimaging of traumatic brain injury and posttraumatic stress disorder. *J Rehabil Res Dev* 46, 717-757.

- VandeVord, P., Bolander, R., Sajja, S., Hay, K. and Bir, C., 2011. Mild neurotrauma indicates a range-specific pressure response to low level shock wave exposure  
Annals of Biomedical Engineering Epub ahead of print,
- VandeVord, P., Bolander, R., Venkata, S., Hay, K. and Bir, C., 2011. Mild Neurotrauma Indicates a range specific pressure response to low level shock wave exposure.  
Annals of Biomedical Engineering epub ahead of print,
- Weidenreich, F., 1947. The trend of human evolution. *Evolution* 1, 221-236.
- Zhang, J., Yoganandan, N., Pintar, F. A. and Gennarelli, T. A., 2006. Role of translational and rotational accelerations on brain strain in lateral head impact.  
*Biomed Sci Instrum* 42, 501-506.
- Zhu, F., Mao, H., Dal Cengio Leonardi, A., Wagner, C., Chou, C., Jin, X., Bir, C., VandeVord, P., Yang, K. H. and King, A. I., 2010. Development of an FE model of the rat head subjected to air shock loading. *Stapp Car Crash J* 54, 211-225.

**ABSTRACT****A MULTI-SPECIES ANALYSIS OF BIOMECHANICAL RESPONSES OF THE HEAD TO A SHOCK WAVE**

by

**RICHARD BOLANDER****May 2012****Advisor:** Dr. Cynthia Bir and Dr. Pamela VandeVord**Major:** Biomedical Engineering**Degree:** Doctor of Philosophy

Shock wave induced brain injury remains a field of research that has great consequences for the rehabilitation of soldiers and civilians that are exposed to an explosion. As such, for the research to be successful in developing strategies to mitigate the effects of these injuries, appropriate research methods need to be developed. Animal models are currently employed to understand the brain's response to a shock wave exposure. Unfortunately no criteria have been established that indicates in what way the mechanical inputs that the cells in an animal's brain are subjected to are similar to a human. The purpose of this dissertation was to investigate these biomechanical responses.

To address this question, the biomechanical responses of the rat, pig, and cadaver were analyzed. Each of the species was exposed to multiple shock waves within a shock tube. Skull strain was measured using strain gages and intracranial pressure was measured using fiber optic pressure sensors. The effect of orientation was also addressed for the cadaver and the pig.

The results of the project indicate that for all three species, as the incident shock wave amplitude increases, the peak strain and ICP also increases. Also, the response of the head is unique to orientation. A front facing head will respond differently than a side facing head. The relationships between skull strain and ICP were also demonstrated. Skull flexure has a dominate effect on the ICP response. Additionally key characteristic waveforms describing the skull surface and ICP wave dynamics were identified.

Overall this project provides much needed information in the field of blast biomechanics. The results of the study indicate that each species will experience pressure wave profiles in the brain partially by means of skull flexure. And that the intracranial pressure environment is dependent on intensity, orientation of the head, and species being tested. It is possible that the responses of each species can be simplified into relative contributions of the identified waveforms. This research provides a basis for further studies that will either investigate methods for mitigating the effects of shock wave exposure or investigating brain cell response to pressure waveforms that are generated within the brain when exposed to a shock wave.

## AUTOBIOGRAPHICAL STATEMENT

### RICHARD BOLANDER

**PLACE OF BIRTH:** Bay City, Michigan

**EDUCATION:**

2012	PhD	Biomedical Engineering	Wayne State University
2009	MS	Biomedical Engineering	Wayne State University
2007	BS	Biomedical Engineering	Michigan Tech University

**HONORS AND AWARDS:**

Member of Golden Key Honor Society (2011)  
 First Place Poster Award, *The Eighth World Congress on Brain Injury* (2010)  
 Thomas Rumble Graduate Student Fellowship (2007-2008, 2010-2011), Wayne State University

**ACADEMIC WORK:**

Bolander, R., Mathie, B., Bir, C., Ritzel, D., VandeVord, P. (2011). Skull flexure as a contributing factor in the mechanism of injury in the rat when exposed to a shock wave. *Ann Biomed Eng.* 39: 2550-9.

VandeVord, P., Bolander, R., Sajja, S., Hay, K., Bir, C. (2011). Mild neurotrauma indicates a range-specific pressure response to low level shock wave exposure. *Ann Biomed Eng.*

Bolander, R.P., Neto, O.P., Bir, C.A. (2009). The effects of height and distance on the force production and acceleration in martial arts strikes. *Journal of Sports Science and Medicine, CSSI* 3: 47-52.

Neto, O.P., Bolander, R., Pacheco, M.T., Bir, C.A. (2009). Force, reaction time, and precision of Kung Fu strikes. *Percept Mot Skills.* 109: 295-303.

Neto OP, Silva JH, Marzullo ACD, Bolander RP, Bir CA. (2011). The effect of hand dominance on martial arts strikes. *Human Movement Science*, in press.